ENZYME-INHIBITORY SECONDARY METABOLITES AND THEIR EXUDATION IN THE MARINE-DERIVED FUNGUS *EPICOCCUM NIGRUM* Link

Dissertation

zur

Erlangung des Doktorgrades (Dr. rer. nat.)

der

Mathematisch-Naturwissenschaftlichen Fakultät

der

Rheinischen Friedrich-Wilhelms-Universität Bonn

vorgelegt von

Peter Hufendiek

ENZYME-INHIBITORY SECONDARY METABOLITES AND THEIR EXUDATION IN THE MARINE-DERIVED FUNGUS *EPICOCCUM NIGRUM* LINK

Dissertation

zur

Erlangung des Doktorgrades (Dr. rer. nat.)

der

Mathematisch-Naturwissenschaftlichen Fakultät

der

Rheinischen Friedrich-Wilhelms-Universität Bonn

vorgelegt von

Peter Hufendiek

aus

Bielefeld

Bonn, 2016

Angefertigt mit Genehmigung der Mathematisch-Naturwissenschaftlichen Fakultät der Rheinischen Friedrich-Wilhelms-Universität Bonn

1. Gutachter: Prof. Dr. G. M. König
2. Gutachter: Prof. Dr. V. Gieselmann

Erscheinungsjahr: 2017

Tag der Promotion: 30.03.2017

IN ADVANCE PUBLICATIONS OF THE DISSERTATION

Parts of this study have been published in advance by permission of the Mathematisch-Naturwissenschaftlichen Fakultät, represented by the supervisor of this study:

Research papers:

Hufendiek, P.; Stölben, S. S. M; Kehraus, S.; Merten, N.; Harms, H.; Crüsemann, M.; Arslan, I.; Gütschow, M.; Schneider, T.; König, G. M. Biosynthetic studies on acetosellin and structure elucidation of a new acetosellin derivative. Planta Medica 2017. Advance online publication. doi: 10.1055/s-0042-124493.

*Dávila-Céspedes, A.; *Hufendiek, P.; *Crüsemann, M.; Schäberle, T. F.; König, G. M. Marine-derived myxobacteria of the suborder Nannocystineae: An underexplored source of structurally intriguing and biologically active metabolites. Beilstein Journal of Organic Chemistry 2016, 12, 969–984.

*These authors contributed equally.

Harms, H.; Kehraus, S.; Nesaei-Mosaferan, D.; Hufendiek, P.; Meijer, L.; König, G. M. Aβ-42 lowering agents from the marine-derived fungus Dichotomomyces cejpii. Steroids 2015, 104, 182–188.

Harms, H.; Rempel, V.; Kehraus, S.; Kaiser, M.; Hufendiek, P.; Müller, C. E.; König, G. M. Indoloditerpenes from a Marine-Derived Fungal Strain of Dichotomomyces cejpii with Antagonistic Activity at GPR18 and Cannabinoid Receptors. Journal of Natural Products 2014, 77, 673–677.

Research presentations:

Hufendiek, P.; Kehraus, S.; König, G.M. Chemical and pharmacological investigation of metabolites from the marine-derived fungus *Epicoccum nigrum* LINK. Poster presentation at the ´14th International Symposium on Marine Natural Products joint with the 8th European Conference on Marine Natural Products 2013´, September 15-20, 2013, La Toja Island, Spain.

Hufendiek, P.; Kehraus, S.; Gütschow, M.; König, G.M. Epipyrones from the marine-derived fungus *Epicoccum nigrum* LINK inhibit the proteases cathepsin K and S. Poster presentation

at the ´2nd European Conference on Natural Products 2015´, September 6-9, 2015, Frankfurt, Germany.

Schrör, J.; Hufendiek, P.; Kehraus, S.; Gütschow, M.; König, G.M. Secondary metabolites of the fungus *Stemphylium globuliferum* and their biological activity. Poster presentation at the ´2nd European Conference on Natural Products 2015´, September 6-9, 2015, Frankfurt, Germany.

Hufendiek, P.; Kehraus, S.; Gütschow, M.; König, G.M. Epipyrones from the marine-derived fungus *Epicoccum nigrum* LINK inhibit the proteases cathepsin K and S. Poster presentation at the ´9th conference of Marine Natural Products 2015´, August 30 - September 2, 2015, Glasgow, Scotland.

Hufendiek, P.; Kehraus, S.; Gütschow, M.; König, G.M. Epipyrones from the marine-derived fungus *Epicoccum nigrum* LINK inhibit the proteases cathepsin K and S. Poster presentation at the ´1st International Conference of the Marine Fungal Natural Products Consortium joint with the 14th International Marine and Freshwater Mycology Symposium 2015´, July 21-24, 2015, Nantes, France.

ACKNOWLEDGEMENTS

ABBREVIATIONS

°C	degree Celsius
[1-^{13}C]acetate	acetate enriched with ^{13}C at position C-1
^{1}H-NMR	proton NMR
^{13}C-NMR	carbon-13 NMR
α	optical rotation
$[\alpha]_D^T$	specific optical rotation; T = temperature; D = D-line of sodium at 589 nm
δ	chemical shift in NMR spectroscopy [ppm]
Δδ	difference of chemical shifts
λ	wavelength [nm]
μ	micro = 10^{-6}
μL	microliter
μm	micrometer
A	adenine
Ac$_2$O	acetic anhydride
ACN	acetonitrile
ACP	acyl carrier protein (domain of polyketide synthases)
ARSA or ASA	Arylsulfatase A
Asp	L-aspartic acid
ASW	artificial sea water
Å	Ångström = 0.1 nm
BGC	biosynthetic gene cluster

C	cytosine
^{13}C	carbon-13 isotope
C_{18} silica	octadecylsilylated silica gel (= ODS, RP-18 silica)
CD	Circular dichroism
CDA	Czapek-Dox agar
CDA+Cu^{2+}	Czapek-Dox agar supplement with $CuSO_4$
CDA+Zn^{2+}	Czapek-Dox agar supplement with $ZnSO_4$
CDT	Czapek-Dox agar with TMS
CMeT	C-methyl transferase (domain of polyketide synthases)
CoA ≡ CoASH	coenzyme A
(h)CST	(human) cerebroside sulfotransferase
Cys	L-cysteine
MeOH-d_4	fully deuterated MeOH
DMSO-d_6	fully deuterated DMSO
DAD	diode array detector
DEPT-135	distortionless enhancement by polarization transfer (flip angle 135°)
DMSO	dimethyl sulfoxide
e.g.	for example
ELSD	evaporative light scattering detector
ESI	electrospray ionization (in mass spectrometry)
EtOAc	ethyl acetate
EtOH	ethanol
FAS	fatty acid synthase
FC	flash chromatography

g	gram
G	guanine
H,H-COSY	homonuclear correlation spectroscopy
His	L-histidine
HMBC	heteronuclear multiple bond correlation spectroscopy
HPLC	high pressure liquid chromatography
HSQC	heteronuclear single quantum coherence spectroscopy
Hz	Hertz (frequency)
i.e.	that is to say (*id est*)
IR	infrared
ITS	Internal transcribed spacer (gene region)
J	coupling constant [Hz]
keV	kiloelectron volt
L	liter
LC	liquid chromatography
LC-MS	HPLC or UPLC coupled to a mass spectrometer
log *D*	Distribution coefficient (pH-dependent)
log *P*	Partition coefficient
m/z	mass to charge ratio (in mass spectrometry)
mAU	milli absorption units
MAzP	*Monascus* azaphilone pigment
mg	milligram
MEA	malt extract agar
MEN	MEA supplemented with ASW and NaOAc
MES	MEA supplemented with ASW

Abbreviations

MeOH	methanol
MHz	Megahertz
min	minutes
mL	milliliter
mol	mole (unit)
mmol	millimole
MPLC	medium pressure liquid chromatography (syn. flash chromatography)
M_r	molecular weight
ms	milliseconds
MS	mass spectrometry
MS/MS ≡ MS^2	Tandem mass spectrometry
NADPH	nicotinamide dinucleotide phosphate (reduced form)
NaOAc	sodium acetate
nL	nanoliters
nm	nanometer
NMR	nuclear magnetic resonance
NOESY	Nuclear Overhauser enhancement spectroscopy
NP	normal phase (in chromatography)
NR-(f)PKS	non-reducing (fungal) polyketide synthase
OSMAC	one strain many compounds
(f)PKS	(fungal) polyketide synthase
ppm	parts per million
R^2	correlation coefficient
ROESY	rotating frame Nuclear Overhauser effect spectroscopy
RP	reversed phase (in chromatography)

S	Svedberg unit (sedimentation rate of ribosomal subunits)
SAM	S-adenosyl methionine
SAW	surface acoustic wave (type of biosensor)
sec	seconds
SEC	size exclusion chromatography
Ser	L-serine
SM	secondary metabolite
SPE	solid phase extraction
T	thymine
T_M	melting point [°C]
t_R	retention time [min]
TFA	trifluoroacetic acid
TIC	total ion chromatogram (in mass spectrometry)
TMS	trace metal solution (as defined in section 3.1.3)
TWC	total wavelength chromatogram (in mass spectrometry)
UPLC ≡ UHPLC	ultrahigh pressure liquid chromatography
UV	ultraviolet
VLC	vacuum liquid chromatography
vol%	percentage by volume (v/v)
wt%	percentage by mass (w/w)

Abbreviations

CONTENTS

Contents

Contents

Contents

1   INTRODUCTION

1.1   WHY FUNGI? SECONDARY METABOLISM AND ITS RELEVANCE IN DRUG DISCOVERY

As pointed out by Newman and Cragg [1], secondary metabolites are an indispensable source for drugs in medicine. Of the therapeutic agents, which were approved from 1981 – 2014, 51% were derived from natural products. 4% of all introduced drugs were unmodified, original natural products. The long evolutionary history of metabolic adaption may be the reason, why natural products in general often lead to positive hits in drug screening programs. It was hypothesized by Kellenberger et al. that there are similar recognition sites in the biosynthetic proteins and in human protein targets used in drug discovery [2]. For the search of new chemical entities, mainly plants, bacteria and fungi, but also vertebrates and invertebrates have been employed as sources [3]. Among the mentioned groups, fungi are highly diverse, with ca. 100.000 known species and an estimated 1.5 - 5.1 million species [4]. They colonize virtually any substrate, ranging from exposed rocks and deserts to freshwater and marine habitats. Most importantly, they interact with other organisms as parasites, symbionts or decomposers and thus remineralize decaying organic material [5].

However, the vast diversity of metabolic scaffolds from fungi cannot only be explained by the number of species. In their natural environments, they are exposed to often harsh conditions, *e.g.*, intense sun light, low nutrient availability or osmotic stress in saline habitats [6–8]. What may be even more important is the close contact to other, often concurring organisms (*e.g.*, in soil or on plant surfaces). In soil, up to 10^{11}-10^{12} prokaryotic cells can be found per gram dry sample via microscopic methods [9,10]. Adaption to the numerous different ecological niches is of course also reflected by a variety of morphological and physiological characteristics. Consequently, fungi developed a vast array of specific enzymes and metabolic capabilities. Therefore they are a prolific source of primary and secondary metabolites [11–18]. This applies mainly to the Ascomycota and the Basidiomycota, which comprise more than 90% of the known fungal species (see **fig. 1.1**) and are also the most productive producers of secondary metabolites [19].
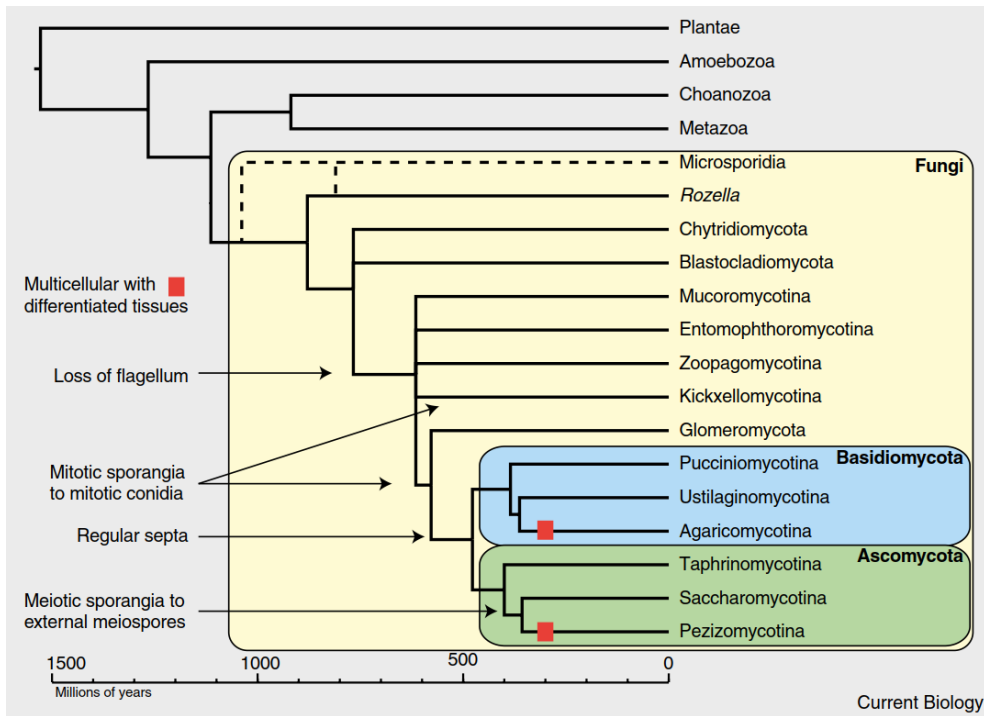
Fig. 1.1: A phylogenetic tree, showing the fungi as a distinct group. The picture is taken from Stajich et al. [5].

In order to exploit the metabolic potential of fungi, the so called OSMAC (one strain many compounds) approach was developed and used over the last decades [20–22]. The simple, yet efficient idea behind this method is to stimulate the biosynthesis of a wide range of secondary metabolites by applying different cultivation conditions.

This can be done by offering completely different sets of nutrients: Fermentation on nutrient-rich complex media (*e.g.*, yeast extract or malt extract) versus cultivation on nutrient-limited, defined media like Czapek-Dox agar (CDA).

Another variant of this approach is to provide the fungus with different supplements or abiotic factors while cultivating it on the same substrate. Variations can be the addition of trace metal ions [23] as well as altered physical variables: temperature, lighting, oxygen concentration, to name just a few. These slight modifications can lead to major changes in the metabolic profile [24,25]. In recent years, co-cultivation and the addition of epigenetic modifiers emerged as powerful tools in this field [26].

Thus, the chemical diversity and strong bioactivities of different fungal natural products led to the development of a number of drugs and drug candidates for the medicinal use. **Fig. 1.2** shows one examples of a fungal meroterpenoid, namely fumagillin, which was first isolated from *Aspergillus fumigatus* (Trichocomaceae, Eurotiales). Biosynthetically, it is composed of

a sesquiterpenoid unit and a polyenic polyketide moiety [27]. The epoxy group is the pharmacophore, which irreversibly binds to a histidine residue of methionine aminopeptidase type 2 (MetAP2) [28]. Methionine aminopeptidases are cytosolic enzymes, which cleave terminal methionine residues from nascent proteins. They are therefore essential for the activation of newly synthesized proteins and cell survival [29]. While higher eukaryotes have two isoforms, MetAP1 and MetAP2, microsporidia only produce MetAP2. Microsporidia (*e.g.*, *Enterocytozoon bieneusi*) are obligate intracellular parasites of vertebrates and invertebrates, which presumably form an ancient clade of the fungi (see **fig. 1.1**). In rare cases, immunocompromised patients get infected and suffer ocular infections, chronic gastrointestinal symptoms and weight loss. Therefore, fumagillin is used against microsporidiosis in the USA and France [3,30,31]. Since MetAP2 also has a crucial function in angiogenesis, fumagillin is further investigated for the treatment of different types of cancer [29].
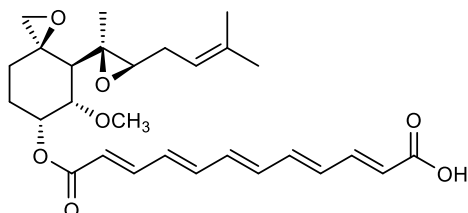
Fig. 1.2: Structure of fumagillin from *Aspergillus fumigatus*.

ASP2397 (see **fig. 1.3**) is a recent example of a fungal hydroxamate siderophore, which is being developed as antifungal agent [32]. It was isolated from *Acremonium persicinum* (Hypocreales), growing on leaf litter and shows strong inhibitory activity on different *Aspergillus* spp. While the exact mechanism is not known, data from *A. fumigatus* show that the efficacy relies on the chelated metal ions (*i.e.,* Al^{3+} or Ga^{3+}), since Fe^{3+} abandons the activity [33]. ASP2397 is taken up by hyphae through the siderophore transporter Sit1. Since humans do not express this protein, fungi are selectively inhibited. Currently, a phase I clinical trial is undertaken in order to assess its application in invasive pulmonary aspergillosis. This is a life-threatening infectious disease in immunocompromised patients [34–36].
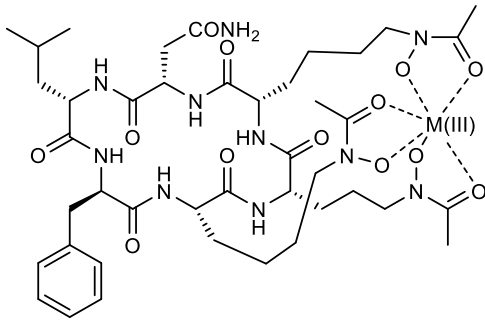
Fig. 1.3: Molecular structure of ASP2397 from *Acremonium persicinum*, a hydroxamate siderophore with antifungal activity. It is currently in phase I clinical trials. M(III) = Al^{3+}.

1.2 PLANT-ASSOCIATED FUNGI AS SOURCES OF SECONDARY METABOLITES

As mentioned earlier, fungi are highly adaptable organisms, able to thrive autonomously or in different relationships. These relationships involve symbiotic or parasitic ties with plants, bacteria or animals [5,37–42]. Regarding symbiotic relationships with plants, a distinction between mycorrhizal fungi and endophytic fungi is important: The term *mycorrhiza* is used to characterize specifically a fungal association with plant roots, where significant parts of the fungus still live outside of the plant tissue [43]. Microorganisms (including bacteria and even unicellular algae [44,45]) living asymptomatically in plant tissue are commonly referred to as *endophytes*. Endophytes can infect different plant parts and live exclusively inside of the plant during the association. They were found in all large groups of plants, including mosses, ferns, gymnosperms, angiosperms and algae. Finally, epibionts live on plant surfaces [46].

Endophytes are usually regarded as a means to strengthen the competitiveness of the host plant. They influence the resistance against abiotic (*e.g.*, light stress, drought/ salt/ oxidative stress) and biotic stress factors (*e.g.*, herbivores, pathogens) [47]. Different mechanisms are involved in the mentioned effects. Drought stress and salt stress can be alleviated by the production of compatible solutes [48]. Oxidative stress, resulting from different abiotic and biotic stressors, was also found to be reduced in infected plants. Barley roots (*Hordeum vulgare*, Poaceae), associated with the fungal endophyte *Piriformospora indica* (Sebacinales), exhibited higher levels of antioxidant metabolites, *i.e.,* glutathione and ascorbic acid [49].

The association of different grasses with fungi from the family Clavicipitaceae (Hypocreales, Ascomycota; the so-called *clavicipitalean endophytes*) is the subject of numerous studies.

This is due to its agricultural and economic importance for livestock farming and crop growing [50]. On the one hand, clavicipitalean fungi can act as parasites on grasses, *e.g.*, the ergot fungus (*Claviceps purpurea*). It produces different ergoline alkaloids, of which ergotamine is one of the main constituents (see **fig. 1.4**). Due to its agonist activity on serotonin- (5-HT$_{1B}$-/5-HT$_{1D}$-)receptors, it is in use against migraine (Ergo-Kranit[®]). On the other hand, clavicipitalean fungi also form symbiotic relationships with plants, as epibionts or endophytes. In those cases, the fungal partner produces antioxidant phenolic substances as well as insecticidal and antifeedant alkaloids, which can be toxic to grazing cattle (*e.g.*, loline or ergoline alkaloids) [51,52].

From a pharmaceutical perspective, another finding may even be more intriguing: A couple of secondary metabolites from terrestrial plants are actually produced by fungal endophytes or by both symbiotic partners, plant and fungus. The discovery of plant-derived drugs being produced by fungal endophytes spurred the search for fungal strains, which could be exploited for the large-scale production of these compounds. Industrial production of plant secondary metabolites by plant cell cultures can be cumbersome. Thus, the replacement of plant cells by fungal biomass is a promising field of current research projects [53]. Examples include the microtubule-stabilizing anticancer drug paclitaxel from *Taxus brevifolia* (see **fig. 1.4**). It is most likely produced by the host plant together with different endophytic fungi (*e.g.*, *Taxomyces andreanae* or *Paraconiothyrium* sp. SSM001) [54], though there has been some controversy over the real capabilities of the endophytes to produce taxane alkaloids [55]. Furthermore, some of the flavonolignans (*e.g.,* silybin A, see **fig. 1.4**) from the fruits of the milk thistle (*Silybum marianum*) have also been produced in axenic culture by an endophytic fungus, *i.e., Aspergillus iizukae* (Trichocomaceae, Eurotiales) [56]. A complex of at least seven flavonolignans, called silymarin, is used as hepatoprotective agent and antidote against poisoning by hepatotoxic compounds, *e.g.*, amatoxins. Silymarin presumably acts by preventing lipid peroxidation in the plasma membrane and by regulating the membrane permeability of liver cells, thus inhibiting absorption of the toxic agents [57].

Paclitaxel

Ergotamine
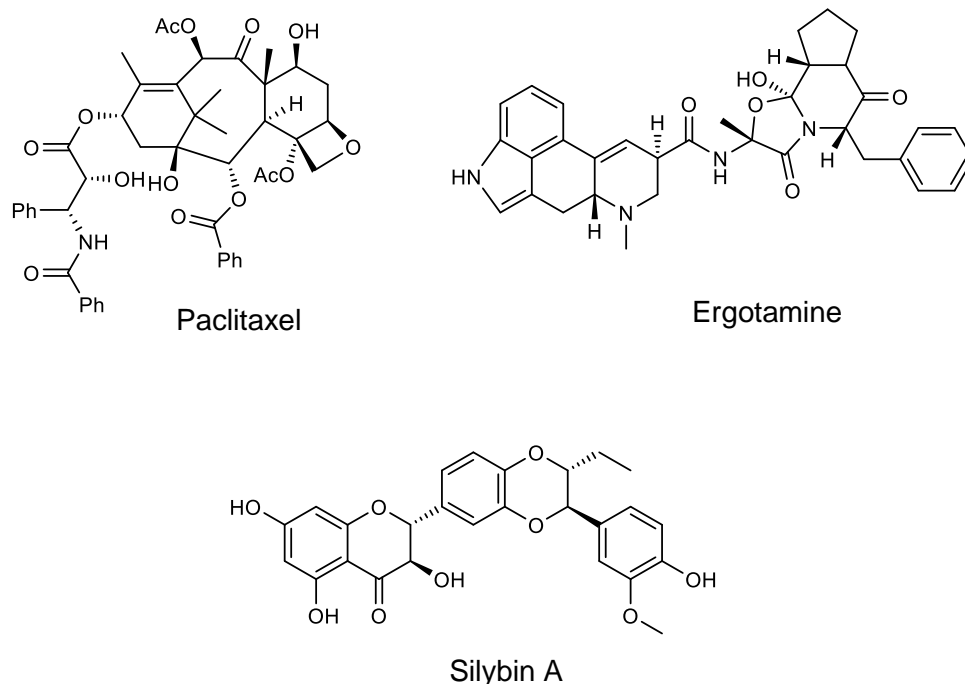
Silybin A

Fig. 1.4: Structures of approved drugs, which are produced by fungi associated with vascular plants: Ergotamine is produced by the parasitic fungus *Claviceps purpurea*. Paclitaxel and silybin A were first isolated from vascular plants and are now thought to be produced additionally by fungal endophytes. Ph = Phenyl ring.

1.3 MARINE FUNGI - ALGICOLOUS STRAINS AND THEIR POTENTIAL AS PRODUCERS OF LEAD STRUCTURES

Though most of our planet is covered by oceans, fungi were mainly sampled or studied from terrestrial biotopes. Nevertheless, they are also frequently isolated from marine and freshwater habitats [58,59]. Some fungi even specialized on freshwater environments. These are commonly referred to as ´Ingoldian fungi´, though they do not form a monophyletic group [60]. Instead, they are defined by their ecophysiological and morphological traits. Similar to the Ingoldian fungi, obligate marine species belong to different phylogenetic groups mainly within the Ascomycota and Basidiomycota (according to the current state of knowledge). Thus, adaptation to marine habitats may have occurred multiple times independently during evolution [61,62]. Apart from that, common terrestrial lineages make up the majority of samples from marine habitats, thus highlighting the high adaptability of certain fungi to different ecological niches and degrees of salinity. Many of them live on the surface of algae or in their tissue as endophytes. Those species are referred to as algicolous fungi [63]. To

date, macroalgae from the Chlorophyta (green algae), Rhodophyceae (red algae) and Phaeophyceae (brown algae) were found to harbor fungal endophytes [64].

Similar to marine-derived fungi in general, secondary metabolites from marine sources have long been neglected due to the difficulty in sampling. Since it is becoming increasingly harder to find new chemical entities in terrestrial strains, marine-derived fungi are an advancing research area [65,66]. As mentioned before, a number of studies on terrestrial endophytes focus on the ability of fungi to produce plant secondary metabolites. However, research on marine endophytes or epibionts concentrates more on the discovery of new chemical entities. Clinical studies already have been undertaken with fungal metabolites from marine sources. Unfortunately, however, none has been approved yet [67].

A promising example for a marine-derived lead structure is (-)-phenylahistin (syn. halimide, see **fig. 1.5**), which is produced by an *Aspergillus* sp., isolated from a green alga near the Philippine Islands. Chemically, it is a diketopiperazine derivative with cytotoxic activity. In order to improve its bioactivity, it was semi-synthetically modified to yield plinabulin [68,69]. The mechanism of action of plinabulin is believed to be the induction of caspase- and JNK (c-Jun N-terminal kinase)-dependent apoptosis. Additionally, it leads to microtubule depolymerization in vascular endothelial cells in the tumor [70]. Currently, a phase III clinical trial is under way in order to assess its efficacy in combination with docetaxel against advanced NSCLC (non-small cell lung cancer) [71].

(-)-Phenylahistin   Plinabulin
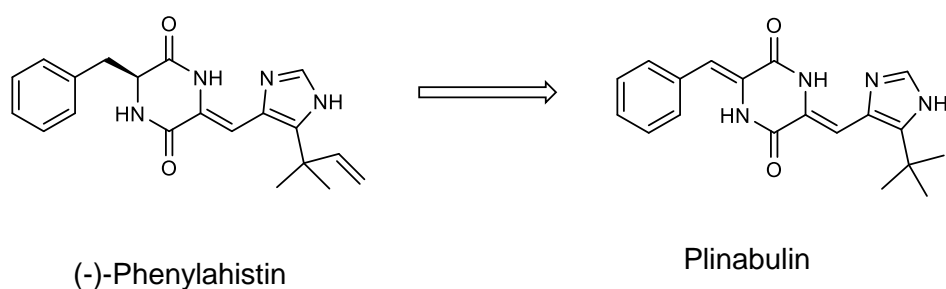
Fig. 1.5: Structures of (-)-phenylahistin (syn. halimide) and the semi-synthetic derivative plinabulin (syn. NPI-2358).

1.4 INTRODUCTION TO THE ENZYMATIC TARGETS AND THEIR ROLE IN HUMAN DISEASES

Cerebroside sulfotransferase:

Human cerebroside sulfotransferase (hCST) catalyzes the sulfonation of galactose residues of glycolipids. One of the major substrates is galactosyl ceramide, a glycosphingolipid, which is converted by hCST into sulfatide (see **fig. 1.6**) [72–74]. The enzyme is located in the membrane of the Golgi apparatus with the catalytic domain localized to the lumen. To date, neither the crystal structure of the hCST was published, nor is the exact catalytic mechanism known [72].

Arylsulfatase A (ASA or ARSA) is the physiological opponent of hCST, since it recycles sulfatide into cerebroside, thereby preventing the accumulation of sulfatide in healthy individuals [75]. Mutations in the gene, which codes for ASA, can lead to ASA deficiency and subsequently to increased concentrations of sulfatide in lysosomes of different cell types, especially in the central (CNS) and peripheral nervous system (PNS), where the myelin sheath is most affected. As a consequence, the accumulation of sulfatide leads to a degradation of the myelin sheath (´demyelination´) and to lesions of the white matter in the brain [76]. This observation led to the name for this disease - metachromatic leukodystrophy (MLD). It is a rare, autosomal recessive disorder [75,77]. Based on the lysosomal location of sulfatide accumulation, it is grouped into the lysosomal storage diseases. Symptoms mostly include neurological signs like seizures, paresis, movement disorders, speech disorders and a dramatically decreased expectancy of life. Patients often die during childhood.

While ASA deficiency is usually responsible for the development of MLD, in a few cases ASA activity seems to be normal. Instead, the putative cofactor of ASA is affected. This glycoprotein - saposin-B and its precursor prosaposin – stimulates ASA activity [78]. In rare cases, mutations in the gene coding for prosaposin (*psap*) lead to symptoms, which resemble those of the metachromatic leukodystrophy. The difference is that ASA activity is normal in those cases [79].
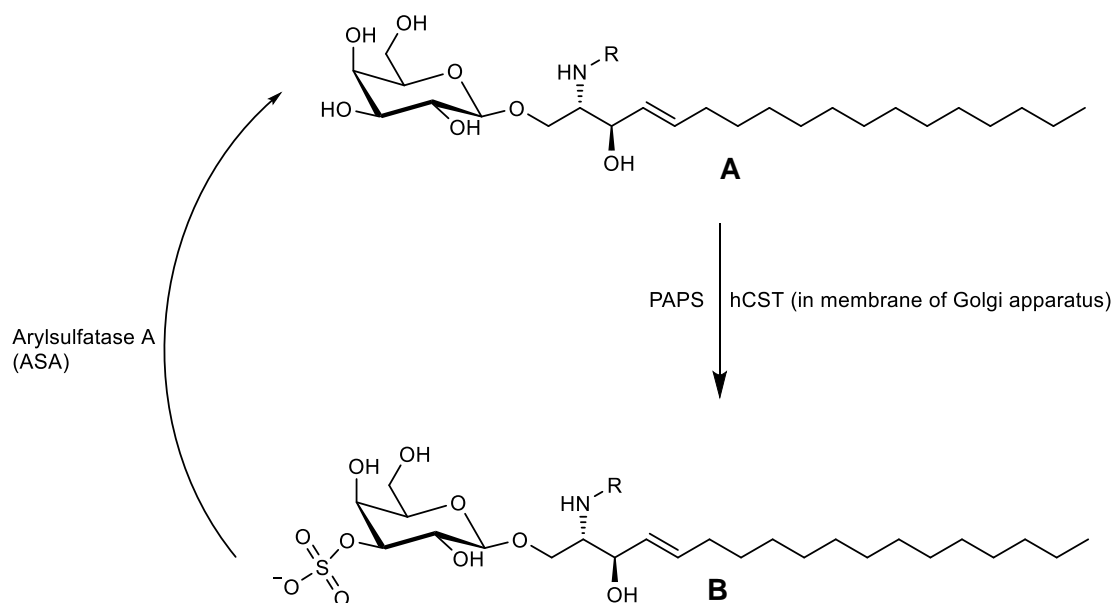
Fig. 1.6: Reaction scheme, showing the sulfonation reaction catalyzed by hCST and sulfatide breakdown by ASA [72,76].
R = fatty acyl substituent with different chain lengths.
A: Galactosyl ceramide ≡ cerebroside
B: Sulfatide
PAPS = 3´-Phosphoadenosine-5´-phosphosulfate
hCST = Cerebroside sulfotransferase

Currently, there is no causal therapy or cure available for MLD, regardless of whether ASA activity is affected or the activity of saposin-B [75]. Recent attempts to introduce new treatments include the intrathecal application of a recombinant human arylsulfatase A (enzyme replacement therapy, ERT) [80] or hematopoietic stem cell transplantation [81]. None of these methods was approved for clinical use, yet. A third approach would be substrate reduction therapy [72,82], which requires an inhibitor of hCST in order to prevent the accumulation of sulfatide. For other lysosomal storage diseases, this approach is already in clinical use: Miglustat (n-butyldeoxynojirimycin) was approved for use against Morbus Gaucher (type I) and Niemann-Pick disease (type C) [83], while migalastat (1-deoxygalactonojirimycin) was approved recently (in 2016) in the EU for use against Morbus Fabry [84,85]. The latter was isolated from the actinomycete *Streptomyces lydicus* [86]. However, no inhibitor of hCST was known at the beginning of this study [72]. But the last example shows that it is worth searching for lead structures against lysosomal storage diseases in microorganisms.

Cysteine and serine proteases:

Proteases can be found in every domain of life, including viruses [87]. More than 2% of the human genome consist of sequences coding for proteases or protease inhibitors, which points to their physiological importance [88]. Based on functionally important amino acids in their active site, they were subdivided into six broad subgroups, amongst them are cysteine- and serine-proteases. These subgroups are further subdivided into clans and families according to catalytic mechanism and ancestry [89]. A common trait of cysteine and serine proteases is that they employ a nucleophile – either a Cys or a Ser residue – to attack the carbonyl function of the substrate and thereby cleave the peptide bond.

Serine proteases make up more than one third of the known proteases. Most serine proteases are endoproteases, which are involved in blood coagulation, cell development, digestion [90]. They also contribute to inflammatory diseases, like lung emphysema [91]. In plants, serine proteases were proven to have important functions in defense against pathogens [92]. The active site is usually formed by a catalytic triad of Asp, His, Ser. The hydroxyl group of serine is deprotonated by a histidine residue and thereby activated. Asp has the role of stabilizing the protonated His residue [93]. This is especially true of chymotrypsin-like peptidases, of which some representatives were assayed for this study, *i.e.,* chymotrypsin, trypsin, neutrophil elastase (human leukocyte elastase, HLE). Chymotrypsin and trypsin are both part of the digestive system, where they break down proteins. Both are synthesized in the pancreas as proenzymes and activated later in the small intestine [94]. HLE is secreted by neutrophil granulocytes and is connected with degradation of pathogens under physiological conditions [95].

Like serine proteases, cysteine proteases are distributed among all domains of life [96]. The common property of cysteine proteases is a catalytic dyad, formed by a Cys and a His residue. Similar to serine proteases, the His residue deprotonates the thiol group of Cys, the resulting thiolate ion acts as a nucleophile on the carbonyl bond of the peptide substrate. Among the members of papain-like proteases (clan CA, according to the MEROPS-database [89]), which encompasses the cysteine cathepsins, Gln and Asn (or Asp) have supportive roles in the active site [97]. Papain-like proteases are distributed widely, *e.g.,* in plant latices, where they are supposed to play a role against herbivores [98]. In contrary, human cathepsins are predominantly located in the lysosomes [99]. Regarding the physiological and pathological relevance of serine and cysteine proteases, please refer to **table 1.1**.

In recent years, a few reports were published about inhibitors of cysteine and serine proteases from natural origin, especially against cathepsins B, L and K or HLE [100–105]. Among them are also fungal metabolites, like the anthraquinone chrysophanol isolated from

Penicillium citrinum, which is active against cathepsin B [101]. HLE inhibitory activity was found for a tetramic acid derivative (Sch210972) from a *Microdiplodia* sp. [106] and for two enantiomeric phthalimides from a *Stachylidium* sp. [107]. In both cases, activities are in a low micromolar range, underlining the high potential of natural products of fungal origin for novel drug leads.

Tab. 1.1: Main physiological functions and pathological relevance of the tested enzyme types.

Enzyme	Main physiological functions	Main pathological relevance
Trypsin	Proenzyme produced in pancreas, activation in small intestine; involved in digestion of food proteins	Pancreatitis through premature activation already in the pancreas [108]
Chymotrypsin		
HLE	Secretion by neutrophil granulocytes (degradation of pathogens)	COPD (chronic obstructive pulmonary disorder), rheumatoid arthritis [109,110]
Cathepsin B	In different cell types, involved in degradation of extracellular matrix (ECM)	Cancer [111,112]
Cathepsin L	In different cell types involved in protein turnover	Cancer and metastasis [113]
Cathepsin K	Mainly found in osteoclasts; responsible for resorption of non-mineral bone matrix	Osteoporosis [111]
Cathepsin S	Antigen presentation in antigen presenting cells; endothelial cells	Different chronic inflammatory diseases (rheumatoid arthritis, psoriasis, asthma,…), [114]; neuropathic pain [115]; psoriasis [116]

1.5   EXUDATION IN FUNGI AND ITS SIGNIFICANCE

Fungi in general follow an ´absorptive lifestyle´: They secrete enzymes in order to break down organic macromolecules and subsequently ingest the products. Additionally, small organic acids (*e.g.*, oxalic acid) and different siderophores are employed for the supply with inorganic nutrients (*e.g.*, trace metals and phosphate) [43,117]. Moreover, the buildup of the fungal cell wall depends on the vesicular secretion of chitinases and β-1,3-D-glucan synthases for the formation of cell wall components [118]. Thus it becomes evident that fungi rely heavily on different secretory mechanisms for their growth. By means of exudation or secretion of metabolites into their surrounding space, fungi also change their environment and may thereby control the community structure in the respective ecological niche [119]. For this purpose, fungi can either secrete primary metabolites, *e.g.,* trehalose, which can be used as substrate by certain bacteria [120]. Toxic secondary metabolites may, in turn, be used as defense weapons. Furthermore, secreted chemical signals may also induce symbiotic or parasitic relationships to plants or even humans [121]. *Cryptococcus neoformans*, a basidiomycete causing life-threatening infections in immunocompromised patients, releases virulence factors into the host tissue via exocytosis. The vesicles presumably pass the cell wall through preformed pores [122].

Since fungi produce a large number of highly bioactive metabolites, secretion can also serve as a detoxification mechanism for toxic metabolic end-products [123]. The secreted compounds can further act as virulence factors or defense substances. Such a dual role for secretion, *i.e.* for waste disposal and defense or host invasion, was shown for gliotoxin and aflatoxin [124,125].

Apart from exocytosis, two types of transporters are used for the secretion of specific secondary metabolites. MFS (major facilitator superfamily) transporters use the electrochemical gradient at the plasma membrane as the driving force. Their role was proven for the expulsion of cephalosporin and gliotoxin [124,126]. ABC (ATP-binding cassette) transporters hydrolyze ATP. They were proposed to carry out the secretion of penicillin in *Aspergillus nidulans* [127].

Guttation (Latin *gutta* = drop) is a special means for the exudation of solutes from the cell. It occurs widely in plants, bacteria and fungi, *i.e.,* Basidiomycota, Ascomycota and Mucoromycotina [128,129]. Originally, it was described for plants, which are able to exude liquid water actively onto the leave surface. Guttation droplets are commonly observed under conditions of high humidity, when the capacity of the transpiration-driven water flow

from the roots up to the leaves cannot be exploited sufficiently [130]. Among the Basidiomycota, guttation is also frequently observed in the wild on fruiting bodies, while in the Ascomycota guttation droplets in axenic culture have been used as taxonomic markers [131–133]. In contrary to plants, only little is known about the reasons for guttation and the underlying cellular structures in fungi [133]. Guttation droplets can be regarded as exudates, which form droplets on the mycelium due to the highly hydrophobic cell wall of the fungal hyphae [134]. These droplets were shown in a few cases to harbor reasonable amounts of primary (*e.g.*, carbohydrates, amino acids, enzymes) and secondary metabolites, both, in plants and in fungi [133,135,136].

Hypotheses on the role of guttation in fungi include the relevance for storage or disposal of primary and secondary metabolites. Fungi, especially at the hyphal tip, do not have extensive storage capacities such as plants, which usually form a large central vacuole [119]. Guttation droplets were also shown to exert antifeedant or antimicrobial activity and to mediate plant cell wall degradation [136–138]. Finally, a role in the growth of hyphae was proposed, specifically as a water reservoir to keep up the intracellular turgor [139]. These observations, together with the fact that guttation droplets can be analyzed without extensive processing, renders guttation droplets interesting subjects to assess their ecological significance and their usability during drug discovery projects.

2   AIM OF THE PRESENT STUDY

The main goal of the present study is to identify bioactive metabolites from marine-derived fungi, which could serve as lead structures for the development of medicinal drugs. For this purpose, two fungal strains, *Epicoccum nigrum* strain 749 and 800, were chosen based on preliminary screening results to be cultivated under different conditions in order to search for inhibitors of human cerebroside sulfotransferase as well as against serine- and cysteine proteases.

First, the two fungal strains are to be subjected to different substrates and cultivation conditions, in order to examine their ability to produce secondary metabolites. Besides the medium, abiotic factors like light and trace element supplementation are included in the fermentation experiments. The most promising cultivation conditions are then chosen for large scale fermentation.

In the next step, preparative analytical methods are employed for the fractionation of promising crude extracts and isolation of secondary metabolites, which will be characterized via different analytical techniques.

One of the known metabolites from polyketide origin – acetosellin – will be investigated regarding its biosynthesis through feeding of labeled precursors. Thus, its construction from two separate polyketide units shall be proven.

Second, the isolated secondary metabolites will be subjected to different pharmacological assays for the assessment of their biological effects with an emphasis on the aforementioned targets.

In the end, guttation droplets, which are formed by *E. nigrum* strain 749 under certain conditions, are to be examined for their content in secondary metabolites. The metabolic pattern will be compared between the guttation droplets and the fungal crude extracts. In this way, their applicability for drug discovery during the screening for bioactive metabolites shall be assessed. Therefore, a thorough qualitative and quantitative chemical examination will be carried out, taking into account the effect of different cultivation conditions on the constituent levels.

3   MATERIALS AND METHODS

3.1   THE FUNGAL STRAINS

During this study, two fungal strains of the species *Epicoccum nigrum* LINK were cultivated and studied for their chemical constituents:

Strain 749 was isolated from the surface of an unspecified green alga on water agar (WA, see below). The alga was collected at Cabrera (Spain).

Strain 800 was isolated as an endophyte from a *Fucus* sp. (Fucaceae, Phaeophyceae [≡ brown algae]) on chitin malt extract agar (CM, see below). The alga was collected at Büsum, Germany.

Collection of the algae, isolation of fungal strains and early examinations (see section 3.1.1) were carried out by Ekaterina Egereva (Institute of Pharmaceutical Biology, University of Bonn). For the isolation of fungal samples, following procedure was applied:

The algal samples were first sterilized with 70 vol% EtOH, then rinsed with sterile water and pressed onto sterile agar surfaces (control samples). Viable spores or hyphae on the surface of the alga were to be detected through incubation of these agar plates. The remaining sterilized algal samples were then cut into pieces and incubated on agar separately (´endophyte-revealing samples´). Mycelia growing out of the cut surface were deemed as endophytes. Mycelial mats, which were also observed on the control samples, were marked as ´non-endophytic´, *i.e.,* epibionts or contaminants. Promising fungal colonies were separately transferred onto new plates containing MES medium. The media, which were used during the isolation process are the following. Each isolation medium was supplemented with 250 mg/L benzylpenicillin (= penicillin G) and 250 mg/L streptomycin sulfate.

Water agar (WA): 15 g agar, 1 L ASW.

Glucose yeast agar (GYA): 15 g agar, 1 g glucose, 0.1 g yeast extract, 1 L ASW.

Chitin malt extract agar (CM): 15 g agar, 2 g chitin, 10 g malt extract, 1 L ASW.

Cellulose agar (CA): 15 g agar, 20 g cellulose, 1 L ASW.

3.1.1 EARLY EXAMINATION OF ISOLATED FUNGAL STRAINS

The isolated strains were subjected to medium scale fermentation on solid agar media. The resulting extracts were used for the investigation of promising chemical bioactivities. Following media were employed for the cultivation (see section 3.1.3 for media composition):

MEA (malt extract agar)

MES (malt extract agar with addition of artificial sea water)

3.1.2 IDENTIFICATION AND TAXONOMY

Microscopy was carried out using an Olympus BX51 microscope. Pictures were recorded with Cell^A 2.4 software (Cell^A Soft Imaging Systems GmbH, Münster).

3.1.2.1 MOLECULAR IDENTIFICATION

For the molecular identification of the two strains, the ITS (internal transcribed spacer) region was employed. ITS sequences are linker regions within the rDNA (ribosomal DNA), which codes for the ribosomal RNA (rRNA). Typically, high copy numbers of rDNA occur as tandem repeats on one DNA molecule. These repeats are connected by linker regions, which are divided into a NTS (non-transcribed spacer, harboring the promotor) and the ETS (external transcribed spacer). Transcription of rDNA is carried out by RNA-polymerase I in eukaryotes [140].

Each transcription unit consists of an external transcribed spacer (ETS), a small (SSU, 18S), a large (LSU, 28S) and a 5.8S subunit. The linker sequences – ITS1 and ITS2 – between these subunits are called ITS *sequences*, whereas the ITS1, 5.8S subunit and ITS2 taken together are referred to as ITS *region*. Due to the high variability and copy number, the ITS region is frequently used for the molecular identification of fungi and was proposed as a universal barcode marker [141,142].
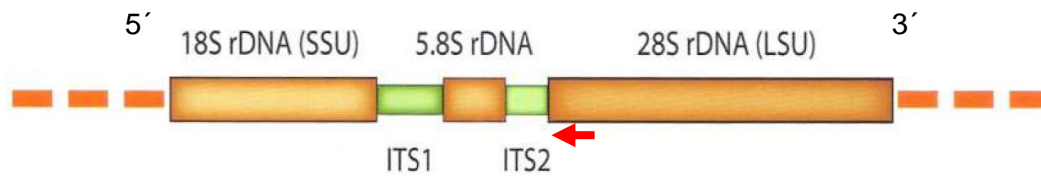
Fig. 3.1: Schematic drawing of the eukaryotic rDNA. The arrow represents the hybridization region of the ITS4 primer, with the head being the 3´-end. The interrupted orange lines stand for the NTS (non-transcribed spacer, including the promoters) and the ETS. SSU = Small subunit; LSU = Large subunit. (Picture modified from: Schmidt-Stohn, G.; Oertel, G. "DNA-Analysen in der Pilz-Taxonomie." Journal Des Journee Europeennes Du Cortinaire, 11 (2009): 10–19.)

During this study, the ITS4 primer, described by White et al. [143] was used. The primer was provided by Eurofins MWG Operon (Ebersberg, Germany):

Sequence (5´ → 3´):

TCCTCCGCTTATTGATATGC (T_M = 55.3°C, according to the manufacturer)

The identification process included following six steps:

1) For the extraction of fungal DNA, static liquid cultures, grown in 100 ml MEB (malt extract broth: 2g malt extract, 100 ml demineralized water) under artificial light for two weeks were chosen. At the end of the cultivation, the fungal biomass was separated from the liquid medium and dried in a freeze drier. The DNA was then extracted with the E.Z.N.A.® SP Fungal DNA Mini Kit (Omega Bio-tek, Norcross, USA).

2) Polymerase chain reaction: PCR was performed applying a T3-thermocycler. For PCR amplification of template DNA, PCR-buffers supplied with the GoTaq® Flexi DNA Polymerase were applied.

Tab. 3.1: PCR reaction mixture:

5x GoTaq® Flexi Buffer		10.0 µl
MgCl$_2$	(25 mM)	2.5 µl
dNTP	(each 10 mM)	1.0 µl
GoTaq-Polymerase	(5 unit/µl)	0.5 µl
Primer	(100 µM)	1.0 µl
DMSO		2.5 µl
Template		2.0 µl
H$_2$O (nuclease-free)		**ad 50.0 µl**

A modified version of the thermocycling sequence described in [143] was applied:

Tab. 3.2: Thermocycling sequence

	Step	**Temperature [°C]**	**Duration [s]**
	Initial denaturation	95	120
35 cycles of:	Denaturation	95	30
	Annealing	55	30
	Extension	72	60
	Final extension	72	600

3) After amplification, the fragments were separated through agarose gel electrophoresis and the bands with a size of ca. 450 – 600 bp were excised. Agarose gel electrophoresis was employed for the purification of the PCR products. Gels consisted of 1% peqGOLD Agarose in 1 x TBE buffer. Simple gels were usually run for 20 min at a voltage of 120 V in Life Technologies Horizon® 58 chambers. Nucleic acid probes were mixed with gel loading dye before loading them into the slots. DNA standards were applied to each gel for size estimation.

The gels were stained subsequently to the separation run. The dye bath contained 100 ml ethidium bromide solution (10 mg/ml), the gels were stained for 1-3 min, followed by a washing step in water for another 3-5 min. Bands containing nucleic acids were visualized in under UV light (254 nm).

Detected PCR fragments were directly cut out from the gel and purified using the Wizard® SV Gel and PCR Clean-up System (Promega, Mannheim, Germany), following the manufacturer's protocol.

4) DNA sequencing was carried out by GATC Biotech AG (Konstanz, Germany) using a 454 pyrosequencing method [144].

5) The obtained sequence data were checked for errors and edited using Geneious® Basic 5.6.7 (www.geneious.com, [145]), then analyzed with other sequences obtained in this lab and from Genbank [146], using the blastn suite of BLAST (Basic Local Alignment Search Tool; http://blast.ncbi.nlm.nih.gov/Blast.cgi; [147]).

6) The first four hits in the nucleotide search were used for phylogenetic analysis (for each strain), together with three further sequences of fungi (*Phoma exigua* strain PB5, *Phoma betae* strain 815, *Gliomastix murorum* strain 469), which were isolated before in our lab (see appendix for sequences or accession numbers). The two *Phoma* species were chosen for their close relationship (both belong to the order Pleosporales), whereas *Gliomastix murorum* is distantly related (order Hypocreales).

The evolutionary history was inferred by using the Maximum Likelihood method based on the Tamura-Nei model [148]. The tree with the highest log likelihood (-1237.5214) is shown. The percentage of trees in which the associated taxa clustered together is shown next to the branches. Initial tree(s) for the heuristic search were obtained automatically by applying Neighbor-Join and BioNJ algorithms to a matrix of pairwise distances estimated using the Maximum Composite Likelihood (MCL) approach, and then selecting the topology with superior log likelihood value. The tree is drawn to scale, with branch lengths measured in the number of substitutions per site. The analysis involved 12 nucleotide sequences. All positions with less than 95% site coverage were eliminated. That is, fewer than 5% alignment gaps, missing data, and ambiguous bases were allowed at any position. There were a total of 423 positions in the final dataset. Evolutionary analyses were conducted in MEGA6 [149].

3.1.3 CULTURE CONDITIONS AND MEDIA FOR LARGE SCALE FERMENTATION

In this section, the constituents for the media used in this study will be given. If nothing else is mentioned, all ingredients were added and mixed on a magnetic stirrer before autoclaving the media. Each preculture was prepared by cultivating the respective strain at 25°C in an incubation chamber in darkness. After autoclaving, either ca. 100 mL of the respective medium was poured into each petri dish (145 x 20 mm), or 250 mL were used in Fernbach flasks for large scale cultivation. Inoculation was carried out using 3 agar plugs of precultures per plate. After inoculation, the plates were sealed with parafilm and incubated at 26°C under constant artificial illumination (white light). Cultures grown in darkness were stored in the same room in a closed box.

Malt extract agar (MEA): 20 g malt extract, 16 g agar (Sigma-Aldrich), 1000 mL demineralized water.

> **MES (MEA + ASW):** 20 g malt extract, 16 g agar, 500 mL ASW stock solution, 500 mL demineralized water.
>
> **MEN (MEA + ASW + NaOAc):** 20 g malt extract, 16 g agar, 1 g NaOAc, 500 mL ASW stock solution, 500 mL demineralized water.
>
> **MPY (malt extract – peptone – yeast extract agar):** 20 g malt extract, 2.5 g peptone from animal tissue (Roth), 2.5 g yeast extract (Roth).

Czapek-Dox agar (CDA): 35 g Czapek-Dox broth, 16 g agar, 1000 mL demineralized water.

For the preparation of CDA and CDT, Difco Czapek-Dox broth was used. The constituents are as follows [g/L medium]:

Tab. 3.3: Constituents of Difco Czapek-Dox broth:

Compound	Amount [g]
Sucrose	30.0
$NaNO_3$	3.0
K_2HPO_4	1.0
$MgSO_4$	0.5
KCl	0.5

Czapek-Dox agar + TMS (CDT): 35 g Czapek-Dox broth, 16 g agar, 1 mL TMS stock solution, 1000 mL demineralized water.

Czapek-Dox agar + Cu^{2+} (CDA+Cu^{2+}): 35 g Czapek-Dox broth, 16 g agar, 1 mL CuSO$_4$ stock solution, 1000 mL demineralized water.

Czapek-Dox agar + Zn^{2+} (CDA+Zn^{2+}): 35 g Czapek-Dox broth, 16 g agar, 1 mL CuSO$_4$ stock solution, 1000 mL demineralized water.

Artificial seawater (ASW): Artificial seawater was prepared by dissolving defined salts in demineralized water. It was mixed as a stock solution in double concentration. Per Liter agar medium, 500 mL of ASW were added and filled up with 500 ml of demineralized water. The stock solution contains following salts:

Tab. 3.4: Constituents of artificial sea water (ASW) stock solution (per Liter demineralized water):

Constituent	amount [g]
KBr	0.2
NaCl	46.96
MgCl$_2$ x 6 H$_2$O	21.22
CaCl$_2$ x 2 H$_2$O	2.94
KCl	1.32
SrCl$_2$ x 6 H$_2$O	0.08
Na$_2$SO$_4$	7.84
NaHCO$_3$	0.38
H$_3$BO$_3$	0.06

Trace metal solution (TMS): According to Frisvad [20], 1 g ZnSO$_4$ x 7 H$_2$O and 0.5 g CuSO$_4$ x 5 H$_2$O were dissolved in 100 ml demineralized water. Of this solution 1 ml was taken for the preparation of 1 L CDT or any other TMS-supplemented medium. The final concentration in the medium was: c(Zn^{2+}) = 35 µM; c(Cu^{2+}) = 20 µM.

CuSO$_4$ stock solution: 0.5 g CuSO$_4$ x 5 H$_2$O was dissolved in 100 ml demineralized water. Of this solution 1 ml was taken for the preparation of 1 L Cu^{2+}-supplemented medium (CDA+Cu).

ZnSO$_4$ stock solution: 1 g ZnSO$_4$ x 7 H$_2$O was dissolved in 100 ml demineralized water. Of this solution 1 ml was taken for the preparation of 1 L Zn^{2+}-supplemented medium (CDA+Zn).

3.1.4 EXTRACTION OF THE CULTIVATED FUNGI

When nothing else is stated, the fermented cultures – containing mycelium and agar medium – were harvested after 4 weeks and minced using a blender. Aliquots were transferred to 1L round flasks and covered with 300 – 400 mL EtOAc. The saturated solution was decanted and exchanged for pure EtOAc. Decanting was carried out successively four times during two days, in order to exhaustively extract the secondary metabolites. The collected four aliquots were then unified, dried in a rotary evaporator to dryness and stored under -18°C.

3.1.5 CULTIVATION AND EXTRACTION CONDITIONS FOR THE ´TIME COURSE EXPERIMENTS´ AND ISOTOPIC LABELING

3.1.5.1 STRAIN 800 – TIME COURSE EXPERIMENT

To determine the optimal cultivation time for the labeling experiment with sodium [1-^{13}C]acetate, a large scale culture of *Epicoccum nigrum* strain 800 on MEN (6.25 L, divided into 25 Fernbach flasks; continuous illumination with artificial white light; 26 °C) was prepared and divided into five equal parts. Extraction was carried out in time intervals of 1 week, starting at week 1 and ending at week 5.

For each time point, five cultures, equal in size (total volume of medium: 1.25 L), were extracted three times with ca. 400 mL EtOAc, a sufficient amount to cover the agar pieces. The solvent was evaporated at 40 °C, using a rotary evaporator. For the yields of extracts see **fig. 3.2**.

800-1W	800-2W	800-3W	800-4W	800-5W
1 week	2 weeks	3 weeks	4 weeks	5 weeks
95.1 mg	285.3 mg	282.7 mg	159.5 mg	111.4 mg
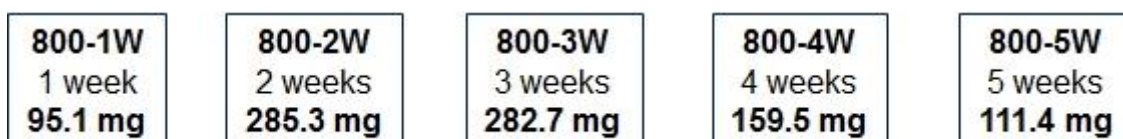
Fig. 3.2: Yields for the extractions of the time cultures of *E. nigrum* strain 800.

3.1.5.2   STRAIN 749 – ISOTOPIC LABELING EXPERIMENT

Since *E. nigrum* strain 749, grown on CDA, proved to be a superior production system than strain 800 on MES, labeling cultures were prepared using following protocol:

Strain 749 was cultivated for 3 weeks on 500 mL of CDA under continuous illumination with artificial white light at 26 °C.

A solution was prepared containing 55.6 mg/mL sodium[1-^{13}C,99%]acetate (Cambridge Isotope Laboratories Inc.) in demineralized H_2O.

3 mL of this solution were added to each Fernbach flask during the cultivation period on days 4, 7 and 10, respectively. The solution was spread evenly on the agar surface in order to enable every part of the mycelium to get in contact to the labeled precursor. The total amount of added precursor was 500 mg sodium[1-^{13}C,99%]acetate per flask, which equals a concentration of 2 g/L medium.

After 21 days, the labeling culture underwent the same extraction procedure as described in **section 3.1.5.1**, yielding 111 mg of crude extract (´749-13C-EtOAc´).

3.2   CHROMATOGRAPHY

3.2.1   SIZE EXCLUSION CHROMATOGRAPHY (SEC)

The sorbent used for SEC was Sephadex® LH-20 (Sigma Aldrich), pure MeOH served as the mobile phase. The stationary phase was swollen overnight in the eluent prior to packing of the column. The column was packed with the sorbent being suspended in the eluent. The flow was set to ca. 2-4 drops/second.

3.2.2.   VACUUM LIQUID CHROMATOGRAPHY (VLC)

Separations were performed using either silica gel 60 (0.063-0.2 mm, Merck), silica gel 60M (0.04-0.063 mm, Macherey-Nagel) or Polygoprep 60 C_{18} (0.05 mm, Macherey-Nagel). Columns were packed under vacuum with the sorbent being suspended in the eluent, using

PE or dichloromethane for normal-phase, and MeOH for RP separations. Each column was equilibrated prior to the separation with the first designated eluent. Vacuum was applied using a water-jet vacuum pump.

3.2.3. SOLID PHASE EXTRACTION (SPE)

For solid phase extraction, a Bakerbond C_{18} column (2000 mg/6ml; column A) or Bakerbond C_{18} (1000 mg/3 ml, column B) was used. Separations were performed using a water-jet vacuum pump. Columns were equilibrated with the first designated eluent.

3.2.4. FLASH CHROMATOGRAPHY (FC)

A Reveleris X2 Flash Chromatography System with UV-detector and ELSD was used. Software: Navigator. For the introduction of samples, either a 3 g- or a 12 g-solid loader was used. Packing of the solid loaders was achieved through adsorption of the sample onto silica gel 60 (0.063–0.200 mm, Merck) or Polygoprep 60 C_{18} (0.05 mm, Macherey-Nagel), respectively. The dried material was then filled into the solid loader. Reveleris® flash cartridges, prefilled either with 4 g or 12 g of silica or C_{18}-silica, were used (with 40 µm particle size).

3.2.5. HIGH PERFORMANCE LIQUID CHROMATOGRAPHY (HPLC)

Following systems were used:

System A: Waters 1525µ binary pump with Waters 2998 diode array detector (DAD). Software: Breeze 2 (© 2008 Waters Co.).

System B: Waters HPLC system equipped with a 2695 separations module, a 996 DAD and QuickStart Empower 2 software (© 2005 Waters Co.).

System C: HPLC system composed of a Waters 515 pump with a Knauer K-2300 differential refractometer.

System D: Merck-Hitachi system equipped with an L-6200A pump, an L-4500A photodiode array detector and a D-6000 interface.

Columns:

Column A: Macherey-Nagel Nucleodur C_{18} ec (250 x 8 mm, 5 μm).

Column B: Kinetex C_{18} column (Phenomenex, 250 mm x 4.6 mm, 5 μm).

Column C: Kinetex PFP column (Phenomenex, 250 mm x 4.6 mm, 5 μm).

Column D: Macherey-Nagel Nucleoshell RP_{18} plus column (250 mm x 4.6 mm, 5 μm).

Column E: Atlantis T3 RP_{18} column (250 x 4.6 mm, 5 μm).

Column F: Phenomenex Aqua C_{18} (250 x 4.6 mm, 5 μm, 125 Å).

Column G: YMC-Triart C_{18} (250 x 4.6 mm, 5 μm).

Column H: Macherey-Nagel Nucleodur PFP (250 mm x 4.6 mm, 5 μm).

3.2.6   ISOLATION PROTOCOLS

3.2.6.1   ISOLATION OF EPIPYRONES (**1**-**3**), EPICOCCONE (**11**) AND 1F4-1-6 (**12**)

E. nigrum strain 749 was cultivated under continuous illumination for 5 weeks on 7 L of MES medium, distributed among 28 Fernbach flasks. The collected medium and mycelium were extracted together five times successively, using EtOAc, yielding 2.66 g of crude extract. VLC on NP (70 g of silica gel 60, 0.063-0.2 mm, Merck) was employed for the first separation step. The step gradient involved the use of DCM, acetone, MeOH (DCM/acetone/MeOH, 90:10:0 → 90:10:0 → 70:30:0 → 50:50:0 → 30:70:0 → 0:100:0 → 0:70:30 → 0:50:50 → 0:30:70 → 0:0:100 → 0:0:100; 100 ml for each step), yielding eleven fractions. The polar fractions 6-11 were pooled (= 1F12) for further fractionation, since they showed strong signals for epipyrones (**1**-**3**) in the LC-MS. Fraction 1F12 was then subjected to SEC (see **section 3.2.1**) with 250 g of Sephadex® LH-20. Fractions were taken with a volume of 50 mL, the total number of fractions being 39. Fractions 12-18 showed strong signals for epipyrones (**1**-**3**) in the LC-MS. Therefore, they were again pooled and purified employing RP-VLC (column packed with 100 g of Polygoprep 60 C_{18} silica gel) and isocratic elution with MeOH/water(0.2% TFA) 80:20. The volume of each fraction was ca. 150 mL (fractions 1-10)

or ca. 250 mL (fractions 11-16). Fraction 5 proved to be purified epipyrones (**1-3**; 79 mg, 11.3 mg/L), while fractions 4, 6, 7, 8, 9 also contained epipyrones (**1-3**) in a semi-pure form. Fraction 5 was used throughout this work for bioactivity testing.

The aforementioned fractions from the NP-VLC separation were also employed for the isolation of further compounds:

Compound **12** was isolated from VLC-fraction 4 via successive use of RP-SPE on C_{18}-silica gel (MeOH/H_2O 50:50 → 100:0 in 10 steps; column A; 30 mL per fraction). SPE-fraction number 1 was purified employing HPLC (system C, column A, MeOH/water 60:40, 1.5 mL/min), with compound **12** eluting after 16 min (m = 2.4 mg).

Epicoccone (**11**) was isolated from VLC-fraction 5 via successive use of RP-SPE (column A, MeOH/water 60:40; 50 mL per fraction, 7 steps), fraction 1 was again subjected to RP-SPE (column B; MeOH/water 10:90; 30 mL per fraction, 4 steps) and fraction 1 of the latter fractionation was purified by HPLC system B [column F, ACN/water 5:95 (t = 0-15 min), 5:95 → 10:90 (t = 15-30 min), 10:90 → 80:20 (t = 30-40 min)], with epicoccone (**11**, 2.7 mg) eluting after 26 min (8% ACN).

3.2.6.2 ISOLATION OF ACETOSELLIN (**4**)

The crude extract of *E. nigrum* strain 749 (m = 576 mg), grown on Czapek-Dox agar (CDA) under continuous illumination for four weeks, was first defatted using liquid-liquid extraction. For this purpose, the sample was dissolved in 100 ml MeOH/water (80:20) and successively shaken three times with 100 ml petrol ether in a separation funnel. The defatted fraction (321 mg) was subjected to flash chromatography (see **fig. 4.13**). For this procedure, the sample was dissolved in MeOH and adsorbed onto 3.5 g C_{18} silica gel (Polygoprep 60 C_{18}, 50 µm, Macherey-Nagel) using a solid loader. Separation was carried out using a C_{18} column (40 µm particle size, 12 g). For the mobile phase MeOH (solvent A) was used in combination with 0.1% aqueous TFA (solvent B). A step gradient with a constant flow of 30 mL/min was applied starting at 20% solvent A (t = 0-5 min), rising up to 100% solvent A (t = 5-17 min), finishing the run with 100% solvent A (t = 17-22 min). The separation process was observed using ELSD and UV-detection (220 nm, 254 nm, 340 nm). Acetosellin (**4**) eluted after 14 min (80% solvent A). In fraction 6, an oxidation product of acetosellin (**4**) in a semi-pure form was detected, 5′,6′-dihydroxyacetosellin (**7**, t_R ≈ 10 min, 6 mg). Epipyrones (**1-3**) were found to be a minor constituent eluting at ca. 95% solvent A (t_R ≈ 16.5 min).

3.2.6.3   ISOLATION OF ^{13}C-LABELED ACETOSELLIN (**4**)

In order to purify the ^{13}C-enriched acetosellin (**4**), the crude extract was subjected to RP Flash chromatography (30 mL/min, Reveleris® C$_{18}$ column, 4 g, particle size 40 µm), starting with H$_2$O:MeOH 80:20 (min 0-5) and then switching to gradient elution (MeOH 20 % $\rightarrow$ 100 %, min 5-15), ending up with 34.5 mg of semi-pure compound (t$_R$ = 12 min, 70% MeOH).

3.2.6.4   FRACTIONATION OF CRUDE EXTRACT FROM ´TIME COURSE CULTURES´ OF STRAIN 800

The five ´time course´ cultures (for cultivation details see **section 3.1.5.1**) were pooled, resulting in 934 mg of crude extract (800Z-total). The extract was then defatted using liquid-liquid extraction (n-hexane/MeOH:H$_2$O [90:10]). This resulted in 509 mg of defatted crude extract (800Z).The defatted crude extract 800Z was subjected to fractionation via RP flash chromatography (FC, flow: 30 mL/min, column: Reveleris® C$_{18}$-silica, 12 g, 40 µm), starting with H$_2$O:MeOH 80:20 (min 0-7) and then switching to linear gradient elution (MeOH 20 % $\rightarrow$ 100 % min 7-15; t = 15-20 min: 100% MeOH). Ten fractions were obtained.

The so obtained fractions were further separated using HPLC system B (see **section 3.2.5**). FC-Fraction 4 (eluting after 10.5 min) was separated with RP-HPLC (H$_2$O:ACN 80:20; column D; flow: 0.7 mL/min), fraction 1 giving purified (3*R*,4*S*)-4-hydroxymellein (**10**, 2.0 mg). The same compound was isolated from fraction 5 of flash chromatography by HPLC (H$_2$O:ACN 76:24, column E, 0.7 mL/min).

FC-Fraction 7 (eluting after 14 min) was separated with RP-HPLC (H$_2$O:ACN 70:30, column D, 1.0 mL/min) into 7 fractions (F7-1 – F7-7), of which fraction 6 proved to be the new compound epicaronic acid (**13**, 2.7 mg).

FC-Fraction 8 (eluting after 15 min) was separated with RP-HPLC (H$_2$O:ACN 62:38, column D, 1.0 mL/min) into 8 fractions, of which fraction 5 yielded tricinonoic acid (**14**, 1.5 mg).

3.2.6.5 ISOLATION OF EPICOCCOLIDE B (**9**), FLAZIN (**15**) AND EPICARONIC ACID (**13**) FROM STRAIN 800

Two cultures of *E. nigrum* strain 800 were used:

1) The first culture was prepared on 10 L of MEN medium and fermented for four weeks. Extraction with EtOAc afforded 1.35 g of crude extract (see **section 3.1.4** for the protocol), which was subjected to NP VLC on silica gel (200 g silica gel 60M, 0.04-0.063 mm, Macherey-Nagel) with a step gradient (n-hexane-EtOAc-MeOH: 100:0:0 → 80:20:0 → 60:40:0 → 40:60:0 → 20:80:0 → 0:100:0 → 0:80:20 → 0:60:40 → 0:40:60 → 0:20:80 → 0:0:100 → 0:0:100, each step 200 ml), yielding 12 fractions. Fractions 6-12 (fraction 6 eluted with 100% EtOAc, fraction 12 eluted with 100% MeOH) were pooled to give 608 mg. This crude material was separated via RP-VLC (using 50 g of Polygoprep 60 C_{18}, 0.05 mm, Macherey-Nagel) with following step gradient: MeOH/aqueous TFA (0.1%) 40:60 → 100:0 (8 steps with 200 mL, respectively). Fractions 4 and 5, eluting at 70-80% MeOH, were again pooled (m = 177 mg) and subjected to SEC (packed with 25 g of Sephadex LH-20), employing 100% MeOH as eluent.

   Eight fractions were obtained, fraction 4, eluting as a red solution, was purified on HPLC system D with column G (see section 3.2.5 for details) with a flow of 0.9 mL/min and a gradient of MeOH/water 60:40 (t = 0-23 min) → 75:25 (t = 24-50 min). Fraction 4 of this HPLC-separation, eluting after 24 min, proved to be epicaronic acid (**13**, 2.2 mg), which was also found in another extract of *E. nigrum* strain 800 (see **section 3.2.6.4**).

   Fraction 6 of the separation using size exclusion chromatography, eluting as a yellow solution, was purified on HPLC system D with column G. A gradient was used with a flow of 0.9 mL/min, starting with MeOH/water 60:40 (t = 0 → t = 30 min), ending up with 100% MeOH (t = 31-60 min). From this HPLC-separation, fraction 2 proved to be flazin (**15**, t_R = 25 min; 1.2 mg).

2) The next culture of *E. nigrum* strain 800 was grown on 500 mL of malt extract agar with trace metal solution in darkness, yielding 0.2 g of crude extract through extraction with EtOAc (see **section 3.1.4**). This extract was subjected to NP FC (15 mL/min, Reveleris® flash cartridge, with 4 g of silica, 40 µm particle size), using a linear gradient starting with petrol ether (t = 0 min: 80%, t = 5 min: 0%), with increasing amounts of EtOAc (t = 0 min: 20% → t = 5-8 min: 100%) and MeOH (t = 8

min: 0% → t = 16-18 min: 100%). Fraction 2, eluting at = 3.5-7 min, was purified on HPLC system A with column D, a following gradient was applied: ACN/water 20:80 (t = 0-10 min) → 30:70 (t = 12-21 min) → 100% MeOH (t = 22-26 min), the flow was set to 1.0 mL/min. Epicoccolide B (**9**, 1.3 mg) eluted after 20 min with 30% ACN.

This compound was later again isolated, in order to get a larger amount of substance. For this purpose, four exploratory crude extracts from *E. nigrum* strain 800 were pooled to give a total mass of 0.4 g (see **section 3.1.3** for media composition):

- 800 MES (grown under continuous illumination)
- 800 MEA+TMS (grown in darkness)
- 800 MEA+TMS (grown under continuous illumination)
- 800 MES+TMS (grown under continuous illumination)

Fractionation was achieved through successive use of RP FC(flow: 30 mL/min, column: Reveleris® C_{18}-silica, 12 g, 40 μm, ACN/water 10:90 → 80:20 and HPLC with ACN/water (system A, column B, gradient: t = 0-4 min: 20:80 → t = 5-16 min: 30:70 → t = 17-20 min: 100:0, 1.0 mL/min), with compound **9** eluting after 14.5 min (m = 4.8 mg).

3.3   STRUCTURE ELUCIDATION

3.3.1.   NMR

All NMR spectra were recorded in acetone-d_6, methanol-d_4, or in DMSO-d_6 using either a Bruker Avance 300 DPX spectrometer operating at 300 MHz (^{1}H) and 75 MHz (^{13}C), a Bruker Avance 500 DRX spectrometer operating at 500 MHz (^{1}H) and 125 MHz (^{13}C) and a Bruker Ascend 600 spectrometer operating at 600 MHz (^{1}H) and 150 MHz (^{13}C). Spectra were referenced to residual solvent signals with resonances at $\delta_{H/C}$ 2.04/29.8 (acetone-d_6), $\delta_{H/C}$ 3.35/49.0 (methanol-d_4) and $\delta_{H/C}$ 2.50/39.51 (DMSO-d_6) respectively. Spectra were processed using Bruker XWIN-NMR version 3.5 software and Mestrenova version 8.0.1-10878 (Mestrelab Research S.L.). ChemSketch version 11.02 (ACD/Labs 2012) was used to compare characteristic chemical shifts of isolated compounds to calculated values. The following NMR experiments were performed: ^{1}H-NMR, ^{13}C-NMR, DEPT-135, COSY, ^{1}H-^{13}C-HSQC, ^{1}H-^{13}C-HMBC and ^{1}H-^{1}H-ROESY, ^{1}H-^{1}H-NOESY.

3.3.2.   MASS SPECTROMETRY

Mass spectrometry was performed on the following four systems:

1) LC-ESI-MS using an HPLC coupled to a quadropole analyzer (system A)

LC-ESI-MS measurements were conducted by E. Eguereva (Institute for Pharmaceutical Biology, University of Bonn). The samples were diluted with MeOH to a concentration of 1 mg/mL and were analyzed using an Agilent 1100 system including a diode array detector (DAD) and an API 2000 Triple Quadrupole LC/MS/MS with ESI source (Applied Biosystems/MDS Sciex, Analyst Software). An RP-18 column (Macherey-Nagel Nucleodur 100, 125 x 2mm, 5 µm) served as stationary phase. Gradient elution was used with following parameters: It started at MeOH/H_2O (10:90) and was ramped up to 100% MeOH in 20 min, followed by isocratic elution with 100% MeOH for 10 min, NH_4OAc was added as a buffer (c = 2 mM); flow rate: 0.25 mL/min. Experiments were recorded only in positive mode using a declustering potential of either 30 V (experiment 1) or 70 V (experiment 2).

2) LC-MS using a UPLC system coupled to an Orbitrap (system B)

Spectra were recorded by Dr. Marc Sylvester (Institute for Biochemistry and Molecular Biology, University of Bonn). The dried samples were dissolved in 50 µl water per vial. 2µl of this solution were then diluted in an Eppendorf vial using 18 µl of 0.1% formic acid. The resulting solution was centrifuged for several minutes at 12,000 g to separate precipitates.

2 µl (≡ 0.4% of the original sample) were injected onto a C_{18} trap column (20 mm length, 100 µm inner diameter) coupled to a C_{18} analytical column (200 mm length, 75 µm inner diameter), made in house with 1.9 µm ReproSil-Pur 120 C_{18}-AQ particles (Dr. Maisch, Ammerbuch, Germany). Solvent A was 0.1% formic acid. Analytes were separated during a linear gradient from 1% to 35% solvent B (90% ACN, 0.1% formic acid) within 40 min and 35% to 50% B within 7 min at a flow rate of 320 nL/min.

The nanoHPLC was coupled online to an LTQ Orbitrap Velos mass spectrometer using a nanoESI ion source (Thermo Fisher Scientific, Bremen, Germany). Precursor ions between 180 and 700 *m/z* were scanned in the Orbitrap detector with a resolution of 30,000 (maximum fill time 400 ms, AGC target 10^6, lock mass 445.12003 Da). The 10 most intense precursor ions (threshold intensity 5000) were subjected to collision induced dissociation and

fragments also analyzed in the linear ion trap. Fragmented ions were excluded from repeat analysis for 15 s.

3) LC-MS using a UPLC System coupled to Qq-TOF with ESI-source (system C)

Spectra were recorded by Dr. Max Crüsemann (Institute of Pharmaceutical Biology, University of Bonn). A micrOTOF-Q mass spectrometer (Bruker) with ESI-source coupled to a HPLC Dionex Ultimate 3000 (Thermo Scientific) and a EC10/2 Nucleoshell C_{18} 2.7 µm column (Macherey-Nagel) was used. The column temperature was set to 25°C.

MS data were acquired over a range from 100-3000 *m/z* in positive mode. Auto MS/MS fragmentation was achieved with rising collision energy (35-50 keV over a gradient from 500-2000 *m/z*) with a frequency of 4 Hz for all ions over a threshold of 100.

HPLC started with 90 % H_2O containing 0.1% HOAc. The gradient starts after 1 min ending up with 100% Acetonitrile (0.1% acetic acid) in 20 min. The flow was set to 0.3 mL/min. 5 µL per sample solution (1mg/mL) was injected for each run.

4) High resolution ESI-MS (system D)

Dr. M. Engeser (Kekulé Institute of Organic Chemistry and Biochemistry, University of Bonn) conducted HR-ESI-MS measurements on a Bruker Daltonik (Bremen) micrOTOF-Q Time-Of-Flight mass spectrometer for exact mass determination of purified compounds.

3.3.3. UV-SPECTROSCOPY

UV spectra were obtained using a Perkin Elmer Lambda 40 UV/Vis spectrometer with UV WinLab Version 2.80.03 software, using 1.0 cm quartz cell. The molar absorption coefficient ε was determined in accordance with the Lambert-Beer-Law:

$$A = \varepsilon \bullet c \bullet b \leftrightarrow \varepsilon = A/(c \bullet b)$$

ε: molar absorption coefficient [L·mol^{-1}·cm^{-1}]; *A*: absorption at peak maximum; *c*: concentration [mol/L]; *b*: layer thickness of solution [cm]

3.3.4 CD-SPECTROSCOPY

CD spectra were recorded in MeOH at room temperature using a JASCO J-810-150S spectropolarimeter. The CD (circular dichroism) is measured as ellipticity Θ (in mdeg, millidegrees) and subsequently converted into the molar ellipticity $[\Theta]_M$ and finally into $\Delta\varepsilon$ in accordance to the following equation:

$$[\theta]_M = \theta \cdot M / 10 \cdot C \cdot d$$

$[\Theta]_M$ = molar ellipticity [degrees $\cdot$ cm^2/dmol]; θ = ellipticity [degrees]; M_r = molecular weight (g/mol); C = concentration (mg/ml); D = path length (0.1 cm)

Results presented as $\Delta\varepsilon = [\theta]_M / 3300$

3.3.5 IR-SPECTROSCOPY

IR spectra were recorded as film, using a Perkin-Elmer FT-IR Spectrum BX spectrometer. Analysis and reporting were performed with Spectrum v3.01 software.

3.3.6 OPTICAL ROTATION

Optical rotation was measured on a Jasco DIP 140 polarimeter (1 dm, 1 cm^3 cell) operating at wavelength λ=589 nm corresponding to the sodium D line at room temperature. Specific optical rotation $[\alpha]_D^T$ was calculated using following equation:

$$[\alpha]_D^T = \frac{100 \bullet \alpha}{c \bullet l}$$

T = temperature [°C]; D = sodium D line at λ = 589 nm; c = concentration [g/100 ml]; l = cell length [dm]; $α$ = optical rotation

Compounds were dissolved in methanol and the average optical rotation α was calculated based on 5 measurements.

3.4 CHEMICAL DERIVATIZATION

Acetylation of epipyrones (1-3)

For the first attempt, 26 mg ($\equiv$ 4.1825·10^{-5} mol) of epipyrones (**1-3**) were dissolved in 1 mL pyridine and the reaction started with an excess of Ac$_2$O (60 µL). The mixture was stirred at room temperature for 2.5 h under inert gas (argon). TLC was used to monitor the reaction process [C$_{18}$-silica, MeOH/water(TFA 0.1%) 85:15]. The reaction was stopped by adding 300 µL water and evaporating the solvent in a rotary evaporator to yield 34.5 mg of crude product. The crude product was purified in two successive steps using column A on HPLC system B (step 1) or column D and HPLC system A (step 2): For step 1, a gradient with MeOH/water (TFA 0.1%) with a constant flow of 1.5 mL/min was used: t=0 min: 80% MeOH; t=5 min: 85% MeOH; t=20 min: 87% MeOH; t=30 min: 87% MeOH; t=40 min: 95% MeOH. Fraction 5, eluting after 22 min, showed the strongest signals in ^{1}H-NMR and thus was used for purification in step 2 with following gradient (MeOH/water (0.1% TFA)): t=0 min: 75% MeOH; t=3 min: 75% MeOH; t=10 min: 80% MeOH; t=20 min: 80% MeOH; t=21 min: 100% MeOH; t=27 min: 100% MeOH. Peak 4 (compound **6**, 1.4 mg; 5.4% yield) was the main product and was subsequently used for structure elucidation and bioactivity testing.

For the second acetylation approach, the reaction time and amount of Ac$_2$O was increased in order to get the tetraacetate as the main product:

29 mg ($\equiv$ 4.71677·10^{-5} mol) of epipyrones (**1-3**) were dissolved in 1.3 mL pyridine and the reaction started with the addition of 134 µL Ac$_2$O. The reaction was again monitored via TLC [silica gel, DCM/acetone/MeOH (0.1% TFA) 80:15:5]. The reaction was stopped after 48 h by the addition of 5 mL water under cooling with iced water. The solution was extracted seven times successively with 1.5 mL DCM. The pooled DCM phases were washed once with NaHCO$_3$-solution in water (39 mg/mL), then twice with 3 mL water. The organic phase was then evaporated to dryness in the rotary evaporator to yield 39 mg of crude product. Purification was carried out on HPLC system B with column G, using isocratic elution with 78% MeOH/22%water (0.1% TFA) and a constant flow of 1.5 mL/min. Compound **5** eluted after 18 min (compound **5**, 11.8 mg; 40.7% yield).

3.5 EVALUATION OF THE BIOLOGICAL ACTIVITY

3.5.1 CELL VIABILITY ASSAYS

3.5.1.1 RESAZURIN-BASED ASSAY WITH HEK293-CELLS

This assay was carried out by Nicole Merten (working group of Prof. Kostenis, Institute for Pharmaceutical Biology, University of Bonn). Cell viability was assessed using a fluorimetric detection of resorufin (CellTiter-Blue Cell Viability Assay, Promega; see **fig. 3.3**). HEK293 cells were seeded at a density of 25,000 cells per well into black 96-well poly-D-lysine–coated plates with clear bottom. 3h after seeding cells were treated with 0.3% dimethyl sulfoxide (DMSO) or compound dissolved in medium for 24h. To detect cell viability, CellTiter-Blue reagent was added and cells were incubated for 1h at 37°C according to the manufacturer's instructions. Fluorescence (excitation 560nm, emission 590nm) was measured using a FlexStation 3 Benchtop Multimode Plate Reader and data were expressed as percentage of cell viability relative to DMSO control (The cytotoxic anticancer drug etoposide was used as a positive control.).
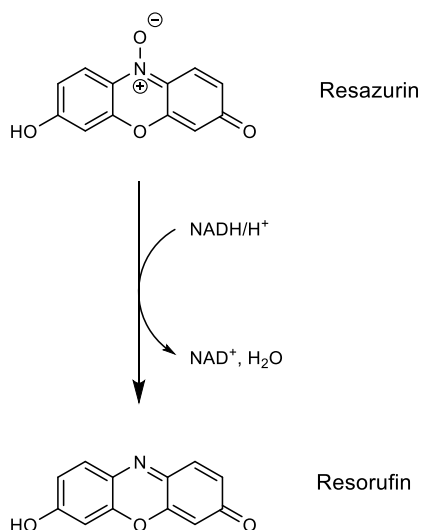

Fig. 3.3: Reaction scheme showing the reduction of resazurin by mitochondrial oxidoreductases. Resazurin itself is only weakly fluorescent, while resorufin shows strong emission at wavelengths above 550 nm upon exposure to green light [150,151].

3.5.1.2　　　　MTT-ASSAY

This colorimetric assay was used to assess the effect of epipyrones (**1**-**3**) on viability of different cell lines according to Zapol´skii et al. [152]. In living cells, MTT [3-(4,5-dimethylthiazol-2-yl)-2,5-diphenyltetrazolium bromide] is reduced by reductases to yield purple formazan. This color change is used as an indicator of cell viability.

The assay was performed by Galina Sergeev in the working group of Prof. Sasse (Helmholtz-Zentrum für Infektionsforschung, Braunschweig). Epipyrones (**1**-**3**) were applied in serial dilutions in MeOH, with a maximum concentration of 60.4 µM. Metabolic activity was determined after 24 h in order to assess acute cytotoxicity with following cell line:

FS4-LTM (immortalized human fibroblasts)

Three additional cell lines were assessed for cell proliferation, using the above mentioned assay. Metabolic activity was determined after 120 h (5 days): L929 (immortalized murine fibroblasts), KB-3-1 (human cervical cancer), MCF-7 (human breast cancer).

3.5.2　　　　ANTIMICROBIAL ACTIVITIES

3.5.2.1　　　　INHIBITION OF BACTERIA AND YEASTS

Agar diffusion assays were provided by Michaele Josten (working group Prof. Schneider, Institute of Pharmaceutical Microbiology, University of Bonn). The following protocol was applied as published before [153].

Culture plates (5% sheep blood Columbia agar, BD) were overlaid with 3 mL Tryptic soy soft agar, inoculated with TSB (Tryptic soy broth, Oxoid) growth suspension of the bacteria to be tested. Compounds were diluted to a concentration of 1mg/mL with DMSO and 3 µL of this dilution were placed on the surface of the agar. Compounds diffused into the agar and the size of the inhibition zone was measured after 24 hours incubation at 37 °C.

Tab. 3.5: Bacterial and yeast strains used to assess antimicrobial activity:

	Strain	No.
1	MSSA	5185
2	MSSA	I-11574
3	MRSA	LT-1334
4	MRSA	LT-1338
5	MRSE	LT-1324
6	*Candida albicans*	I-11301
7	*Candida albicans*	I-11134
8	*Citrobacter freundii*	I-11090
9	*Klebsiella pneumoniae* subsp. *ozeanae*	I-10910
10	*Enterococcus faecium*	I-11305b
11	*Enterococcus faecium*	I-11054
12	*Escherichia coli*	I-11276b
13	*Escherichia coli*	O-19592
14	*Stenotrophomonas maltophilia*	O-16451
15	*Stenotrophomonas maltophilia*	I-10717
17	*Pseudomonas aeruginosa*	I-10968
18	KNS	I-10925
19	*Staphylococcus simulans*	22
20	*Micrococcus luteus*	ATCC 4698
21	*Mycobacterium smegmatis*	ATCC 70084
22	*Bacillus subtilis*	168
23	*Bacillus megaterium*	ATCC 13632
24	*Arthrobacter crystallopoietes*	DSM 20117
25	*Listeria welchimeri*	DSM 20650
26	Bacillus cereus	
28	Corynebacterium xerosis	Va167198
29	Staphylococcus aureus	
30	Staphylococcus aureus	133

MSSA = methicillin-sensitive *Staphylococcus aureus*
MRSA = methicillin-resistant *S. aureus*
MRSE = methicillin-resistant *S. epidermidis*
KNS = coagulase-negative *Staphylococci*

3.5.2.2   INHIBITION OF FILAMENTOUS FUNGI AND YEASTS

The agar diffusion assay using the following set of filamentous fungi and yeasts was provided by Dr. Anne van Diepeningen (CBS-KNAW Fungal Biodiversity Centre, Utrecht, The Netherlands). Paper disks were soaked with 50 µL DMSO (control) or 50 µL of the dissolved compound (1mg/mL DMSO) and placed onto the fungal colonies grown on agar medium. The size of the halo (no growth zone) around the filter paper at two time points was measured, after 2-3 days and after 6-7 days.

Tab. 3.6: Fungal strains used to assess antifungal activity of epipyrones (**1**-**3**):

No.	Strain	Strain number
	Ascomycota:	
1	*Arthroderma obtusum*	CBS 633.82
2	*Arthroderma otae*	CBS 282.63
3	*Arthroderma racemosum*	CBS 633.82
4	*Arthroderma vanbreuseghemii*	CBS 449.74
5	*Aspergillus fumigatus*	CBS 418.64
6	*Candida albicans*	CBS 6431
7	*Candida albicans*	CBS 8758
8	*Cladophialophora carionii*	CBS 160.54
9	*Exophiala jeanselmii*	CBS 507.90
10	*Exophiala phaeomuriformis*	CBS 131.80
11	*Fusarium andiyazi*	CBS 134430
12	*Fusarium petroliphilum*	CBS 135955
13	*Fusarium verticillioides*	CBS 135801
14	*Fusarium sp.*	WLD1-6
15	*Meyerozyma guillermondii*	18.6AIII
16	*Microsporon gypseum*	CBS 130939
17	*Penicillium chrysogenum*	18.6FII
18	*Pleospora sp.*	CBS 134305
19	*Sporothrix schenckii*	CBS 340.35
20	*Trichophyton erinacei*	CBS 344.79

Tab. 3.6 continued

21	*Trichophyton mentagrophytes*	CBS 101546
22	*Trichophyton mentagrophytes*	CBS 120357
23	*Trichophyton verrucosum*	CBS 134.66
24	*Trichophyton violaceum*	CBS 119447
	Basidiomycota:	
25	*Rhodotorula glutinis*	**CBS 20**
	´Zygomycetes´:	
26	*Actinomucor elegans*	CBS 100.13
27	*Mucor indicus*	CBS 120585
28	*Cunninghamella elegans*	WLD1-4

3.5.2.3 ANTI-HIV ACTIVITY

Anti-HIV activity of epipyrones (**1**-**3**) was assessed by Dr. Markus Helfer (Institute of Virology, Helmholtz Zentrum München) following the procedure described by Kremb et al. [154].

3.5.3 INHIBITION OF HUMAN CEREBROSIDE SULFO-TRANSFERASE (HCST)

Isolated and purified hCST was used for the inhibition assay, which was conducted by Isabell Zech (working group Prof. Gieselmann, Institute for Biochemistry and Molecular Biology, University of Bonn), following the modified procedure of Jungalwala et al. [155] as reported in [72]. In principle, the assay measures the activity of hCST by detecting the amount of radioactively labeled sulfatide on a HPTLC plate. Radioactively labeled PAP[^{35}S] (3´-phosphoadenosine-5´-phosphosulfate) was used to monitor the activity of the hCST.

Reaction mixture:

20 µg galactosyl ceramide were dissolved in 10 µl 1% Triton X-100 solution (CHCl$_3$/MeOH 2:1), dried and following solutions added:

3 µl of diluted tested compounds (stock solution: 1 mM in 10 % aqueous DMSO). For positive controls 3 µL 10% DMSO without inhibitor was taken.

16 µl Reaction buffer consisting of:

- Tris-HCl pH 7.1 (final concentration: 80 mM)
- MgCl$_2$ (final concentration: 16 mM)
- PAPS (final concentration: 20 µM; ratio of PAPS and PAP[^{35}S] = 2-10:1)

15 µl shCST solution in Tris-HCl, pH 7.1 (shCST = soluble hCST)

Reaction conditions: 37°C, 700 rpm, 60 min

Termination of the reaction was achieved by addition of 1 ml CHCl$_3$/MeOH (2:1).

After addition of 150 mM NaCl, the mixture was vortexed, centrifuged, the organic phase was transferred into a new vial and washed with 100 µl MeOH/NaCl (150 mM)/CHCl$_3$ (48:47:3). The dried sample was then dissolved in 20 µl CHCl3/MeOH (2:1) und chromatographed using HPTLC (Silica gel 60, Merck, eluent: CHCl$_3$/MeOH/H$_2$O, 65:25:4). Spots with different amounts of reaction buffer served as standards for quantification of the detected signals. After drying the plate, a bioimager screen was applied and incubated for several hours in the dark. The signals were detected using a bioimager screen scanner.

3.5.4   INHIBITION OF CYSTEINE- AND SERINE-PROTEASES

The assays were performed by the working group of Prof. Dr. M. Gütschow (Pharmaceutical Institute, Pharmaceutical Chemistry I, University of Bonn) using the following methods. The tested proteases were used in isolated and purified form.

The panel of tested enzymes involved:

1. Lysosomal cysteine-proteases: Cathepsins B, L, S, K
2. Serine-proteases: HLE (human leukocyte elastase)
                    bovine trypsin
                    bovine chymotrypsin

The assays for cathepsins B and L were based on a method described before [156,157]. Cleavage of the chromogenic substrates was observed spectrophotometrically at 405 nm.

For cathepsin B, Z-Arg-Arg-pNA served as the substrate. Cathepsin L was tested using Z-Phe-Arg-pNA.

The assay against cathepsin S employed the method elsewhere [157]. It employed a spectrophotometric determination of the chromogenic substrate Z-Phe-Arg-pNA (Z-Phe-Arg-para-nitroanilide), which is cleaved by cathepsin S, the detection wavelength was 405 nm.

Inhibitory activities on HLE were performed according to the described method [158]. The spectrophotometric assay employed the chromogenic substrate MeOSuc-Ala-Ala-Pro-Val-pNA, cleavage was monitored at 405 nm.

For bovine trypsin, the method reported in [159] was used. Cleavage of the chromogenic substrate Suc-Ala-Ala-Pro-Arg-p-NA was observed at 405 nm. Bovine chymotrypsin was assayed according to the described method [160].

3.5.5 LUCIFERASE-BASED TRANSIENT REPORTER SYSTEM FOR AGONISTS ON NUCLEAR RECEPTORS

Activities on α-/γ-/δ-PPAR and α-/δ-LXR were assessed by Dr. Paulsen Steinar (The Norwegian Structural Biology Centre and Department of Chemistry, University of Tromsø) using the method described by Tzameli et al. and Ciocoiu et al. [161,162]. Cos-1 cells (cell line from monkey kidneys [163], ATCC no. CRL-1650) were maintained in a humidified atmosphere at 37°C with 5% CO_2, in DMEM (Dulbecco´s Modified Eagle Medium, Invitrogen, CA) containing gentamicin (10 µg/mL) and fetal bovine serum (10%). Prior to sub-culturing or transfection, cell confluence was not more than 80%. 1.7 µg of the expression plasmids and 8.5 µg reporter construct per 1 x 107 cells were employed in order to transiently transfect the Cos-1 cells. Transient transfection was achieved using the Neon electroporation system (Invitrogen, Carlsbad, CA). Prior to the addition of the test compound, the cells were seeded (2 x 104/well) in 96-plates (white F96 microwell, Nalge Nunc Int., Rochester, NY) and allowed to attach for 5 h. The transfected cells were treated with compounds for 19 h (compound solutions made in dilution series in the medium). The values are relative to the luciferase activity obtained by activating the reporter gene system with a known agonist. Luc protein expression was developed (final concentration of D-luciferin: 0.4 mM) in a 30 mM HEPES buffer supplemented with ATP (0.5 mM) and $MgSO_4$ (1 mM) and quantified on a luminometer (Envison, Perkin-Elmer, MA, US).

The pSG5-Gal4-hPPAR-LBD (α, γ and δ isotypes) and pSG5-Gal4-hLXR-LBD (α and δ isotypes) expression constructs were made by Dr. Hilde Nebb, University of Oslo. The pGL3-5xUAS-SV40 luciferase reporter construct was purchased from Promega Corporation (USA).

3.5.6 EXTRACELLULAR AB-42 PEPTIDE PRODUCTION, CELL SURVIVAL AND INHIBITION OF PROTEIN KINASES

The assays were performed with epipyrones (**1-3**) by ManRos Diagnostics (Centre de Perharidy, 29680 Roscoff, France), applying following protocols:

MTS survival assay

This assay is a means to assess cytotoxic effects of the tested compounds, *i.e.,* epipyrones (**1-3**). MTS [3-(4,5-dimethylthiazol-2-yl)-5-(3-carboxymethoxyphenyl)-2-(4-sulfophenyl)-2H-tetrazolium] is reduced by reductases in living cells to a formazan (see **section 3.5.1**). The latter is detected via colorimetry.

N2a cells (= Neuro2a cells, murine neuroblastoma cell line) were transfected with human APP695 and maintained in DMEM in a humidified atmosphere (37°C, 5% CO_2). The medium was supplemented with 5% fetal bovine serum (FBS), 1% penicillin-streptomycin solution and G418 (Sigma, USA) (0.1 mg/mL).

N2a-APP695 cells were cultivated at a density of approximately 10,000 cells per well on 96-well plates in DMEM, supplemented with 0.5% FBS. The media were replaced by new media containing the test compounds after 24 h of incubation. For the initial screen, a 10 µM final concentration was applied. As a control, medium without cells (= blanks) and untreated cells were used. The viability of the cells was measured by the formation of a formazan from MTS, using CellTiter 96 Aqueous One Solution Cell Proliferation Assay (Promega, Madison, WI, USA) at 18 h post treatment. Incubation was carried out for 1h30 (37°C, 5% CO_2 and 95% humidity). Optical density (OD) was measured at 490 Δ 630 nm using a microELISA reader.

$$\text{Cell viability (\%)} = \frac{\text{OD of treated cell} - \text{OD of blanks}}{\text{OD of controls (vehicle treated cells)} - \text{OD of blanks}} \cdot 100$$

Ability of epipyrones (1-3) to induce extracellular production of Amyloid β-42

This assay was performed following the method described by Hochard et al. and Bettayeb et al. [164,165]. It investigates a stimulatory effect of the test substance on the formation of amyloid β-42, which is seen as a causal agent of Alzheimer´s disease.

The effect of epipyrones was tested at a final concentration of 10 µM. Following controls were used: (1) Blank (without cells), (2) Vehicle treated cells; (3) cells + 100 µM Aftin-5 (Aftin-5 is a reference compound for the induction of extracellular Aβ-42 production [164]). Aftin-5 was produced by ManRos Reagents.

Inhibition of Amyloid β-42 production induced by Aftin-5

In addition to the previous assay, this method measures the effect of compounds on the production of extracellular Amyloid β peptides induced by a pre-treatment with 100 µM of Aftin-5. Thus, an inhibitory effect of the test substance on the formation of amyloid β-42, which is seen as a causal agent of Alzheimer´s disease, is investigated. The effect of epipyrones was tested at a final concentration of 10 µM. The following controls were used (1-4): (1) Blank (no cells); (2) vehicle treated cells; (3) cells + 100 µM Aftin-5, the reference activator of extracellular Aβ-42 production [2]. Aftin-5 was produced by ManRos Reagents; (4) cells + 10 µM DAPT (N-[(3,5-difluorophenyl)acetyl]-Lalanyl-2-phenyl]glycine-1,1-dimethylethyl ester), a ɣ-secretase inhibitor, which inhibits the production of extracellular Amyloid β peptides induced by a pre-treatment with 100 µM Aftin-5.

N2a cells were transfected with human APP695 and cultivated as described for the MTS-assay (see above). The N2a-APP695 cells were cultivated with a density of approximately 10,000 cells per well in DMEM/optiMEM with 0.5% FBS. After 18 h incubation, the media were replaced by new media containing the test compounds. After 1 h incubation, Aftin-5 was added (100 µM 1% DMSO final). The cultured media were taken for Amyloid β-42 determination by ELISA assay after 18 h of incubation.

Protein kinase assays

The assays were performed using following protocols: The assays were performed in buffer A or C (see below), with their corresponding substrates, in the presence of 15 µM [ɣ-33P] ATP (3,000 Ci/mmol; 10 mCi/mL, PerkinElmer, France) in a final volume of 30 µL. The reaction was stopped by harvesting on a FilterMate harvester (Packard) onto P81 phosphocellulose papers (GE Healthcare) after 30 min of incubation at 30°C. Filters were washed in 1% phosphoric acid. 20 µL of scintillation fluid were added and the incorporated radioactivity was measured in a Packard counter. Blank values were subtracted and activities calculated as pmoles of phosphate incorporated during the 30 min incubation. The activities

were expressed in % of the maximal activity, *i.e.,* in the absence of inhibitors. Controls were performed with appropriate dilutions of DMSO. CDK1/cyclin B was prepared as previously described [166]. Kinase activity was assayed in buffer A, with 1 mg histone H1/mL. CDK2/cyclin A (human, recombinant, expressed in insect cells) was tested as described for CDK1/cyclin B. CDK5/p25 (mammalian, recombinant, expressed in *E. coli*) was tested as described for CDK1/cyclin B. CDK9/cyclin T (human, recombinant, expressed in insect cells) was tested as for CDK1/cyclin B using the Tide 7/9 substrate (YSPTSPSYSPTSPSYSPTSPSKKKK, Proteogenix, France) (500 µM). CK1δ/ε (porcine brain, native, affinity purified on axin-2 beads [6]) was tested as described for CDK1 but in buffer C and using the CK1-specific peptide substrate (CKs: RRKHAAIGSpAYSITA, Proteogenix, France) (1 mM). CLK1 (Human, recombinant, expressed in *E. coli* as GST fusion protein) was tested in buffer A (+ 0.15 mg BSA/ml) with RS peptide (GRSRSRSRSRSR, Proteogenix, France) (1 µg/assay). DYRK1A (human, recombinant expressed in *E. coli* as a glutathione S-transferase fusion protein) were purified by affinity chromatography on glutathione-agarose and tested as described for CDK1/cyclin B using Woodtide (KKISGRLSPIMTEQ, Proteogenix, France) (1.5 µg/assay) as a substrate, a residue of transcription factor FKHR. GSK-3α/β (porcine brain, native, affinity purified on axin-1 beads [7]) was tested as described for CDK1 using a GSK-3–specific substrate (GS-1: YRRAAVPPSPSLSRHSSPHQSpEDEEE; Sp = phosphorylated serine, Proteogenix, France) (250 µM).

Two protein kinase assay buffers were used during this assay: Buffer A : 10 mM MgCl2, 1 mM EGTA (MW 380.4), 1 mM DTT (MW 154.2), 25 mM Tris/HCl (MW 121.1) and 50 µg/ml Heparin. Buffer C : 20 mM ß-glycerophosphate, 10 mM p-nitrophenylphosphate, 25 mM MOPS, 5 mM EGTA, 15 mM MgCl2, 1 mM DTT and 0.1 mM sodium vanadate.

3.5.7   BINDING OF EPIPYRONES (1-3) TO A MODEL MEMBRANE

Binding of epipyrones (**1-3**) to a model membrane consisting of POPC (1-palmitoyl-2-oleoyl-phosphatidylcholine) was studied using a SAW (surface acoustic wave) sensor (S-sens® K5, Biosensor GmbH, Bonn) by Hildegard Falkenstein-Paul in the working group of Prof. Bendas (Pharmaceutical Institute, Pharmaceutical Chemistry II, University of Bonn). The method described by Schmitz [167] was used.

Briefly, a solution of the tested substance is injected into the SAW sensor setup (surface acoustic wave, a piezoelectric crystal element), which is loaded with an artificial membrane

bilayer consisting of POPC (1-palmitoyl-2-oleoyl-phosphatidylcholine). During the measurements, an alternating current is applied. This current leads to a rhythmic deformation of the piezoelectric crystal with specific frequency and amplitude. The type of wave, which is observed, is named ´Love shear wave´. It is a surface wave with horizontal polarization. Adsorption of particles onto the surface leads to an altered oscillation of the crystal.

The membrane surface is separated into five single chambers, in which parallel measurements can be performed. It is continuously flushed with buffer (PBS buffer, pH 7.4). In defined intervals, increasing concentrations of a test compound are injected into the buffer flow. According to phase shift and amplitude of the detected Love shear wave, conclusions can be drawn on whether the tested substance binds to the membrane, whether it is inserted into the membrane or whether it does not show any affinity towards the membrane. During the delay period following each injection, the test compound is allowed to elute from the membrane. The next injection cycle can proceed with an increased concentration of the test compound. For further descriptions and theory, see following literature [167–169].

3.6 GUTTATION FLUIDS – CULTIVATION AND ANALYSIS

Fungal cultures of *E. nigrum* strain 749 were grown on Czapek-Dox agar with and without trace metals. 4 – 5 L of each medium were prepared. Ca. 100 mL were filled into each petri dish (145 x 20 mm; see **section 3.1.3** for media composition and **section 3.1.4** for extraction).

Tab. 3.7: Experimental setup of the cultivation of *E. nigrum* strain 749 on Czapek-Dox medium for the induction of guttation droplet formation. For each experiment, 10-25 petri dishes with agar medium were prepared and inoculated with three agar plugs from precultures.

	No additives	Trace metals (Cu^{2+}, Zn^{2+})
Without illumination	Experiment 1	Experiment 2
Continuous illumination	Experiment 3	Experiment 4

Fungal cultures on each medium were divided into two groups, respectively: One half was grown in darkness, while the other half was grown under continuous illumination with artificial white light over the whole fermentation period (see table **3.7**). In this way 10-25 petri dishes were prepared for each of the four conditions. Each plate was inoculated with three agar plugs (three-point inoculation) from fungal precultures grown on agar medium (either malt extract agar or Czapek-Dox agar). The whole experiment was performed three times. Each culture was fermented at 26 °C for 30 days. On day 14 and 28, cultures were checked for production of guttation droplets. Droplets were drawn with a syringe (10 µl, Hamilton, USA) and collected in glass vials. Each vial was supplemented with 20 µL of MeOH (LC-MS grade, Merck, Germany) as an antifoam agent. Volumes of the samples were measured with an HPLC-syringe (100 µL, Hamilton, USA). The solution was then dried under nitrogen gas flow and stored under -18 °C until further use.

On day 30, the fermented cultures – containing mycelium and agar medium – were extracted four times successively during two days using EtOAc. The collected four aliquots were then unified, dried in a rotary evaporator to dryness and stored under -18 °C.

Guttation droplets were analyzed qualitatively using LC-HRMS (with systems B and C, see **section 3.3.2**). Crude extracts of the fungal cultures were measured via ^{1}H-NMR (in MeOH-d_4) and LC-HRMS (with system C) for qualitative analysis.

Quantitative determination of epipyrones (**1-3**) and acetosellin (**4**) in guttation droplets and crude extracts was performed on LC-MS system A in one single run, using the peak area in the TWC (total wavelength chromatogram) of the diode array detector for quantification. For this purpose, the dried guttation fluid was dissolved in 180 µl MeOH/water (50:50), centrifuged (13g, 2 min) and the supernatant was taken for analysis. The crude extracts were defatted prior to quantification using VLC [the column was packed with 10 g C_{18}-silica and repeatedly used for every sample (see **section 3.2.2**; eluent: 50 mL MeOH/water (90:10)]. The crude extract samples were then dried at 40 °C using a rotary evaporator and resolved in 100% MeOH (LC-MS grade, Merck, Germany) to a final concentration of 1 mg/mL.

Following standards were prepared for acetosellin (**4**) and epipyrones (**1-3**) in ascending concentrations using 100% MeOH (LC-MS grade, Merck, Germany; values given in mg/mL): 0.002; 0.01; 0.05; 0.1; 0.5; 1.0.

From the peak area of standard solutions (expressed in [mAU·sec]) a standard curve was prepared and the concentration values of each sample was calculated on basis of the standard curves (see **figures 3.4a** and **3.4b**). Statistical evaluation was performed on Prism 5 (GraphPad Software Inc.), including the SEM (standard error of the mean) and statistical evaluation employing the Mann-Whitney test (one-tailed). Concentration values for the

guttation fluid refer to the concentration in the original fluid prior to processing. Concentration values for the crude extracts refer to the original, non-defatted, extracts.
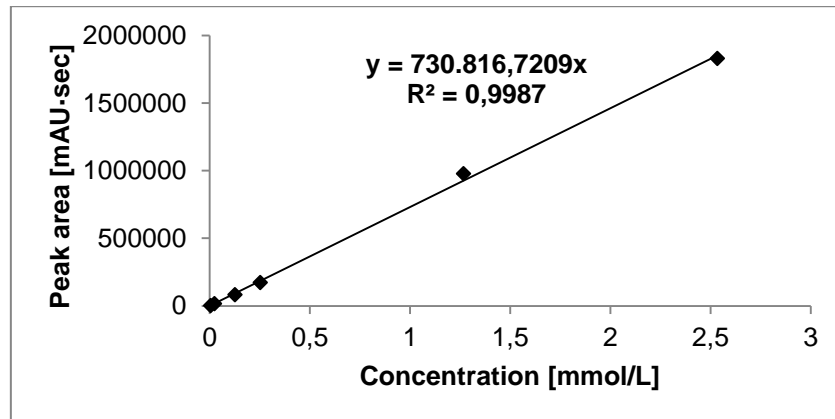

Fig. 3.4a: Linearity for the LC-MS results of standard solutions for acetosellin (**4**) (concentration given in mmol/L), inferred by linear regression. Peak areas, expressed in mAU·sec, were taken from the diode array detector.
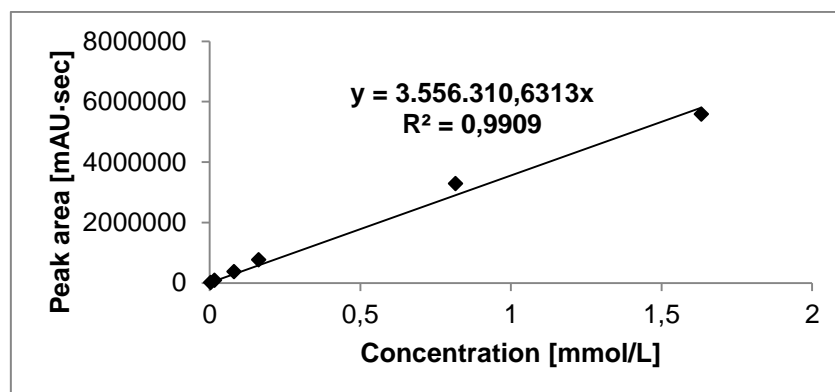

Fig. 3.4b: Linearity for the LC-MS results of standard solutions for epipyrones (**1-3**) (concentration given in mmol/L), inferred by linear regression. Peak areas, expressed in mAU·sec, were taken from the diode array detector.

3.7   CHEMICALS AND SOLVENTS

Acetic anhydride (99.6%)	VWR International (France)
Acetone-d_6 99.8%	Deutero GmbH (Germany)
Acetonitrile (HPLC grade)	VWR International (France)
Agar	Sigma-Aldrich (USA)
Benzylpenicillin	Fluka (Switzerland)
Chitin from crab shells	Fluka (Switzerland)
Chloroform-d_1	Deutero GmbH (Germany)
Copper sulfate pentahydrate (p.a.)	Merck (Germany)
Difco Czapek-Dox broth	Becton Dickinson (USA)
DMSO-d_6, 99.8%	Deutero GmbH (Germany)
Malt extract	Villa Natura GmbH (Germany
Methanol (HPLC grade)	Avantor (Poland)
Methanol (LC-MS grade)	Merck (Germany)
Methanol-d_4 99.8%	Deutero GmbH (Germany)
Peptone (from animal tissue)	Roth (Germany)
Pyridine (99%)	Roth (Germany)
Sodium[1-^{13}C,99%]acetate	Cambridge Isotope Laboratories Inc. (USA)
Streptomycin sulfate	Fluka (Switzerland)
Trifluoroacetic acid (TFA), 99.9%	Roth (Germany)
Yeast extract (micro-granular)	Roth (Germany)
Zinc sulfate heptahydrate (p.a.)	Roth (Germany)

4   RESULTS

4.1 IDENTIFICATION OF THE FUNGAL STRAINS

As of 2011, nearly 100,000 fungal species have been described [170]. Ascomycota make up the largest group with 68,000 species. The major characteristic of this phylum is the formation of asci, which harbor the ascospores, *i.e.,* meiospores that are built after genetic recombination in a sexual process. Among these fungi are the Pleosporales, which form a large group with 4705 species, according to Moore et al. [170]. Typically, they live as epiphytes, endophytes, plant parasites, saprobes on dead plant matter or on dung [171]. Inside the order Pleosporales, the family Didymellaceae, which was delineated by genetic methods, harbors the genus *Epicoccum*. Currently, eight species are accepted for this genus, all of which are highly variable anamorphic fungi, *i.e.,* sexual reproduction has not been observed [172,173]. Specifically, the herein described species – *Epicoccum nigrum* – has been the subject of some recent phylogenetic studies [14,174]. Remarkable variability, together with frequent occurrence and the importance for agriculture, may be the reasons.

The two fungal strains, which are the basis of this work, were identified based mainly on their ITS sequences. Additionally, microscopic evaluation was performed. According to Chen et al. [173], the genus *Epicoccum* is characterized by the formation of unicellular or multicellular, smooth or verrucose chlamydospores, which can vary in size (5 – 35 µm) and pigmentation (subhyaline to dark brown). This was confirmed through microscopical examination of mycelium grown on Czapek-Dox agar with trace metal solution (see **fig. 4.1** and **4.2**). However, pycnidia or sporodochia, which were also described for the genus, could not be observed on the cultures.

For the confirmation of the microscopical data and to further narrow down the identity of the strains to species level, molecular identification via the ITS sequence was used. This approach has already been applied successfully for this genus [14]. Comparison of the obtained genetic sequences with the top hits in blastn revealed the identity of both strains to be *Epicoccum nigrum* with a sequence identity of 100% compared to the strains obtained from Genbank [146] (see **fig. 4.3**).
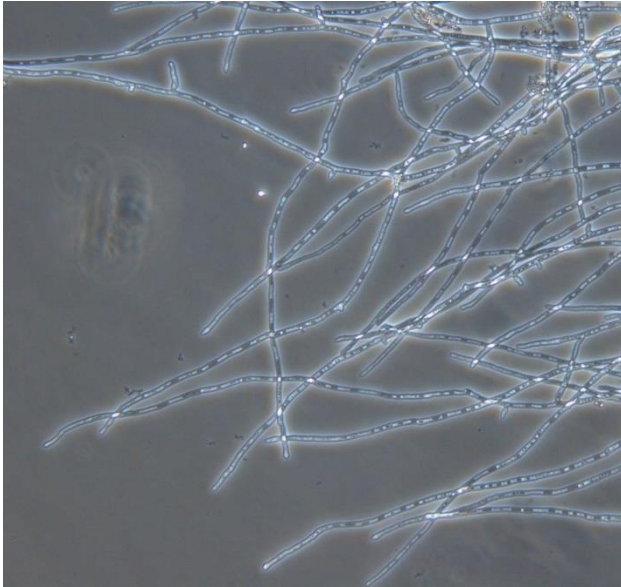
Fig. 4.1: Branched vegetative mycelium of *E. nigrum* strain 749 grown in MEB (malt extract broth), imaged by phase-contrast microscopy. Magnification: 200x.
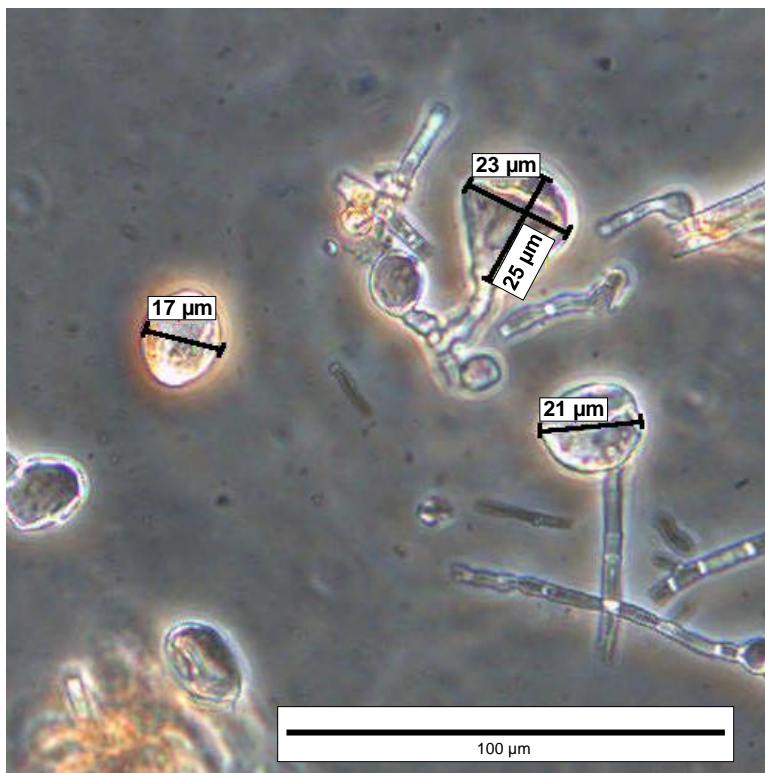

Fig. 4.2: Chlamydospores of *E. nigrum* strain 749 grown on Czapek-Dox agar with trace metal solution in darkness. Spores were imaged through phase-contrast microscopy after 4 weeks culture. Magnification: 200x. Spore sizes are included in the picture.
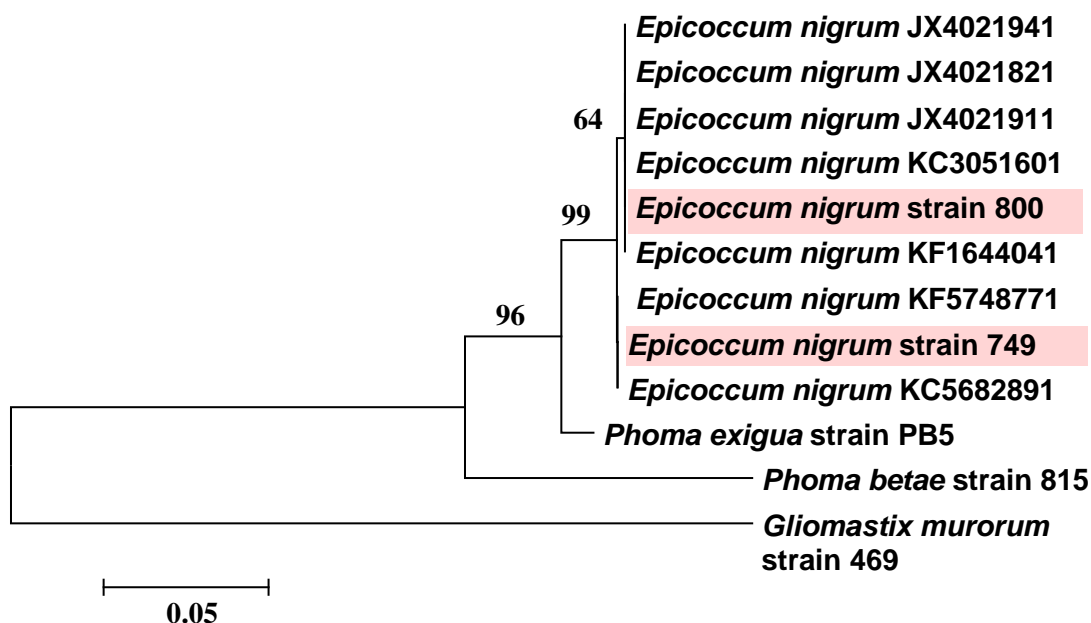
Epicoccum nigrum JX4021941
Epicoccum nigrum JX4021821
Epicoccum nigrum JX4021911
Epicoccum nigrum KC3051601
Epicoccum nigrum strain 800
Epicoccum nigrum KF1644041
Epicoccum nigrum KF5748771
Epicoccum nigrum strain 749
Epicoccum nigrum KC5682891
Phoma exigua strain PB5
Phoma betae strain 815
Gliomastix murorum strain 469

0.05

Fig. 4.3: Evolutionary relationships of the herein described taxa. ITS sequences for *E. nigrum* strains obtained in this study are highlighted. *Gliomastix murorum* strain 469 (Hypocreales, Sordariomycetes) was chosen as the outgroup, all of the remaining taxa belong to the Pleosporales (Dothideomycetes). Calculation of the phylogenetic tree was carried out with Mega6 [149]. The evolutionary history was inferred by using the Maximum Likelihood method based on the Tamura-Nei model. The tree with the highest log likelihood (-1237.5214) is shown. The percentage of replicate trees in which the associated taxa clustered together (1000 replicates) are shown next to the branches. The tree is drawn to scale, with branch lengths measured in the number of substitutions per site (scale bar: 5 substitutions per 100 nucleotides; see **section 3.1.2** for the method and references).

4.2   SECONDARY METABOLITES OBTAINED DURING THIS STUDY

During the initial screening of *E. nigrum* strain 749, carried out by Ekaterina Egereva, an inhibitory activity of crude extracts against human leukocyte elastase (HLE) (see **table 4.1**). Consequently, a large scale fermentation of strain 749 was attempted on MES medium (malt extract agar with artificial sea water) first. During this work, an additional strain of *E. nigrum* was isolated (see **section 4.1**), the strain 800. The latter was initially envisaged as the producing strain for acetosellin in order to elucidate its biosynthesis, since it initially produced a higher amount of this compound (see **section 4.4**). Later, strain 749 proved to be the superior producer of acetosellin (**4**) during cultivation experiments. Therefore, strain 800 was only used for the isolation of additional bioactive secondary metabolites (see **fig. 4.5**).

Table 4.1: Inhibitory activity on human leukocyte elastase (HLE) of extracts from cultures of *E. nigrum* strain 749 grown under continuous illumination.

Growth medium	Residual enzyme activity [%] at a concentration of 10 µg/ml[*]
MES[**]	33.3
MEA[***]	9.9

*Experiments performed in the working group of Prof. Gütschow.

**MES = Malt extract agar with artificial sea water. ***MEA = Malt extract agar.

Both strains – 749 and 800 – were fermented under different conditions, in order to change the secondary metabolism (OSMAC approach, see **section 1.1** for the definition).

Strain 749 was cultivated first on MES (malt extract agar with artificial sea water) under continuous illumination with artificial light. From this extract, epipyrones (**1**-**3**) were isolated using size exclusion chromatography and RP-VLC in high yields (78.8 mg). Two 5-methyl orsellinic acid derivatives, 1F4-1-6 (**12**) and epicoccone (**11**), were obtained via further purification by RP-SPE and RP-HPLC. For details see **section 3.2.6.1** and **fig. 4.4**.

Later, acetosellin (**4**) and its dihydroxy derivative (compound **7**) were isolated from a culture of strain 749 on CDA (Czapek-Dox agar), grown under continuous illumination with white light, again in a high yield (104 mg).
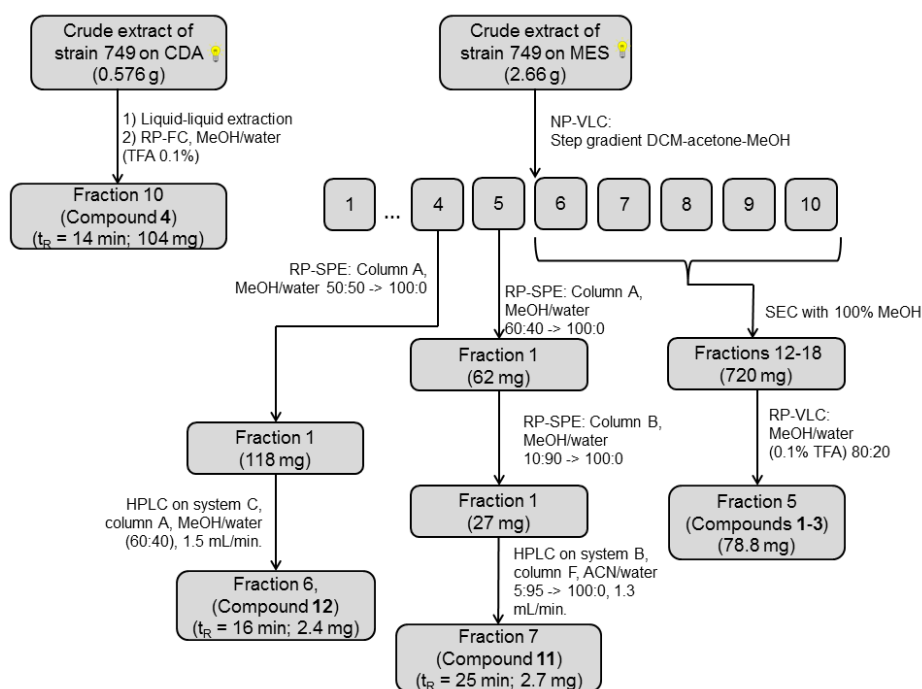
Fig. 4.4: Separation scheme for *E. nigrum* strain 749 grown on MES (malt extract agar with artificial sea water) and on CDA (Czapek-Dox agar). Both cultures were grown under continuous illumination. For details on cultivation conditions and media see **section 3.1.3**, for details on extraction and fractionation see **section 3.2.6.1**.
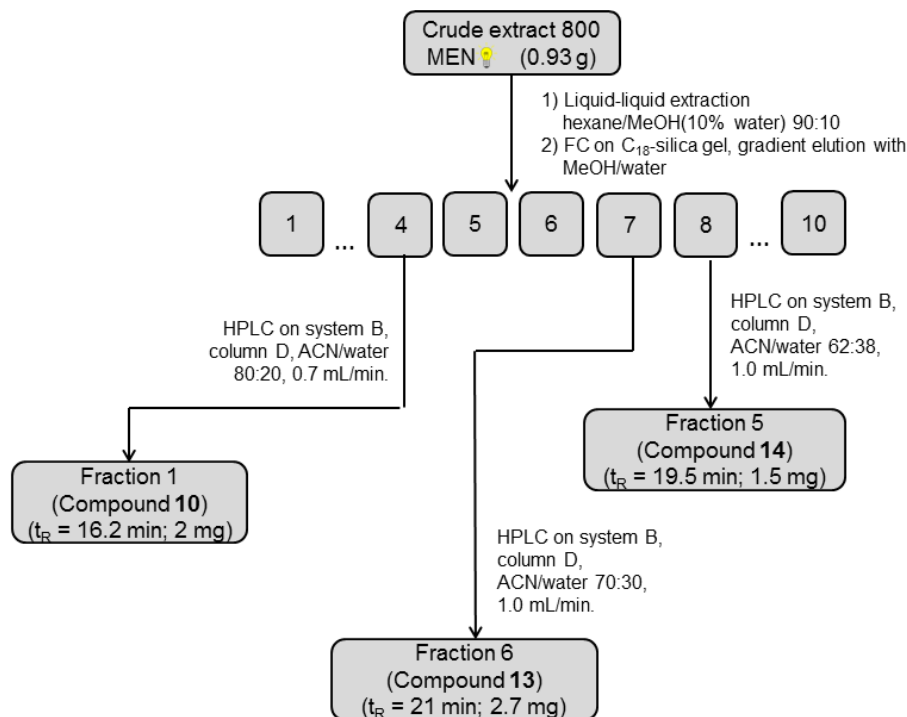
Strain 800

E. nigrum strain 800 was cultivated three times on different media:

1) The first culture was prepared on MEN medium (malt extract agar with artificial sea water and sodium acetate) under continuous illumination with white light. Separation of this first extract by successive use of NP VLC, SPE and HPLC afforded two metabolites (see **section 3.2.6.5** and **fig. 4.5**): Epicaronic acid (**13**, also found in the third culture extract of strain 800 mentioned below) and flazin (**15**).

2) Epicoccolide B (**9**) was isolated from a second culture on MEA+TMS (malt extract agar with trace metal solution), grown in darkness, through successive use of NP flash chromatography and RP-HPLC (see **fig. 4.5** and **section 3.2.6.5**).

3) The third culture (´time course´ culture) was initially prepared for studies on the biosynthesis of acetosellin (**4**) (**section 4.3.4**). Isolation of metabolites was achieved by successive use of RP flash chromatography and RP-HPLC (see **section 3.2.6.4** and **fig. 4.6**). Three compounds were isolated: Epicaronic acid (**13**), tricinonoic acid (**14**) and (3*R*,4*S*)-4-hydroxymellein (**10**).
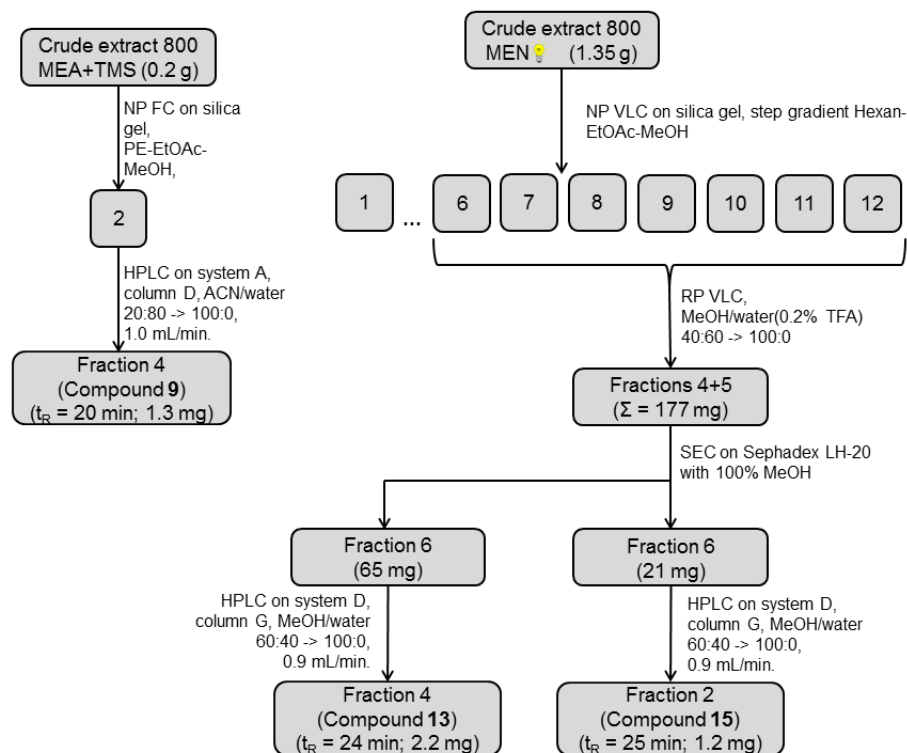
Fig. 4.5: Separation scheme for the first two fermentations of *E. nigrum* strain 800 on MEA+TMS (malt extract agar with trace metal solution, grown in darkness) and on MEN (malt extract agar with artificial sea water and sodium acetate, grown under continuous illumination). For details on cultivation conditions and media see **section 3.1.3**.

Fig. 4.6: Separation scheme for the third cultivation of strain 800. These ´time course´ cultures of *E. nigrum* strain 800 were grown on MEN (malt extract agar with artificial sea water and sodium acetate). The culture was grown under continuous illumination. For details on cultivation conditions and media see **section 3.1.5**, details on fractionation are given in **section 3.2.6.4**.

4.3 EPIPYRONES (1-3)

4.3.1 CULTIVATION EXPERIMENTS AND FERMENTATION CONDITIONS

As indicated in the last section, different culture conditions were used to alter the secondary metabolism of *E. nigrum* strains 749 and 800 (for basic cultivation techniques, see **section 3.1.3**). For this purpose, two of the aforementioned procedures (see **section 4.2**) were chosen: Variation of the substrate and of abiotic factors, including trace metal supplementation and growth under continuous illumination with white light or darkness.

Concerning strain 749, following observations were made: The metabolic pattern proved to be remarkably stable, concerning the experiments on malt extract agar medium (MEA) (see **table 4.2** and appendix: **fig. 8.1**). Epipyrones (**1**-**3**, **fig. 4.7**) can be distinguished as the main metabolites on different growth conditions, with a retention time of ca. 18.4-19.5 min in the UV trace of the LC-MS-DAD chromatogram (see **table 4.2** and **fig. 8.1** in appendix). The striking exception is an extract prepared from strain 749 grown on malt extract agar with trace metal solution under continuous illumination (**No. 5** in **table 4.2**). In this case, only minute amounts of epipyrones (**1**-**3**) could be detected, probably due to the artificial light applied during the whole cultivation period. It can be concluded from the depicted data that – during fermentation on MEA – either darkness is needed to induce production of epipyrones (**1**-**3**) or a (osmotic) stress-inducing supplement. This can be ASW (artificial sea water) or NaOAc.

The second major compound found in strain 749 is acetosellin (**4**) (see **fig. 8.1** in appendix for a comparison of chromatograms from crude extracts) with a retention time of approximately 18 min. This compound is a polyketide with a partly reduced azaphilonoid core structure. It will be further discussed in **section 4.4**. In contrary to strain 749, production of epipyrones (**1**-**3**) was not observed for strain 800 (see **fig. 8.2** in appendix) with neither of the cultivation conditions. Production of acetosellin (**4**), however, is upregulated during growth on malt extract agar with ASW (artificial sea water) and sodium acetate. Also, addition of trace metals causes a marked decrease in acetosellin (**4**) production in both strains. As will be mentioned in **section 4.7**, production of acetosellin (**4**) on Czapek-Dox agar (CDA) in strain 749 relies mainly on the absence of trace metal solution (TMS). More details on the metabolism of strain 749 on CDA will be given in **section 4.7**.

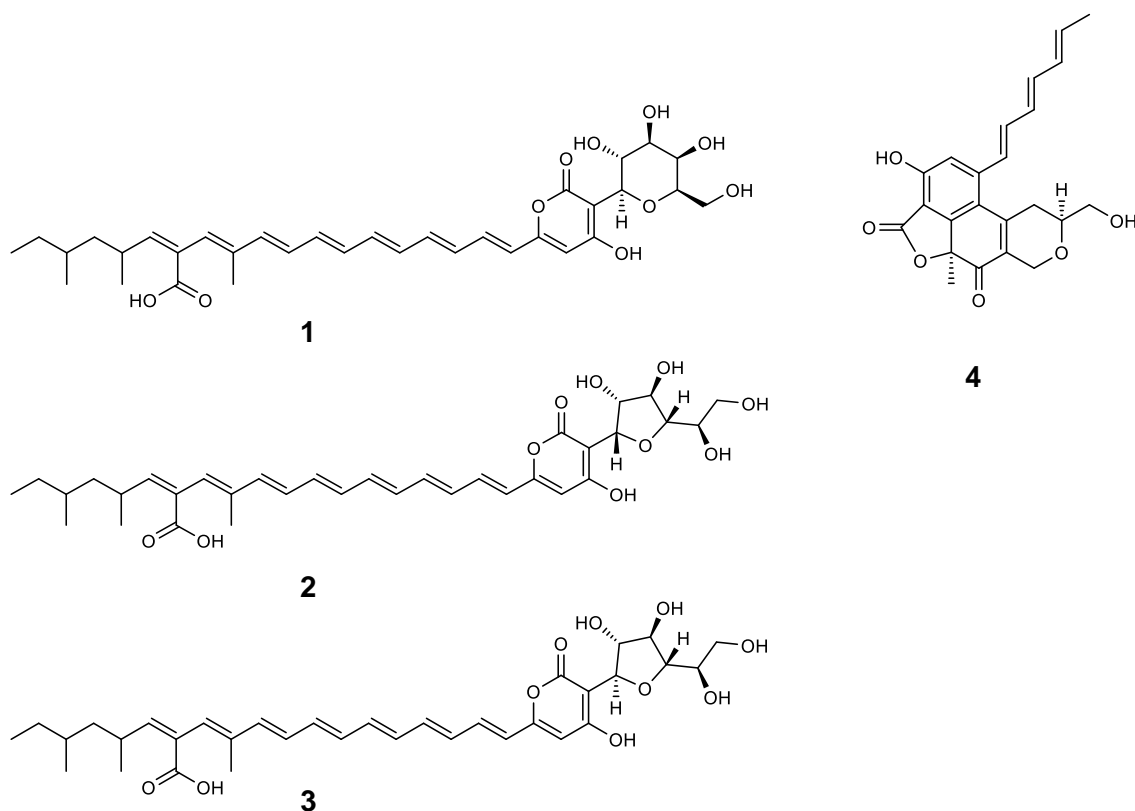**Fig. 4.7:** Major secondary metabolites found in *E. nigrum* strain 749. Epipyrone A (**1**), epipyrone B (**2**), epipyrone C (**3**), acetosellin (**4**).

Table 4.2: Relative abundance of the major metabolites from extracts fermentation experiments (each strain was cultivated on five petri dishes under each condition). The data were calculated from the peak area in the TWC in relation to epipyrones (**1**-**3**) or acetosellin (**4**) standard solution (1 mg/ml), respectively. Shown are the data from extracts of two strains (strains 749 and 800).

		Relative abundance of major metabolites in crude extract [wt%]			
		epipyrones		acetosellin	
No.	Culture conditions	strain 749	strain 800	strain 749	strain 800
1	MEA + ASW 💡	16	*n.d.*	9	2
2	MEA + ASW +NaOAc 💡	38	*n.d.*	3	8
3	MEA + TMS +ASW 💡	50	*n.d.*	3	1
4	MEA + TMS	24	*n.d.*	*n.d.*	0
5	MEA + TMS 💡	1	*n.d.*	0	1
6	CDA + TMS 💡	58	*n.d.*	*n.d.*	*n.d.*

n.d. = not detected, MEA = malt extract agar, ASW = artificial sea water
TMS = trace metal solution (containing Zn^{2+} and Cu^{2+}, see **section 3.1.3** for details), CDA + TMS = Czapek-Dox agar with trace metal solution. Lightbulbs indicate continuous illumination of the fungal cultures with artificial white light.

4.3.1.1 ISOLATION AND STRUCTURE ELUCIDATION OF EPIPYRONES (1-3)

As described in **section 3.2.6.1**, epipyrones (**1-3**) were isolated from strain 749 grown on MEA + TMS via successive use of NP-VLC, SEC and RP-VLC. Structure elucidation was achieved by comparison of the exact mass measurement, 1D-/2D-NMR data, as well as of the UV and IR data with data from the literature [175,176]. In this way the configuration of the side chain and the identity of the *C*-glycosyl moiety could be confirmed. The signals in the ^{1}H-NMR and ^{13}C-NMR also point to the presence of isomers B (**2**) and C (**3**), which arise from **1** by rearrangement of the glycosidic part (see **tables 4.3a-c**). Integration of the signals also confirms that epipyrone A (**1**) accounts for ca. 70% of the mixture, which was reported before [175].
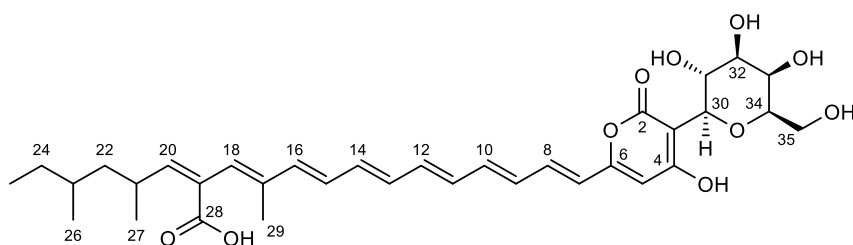
Fig. 4.8: Structure of epipyrone A (**1**) with numbering.

Table 4.3a: NMR-data of epipyrone A (**1**), measured in MeOH-d_4, at 300 MHz (^{1}H-NMR) and 75 MHz (^{13}C-NMR), respectively.

Carbon No.	δ_C [ppm] [a,c]	δ_H [ppm][c]; *(J [Hz])*	COSY	HMBC[b,c]
2	166.1, qC	-		
3	101.7, qC	-		
4	170.4, qC	-		
5	102.3, CH	6.12 (1 H, s)		3,6,7
6	160.6, qC	-		
7	122.4, CH	6.20 (1 H, br d, 15.0)	8	
8	137.6, CH	7.13 (1 H, dd, 11.3; 15.0)	7	
9	132.2, CH	6.45[†]		
10	140.6, CH	6.61 (1 H, br d, 11.3)		
11	134.1, CH	6.44[†]		
12	133.6, CH	6.40[†]		
13	137.0, CH	6.44[†]		
14	130.1, CH	6.44[†]		
15	138.1, CH	6.47[†]		
16	140.3, CH	6.44[†]		
17	136.6, qC	-		
18	131.4, CH	6.18 (1 H, s)	20,29	20,21,28
19	132.2, qC	-		
20	149.1, CH	5.65 (1 H, d, 10.3)	18,21	18,28
21	33.1, CH	3.08 (1 H, m)	22,27	
22	45.8, CH$_2$	1.16 (1 H, m[†]) 1.40 (1 H, m[†])		21
23	33.8, CH	1.36 (1 H, m[†])	22,24	25
24	31.2, CH$_2$	1.21 (1 H, m[†]) 1.36 (1 H, m[†])		22
25	11.7, CH$_3$	0.915 (3 H, t[†])	24	23
26	19.5, CH$_3$	0.90 (3 H, d[†])		22,24
27	21.8, CH$_3$	1.07 (3 H, d, 6.6)	21	21,22
28	172.0, qC	-		
29	13.8, CH$_3$	1.92 (3 H, s)		
30	76.2, CH	4.58 (1 H, d, 9.5)	31	2,3,4
31	70.2, CH	4.28 (1 H, t, 9.5)	30,32	
32	76.5, CH	3.57 (1 H, dd, 2.9; 9.5)	31,33	
33	71.1, CH	3.97 (1 H, br d, 2.9)	32,34	
34	80.9, CH	3.67 (1 H, m)	33,35	
35	62.7, CH$_2$	3.80 (1 H, m)	34	

referenced in Mestrenova using MeOH-d_4 signal.
[a] multiplicities deduced from DEPT-135 experiments
[b] numbers refer to ^{13}C resonances
[c] measured in MeOH-d_4
[†] overlapped

Table 4.3b: NMR-data of epipyrone B (**2**), measured in MeOH-d_4, at 600 MHz (^{1}H-NMR) and 125 MHz (^{13}C-NMR), respectively.

Carbon No.	δ_C [ppm] [a,c]	δ_H [ppm][c]; (J [Hz])
30	83.0, CH	5.27 (1 H, d, 2.5)
31	78.8, CH	4.23[†]
32	80.6, CH	4.27[†]
33	87.3, CH	4.09[†]
34	72.5, CH	3.82[†]
35	64.5, CH$_2$	3.69[†]

referenced in Mestrenova using MeOH-d_4 signal.
[a] multiplicities deduced from DEPT-135 experiments
[b] numbers refer to ^{13}C resonances
[c] measured in d$_4$-MeOH
[†] overlapped

Table 4.3b: NMR-data of epipyrone C (**3**), measured in MeOH-d_4, at 600 MHz (^{1}H-NMR) and 125 MHz (^{13}C-NMR), respectively.

30	78.3, CH	5.16[†]
31	79.5, CH	4.69[†]
32	71.0, CH	4.17[†]
33	83.6, CH	4.12[†]
34	72.4, CH	3.82[†]
35	62.7, CH$_2$	3.71[†]

referenced in Mestrenova using MeOH-d_4 signal.
[a] multiplicities deduced from DEPT-135 experiments
[b] numbers refer to ^{13}C resonances
[c] measured in d$_4$-MeOH
[†] overlapped

Epipyrones (**1-3**): Red-orange amorphous powder (79 mg, 11.3 mg/L). $[\alpha]_D^{20}$ +121.0 (c 0.04, MeOH). UV (CH$_3$OH) λ_{max} (ε), 239 (1990) nm, 427 (69346); IR (ν_{max}) 3261, 2961, 1664, 1538, 1421, 1138, 1003 cm^{-1}. ^{1}H-/^{13}C-NMR-data see **table 4.3**. HR-ESI-MS m/z 635.2780 [M+Na]$^+$ (calcd. for C$_{34}$H$_{44}$NaO$_{10}{}^+$, 635.2827).

4.3.2   ACETYLATION PRODUCTS (5-6)

Acetylation of epipyrones (**1**-**3**) was attempted according to the protocols mentioned in **section 3.4** in order to determine the structure-activity relationships for the *C*-glycosyl moiety and to inhibit isomerization of the pyranosyl isomer into the two furanosyl isomers. Isomerization reportedly happens spontaneously in solution [175]. However, for purification, chemical analysis and biological activity testing, a defined substance is preferable. The desired compound **5** (see **fig. 4.9**) was obtained in 40.7% yield, while the yield for compound **6** (see **fig. 4.9**) was 5.4%. Structure elucidation involved comparison of the 1D- and 2D-NMR data with the data obtained from epipyrones (**1**-**3**), high accuracy mass measurements, as well as IR- and UV-data. For compound **5**, the ^{1}H-NMR (see **table 4.4**) already showed the presence of four additional signals between δ 1.93 and δ 2.22, typical for methyl protons in α-position of an acetyl unit. The ^{1}H-NMR coupling constants of the *C*-glycosyl moiety further confirmed the presence of a pyranose ring. HMBC correlations, together with the changed chemical shift values of methine and methylene groups in the ^{1}H-NMR, served to elucidate the acetylation pattern of the pyranosyl moiety.

Remarkably, the signal for H-20 was shifted downfield (Δδ = 0.95), which pointed to an isomerization from *Z*- to *E*-configuration at the terminal double bond, which is especially prone to isomerization. This was confirmed by the ROESY correlation between H-18 and H-21. Additional evidence for isomerization was obtained from the lower UV-maximum at 422 and the lower molar absorptivity compared to epipyrones (**1**-**3**) (Δλ = 5 nm, Δε = 39840).

The ^{1}H-NMR of compound **6** (see **table 4.5**) revealed the presence of three acetyl units (δ 1.93 – 2.11). Again, the ^{1}H-NMR coupling constants for the *C*-glycosyl moiety confirmed the presence of a pyranose partial structure and HMBC correlations provided evidence for the acetylation pattern. The chemical shift value of H-20 pointed to the fact that the original *Z*-configuration of the terminal double bond was retained.

Finally, high resolution mass spectrometry confirmed the acetylation rate for both compounds **5** and **6** (see **fig. 4.9**).

Table 4.4: NMR-data of epipyrone tetraacetate (**5**), measured in MeOH-d_4, at 600 MHz (^{1}H-NMR) and 150 MHz (^{13}C-NMR), respectively.

Carbon No.	δ_C [ppm] [a,c]	δ_H [ppm][c]; (*J* [Hz])	COSY	HMBC[b,c]
2	165.3, qC	-		
3	99.1, qC	-		
4	170.7, qC	-		
5	101.4, CH	6.09 s		
6	161.2, qC	-		
7	122.3, CH	6.24 (1H, d, 15.0)		
8	138.1, CH	7.21 (1 H, dd, 11.2; 15.0)		
9	132.2, CH	6.49[†]		
10	140.8, CH	6.72 (1 H, dd, 11.4; 14.5)		
11	134.3, CH	6.48[†]		
12	133.6, CH	6.45[†]		
13	136.9, CH	6.53[†]		
14	130.3, CH	6.51[†]		
15	138.2, CH	6.59[†]		
16	138.9, CH	6.53[†]		
17	139.8, qC	-		
18	127.0, CH	6.14 (1 H, s)	20	
19	130.1, qC	-		
20	152.1, CH	6.60 (1 H, br d, 10.5)	18	19,28
21	32.9, CH	2.57 (1 H, br m)		
22	45.3, CH$_2$	1.18 (1 H, m[†]) 1.40 (1 H, m[†])		
23	33.6, CH	1.27 (1 H, m[†])		
24	31.1, CH$_2$	1.18 (2 H, m[†])		
25	11.6, CH$_3$	0.90 (3 H, t, 7.5)		
26	19.6, CH$_3$	0.84 (3 H, d, 6.4)		
27	20.3, CH$_3$	1.06 (3 H, d, 6.4)		
28	170.6, qC	-		
29	14.7, CH$_3$	1.78 (3 H, br s)	18	19
30	73.6, CH	4.88 (1 H, d, 9.9)		
31	68.2, CH	6.04 (1 H, t, 9.9)		36
32	74.2, CH	5.20 (1 H, dd, 3.4; 9.9)		38
33	69.3, CH	5.50 dd (1 H, dd, 0.7; 3.4)		40
34	75.6, CH	4.15 (1 H, m[†])		
35	63.1, CH$_2$	4.17 (2 H, m[†], 5.5; 10.1)		42
36	171.4, qC	-		
37	20.6[†], CH$_3$	1.93 (3 H, s)		36
38	171.7, qC	-		
39	20.6[†], CH$_3$	2.00 (3 H, s)		38
40	172.3[†], qC	-		

Tab. 4.4 continued

41	20.6[†], CH_3	2.22 (3 H, s)		40
42	172.2[†], qC	-		
43	20.6[†], CH_3	2.06 (3 H, s)		42

referenced in Mestrenova using MeOH-d_4 signal.
[a] multiplicities deduced from DEPT-135 experiments
[b] numbers refer to ^{13}C resonances
[c] measured in MeOH-d_4
[†] overlapped

Table 4.5: NMR-data of epipyrone triacetate (**6**), measured in MeOH-d_4, at 600 MHz (^{1}H-NMR) and 150 MHz (^{13}C-NMR), respectively.

Carbon No.	δ_C [ppm] [a,c]	δ_H [ppm][c]; (J [Hz])	COSY	HMBC[b,c]
2	166.6, qC	-		
3	99.0, qC	-		
4	n.d.			
5	104.2, CH	6.02 (1 H, br s)		
6	160.3, qC	-		
7	122.8, CH	6.21 (1 H, d, 15.2)		
8	137.2, CH	7.17 (1 H, br t)		
9	132.3, CH	6.47[†]		
10	140.2, CH	6.69 (1 H, br t, 11.9)		
11	134.0, CH	6.45[†]		
12	133.6, CH	6.45[†]		
13	136.9, CH	6.47[†]		
14	130.0, CH	6.45[†]		
15	137.8, CH	6.55[†]		
16	140.3, CH	6.45[†]		
17	136.5, qC	-		
18	131.5, CH	6.16 (1 H, s)	20	
19	n.d.			
20	148.3, CH	5.61 (1 H, d, 10.3)	18	
21	33.1, CH	3.05 (1 H, br m)		
22	45.9, CH_2	1.16 (1 H, m[†]) 1.40 (1 H, m[†])		
23	33.8, CH	1.37[†]		
24	31.2, CH_2	1.21 (2 H, m[†])		
25	11.7, CH_3	0.91 (3 H, br s)		
26	19.5, CH_3	0.91 (3 H, s[†])		
27	21.8, CH_3	1.07 (3 H, br d)		
28	172.6, qC	-		
29	13.7, CH_3	1.93 (3 H, s[†])		
30	74.1, CH	4.83 (1 H, d[†], 8.8)		

Tab. 4.5 continued

31	69.0, CH	5.94 (1 H, br t, 9.7)		36
32	76.7, CH	5.03 (1 H, d†, 9.7)		38
33	68.7, CH	4.14 (1 H, br s)		
34	77.7, CH	3,96 (1 H, br s)		
35	64.7, CH$_2$	4.28 (2 H, br m)		40
36	171.6, qC	-		
37	20.6, CH$_3$	1.93 (3 H, s†)		36
38	172.1, qC	-		
39	20.8, CH$_3$	2.11 (3 H, br s)		38
40	172.6, qC	-		
41	20.7, CH$_3$	2.08 (3 H, br s)		40

referenced in Mestrenova using MeOH-d_4 signal.
[a] multiplicities deduced from DEPT-135 experiments
[b] numbers refer to ^{13}C resonances
[c] measured in MeOH-d_4
[†] overlapped
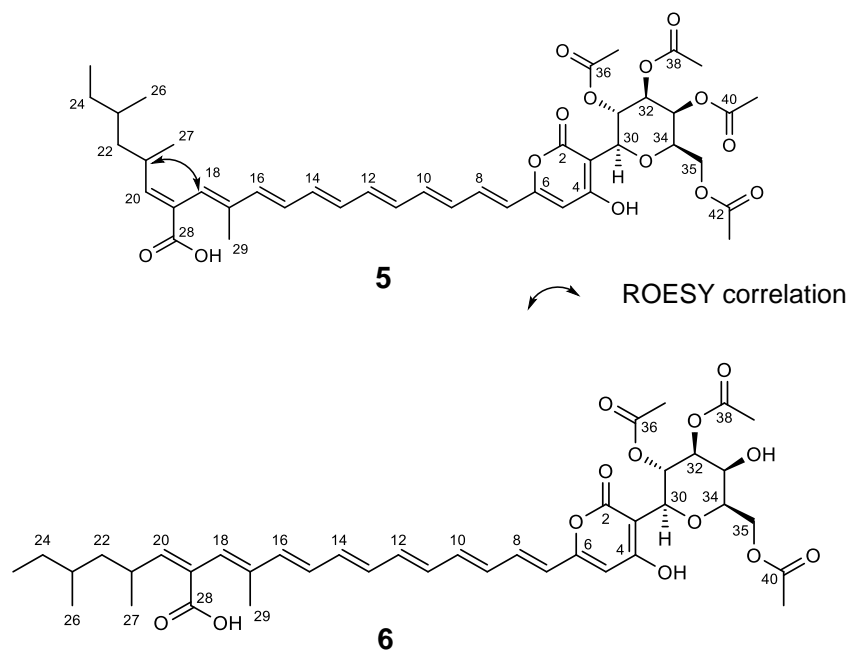
Fig. 4.9: Acetylation products **5** and **6** obtained from reaction of epipyrones (**1-3**) with Ac$_2$O in pyridine.

Epipyrone tetraacetate (**5**): Red-orange amorphous solid (11.8 mg). $[\alpha]_D^{20}$ -46.0 (*c* 0.20, MeOH). UV (CH$_3$OH) λ_{max} [nm] (ε [L·mol^{-1}·cm^{-1}], 219 (16299), 330sh (12976), 422 (29506); IR (v_{max}) 3385, 2924, 1745, 1682, 1541, 1420, 1368, 1223 cm^{-1}. ^{1}H-/^{13}C-NMR-data see **table 4.4**. HR-ESI-MS *m/z* 781.3359 [M+H]$^+$ (calcd. for C$_{42}$H$_{53}$O$_{14}^+$, 781.3430), 803.3232 [M+Na]$^+$ (calcd. C$_{42}$H$_{52}$NaO$_{14}^+$, 803.3249).

Epipyrone triacetate (**6**): Red-orange amorphous solid (1.4 mg). $[\alpha]_D^{20}$ +9.0 (*c* 0.10, MeOH). UV (CH$_3$OH) λ_{max} [nm] (ε [L·mol^{-1}·cm^{-1}]) 345sh (9134), 424 (34163); IR (v_{max}) 3395,

2922, 1728, 1639, 1538, 1440, 1370, 1240 cm^{-1}. ^{1}H-/^{13}C-NMR-data see **table 4.5**. HR-ESI-MS *m/z* 739.3284 [M+H]$^+$ (calcd. for $C_{40}H_{51}O_{13}^+$, 739.3324).

4.4 ACETOSELLIN (4) AND 5´,6´-DIHYDROXYACETOSELLIN (7)

Acetosellin (**4**) is believed to be a polyketide-derived secondary metabolite, which belongs to the widespread fungal subgroup of azaphilonoid compounds [177,178]. A highly oxygenized pyran-quinone core structure is characteristic. A remarkable feature of acetosellin (**4**) is the reduced pyran moiety, since the usually present double bond at C-1 is responsible for the high reactivity regarding primary amines (see **fig. 4.10** and **4.11**) [177,179–181]. The enone partial structure usually acts as a Michael acceptor for the nucleophilic amine group. Depending on the degree of unsaturation in the pyran moiety, either a pyridylidene- or an enamine formation is favored. In the case of epicocconone (**8**), it was shown that reaction with amines only leads to a reversible enamine formation. Though the reactivity of acetosellin (**4**) with regard to amines has not been studied to the best of my knowledge, it can thus be assumed that acetosellin (**4**) is not as reactive under physiological conditions.

Compound **4** was discovered in an extract of the ascomycete *Pseudocercospora acetosellae* (syn. *Cercospora acetosellae*, Mycosphaeraceae, Capnodiales), though only weak bioactivities were reported against *Micrococcus luteus* and *Saccharomyces cerevisiae*, as well as phytotoxic activity [182]. In 2013, a report about the occurrence in an *Epicoccum* sp. CAFTBO, endophytically growing in *Theobroma cacao*, was published [183]. The authors confirmed moderate antibacterial activity.

The biosynthesis of acetosellin (**4**) was subject of a dissertation published in 2007 [184]. However, since the employed strain lost the ability to produce acetosellin (**4**) during these studies, the biosynthetic origin could not be clarified.
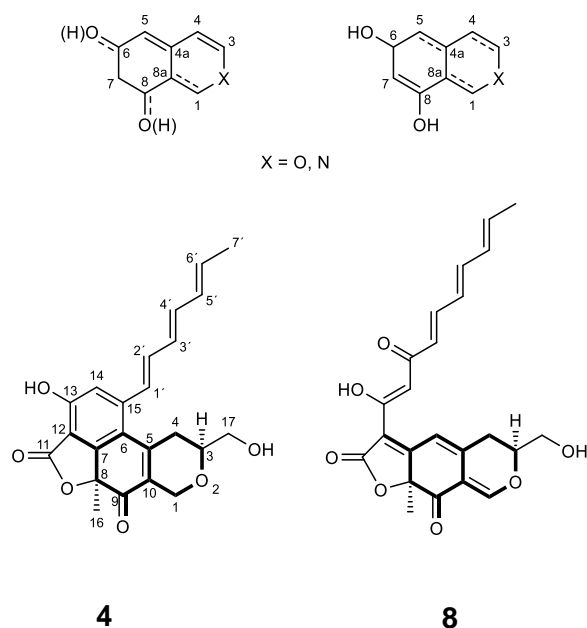
Fig. 4.10: Generic azaphilonoid scaffold (modified from [177]), in comparison with acetosellin (**4**) and epicocconone (**8**). The characteristic core structure is shown in bold for compounds **4** and **8**.
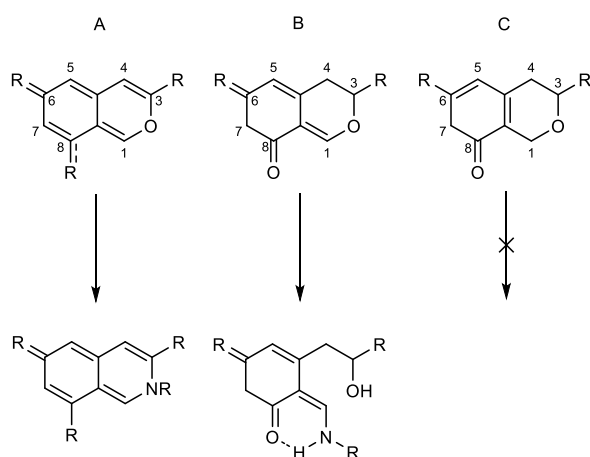
Fig. 4.11: Reactivity of different azaphilonoid scaffolds with ammonia and primary amines (A + B) and proposed diminished reactivity of acetosellin (**4**). Reactions: A = generic azaphilonoid scaffold, *e.g.,* (+)-sclerotiorin; B = epicocconone (**8**) core structure; C = acetosellin (**4**) core structure.

In early cultivation experiments during this study, acetosellin (**4**) was only found as a byproduct in strain 749 grown on different cultivation media. Different approaches to isolate this compound, proved to be cumbersome, yielding minute amounts, which were not sufficient for structure elucidation. Unfavorable chromatographic properties during HPLC and chemical instability are the likely reasons. During the studies on the guttation droplets (see **section 4.7**), a major change in the metabolic pattern was observed: By omitting the TMS supplementation and incubation under constant illumination with artificial light, the fungus was influenced to produce acetosellin (**4**) as major metabolite rather than epipyrones (**1-3**) (see **fig. 4.12,** appendix: **fig. 8.3** and **fig. 8.4**). The acetosellin (**4**) concentration reached ca.

43 wt% in the exploratory crude extract as deduced from the LC-ESI-MS measurement. Additionally, acetosellin (**4**) was found in the agar medium (see appendix: **fig. 8.25**) and in the guttation droplets (also see **section 4.7**).

For the isolation of acetosellin (**4**) this crude extract was harnessed, named 749CDA-h(1). As a consequence, feeding studies on the biosynthesis of acetosellin (**4**) were also carried out under the aforementioned conditions.
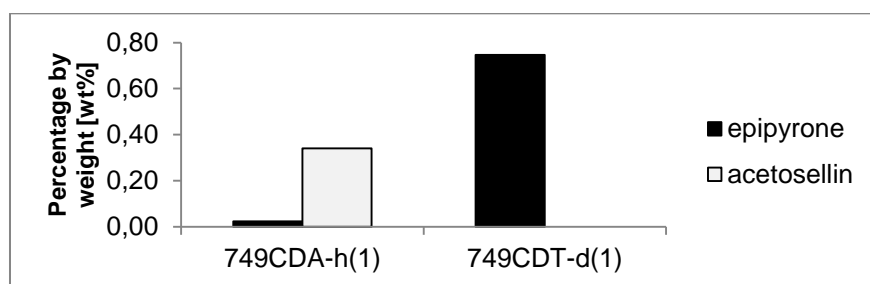
Fig. 4.12: Relative abundance of the main metabolites as calculated from the TWC from LC-MS measurements. Shown are values for acetosellin (**4**) and epipyrones (**1-3**) in the exploratory crude extracts of *E. nigrum* strain 749 on either CDA (Czapek-Dox agar) under continuous illumination with white light or on CDT (Czapek-Dox agar with trace metal solution), grown in darkness. On CDT, acetosellin could not be detected during this cultivation experiment.

4.4.1 ISOLATION PROCEDURE

E. nigrum strain 749 was fermented on 2.5 L of CDA, distributed on 25 petri dishes (for the cultivation and extraction conditions see **sections 3.1.3** and **3.1.4**). 576 mg of a yellow-brown crude extract were separated using flash chromatography (see **section 3.2.6.2**), yielding 15 fractions (see **fig. 4.13**). Fraction 10 ($t_R \approx 14$ min, 80% MeOH/ 20% TFA) proved to be purified acetosellin (**4**, 104 mg, orange solid). In fraction 6, an oxidation product of acetosellin (**4**) in a semi-pure form was detected, dihydroxyacetosellin (**7**, $t_R \approx 10$ min, 6 mg). Epipyrones (**1-3**) were found to be a minor constituent eluting with approximately 95% MeOH (fraction 13, $t_R \approx 16.5$ min).
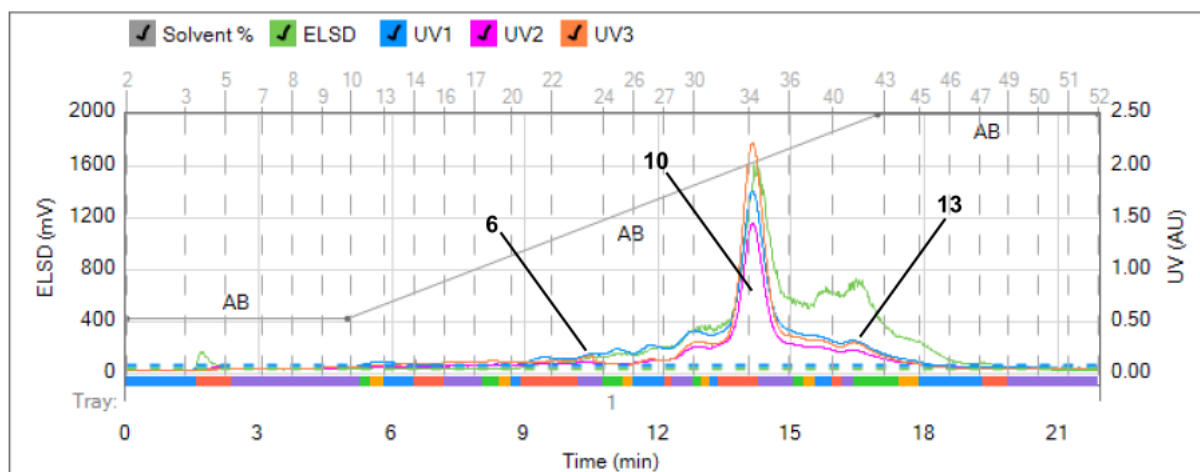
Fig. 4.13: Flash chromatogram from the separation of the defatted crude extract of *E. nigrum* strain 749. Fractions 6 (fraction containing compound **7**), 10 (acetosellin, **4**) and 13 (epipyrones **1**-**3**) are highlighted. Detectors used during this run: ELSD and UV. UV-wavelengths: UV1 = 220 nm, UV2 = 254 nm, UV3 = 340 nm. The solvent gradient is indicated as gray line (AB = composition of the eluents in vol% MeOH). For details see **sections 3.1.3** and **3.2.6.1**.

4.4.2 STRUCTURE ELUCIDATION OF ACETOSELLIN

Comparison of the NMR-data with 1D-NMR values given by Nasini et al. [182] proved to be cumbersome. On the one hand, spectroscopic data were reported without direct assignment to the regarding atoms. On the other hand, deviations of ^{13}C-NMR values for C-10 ($\Delta\delta = 3.3$), C-13 ($\Delta\delta = 9.5$), C-14 ($\Delta\delta = 3.3$) and C-1´ ($\Delta\delta = 5.8$) were higher than expected.

Consequently, the structure of acetosellin (**4**) was deduced from extensive NMR-measurements, using ^{1}H-/^{13}C-NMR, DEPT-135, as well as 2D-NMR-data (see **table 4.6** and **4.7**, **fig. 4.14**). Confirmation of the absolute configuration was achieved by optical rotation measurements and the CD spectrum.
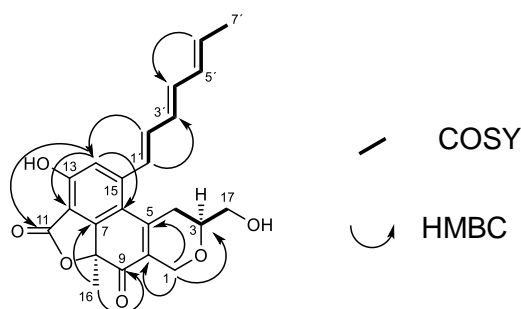
Fig. 4.14: Structure of acetosellin (**4**) showing COSY and key HMBC correlations.

66

Table 4.6: ^{13}C-NMR data of acetosellin (**4**): Comparison of literature values with data from this study. Data were obtained in DMSO-d_6 in both cases. Values with a deviation of Δδ > 2 ppm are marked in bold.

Carbon No.	$δ_C$ [ppm]* according to Nasini et al. [182]	$δ_C$ [ppm] own data
1	63.77	63.8, CH$_2$
3	74.21	74.1, CH
4	32.04	32.0, CH$_2$
5	146.50	145.2, qC
6	117.72	116.5, qC
7	157.78	156.0, qC
8	84.79	84.7, qC
9	196.71	195.7, qC
10	**130.51**	**127.2, qC**
11	164.21	165.6, qC
12	109.03	109.0, qC
13	**146.84**	**156.3, qC**
14	**119.19**	**115.9, CH**
15	144.94	144.6, qC
16	28.78	28.1, CH$_3$
17	63.77	63.6, CH$_2$
1´	**124.24**	**129.0, CH**
2´	134.21	135.4, CH
3´	130.51	130.1, CH
4´	135.44	136.3, CH
5´	131.50	131.7, CH
6´	131.88	132.4, CH
7´	18.18	18.4, CH$_3$

*: Assignment of the data from the given publication was done for this thesis according to best fitting of the values found in this study.

Table 4.7a: NMR-data of acetosellin (**4**), measured in MeOH-d_4, at 300 MHz (^{1}H-NMR) and 75 MHz (^{13}C-NMR), respectively.

Carbon No.	δ_C [ppm] [a,c]	δ_H [ppm] [c], *(J [Hz])*	COSY[c]	HMBC[b,c]
1	65.5, CH$_2$	4.73 (1H$_b$, dd, 17.2; 2.4); 4.35 (1H$_a$, dt, 17.2; 3.0)	1a,4b 1b	3,9,10,15 15
3	75.4, CH	3.73 (1 H, m[†])	17	
4	33.3, CH$_2$	2.84 (1 H$_b$, m); 2.67 (1 H$_a$, d, 17.6)	3,4a,17 1a,4b	15
5	146.7, qC			
6	118.2, qC			
7	157.4, qC			
8	86.6, qC			
9	197.3, qC			
10	128.8, qC			
11	168.3, qC			
12	110.3, qC			
13	157.5, qC			
14	117.2, CH	6.85 (1 H, s)		1´,5,6,11,12,13
15	146.9, qC			
16	28.6, CH	1.83 (3 H, s)		7,8,9
17	65.3, CH$_2$	3.74 (2 H, m[†])	3,4	
1´	129.7, CH	6.99 (1 H, d, 15.0)	2´	3´,13,14,15
2´	137.2, CH	6.69 (1 H, dd, 9.9; 15.0)	1´,3´	4´,15
3´	131.1, CH	6.33 (1 H, dd[†], 9.9; 15.0)	4´,2´	3´
4´	137.9, CH	6.42 (1 H, dd[†], 9.9; 15.0)	3´,5´	5´
5´	132.9, CH	6.17 (1 H, dd, 9.9; 15.0)	4´,6´	4´
6´	133.3, CH	5.86 (1 H, dq, 15.0; 6.8)	5´,7´	4´
7´	18.6, CH$_3$	1.81 (3 H, br d, 6.8)	6´	5´,6´

Data referenced in Mestrenova using MeOH-d_4 signal.

[a] multiplicities deduced from DEPT-135 experiments

[b] numbers refer to ^{13}C resonances

[c] measured in MeOH-d_4

[†] overlapped

Table 4.7b: NMR-data of acetosellin (**4**), measured in DMSO-d_6 or acetone-d_6, at 300 MHz (^{1}H-NMR) and 75 MHz (^{13}C-NMR), respectively.

Carbon No.	δ_C [ppm] [a,d]	δ_H [ppm] [d]; *(J [Hz])*	δ_H [ppm] [e]; *(J [Hz])*
1	63.8 CH$_2$	4.57 (1H, d, 16.5) 4.28 (1H, d, 16.5)	4.65 (1H, d, 15.7) 4.33 (1H, dt, 16.9; 3.5)
3	74.1 CH	3.60 (1H, m [†])	3.71 (H, m)
4	32.0 CH$_2$	2.68 (2H, m)	2.89 (1H, m) 2.74 (1H, br d, 18.0)
5	145.2 qC		
6	116.5 qC		
7	156.0 qC		
8	84.7 qC		
9	195.7 qC		
10	127.2 qC		
11	165.6 qC		
12	109.0 qC		
13	156.3 qC		
14	115.9 CH	6.91 (1H, s)	7.01 (1H, s)
15	144.6 qC		
16	28.1 CH$_3$	1.79 (3H, s [†])	1.83 (3H, s)
17	63.6 CH$_2$	3.57 (2H, m [†])	3.71 (2H, m)
1´	129.03 CH	7.11 (1H, d, 15.0)	7.14 (1H, d, 15.0)
2´	135.4 CH	6.68 (1H, dd, 10.0; 15.0)	6.75 (1H, dd, 10.0; 15.0)
3´	130.1 CH	6.41 (1H, dd, 10.0, 15.0 [†])	6.38 (1H, m)
4´	136.3 CH	6.47 (1H, dd, 10.0, 15.0[†])	6.45 (1H, m)
5´	131.7 CH	6.20 (1H, dd, 10.0; 15.0)	6.16 (1H, dd, 10,0, 15.0)
6´	132.4 CH	5.88 (1H, m)	5.84 (1H, dq, 15.0, 7.0)
7´	18.4 CH$_3$	1.78 (H, d, 7.0[†])	1.76 (3H, br d, 7.0)

Data referenced in Mestrenova using DMSO-d_6 or acetone-d_6 signal, respectively.

[a] multiplicities deduced from DEPT-135 experiments

[d] measured in DMSO-d_6

[e] measured in acetone-d_6

[†] overlapped

Acetosellin (4):   Red-orange amorphous powder (104 mg, 41.6 mg/L). $[\alpha]_D^{20}$ +264 (*c* 0.1, MeOH) [Nasini et al. [182]: $[\alpha]_D^{20}$ +283 (*c* 0.1, MeOH)]. ECD (*c* 0.25 mg/mL, MeOH): λ_{max} (Δ ε) 335 (- 8.1); 214 (+ 9.5) nm; ^{1}H-/^{13}C-NMR-data see **tables 4.6** and **4.7** and **figures 8.26-8.34** in the appendix. HR-ESI-MS *m/z* 412.1762 [M+NH$_4$]$^+$; 395.1483 [M+H]$^+$ (calcd. for C$_{23}$H$_{23}$O$_6^+$, 395.1489); 377.1385 [M-H$_2$O+H]$^+$ (calcd. for C$_{23}$H$_{21}$O$_5^+$, 377.1384).

4.4.3   5´,6´-DIHYDROXYACETOSELLIN

Compound **7** (see **fig. 4.15**) was obtained as the main constituent of a fraction during the isolation process of acetosellin (**4**), eluting with approximately 55% MeOH (see **sections 4.4.1** and **3.2.6.2**). Structure elucidation was performed using mainly 1D- and 2D-NMR measurements. The molecular mass of 428 (Δ = 34 u) already led to the assumption that compound **7** might be a dihydroxylated derivative of acetosellin (**4**). The exact mass confirmed the molecular formula to be $C_{23}H_{25}O_8$, while the hypsochromic shift (Δ = 25 nm) pointed to the shortening of the conjugated polyenic system. Indeed, ^{13}C- and ^{1}H-NMR spectra showed that the alkene signals of C-5´/H-5´ as well as C-6´/H-6´ were missing, compared to the spectra of acetosellin (**4**). In turn, two signals indicative of hydroxymethine functions appeared at δ 3.71/4.06 (^{1}H-NMR) and δ 71.7/77.4 (^{13}C-NMR). Through HMBC and COSY correlations, the side chain was proven to be hydroxylated at C-5´ and C-6´, leading to a vicinal diol partial structure. Comparison of the chemical shift values of all C- and H-atoms confirmed the core structure to be identical with acetosellin (**4**). However, the absolute configuration of C-5´ and C-6´ could not be resolved during this study. In order to elucidate the relative configuration, synthesis of an acetonide at C-5´and C-6´ and subsequent comparison of ^{1}H-NMR coupling constants with literature data could be pursued [185,186]. For the absolute configuration, Mosher´s method [185,187] or X-ray crystallography [188] could be employed. Nevertheless, the configuration at C-8 and C-3 is believed to be identical to acetosellin (**4**), since compound **7** shows the same Cotton effect in the CD-spectrum and is most probably is derived from the latter by oxidation of the terminal double bond (see **fig. 8.44** in the appendix and **section 5.1.2** for the discussion).
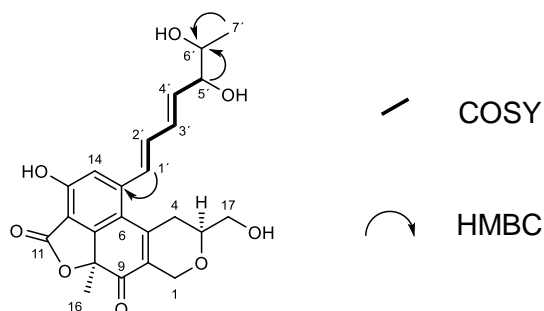
Fig. 4.15: Structure of 5´,6´-dihydroxyacetosellin (**7**) showing COSY and key HMBC correlations.

Table 4.8: NMR-data of 5´,6´-dihydroxyacetosellin (**7**), measured in MeOH-d_4 at 600 MHz (^{1}H-NMR) and 125 MHz (^{13}C-NMR), respectively.

Carbon No.	δ_C [ppm][a,c]	δ_H [ppm][c], (J [Hz])
1	65.5, CH$_2$	4.40 (1 Ha, dt, 17.1; 3.3); 4.78 (1 H$_b$, dd, 2.4; 17.1)
3	75.5, CH	3.72 (1H, m) †
4	33.3, CH$_2$	2.72 (1 H$_a$, br d, 17.6); 2.90 (1 Hb, m)
5	146.6, qC	
6	118.5, qC	
7	157.5, qC	
8	86.6, qC	
9	197.4, qC	
10	129.0, qC	
11	168.3, qC	
12	110.6, qC	
13	157.8, qC	
14	117.8, CH	6.93 (1 H, s)
15	146.9, qC	
16	28.4, CH$_3$	1.88 (1 H, s)
17	65.4, CH$_2$	3.75 (2H, m) †
1´	131.0, CH	7.18 (1 H, d, 15.2)
2´	136.5, CH	6.75 (1 H, dd, 10.2; 15.2)
3´	132.5, CH	6.62 (1 H, dd, 10.2, 15.2)
4´	138.0, CH	6.08 (1 H, dd, 6.5, 15.2)
5´	77.4, CH	4.06 (1 H, m)
6´	71.7, CH	3.75 (2H, m) †
7´	18.9, CH$_3$	1.22 (3 H, d, 6.4)

Data referenced in Mestrenova using MeOH-d_4 signal.

[a] multiplicities deduced from DEPT-135 experiments

[c] measured in MeOH-d_4

† overlapped

5´,6´-Dihydroxyacetosellin (**7**): Yellow amorphous powder (6 mg, 2.4 mg/L). $[\alpha]_D^{20}$ +149.5 (c 0.47, MeOH). UV (CH$_3$OH) λ_{max} [nm] (ε [L·mol^{-1}·cm^{-1}]) 206 (25691), 315 (10816) nm; ECD (c 0.3 mg/mL, MeOH): λ_{max} ($\Delta\,\varepsilon$) 332 (- 8.2), 216 (+ 5.2) nm; IR (v_{max}) 3357, 2914, 2850, 1738, 1694, 1614, 1453, 1261 cm^{-1}. ^{1}H-/^{13}C-NMR-data see **table 4.8**. LC-ESI-HRMS *m/z* 411.1453 [M-H$_2$O+H]$^+$ (calcd. for C$_{23}$H$_{23}$O$_7^+$, 411.1438), 429.1553 [M+H]$^+$ (calcd. for C$_{23}$H$_{25}$O$_8^+$, 429.1544), 446.1794 [M+NH$_4$]$^+$ (calcd. for C$_{23}$H$_{28}$NO$_8^+$, 446.1809).

4.4.4 STUDIES ON THE BIOSYNTHESIS OF ACETOSELLIN (4)

The biosynthesis of azaphilones has been studied in a variety of fungi, most notably in the genera *Penicillium* and *Monascus* (both Aspergillaceae) [189–193]. *Monascus* species are of great interest, since their azaphilonoid pigments (MAzP = Monascus azaphilone pigments [194]) – mainly produced by *M. ruber*, *M. purpureus* and *M. pilosus* – are used in south east Asia as food colorants and are consumed for their alleged health benefits [195]. Traditionally, these species are used for the fermentation of rice, leading to the production of *red mold rice* (RMR, red yeast rice, ang-kak, red koji). RMR is of special importance not only for its azaphilonoid pigments, but for its content of the cholesterol-lowering drug lovastatin [195]. From a toxicological point of view, the capability of the aforementioned genera to produce citrinin as well – a cytotoxic azaphilonoid lacking the extended side chain – is of great concern for the food industry [196].

As of 2015, the full genomes of five different strains in the genus *Monascus* have been sequenced [197]. On the basis of genomic data and labeling studies, a hypothesis was established that azaphilonoids with a side chain similar to acetosellin (**4**) are derived from two distinct polyketide chains. During biosynthesis, an esterification and a following Knoevenagel condensation are responsible for the connection of both parts. Thus, a lactone ring is formed. [177,198–202]. However, the biosynthesis of acetosellin (**4**) could not be resolved in former studies. One attempt by Plitzko et al. [184] failed due to degradation of the cultivated strain and a resulting cessation of acetosellin (**4**) production.

During this study, a successful attempt was made to elucidate the incorporation of precursors by feeding [1-^{13}C]acetate. The results will be discussed in the following section.

4.4.4.1 DETERMINATION OF CULTIVATION CONDITIONS FOR THE LABELING EXPERIMENT WITH *E. NIGRUM*

In order to achieve efficient incorporation of the [1-^{13}C]acetate, experiments on the time course of acetosellin (**4**) production were performed at the beginning. The resulting data are necessary to plan the time points of [1-^{13}C]acetate addition and to estimate the optimal date for harvesting and extraction of the culture. Additionally the consumption of [1-^{13}C]acetate could be reduced by maximizing the yield of the desired product.

To determine the optimal duration of fermentation, *E. nigrum* strain 800 was cultivated and extracted as depicted in **section 3.1.5.1**. The extracts were semi-quantitatively compared via LC-ESI-MS. According to the LC-MS results, the maximum yield of acetosellin (**4**) deploying strain 800 was obtained between two and three weeks (see **table 4.9**).

However, the optimal production of acetosellin (**4**) was observed in test cultures using strain 749 grown on CDA for four weeks. As can be seen in table 4.4, an approximately threefold increase in acetosellin (**4**) production could be achieved. Based on these results, strain 749 growing on CDA was chosen as the production system.

Tab. 4.9: Results of the semi-quantitative analysis of acetosellin (**4**) production by LC-MS for cultures of *E. nigrum* strains 800 and 749. Data were calculated from the TIC by using a mass range from 394 - 396 (**fig. 8.47** in the appendix). Strain 800 was grown on MEN medium, strain 749 was cultivated on CDA. The cultures were extracted with EtOAc after the indicated cultivation period.

E. nigrum strain	Cultivation time [weeks]	Peak area [mAU·s]
800	1	8.0×10^{7}
800	2	1.7×10^{8}
800	3	1.7×10^{8}
800	4	9.8×10^{7}
800	5	4.8×10^{7}
749	4	5.7×10^{8}

Experiences from past cultivations showed that *E. nigrum* grows slower on CDA than on the tested complex media. Therefore, the peak of acetosellin (**4**) production was expected to occur later. A cultivation time of three instead of two weeks was scheduled as compromise in order to yield more product and keep cultivation time limited.

However, strain 800 was still considered for the investigation of new secondary metabolites (see **section 4.5**).

4.4.4.2 CULTIVATION AND FEEDING OF *E. NIGRUM* STRAIN 749 WITH [1-^{13}C]ACETATE

For fermentation, feeding of [1-^{13}C]acetate and extraction of *E. nigrum* strain 749 the protocol mentioned in **section 3.1.5.2** was followed, yielding 111 mg of crude extract.

During the cultivation, exudation of reddish or purple pigments into the medium could be observed. A similar pigmentation was observed for the mycelium, except for young hyphae at the growing front. Additionally, single guttation droplets with orange to dark reddish color appeared at the agar plugs, which were used for the inoculation (see **fig. 4.16**). Above all, phenotype and growth rate were comparable to cultures of strain 749 on pure CDA medium without NaOAc supplementation. In this way, a deleterious effect of precursor addition on the fungus could be excluded already during cultivation.
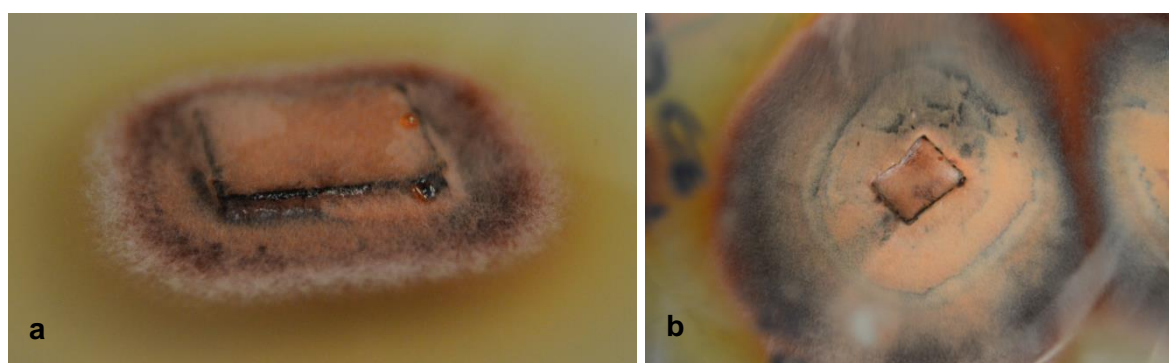
Fig. 4.16: Growth and appearance of a labeling culture of *E. nigrum* strain 749 after 3 days (**a**) and after 21 days of cultivation in Fernbach flasks (**b**). Edge length of agar plugs was ca. 1 cm.

A tentative evidence for successful labeling is given by the LC-ESI-MS data of the crude extract: The chromatogram shows a prominent peak eluting at 18.21 minutes (see **fig. 8.48**), of which the mass (m/z = 395) and UV data (λ_{max} = 340.0 nm) correspond to previous measurements with unlabeled acetosellin (**4**). Additionally, the typical pattern for ^{13}C-labeled metabolites can be identified in the mass spectrum, where the incorporation of at least six ^{13}C-atoms is shown. The remaining ^{13}C-atoms could probably not be resolved due to limited sensitivity of the LC-MS instrument.

4.4.4.3 ISOLATION AND ANALYSIS OF ^{13}C-LABELED ACETOSELLIN (4)

The isolated substance was analyzed via ^{1}H-NMR and ^{13}C-NMR measurements (see **tab. 4.10** and **fig. 4.17**). In order to exclusively see the ^{13}C-enriched atoms, a small number of scans (194 scans) was carried out for the ^{13}C-NMR spectrum. Through comparison of data from the original substance and the ^{13}C-labeled compound, incorporation of eleven [1-^{13}C]acetate units could be confirmed. The alternating labeling pattern complemented this observation.

Tab. 4.10: NMR spectroscopic data of ^{13}C-labeled acetosellin (**4**), measured in MeOH-d_4 at 300 MHz or 75 MHz for ^{13}C-NMR, respectively. The ^{13}C enriched carbons are in bold print.

Carbon No.	δ_C [ppm]	δ_H [ppm] (*J* in Hz)	δ_C [ppm]^a
1	**65.5, CH$_2$**	a 4.76, d (17.2) b 4.38, d (17.2)	65.5, CH$_2$
3	**75.4, CH**	3.73, m	75.4, CH
4	33.3, CH$_2$	a 2.89, m b 2.70, d (17.6)	33.3, CH$_2$
5	**146.7, qC**		146.7, qC
6	118.2, qC		118.2, qC
7	**157.5, qC**		157.4, qC
8	86.6, qC		86.6, qC
9	**197.4, qC**		197.3, qC
10	128.8, qC		128.8, qC
11	**168.3, qC**		168.3, qC
12	110.3, qC		110.3, qC
13	**157.6, qC**		157.5, qC
14	117.3, CH	6.91, s	117.2, CH
15	**147.0, qC**		146.9, qC
16	28.5, CH$_3$	1.86, s	28.6, CH$_3$
17	65.3, CH$_2$	3.73, m	65.3, CH$_2$
1'	129.7, CH	7.08, d (15.0)	129.7, CH
2'	**137.3, CH**	6.74, dd (9.9, 15.0)	137.2, CH
3'	131.1, CH	6.43, m	131.1, CH
4'	**137.9, CH**	6.46, m	137.9, CH
5'	132.9, CH	6.23, dd (9.9, 15.0)	132.9, CH
6'	**133.3, CH**	5.90, dq (15.0, 7.0)	133.3, CH
7'	18.6, CH$_3$	1.84, m	18.6, CH$_3$

^{a}: unlabeled acetosellin (**4**)
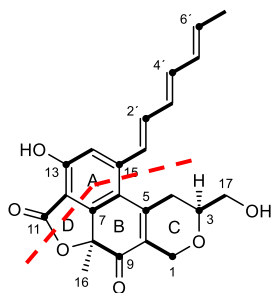
Fig. 4.17: Structure of acetosellin (**4**) with ^{13}C labeling pattern. Bold dots indicate incorporated ^{13}C-atoms. The dashed red lines indicate the two different polyketide units, from which the product presumably originates.

4.4.4.4 SIGNIFICANCE OF THE ^{13}C-LABELING PATTERN

After analysis of the NMR spectroscopic data from the feeding experiment with sodium [1-^{13}C]acetate, eleven ^{13}C-enriched carbons and a pattern of [1-^{13}C]acetate incorporation into acetosellin (**4**) as depicted in **fig. 4.17** were revealed. Thus, the pattern proposed by Plitzko in 2007 [184] could be confirmed.

As a consequence of the incorporation pattern, following conclusions can be drawn: The biosynthesis of the pentaketide unit starting from C-17 through to C-1 forms ring B and C. During the synthesis, two hydroxylations would have to take place to form the hydroxy groups at C-8 and C-17. Condensation between C-10 and C-5 would lead to the formation of ring B, whereas the C-ring would likely be the result of acetal formation and subsequent dehydratation (see **section 5.1.2** for a detailed scheme and further explanations). The methyl group at C-8 presumably arises from methylation via S-adenosyl methionine (SAM) already during chain elongation.

This notion is supported by two observations: First, methylation of polyketides by SAM takes place at the methylene carbon in α-position to the thiolester of the growing chain [203]. In the case of acetosellin (**4**), C-8 does not show ^{13}C-labeling and consequently must have originated from a methylene group during chain elongation. C-16 of the methyl group neither is part of the polyketide backbone nor does it show ^{13}C-labeling. Second, the same methylation pattern and the responsible methyltransferases have been reported as part of the biosynthetic gene clusters of citrinin, azanigerone and the azaphilonoid *Monascus* pigments [177,201,202].

The biosynthesis of the hexaketide unit starting from C-7' through to C-11 and the interconnection with the pentaketide probably leads to the formation of ring A and D. During synthesis, the keto groups at C-6', C-4' and C-2' would have to be reduced to form a conjugated triene with double bonds at C-6', C-4' and C-2'. The carbonyl group at C-13 is enolized.

Both polyketide units would be interconnected at two positions. First, the hydroxy group at C-8 and the carboxylic group at C-11 would undergo an esterification. An additional Knoevenagel condensation between C-12 and the keto group at C-7 would form the γ-lactone ring D, yielding epicocconone (**8**). Another aldol condensation between C-6 and the keto group at C-15 would build the aromatic ring A, leading to the final product, acetosellin (**4**).

4.5   OTHER SECONDARY METABOLITES FOUND IN THIS STUDY

4.5.1.   POLYKETIDES

4.5.1.1   EPICOCCOLIDE B (**9**)
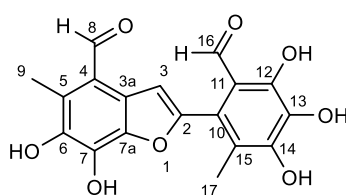
Fig. 4.18: Structure of epicoccolide B (**9**).

Epicoccolide B (**9**) was isolated twice from *E. nigrum* strain 800 following the protocol described in **section 3.2.6.5**. Through comparison of LC-MS data, epicoccolide B (**9**) could be shown to be present in cultures of strain 800 grown on malt extract under different conditions. Through HR-MS measurements of crude extracts from strain 749 grown on CDA (Czapek-Dox agar) medium, compound **9** was also identified. Furthermore, it is excreted into guttation droplets by strain 749, growing on this medium (see **section 4.7** for details).

Structure elucidation of epicoccolide B (**9**) was accomplished through comparison of literature data [183,204] with ¹H- and ¹³C-NMR measurements, mass spectrometry and UV-data.

Epicoccolide B (9): yellow solid (first isolation: 1.3 mg, 4 mg/mL; second isolation: 4.8 mg, 3.4 mg/mL); UV (CH₃OH), λ$_{max}$ [nm] (taken from HPLC-separation): 363, 307, 241; ¹H NMR (300 MHz, DMSO-*d₆*) δ 10.39 (s, H-8), 9.46 (s, H-16), 7.46 (s, H-3), 2.57 (s, H₃-9), 2.00 (s, H₃-17); ¹³C NMR (75 MHz, DMSO-*d₆*) δ 194.8 (C-16, CH), 190.1 (C-8, CH), 151.8 (C-2, qC), 151.6 (C-14, qC), 150.2 (C-12, qC), 142.4 (C-7a, qC), 141.1 (C-6, qC), 136.5 (n.d.), 132.7 (C-13, qC), 127.3 (C-5, qC), 125.0 (C-10, qC), 122.9 (C-3a, qC), 118.8 (C-15, qC), 116.9 (C-4, qC), 112.6 (C-11, qC), 109.0 (C-3, CH), 12.8 (C-17, CH₃), 11.1 (C-9, CH₃); LC-ESI-MS *m/z* 359 [M+H]⁺ (calcd. for $C_{18}H_{15}O_8^+$, 359.1).

4.5.1.2   (3*R*,4*S*)-4-HYDROXYMELLEIN (**10**)
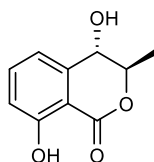
Fig. 4.19: Structure of (3*R*,4*S*)-4-hydroxymellein (**10**).

Retention time, mass fragments and UV maxima obtained by LC-ESI-MS analysis of the flash fractions 4 and 5 already indicated that these fractions contained 4-hydroxymellein (**10**, see also **section 3.2.6.4**), an isocoumarin that was isolated from previously from another strain of *E. nigrum* in this institute [205]. Comparison of ¹H NMR and ¹³C NMR spectra (see appendix) with literature data confirmed the structure. The optical rotation determined for **10** matched the literature data for (3*R*,4*S*)-4-hydroxymellein (**10**) [206,207].

(3*R*,4*S*)-4-hydroxymellein (10): amorphous solid (2.0 mg); $[\alpha]_D^T$ = -27.6 (c 0.001); ¹H NMR (300 MHz, DMSO-*d₆*) δ 10.87 (s, 8-OH), 7.61 (dd, *J* = 7.7, 8.0 Hz, H-6), 7.05 (d, *J* = 7.7 Hz, H-7), 6.94 (d, *J* = 8.4 Hz, H-5), 6.13 (br s, 4-OH) 4.55 (m, H-3, H-4), 1.39 (d, *J* = 4.8 Hz, H₃-11); ¹³C NMR (75 MHz, DMSO-*d₆*) δ 168.1 (C-1, qC), 160.5 (C-8, qC), 143.7 (C-10, qC), 136.6 (C-6, CH), 116.5 (C-7, CH), 116.2 (C-5, CH), 106.9 (C-9, qC), 79.8 (C-3, CH), 69.5 (C-4, CH), 17.7 (C-11, CH₃); LC-ESI-MS *m/z* 195 [M+H]⁺ (calcd. for $C_{10}H_{10}O_4^+$, 195.07).

4.5.1.3 EPICOCCONE (11)
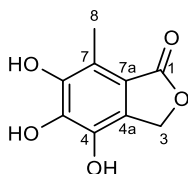
Fig. 4.20: Structure of epicoccone (11).

Fractionation of the crude extract from *E. nigrum* strain 749 – grown on MES – yielded 2.7 mg of compound **11** (see **section 3.2.6.1** for details). The ^{13}C-NMR spectrum already indicated the presence of six aromatic carbons and one carbonyl group, pointing to the presence of an orsellinic acid derivative. Comparison of the NMR spectral data with published data from Abdel-Lateff et al. [205,208] proved the structure to be identical with the phthalide epicoccone (**11**), which was isolated before from the culture of the marine-derived strain *Epicoccum* sp. 353.

Epicoccone (11): greyish-white solid: ^{1}H NMR (300 MHz, MeOH-d_4): δ 5.15 (s, H$_2$-3), 2.44 (s, H-8); ^{13}C NMR (75 MHz, MeOH-d_4): δ 174.6 (C-1, qC), δ 146.2 (C-6, qC), δ 141.4 (C-5, qC), δ 138.0 (C-4, qC), δ 127.9 (C-4a, qC), δ 118.3 (C-7, qC), δ 114.0 (C-7a, qC), δ 68.0 (C-3, CH$_2$), δ 9.7 (C-8, CH$_3$); LC-ESI-MS *m/z* 195 [M-H]$^-$ 151 [M-H-CO$_2$]$^-$ (calcd. for C$_9$H$_9$O$_5^+$: 195.0).

4.5.1.4 1F4-1-6 (12)
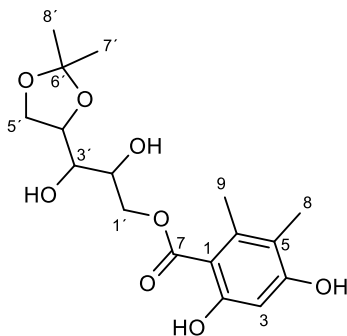
Fig. 4.21: Structure of 1F4-1-6 (12).

The molecular mass of compound **12** (see **fig. 4.21**, for details of the isolation see **section 3.2.6.1**) was deduced to be $C_{17}H_{24}O_8$ by high resolution mass spectrometry, implying six degrees of unsaturation. UV absorption maxima (265 nm, 304 nm) pointed to the presence of an aromatic moiety. Indeed, ^{13}C-NMR data (recorded in MeOH-d_4) showed characteristic resonances for five aromatic carbon atoms (see **table 4.13**), of which one (C-2) was strongly deshielded and thus hypothesized to carry a hydroxyl-substituent. Since one signal from the aromatic moiety could not be observed in MeOH-d_4, additional 1D- and 2D-NMR measurements were undertaken in acetone-d_6, revealing the presence of an aromatic carbon atom (C-4). The chemical shift value (δ 160.5) is in a similar range as for C-2. Accordingly, a dihydroxy phenyl partial structure was assumed. Since only one singlet in the downfield region (H-3) was observed in the ^1H-NMR, three further substituents had to be attributed to the ring system. Extensive 2D-NMR measurements confirmed a spin system consisting of the aromatic moiety, substituted with two hydroxy functions, two methyl groups and one carboxylic ester group. HMBC correlations and comparison of the chemical shift values with calculated values, proved the partial structure to be 5-methyl orsellinic acid. The second spin system – connected to the 5-methyl orsellinic acid moiety – was revealed to be a linear pentitol mainly by its COSY correlations, while the ester bond between C-1´ and C-7 was established by HMBC correlations (see **fig. 4.22**). Finally, the third spin system (C-6´, C-7´, C-8´) showed HMBC correlations to C-5´and C-6´, thus allowing to conclude the presence of an acetonide substructure. However, the configuration at the three chiral centers (C-2´, C-3´, C-4´) could not be resolved, since the substance was lost during an attempt to hydrolyze the ester function.

Literature search did not reveal a report about this specific compound. However, in 2012 Talontsi et al. [209] reported the isolation of paeciloside A (see **fig. 5.11**) in the fungal strain *Paecilomyces* sp. CAFT156 (Trichocomaceae, Eurotiales), including its absolute configuration. Comparison of the NMR-data to compound **12** show a similar pattern and thus confirm the structure. For paeciloside A, weak activity against gram-positive bacteria and cytotoxicity against *Artemia salina* were demonstrated.
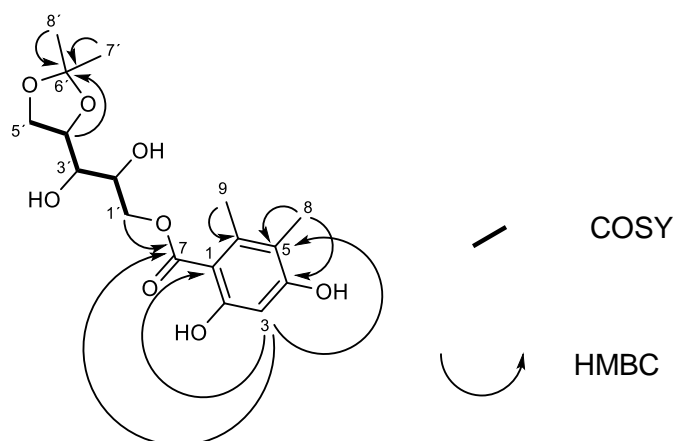
Fig. 4.22: Structure of 1F4-1-6 (**12**) showing COSY and key HMBC correlations.

Tab. 4.13a: NMR-Data for 1F4-1-6 (**12**), obtained in MeOH-d_4.

Carbon No.	δ_C [ppm] [a,c]	δ_H [ppm] [c], (J [Hz])	COSY [c]	HMBC [b,c]
1	108.1, qC			
2	161.3, qC			
3	101.0, CH	6.25 (1 H, s)	8	1,2,5,7
4	n.d.			
5	117.4, qC			
6	141.0, qC			
7	172.6, qC			
8	11.5, CH$_3$	2.10 (3 H, s)	3,9	1,4[*],5,6
9	19.0, CH$_3$	2.45 (3 H, s)	8	2,5,6
1′	67.1, CH$_2$	a: 4.40 (1 H, dd, 5.9; 11.2); b: 4.45 (1H,dd, 7.0, 11.2)		7,2′,3′ 7,2′,3′
2′	69.6, CH	4.14[†] (1 H, m)	1′,3′	1′,4′
3′	73.1, CH	3.60 (1 H, dd, 1.7; 8.0)	4′	1′,4′
4′	76.7, CH	4.23 (1 H, dt, 8.0; 6.0)	3′	5′,6′
5′	68.2, CH$_2$	a: 4.00 (1 H, dd, 6.0, 8.4); b: 4.15[†] (1 H, m)	4′	4′,6′ 4′,6′
6′	110.4, qC			
7′	25.6, CH$_3$	1.37 (3 H, s)		6′
8′	27.1, CH$_3$	1.40 (3 H, s)		6′

referenced in Mestrenova using MeOH-d_4 signal.
[a] multiplicities deduced from DEPT-135 experiments
[b] numbers refer to ^{13}C resonances
[c] measured in MeOH-d_4 (300 MHz)
n.d. = not detected, signal was observed solely in acetone-d_6. [†] overlapped

Tab. 4.13b NMR-Data for 1F4-1-6 (**12**), obtained in acetone-d_6.

Carbon No.	δ_C [ppm] [a,d]	δ_H [ppm] [d]; (J [Hz])
1	107.1, qC	
2	161.0, qC	
3	101.0, CH	6.32 (1 H, s)
4	160.5, qC	
5	117.0, qC	
6	141.4, qC	
7	172.0, qC	
8	11.6, CH$_3$	2.07 (3 H, s)
9	19.1, CH$_3$	2.44 (3 H, s)
1´	67.2, CH$_2$	a: 4.40 (1 H, m) b: 4.45 (1H, m)
2´	69.2, CH	4.14[†] (1 H, m)
3´	72.8, CH	3.60 (1 H, dd, 2.0; 8.2)
4´	76.3, CH	4.17[†] (1 H, m)
5´	67.7, CH$_2$	a: 3.97 (1 H, dd, 5.8; 8.4) b: 4.07 (1 H, dd, 6.2; 8.4)
6´	109.5, qC	
7´	25.6, CH$_3$	1.27 (3 H, s)
8´	27.1, CH$_3$	1.32 (3 H, s)

referenced in Mestrenova using MeOH-d_4 signal.
[a] multiplicities deduced from DEPT-135 experiments
[b] numbers refer to ^{13}C resonances
[d] measured in acetone-d_6 (500 MHz)
[†] overlapped

1F4-1-6 (12): pale yellow solid (2.4 mg): $[\alpha]_D^T$ = +20.0 (c 0.18); UV (CH$_3$OH), λ_{max} [nm] (ε [L·mol^{-1}cm^{-1}]): 304 (11448), 265 (21046); IR (ν_{max}) 3345, 2927, 1704, 1644, 1608 cm^{-1}; ^{1}H and ^{13}C NMR (**tab. 4.13**); HR-ESI-MS *m/z* 379.1362 [M+Na]$^+$ (calcd. for C$_{17}$H$_{24}$NaO$_8^+$: 379.1363).

4.5.2 TERPENOIDS

4.5.2.1 EPICARONIC ACID (**13**)
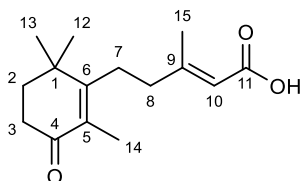
Fig. 4.23: Structure of epicaronic acid (**13**).

Epicaronic acid was isolated from an extract of strain 800, following the method described in **section 3.2.6.5**. The 1D- and 2D-NMR measurements revealed the presence of 15 carbon atoms, including four methyl, four methylene, one methine group and six quaternary centers (see **table 4.14**).

The chemical shift values for C-4 (δ 201.3) and C-11 (δ 170.1) pointed to the presence of a ketone and a carboxylic acid moiety.

The ^{1}H-^{1}H COSY spectrum revealed two spin systems: H_2-2 and H_2-3 as well as H_2-7, H_2-8, H-10 and H_3-15. The small proton coupling constant between H-10 and H_3-15 indicated a long-range coupling through the $^{9,10}\Delta$ double bond and therefore the presence of one sp^2-hybridized quaternary carbon, *i.e.,* C-9. The double bond between C-9 and C-10 was confirmed to be *E*-configured through NOESY correlations between H-10 and H_2-8/H_3-14.

^{1}H-^{13}C HMBC indeed proved C-9 to be the quaternary center between C-8, C-10 and C-15. Additionally, this measurement confirmed most of the acyclic fragment reaching from C-7 to C-15. Furthermore, a six-membered carbon cyclic moiety with the methyl groups C-12 and C-13 both attached to the sp^3 quaternary carbon C-1, a keto function (C-4, δ 201.3) and the methyl group C-14 attached to the sp^2 quaternary carbon C-5, could be established. The HMBC correlations (see **fig. 4.24**) originating from H_2-7, H_2-8, H_3-12, H_3-13 and H_3-14 suggested a connection of the acyclic fragment with the six-membered carbon ring at C-6.

Finally, the quaternary carbon C-11 had yet to be assigned to the structure. A chemical shift value of C-11 in the ^{13}C NMR (δ 170.1) pointed to a carboxylic acid moiety. Since the signal of C-9 was shifted downfield (δ 160.2) and an HMBC correlation of H_3-15 to C-11 was observed, the conclusion was that C-11 is connected to C-10.

The final proof of the proposed structure was achieved through UV, IR and MS analyses. The UV spectrum showed two maxima at 217 and 244 nm; the IR spectrum suggested the presence of alkenes (1644 cm^{-1}) as well as at least one carbonyl group (1694 cm^{-1}). HR-ESI-MS analysis confirmed the chemical formula to be $C_{15}H_{22}O_3$.

Despite extensive search, no literature describing compound **13** could be found, rendering this a new metabolite, named epicaronic acid.
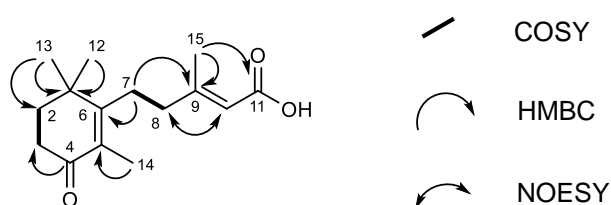
Fig. 4.24: Structure of epicaronic acid (**13**) showing key COSY and HMBC correlations.

Table 4.14: NMR-data for epicaronic acid (**13**) in MeOH-d_4.

No.	δ_C	δ_H (mult, J in Hz)	COSY	HMBC
1	38.3, qC			
2	37.6, CH$_2$	1.89 (2 H, m)	3	1,4,6,7
3	35.1, CH$_2$	2.52 (2 H, t, 6.9)	2	1, 2,4
4	201.3, qC			
5	132.2, qC			
6	166.4, qC			
7	30.2, CH$_2$	2.50 (2 H, m)	8	1,5,6,8,15
8	40.4, CH$_2$	2.35 (2 H, m)	7	6,7,9,10,15
9	160.2, qC			
10	117.1, CH	5.79 (1 H, q, 1.5)	8, 15	15
11	170.1, qC			
12	27.1, CH$_3$	1.26 (3 H, s)		1,2,6,7
13	27.1, CH$_3$	1.26 (3 H, s)		1,2,6,7
14	11.7, CH$_3$	1.82 (3 H, s)		2,4,5,6,8,12,13
15	18.8, CH$_3$	2.26 (3 H, d, 1.5)	8,10	8,9,10

referenced in Mestrenova using MeOH-d_4 signal.
[a] multiplicities deduced from DEPT-135 experiments
[b] numbers refer to ^{13}C resonances

Epicaronic acid (13): yellowish solid (2.7 mg); UV (CH$_3$OH) λ_{max} [nm] (ε [L·mol^{-1}·cm^{-1}) 246 (7055), 217 (7124); IR (ν_{max}) 2926, 1694, 1644, 1443, 1354, 1201, 1137, 1087, 649 cm^{-1}; ^{1}H and ^{13}C NMR (**tab. 4.14**); HR-ESI-MS *m/z* 273.1461 [M+Na]$^+$ (calcd for C$_{15}$H$_{22}$O$_3$Na$^+$, 273.1467).

4.5.2.2 TRICINONOIC ACID (**14**)
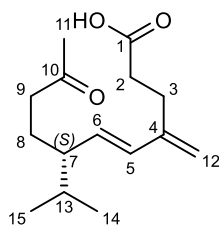
Fig. 4.25: Structure of tricinonoic acid (**14**).

Comparison of the 1D-NMR data (see appendix), molecular mass and the optical rotation proved the structure of **14** (see **fig. 4.25**) to be tricinonoic acid [210], which was found before

in an endophytic *Fusarium tricinctum* (Nectriaceae, Hypocreales) . A second report mentioned the occurrence in an *Hamigera* species (Trichocomaceae, Eurotiales) [211].

Tricinonoic acid (14): light brown solid (1.5 mg); $[\alpha]_D^T$ = +7.3 (c 0.0004, MeOH); ^{1}H NMR (300 MHz, MeOH-d_4) δ 6.06 (d, *J* = 15.7 Hz, H-5), 5.50 (dd, *J* = 9.2, 15.7 Hz, H-6), 4.97 (br s, H_2-12), 2.53 (m, H_2-3), 2.50 (m, H_2-2), 2.45 (m, H_2-9), 2.14 (s, H_3-11), 1.82 (m, H-7, H_2-8), 1.64 (m, H-13), 0.95 (d, *J* = 6.6 Hz, H_3-14), 0.91 (d, *J* = 6.6 Hz, H_3-15); ^{13}C NMR (75 MHz, MeOH-d_4) δ 212.2 (C-10, qC), 177.6 (C-1, qC). 146.2 (C-4, qC), 134.5 (C-5, CH), 133.0 (C-6, CH), 114.6 (C-12, CH_2), 51.0 (C-7, CH), 42.6 (C-9, CH_2), 34.5 (C-2. CH_2), 33.6 (C-13, CH), 30.0 (C-11, CH_3), 28.7 (C-3, CH_2), 21.2 (C-14, CH_3), 19.7 (C-15, CH_3); LC-ESI-MS *m/z* 253.1 [M+H]$^+$ (calcd. for $C_{15}H_{25}O_3$, 253.18).

4.5.3. FLAZIN (15)
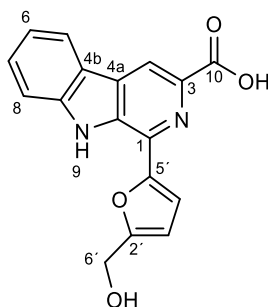
Fig. 4.26: Structure of flazin (**15**).

Fractionation of the crude extract of *E. nigrum* strain 800, grown on MEN, afforded 1.2 mg of flazin (**15**, see **fig. 4.26**). Comparison of the NMR-results and the molecular mass with data reported by Shabaan et al. [212] proved the structure to be flazin. However, flazin was already found to be a constituent of the pure medium:

In order to distinguish medium-derived background signals from fungal metabolites, two extracts were prepared during this study. A: 2 L MES medium (after autoclaving). B: 40 g of commercial malt extract (without autoclaving). Extraction was performed as described in **section 3.1.5.1**.

LC-ESI-MS analysis (see appendix) and ^{1}H-NMR measurement of non-autoclaved malt extract already showed the typical retention time, molecular mass, UV spectrum and ^{1}H NMR resonances for flazin, indicating its presence in commercial malt extract.

Flazin (15): yellow solid: ^{1}H NMR (300 MHz, DMSO-d_6): δ 8.84 (s, H-4), 8.42 (d, J = 8.4 Hz, H-5), 7.83 (d, J = 8.0 Hz, H-8), 7.65 (t, J = 7.6 Hz, H-7), 7.42 (d, J = 3.0 Hz, H-4´), 7.35 (t, J = 7.5 Hz, H-6), 6.63 (d, J = 3.4 Hz, H-3´), 4.68 (s, H$_2$-6´); ^{13}C NMR (75 MHz, DMSO-d_6): δ 168.4 (C-10, qC), δ 159.1 (C-2´, qC), δ 153.1 (C-5´, qC), δ 143.3 (C-8a, qC), δ 134.3 (C-1, qC), δ 133.7 (C-9a, qC), δ 131.7 (C-3, qC), δ 130.7 (C-7, CH), δ 123.9 (C-5, CH), δ 122.8 (C-4a, qC), δ 122.8 (C-4b, qC), δ 122.4 (C-6, CH), δ 117.6 (C-4, CH), δ 114.7 (C-8, CH), δ 112.9 (C-4´, CH), δ 111.1 (C-3´, CH), δ 57.8 (C-6´, CH$_2$); HR-ESI-MS m/z 309.0868 [M+H]$^+$ (calcd. for $C_{17}H_{13}N_2O_4^+$: 309.0870).

4.6 BIOACTIVITIES OF THE ISOLATED METABOLITES

4.6.1 INHIBITION OF CEREBROSIDE-SULFOTRANSFERASE (CST)

During this work, small molecules were tested by Isabell Zech (working group Prof. Gieselmann, Institute for Biochemistry and Molecular Biology, University of Bonn) for their inhibitory activity against hCST using a radioactivity-based assay (see **section 3.5.3** for the method). Epipyrones (**1-3**) showed significant inhibition of this enzymatic target, with an IC$_{50}$-value of 61.4 µM (see **fig. 4.27**).
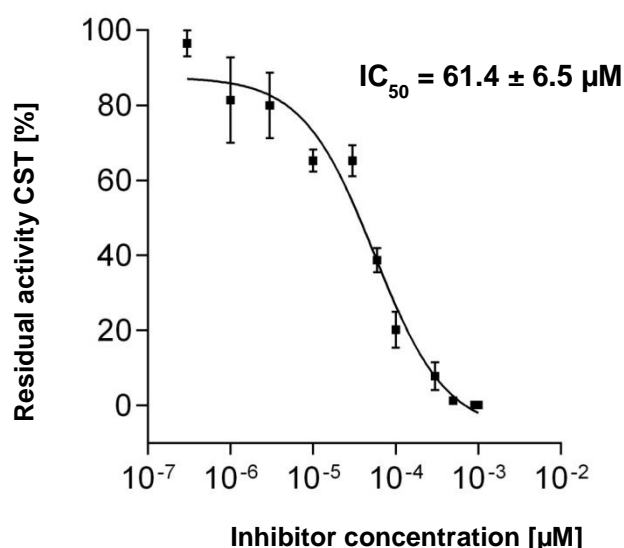
Fig. 4.27: Inhibitory activity of epipyrones (**1-3**) on human cerebroside sulfotransferase (hCST). The assay was performed in duplicates on three days, respectively. The mean values are given with the standard deviation. Assay performed by I. Zech (working group Prof. Gieselmann).

Since epipyrones (**1-3**) were the first inhibitory compounds on this target, more in-depth studies on structure-activity relationships (SAR) were attempted. The structural similarity of the *C*-glycosyl moiety in epipyrones (**1-3**) with the physiological substrate prompted us to undertake a semisynthetic derivatization of epipyrones (**1-3**). Therefore the *C*-galactosyl moiety was acetylated as described in **sections 3.4** and **4.3.2**. The two products **5** and **6** were both probed for their effect on hCST activity (see **fig. 4.28** and **fig. 4.29**): At the concentrations tested – 100 µM and 200 µM – compound **5** exhibited diminished inhibitory potential (100 µM: 61.3%; 200 µM: 42.3% residual activity), compared to epipyrones (**1-3**) (100 µM: 43.3%; 200 µM: 10.2% residual activity). This was also seen for compound **6** (88.4% residual activity at 100 µM) and confirmed that acetylation of the *C*-galactosyl-moiety decreases the activity towards hCST in comparison with epipyrones (**1-3**, 18.2% residual activity).

Since acetylation of the *C*-galactosyl moiety in epipyrones (**1-3**) leads to a marked decrease of inhibitory activity on hCST, a correlation between this moiety and bioactivity on this target seems obvious.

In order to rule out the possibility that only the *C*-glycosyl unit is necessary to inhibit the enzyme, pure β-D-galactose was tested (see appendix). However, no inhibitory activity was observed (see **fig. 8.87** in appendix).

Finally, a search for analogous substances to the epipyrones (**1-3**) was performed via the database ´Zinc´ [213]. One of the compounds – citreoviridin C (see **fig. 4.28**) – was found to exhibit comparable activity as epipyrones (**1-3**, IC_{50} = 58.56 µM, see **fig. 8.88** in appendix for details). Citreoviridins are polyketides of fungal origin, found in *Penicillium* spp. [214] and *Aspergillus* spp. [215].

β-D-galactose   citreoviridin C
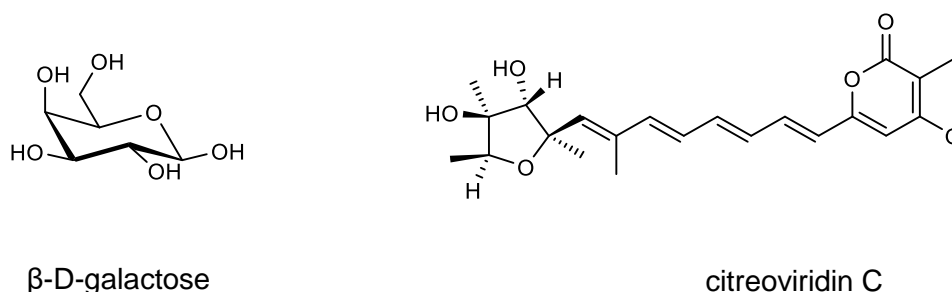
Fig. 4.28: Structures of β-D-galactose and citreoviridin C [215], both tested for their inhibitory effects against hCST.

In conclusion, the galactosyl moiety in the epipyrones (**1-3**) is crucial for the bioactivity, probably as a hydrophilic head group, but it is not solely responsible for the observed

inhibitory activity at the hCST. The two hydrophilic end portions, connected by a rigid polyenic spacer are common structural features of both inhibitors, epipyrones (**1-3**) and citreoviridin C. The exact role of different structural moieties remains unknown. Further studies would be needed to reveal the complete structure activity relationships.

After succeeding in characterizing the first inhibitor for the hCST, *i.e.*, epipyrones (**1-3**), more secondary metabolites from *E. nigrum* were tested for their inhibitory potential (see **fig. 4.31**). Compounds **10**, **13**, **14** and **15** showed weak or no inhibition of hCST at a concentration of 100 µM.

While acetosellin (**4**) showed a stronger inhibitory activity (11.9% residual activity) when compared to epipyrones (**1-3**), the results for compound **4** were not reproducible when retested with a second sample of compound (**4**). This led to the assumption that the observed inhibition may have been an experimental artefact. Another explanation could be the instability of acetosellin (**4**), which became apparent during purification by HPLC (see **section 3.2.6.2**).

Overall, the importance of natural products in the search for inhibitors of hCST could be demonstrated, since epipyrones (**1-3**) were proven to be the first inhibitors of this target. Further work will be needed to establish molecular tools or lead structures for research and therapy.
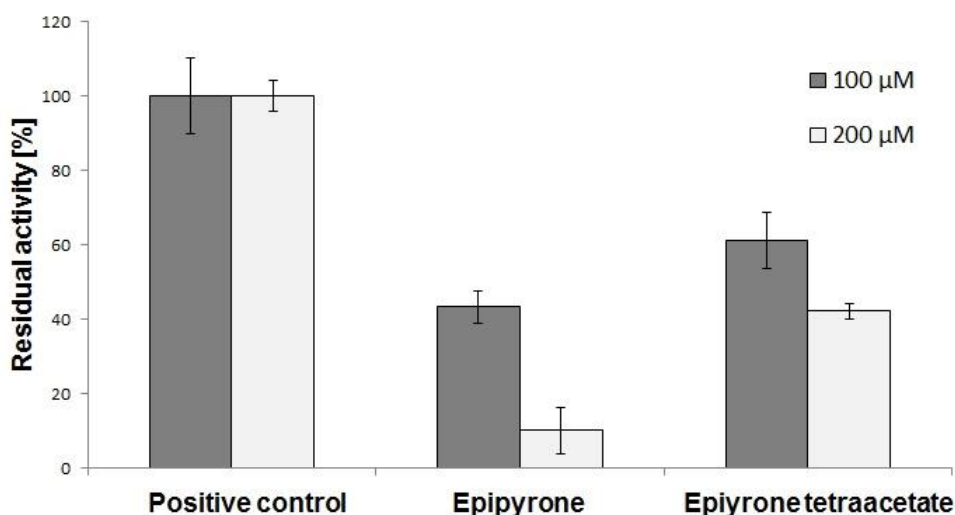
Fig. 4.29: Inhibitory activity of epipyrones (**1-3**) and epipyrone tetraacetate (**5**) on human cerebroside sulfotransferase (hCST). The assay was performed in triplicates. For the positive control, the assay was carried out without inhibitor. The mean values are given with the standard deviation. Assay performed by I. Zech (working group Prof. Gieselmann).
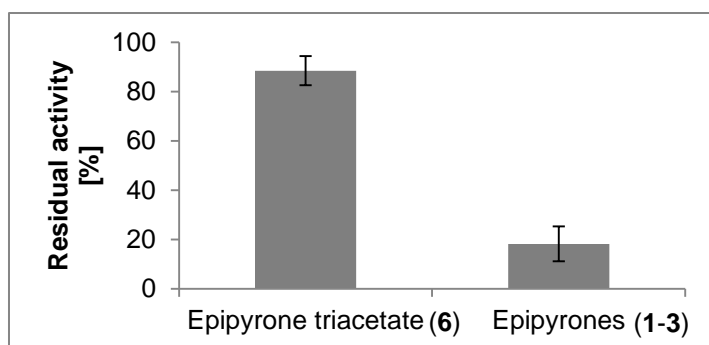
Fig. 4.30: Inhibitory activity of compound **6** (epipyrone triacetate) on human cerebroside sulfotransferase (hCST) at a concentration of 100 µM, compared with that of epipyrone (**1-3**). Inhibitory activity is given as residual activity of the tested enzyme in %. Assay was performed in duplicates on two days, respectively. The mean values are given with the standard deviation. Assay performed by I. Zech (working group Prof. Gieselmann).
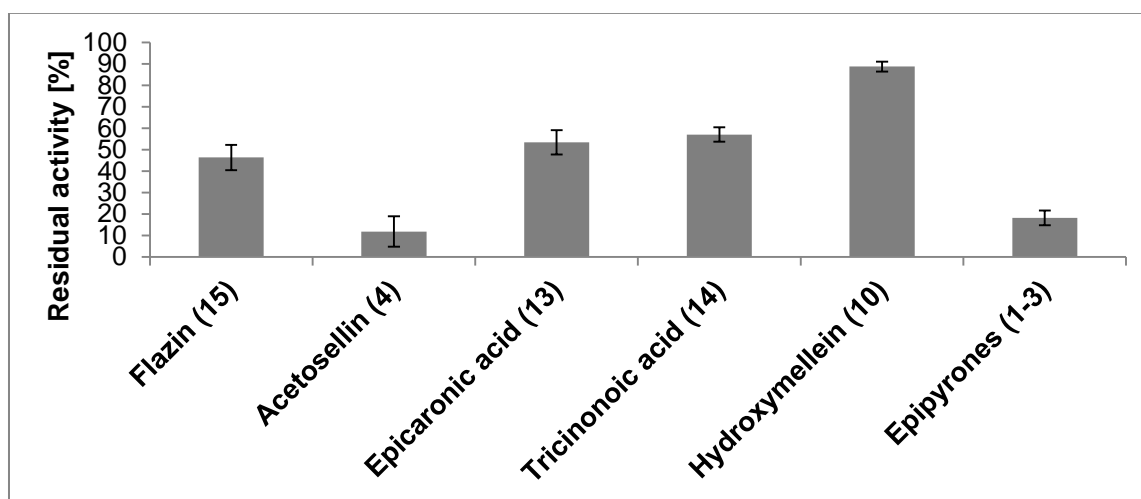
Fig. 4.31: Inhibitory activity of compounds epipyrones (**1-3**), acetosellin (**4**), hydroxymellein (**10**), epicaronic acid (**13**), tricinonoic acid (**14**), flazin (**15**) on human cerebroside sulfotransferase (hCST) at a concentration of 100 µM. Inhibitory activity is given as residual activity of the tested enzyme in %. Assay was performed in duplicates on two days, respectively. The mean values of are given with the regarding standard deviation. Assay performed by I. Zech (working group Prof. Gieselmann).

4.6.2 INHIBITION OF CYSTEINE AND SERINE PROTEASES

During this project, secondary metabolites were tested by the working group of Prof. Gütschow (Pharmaceutical Institute, Pharmaceutical Chemistry I, University of Bonn) for their inhibitory activity against different proteases (see **section 3.5.4** for the methods). While acetosellin (**4**), epicaronic acid (**13**) and flazin (**15**) did not show any activities towards serine

or cysteine proteases at concentrations of 20 µM, epipyrones (**1**-**3**) exhibited potent inhibition of selected target enzymes (see **tab. 4.15**, **fig. 4.32** and **fig. 4.33; inhibition curves for epipyrones in fig. 8.89 - 8.91 in the appendix**): The IC_{50} values range from 4.63 to 11.4 µM for HLE (human leukocyte elastase), cathepsin K and S. Interestingly, cathepsins B and L were not inhibited by epipyrones (**1**-**3**). This observation is intriguing, since the latter both are found ubiquitously in the human body, in contrary to cathepsins K and S (see **section 1.4**): Cathepsin K is mainly synthesized by osteoclasts, while antigen presenting cells are the main producers of cathepsin S, though additional cell types have been attributed to the latter quite recently [116]. Additionally, the digestive enzymes – trypsin and chymotrypsin – were not inhibited.

Tab. 4.15: Activities of the tested compounds against cysteine and serine proteases: Shown are the IC_{50} values, inhibitory constants (*K_i*) in brackets. Compounds **4**, **13**, **15** were assayed at a final concentration of 20 µM in all assays. Compounds **1-3**, **5** and **6** were assayed in following concentrations: Against HLE, six concentration were tested. For cathepsins B and L, compounds **5** and **6** were tested at 10 µM, epipyrones (**1**-**3**) were tested at 20µM. For cathepsins K and S, compounds **5** and **6** were tested at 20 µM, epipyrones (**1**-**3**) were tested with six concentrations.

Comp.	Enzymes						
	trypsin[2]	chymo-trypsin[2]	HLE [2]	cath. B [2]	cath. L [2]	cath. K [2]	cath. S [2]
1-3	-	-	4.63±0.64 (1.62±0.23)	-	-	11.4±1.8 (0.795±0.123)	6.61±0.42 (3.80±0.24)
5	-	-	5.19±0.77 (1.82±0.27)	-	-	64[1]	29[1]
6	-	-	10.0±2.1 (3.52±0.73)	-	-	54[1]	83[1]
4	-	-	-	n.i.	-	n.i.	n.i.
13	-	-	-	n.i.	-	n.i.	n.i.
15	-	-	-	n.i.	-	n.i.	n.i.

cath. = cathepsin;
n.i. = not investigated.
´-´ = no inhibitory activity found.
[1] When only one concentration was measured to calculate the **IC_{50}** value, then the data are shown without standard error and inhibitory constant (see **section 3.5.4** for the methods).
[2] Shown are the values of duplicate measurements under the assumption of competitive inhibition [µM ± standard error] (the mode of inhibition was not examined in the experiments).

In accordance with the previous observations on hCST (human cerebroside sulfotransferase, see **section 4.6.1**), acetylation of epipyrones (**1**-**3**) leads to a diminished activity toward the protease targets (see **fig. 4.32** and **fig. 4.33**). While the activity on HLE seems to be weakly affected, the inhibitory activity towards cathepsins K and S was strongly decreased. Apart from that, epipyrone tetraacetate (**5**) has the advantage that it is a single defined molecule, which apparently does not isomerize at its *C*-glycosyl moiety, contrary to epipyrones (**1**-**3**).
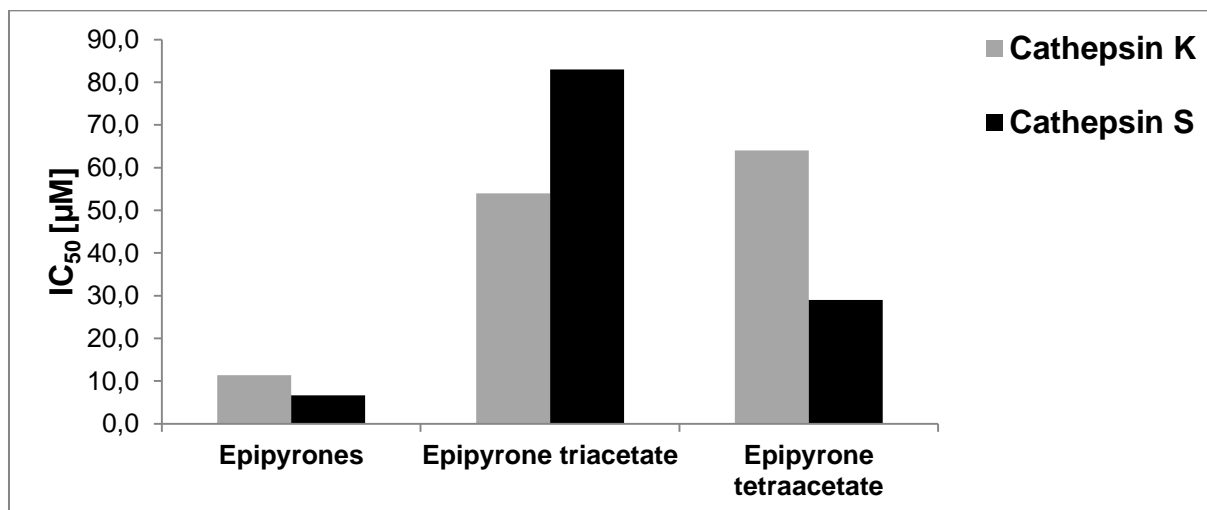
Fig. 4.32: Inhibition of cathepsins K and S by epipyrones (**1**-**3**), epipyrone triacetate (**6**) and epipyrone tetraacetate (**5**). Shown are the IC$_{50}$ values. For epipyrones (**1**-**3**), six measurements (0 – 25 µM) were performed in duplicate. For compounds **5** and **6**, the IC$_{50}$ was determined based on two measurements at 20 µM and subsequent non-linear regression analysis. The assays were all performed in the working group of Prof. Gütschow.
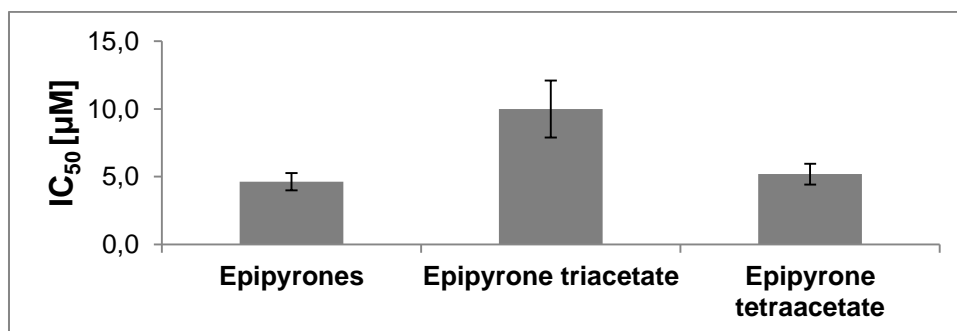
Fig. 4.33: Inhibition of neutrophil elastase (HLE) by epipyrones (**1**-**3**), epipyrone triacetate (**6**) and epipyrone tetraacetate (**5**). Shown are the IC$_{50}$ values. For all compounds, six measurements at different concentrations were performed in duplicate. Error bars display the standard error, which has been calculated based on non-linear regression analysis. The assays were all performed in the working group of Prof. Gütschow.

4.6.3   OTHER BIOACTIVITIES

4.6.3.1   CYTOTOXICITY

Resazurin-based assay

At a concentration of 30 µM there was no cytotoxicity in the resazurin-based cell viability assay for acetosellin (**4**) and epicoccolide B (**9**) (see **fig. 4.34** and **4.35**; for details see **section 3.5.1.1**).
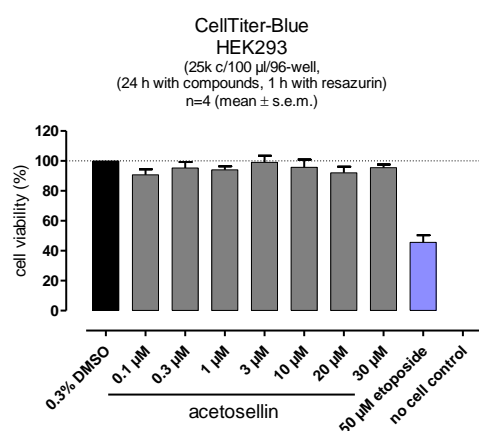
Fig. 4.34: Cell viability measured with acetosellin (**4**) using the resazurin assay. Displayed are mean values of 4 replicates. Etoposide was taken as the positive control.
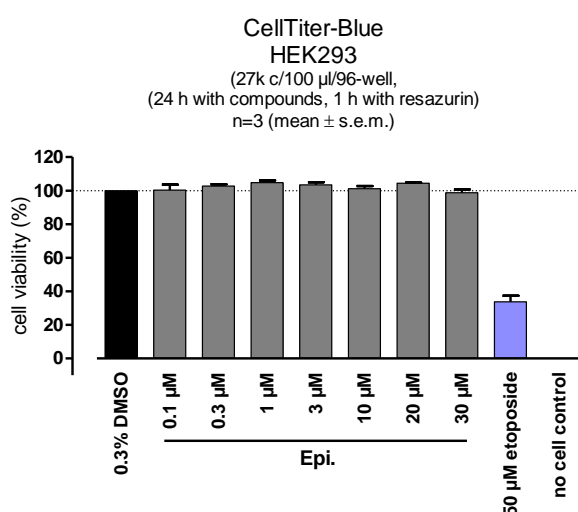
Fig. 4.35: Cell viability measured with epicoccolide B (**9**) using the resazurin assay. Displayed are mean values of 4 replicates. For data of single measurements see appendix. Etoposide was taken as the positive control.

MTT-based assay:

Epipyrones (**1**-**3**) did not show cytotoxic or antiproliferative effects against four different human or murine cell lines at a concentration of 37 µg/mL (= 60.4 µM). For the method see **section 3.5.1.2**.

4.6.3.2   ANTIMICROBIAL ACTIVITIES

Antibacterial activity

Epipyrones (**1**-**3**), acetosellin (**4**), epicoccolide B (**9**), epicaronic acid (**13**), tricinonoic acid (**14**) and (3R,4S)-4-hydroxymellein (**10**) were subjected to agar diffusion assays. None of the tested compounds displayed antibacterial activity (see **section 3.5.2.1** for the tested strains).

Antifungal activity

Since epipyrones (**1**-**3**) were previously found to exert antifungal activity against plant pathogens [175,216], a wide array of fungal strains was tested for inhibitory activity in an agar diffusion assay (see **section 3.5.2.2** for the method and **table 4.16**). 50 µg of epipyrones (**1**-**3**) were applied per test disk. Antifungal activity was observed mainly for dermatophytic ascomycetes from the genera *Arthroderma* and *Trichophyton* (both Arthrodermataceae, Onygenales). This is noteworthy, since these two genera are phylogenetically related. None of the tested mucoralean (*Mucor indicus*, *Actinomucor elegans*, *Cunninghamella elegans*) or basidiomycetous fungi (*Rhodotorula glutinis,* Sporidiobolales) showed inhibition by epipyrones (**1**-**3**). Fungi from the Hypocreales (*Fusarium* spp.), Eurotiales (*Penicillium* spp, *Aspergillus* spp.) or Chaetothyriales (*Exophiala* spp., *Cladophialophora* spp.) or Pleosporales (*Pleospora* sp.) did not show significant inhibition or only slight inhibition by epipyrones (**1**-**3**), the only exception being *Exophiala phaeomuriformis.* However, the sensitivity of dermatophytes to epipyrones (**1**-**3**) could not be scientifically interpreted.

Tab. 4.16: Agar diffusion assay with epipyrones (**1**-**3**). The size of the halo (no growth zone) around the filter paper with 50 µl DMSO (control) or 50 µl epipyrones-solution (1 mg epipyrones/ml DMSO) at two time points.

Strain	Strain number	Inhibition zone in mm after 2-3 days	Inhibition zone in mm after 6-7 days[***]
Ascomycota:			
Arthroderma obtusum	CBS 633.82	2.00±0	1.16±0.23
Artroderma otae	CBS 282.63	0±0	0±0
Arthroderma racemosum	CBS 633.82	0.37±0.12	0.32±0.37
Arthroderma vanbreuseghemii	CBS 449.74	-	0.63±0.29
Aspergillus fumigatus	CBS 418.64	-	0.38±1.01
Candida albicans	CBS 6431	0±0	0±0
Candida albicans	CBS 8758	0±0	0±0
Cladophialophora carionii	CBS 160.54	-	0±0
Exophiala jeanselmii	CBS 507.90	0.84±0.22	-
Exophiala phaeomuriformis	CBS 131.80		2.22±0.74
Fusarium andiyazi	CBS 134430	0±0	0±0
Fusarium petroliphilum	CBS 135955	0±0	0±0
Fusarium verticillioides	CBS 135801	0±0	0±0
Fusarium sp.	WLD1-6	0±0	0±0
Meyerozyma guillermondii	18.6AIII	0±0	0±0
Microsporon gypseum	CBS 130939	1.18±0.38	
Penicillium chrysogenum	18.6FII	0±0	0±0
Pleospora sp.	CBS 134305	-	0.375±1.1
Trichophyton erinacei	CBS 344.79	2.00±0.32	
Trichophyton mentagrophytes	CBS 101546	4.44± 0.45	5.0±0.71
Trichophyton mentagrophytes	CBS 120357	1.35± 0.42	
Trichophyton verrucosum	CBS 134.66	0±0	0±0
Trichophyton violaceum	CBS 119447	-	0.10±0.13
Basidiomycota:			
Rhodotorula glutinis	CBS 20	1.18±0.24	0.45±0.42
Mucorales:			
Actinomucor elegans	CBS 100.13	0±0	0±0
Mucor indicus	CBS 120585	0±0	0±0
Cunninghamella elegans	WLD1-4	0.83±0.33	0±0

- = no growth observed at that time point, [***] Mean values are given with the respective standard deviation.

Anti-HIV testing

Epipyrones (**1-3**) were also assayed for inhibitory activity against HIV-1 using the EASY-HIT assay [154] (see **section 3.5.3**). No inhibitory activity was observed (see **fig. 4.36**).
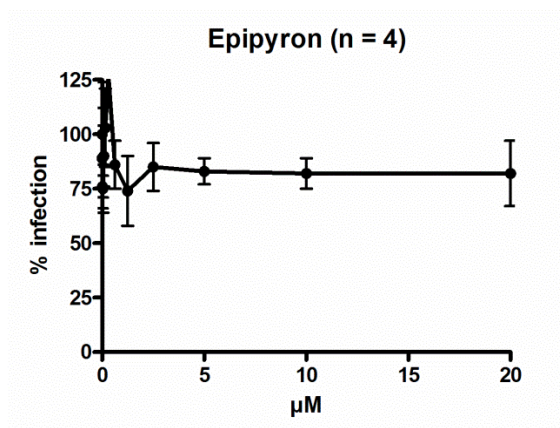
Fig. 4.36: Effect of epipyrones (**1-3**) on the ability of HIV-1 to infect HeLa-derived cells. The y-axis displays the rate of infection of the susceptible cells, while the x-axis shows the final concentration of epipyrones (**1-3**). Experiments were done in four replicates (n = 4). No inhibitory activity can be attributed to epipyrones (**1-3**).

4.6.3.3   NUCLEAR RECEPTORS (LXR, PPAR)

Epipyrones (**1-3**) were tested against five nuclear receptors (LXRα, LXRβ, PPARα, PPARγ, PPARδ). Only PPARγ was activated at a final concentration of 125 μM (see **fig. 4.37**), while all other receptors did not show significant activation at the same concentration. Nevertheless, the observed activity on the PPARγ receptor is not pronounced enough for further tests on these targets.
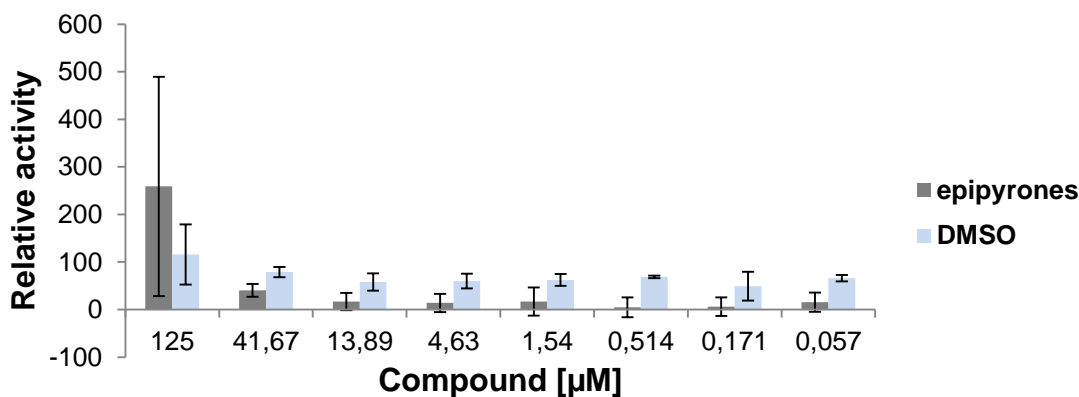
Fig. 4.37: Agonist activity of epipyrones (**1**-**3**) at the PPARγ-receptor in comparison with a negative control (DMSO), with a concentration range between 7.81 – 125 µM. Values are given relative to the activity, which is obtained by activation with the agonist rosiglitazone. The assay was carried out in triplicate. Error bars display the standard deviation. For the method see **section 3.5.5**.

4.6.3.4   EXTRACELLULAR AB-42 PRODUCTION AND INHIBITION OF PROTEIN KINASES

No activity of epipyrones (**1**-**3**) was observed towards Aβ-42 production or protein kinase activity in the assays of ManRos Diagnostics (see **section 3.5.6** for the methods).

4.6.3.5   BINDING OF EPIPYRONES (1-3) TO A MODEL MEMBRANE

In this assay, performed in the working group of Prof. Bendas (Institute of Pharmaceutical Chemistry, University of Bonn), the ability of epipyrones (**1**-**3**) to bind to or to integrate into a phospholipid-bilayer was studied. The purpose of this experiment was to get insights into a possible generic mode of action for epipyrones (**1**-**3**), which would be an explanation for the different bioactivities. For this purpose a model membrane, bound to a surface acoustic wave sensor (SAW) was used (see **section 3.5.7** for the method). The oscillation on its surface, called Love shear wave, was observed and interaction of the test compound with the model membrane was indicated by a phase shift and changes in the amplitude.

Upon injection of epipyrones (**1**-**3**) onto the SAW sensor, a phase shift (observed as a peak) occurs, which points to adsorption onto the membrane, while the overall rise of the curve

indicates that epipyrones (**1**-**3**) do not elute completely from the membrane after cessation of the injection but instead keep on binding to it (see **fig. 4.38**). The decreased amplitude of the detected shear wave during injection indicates an adsorption of epipyrones (**1**-**3**) rather than an integration into the membrane, since the latter would lead to an increased amplitude (see **fig. 4.39**).

As can be seen from the measured phase shift and change in amplitude of the Love-shear wave, epipyrones (**1**-**3**) bind to the model membrane at a physiological pH (pH 7.4). These data indicate that epipyrones (**1**-**3**) are able to bind to plasma membranes at physiological conditions and thus could perturb membrane organization or function of membrane proteins or receptors (see **section 5.1.1** for discussion).
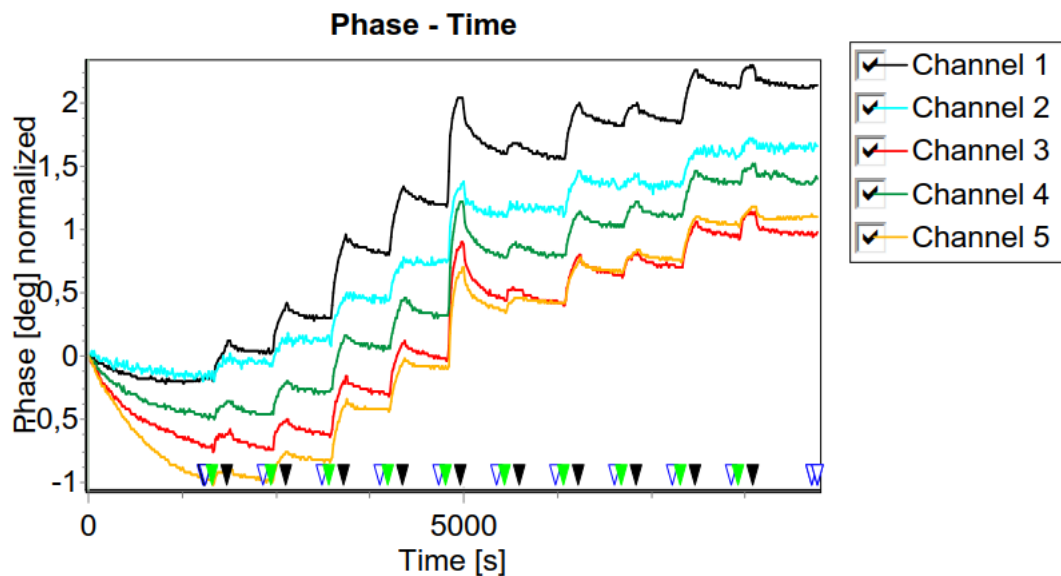
Fig. 4.38: Phase shift (in degrees [deg]) of the Love-shear wave through application of epipyrones-containing solution (increasing concentrations of epipyrones (**1**-**3**), in PBS buffer at pH 7.4, from 10^{-15} to 10^{-6} M). Green arrows at the bottom indicate the beginning of the injection, black arrows indicate termination of the injection. Blue arrows indicate preparation for the injection. The measurement was carried out in 5 consecutive channels.
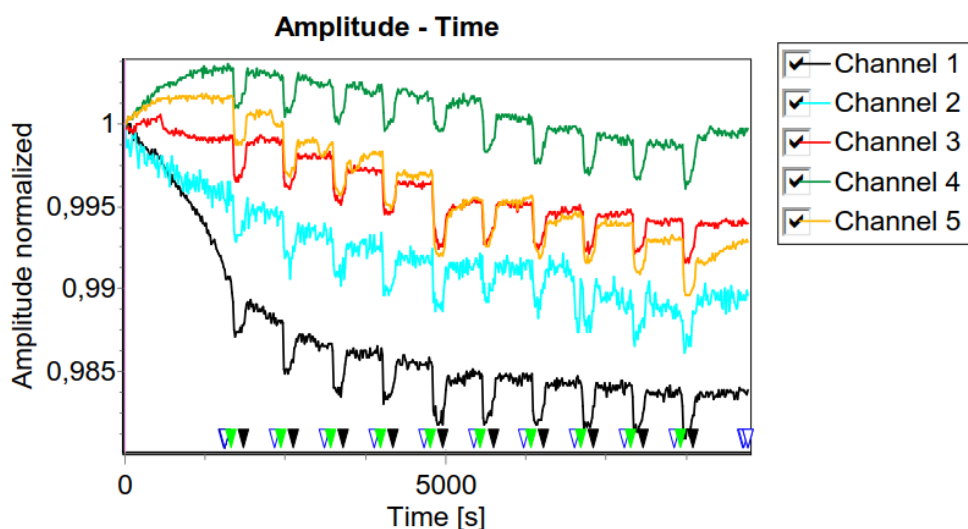
Fig. 4.39: Change in the amplitude of the Love-shear wave through application of epipyrones-containing solution (increasing concentrations of epipyrones (**1**-**3**), in PBS buffer at pH 7.4, from 10^{-15} to 10^{-6} M). Green arrows at the bottom indicate the beginning of the injection, black arrows indicate termination of the injection. Blue arrows indicate preparation for the injection. The measurement was carried out in 5 consecutive channels.

4.7   GUTTATION FLUIDS – QUALITATIVE AND QUANTITATIVE ANALYSIS

4.7.1   INTRODUCTION

The aim of the herein described experiments was to alter the production of different secondary metabolites in an efficient, simple way and to assess the applicability of guttation droplets to monitor these metabolic changes. The increase in the production of guttation fluid was a further aim, in order to get a sufficient amount for in-depth chemical analyzes. Furthermore, they can be analyzed chemically without the need of extraction or purification. Thus, their analysis could provide a time- and cost-saving tool for drug discovery in fungi, since they were shown to harbor a wide array of primary and secondary metabolites (see **section 1.5**). Additionally, they are interesting from an ecological perspective. The exudation of reasonable amounts of secondary metabolites implicates that guttation droplets exert important functions for the producing strain. However, their role has not been elucidated clearly. Thus, the study of their metabolite content could also shed light on the reasons of their production. In the following section the experimental setup and the results will be described, for the methods see **section 3.6**, for the discussion see **section 5.2**.

4.7.2   CULTIVATION AND PHENOTYPE

E. nigrum strain 749 was cultivated on Czapek-Dox agar with variation of two parameters: Illumination and supplementation with trace metals (Zn^{2+} + Cu^{2+}), giving four distinct fermentation conditions (see **table 4.17**). For each condition, ca. 10 - 25 single cultures were prepared and the cultivation was repeated three times (see **section 3.6** for details on the method). Liquid droplets are drawn with a syringe after 14 and 28 days, respectively. The cultures were extracted on day 30.

	No additives	**Trace metals**[*]
Darkness	Experiment 1	Experiment 2
Continuous illumination	Experiment 3	Experiment 4

Table 4.17: Setup of the cultivation experiments, altering illumination (artificial white light) and trace metal supplementation.
*Concentration of trace metals (applied as $ZnSO_4$ and $CuSO_4$; final concentration in the medium): $c(Zn^{2+})$ = 35 µM; $c(Cu^{2+})$ = 20 µM

As can be seen from the photos (see **fig. 4.40**), variations in the cultivation conditions provoke a major change in culture morphology, pigmentation and guttation. While the morphology of the mycelium is influenced mainly by the trace metal content, illumination primarily affects pigmentation and guttation. This also applies to the production of the main metabolites, as will be pointed out in the next section (**section 4.7.3**). Following observations were made regarding the phenotype of *E. nigrum* strain 749:

Morphology: Mycelium on Czapek-Dox agar supplemented with trace metals shows a tomentose (cottony) growth, while a powdery morphology can be observed without trace metals. Light does not seem to have a significant influence. **Pigmentation:** In contrast to the morphology, pigment production is susceptible to changes of illumination and trace metal content. Without additives, reddish-violet pigmentation is more pronounced under continuous illumination, while it is quite faint in darkness. Trace metal addition leads to an inverted correlation: Production of orange pigments is much stronger in darkness and decreases under light. These observations are probably related to the metabolite content of the extracts and guttation droplets (see **section 4.7.3**).

Guttation: The spatial distribution, onset of production and metabolite content differ with each of the four variations of cultivation conditions. While guttation on medium without trace metals occurs already a few days after inoculation (during the first week of cultivation), the amount on day 14 is high and is similar on day 28. The overall volume of guttation droplets is higher as with trace metal supplementation (see appendix, **table 8.3c**). However the volume of droplets could not be measured accurately, since it was not possible to collect the liquid exhaustively. Thus, the data for the droplet volume are approximations.

Additionally, trace metals lead to a delayed onset of guttation production (later than one week after inoculation) and the volume increases over time comparing the drawn droplets from day 14 and day 28. Remarkably, without additives the droplets mainly occur in the center of the mycelium on the agar plug, which was used for the inoculation of the cultures. Trace metal addition leads to droplet formation scattered mainly in the middle section or nearer the growing zone

	No additives	**Trace metals (Cu^{2+}, Zn^{2+})***
Darkness		
Continuous illumination		
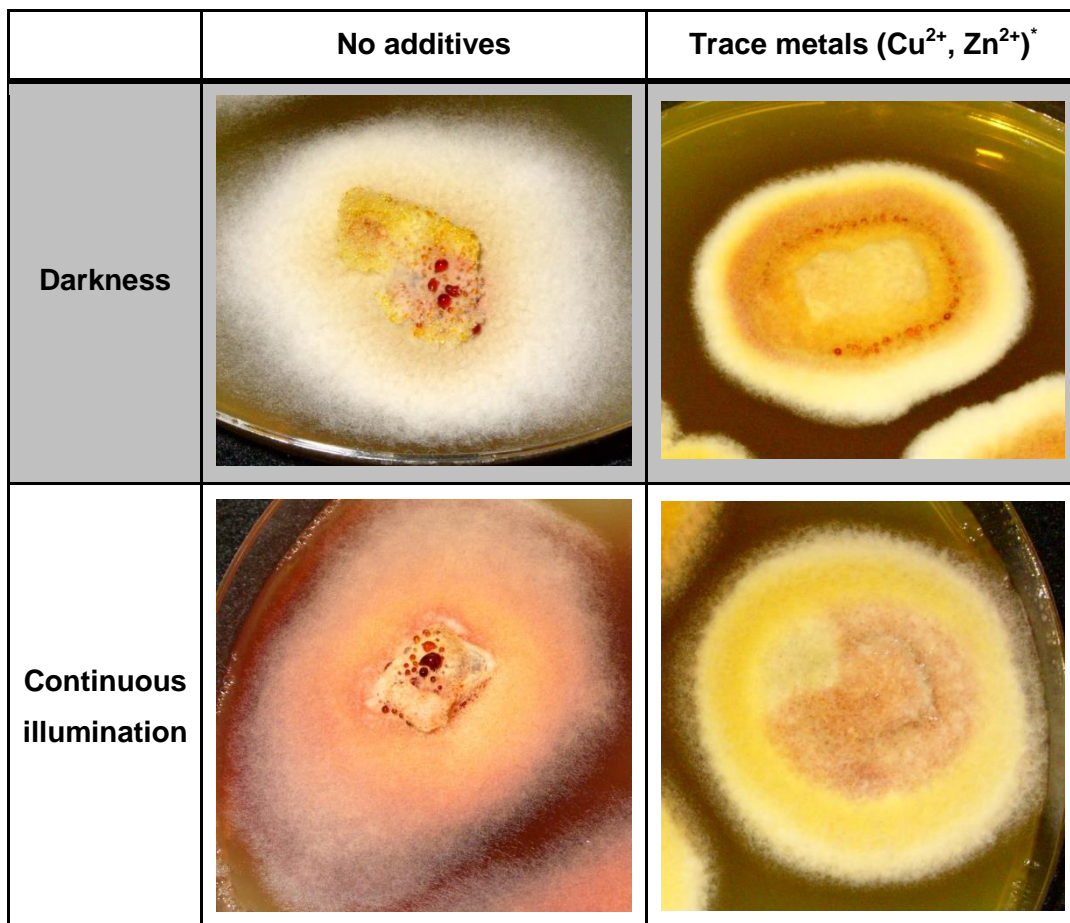
Fig. 4.40: Phenotypic plasticity of strain 749 as exemplified by photos of 14 day old cultures with a typical habit, grown on CDA (Czapek-Dox agar) or CDT (Czapek-Dox agar supplemented with trace metals).

| 4.7.3 | **SECONDARY METABOLITE CONTENT IN _E. NIGRUM_ STRAIN 749** |

4.7.3.1 QUALITATIVE ANALYSIS OF MINOR CONSTITUENTS

The metabolic content of the extracts and guttation fluid of _E. nigrum_ strain 749 was first analyzed for known metabolites from _E. nigrum_ mainly by high resolution LC-MS and comparison with own or literature data. Mass to charge ratio of the pseudomolecular ions as well as fragmentation pattern were taken for this purpose. In this way, epipyrones (1-3) and acetosellin (4) were identified as main constituents of extracts and guttation fluid. Additionally, the presence of 5´,6´-dihydroxyacetosellin (**7**) and epicoccolide B (**9**) could be proven in the guttation fluid and the extracts of strain 749 grown on Czapek-Dox agar. Furthermore, epicocconone (**8**) was found via high resolution LC-MS in extracts and guttation droplets [see **fig. 8.92-8.94** in the appendix for MS-data of epicocconone (**8**)].

Epicocconone (**8**): HR-ESI-MS _m/z_ 411.1454 [M+H]$^+$; ESI-MS/MS _m/z_ 393; 375; 317; 249; 163.

4.7.3.2 QUALITATIVE AND QUANTITATIVE ANALYSIS OF THE MAJOR CONSTITUENTS

The quantification of the main constituents, epipyrones (**1-3**) and acetosellin (**4**), in guttation droplets and extracts of _E. nigrum_ strain 749 was achieved with the DAD-data from LC-MS measurements, while ^{1}H-NMR was used additionally for the extracts in order to underpin these results (see appendix, **fig. 8.3, fig. 8.4** and **tables 8.3a – 8.3e**). Serial dilutions of the two compounds were employed as standard solutions (see **section 3.6** for the method, **fig. 3.4a** and **fig. 3.4b** for linearity of values from the standard solutions).

The data for the extracts clearly showed that production of epipyrones (**1-3**) and acetosellin (**4**) is influenced differentially by constant illumination and trace metal content (see **fig. 4.41**). Under optimal conditions (without trace metal addition), acetosellin mean concentration (per Liter medium) was found to be 0.165 mM (with illumination) or 0.264 mM (without illumination). For epipyrones, the concentrations are at 0.187 mM (with illumination) or 0.308

mM (without illumination) under its respective optimal production conditions (with trace metal addition).

Without trace metals, mainly acetosellin (**4**) is produced, while addition of trace metals favors the synthesis of epipyrones (**1**-**3**). The effect of illumination is not as pronounced, but still an effect on the metabolism can be observed: Epipyrones (**1**-**3**) production favors darkness, while the effect on acetosellin (**4**) biosynthesis is not as clear, since the variation without illumination is much higher than with illumination. In general, the variability of metabolism among the replicate cultures is remarkable. Specifically, the results for acetosellin (**4**) vary conspicuously throughout the experiments. However, it can be concluded that both factors – illumination and trace metals – have a remarkable effect on the production of these two major secondary metabolites.

Based on the above mentioned observations, one would expect a similar pattern in the guttation droplets according to the cultivation conditions. Indeed, acetosellin (**4**) appears mainly on medium without trace metal supplementation, while epipyrones (**1**-**3**) production is still increased by TMS addition without illumination. Thus, an influence of trace metals can still be observed, while the effect of illumination is not as pronounced. Surprisingly, there are some remarkable differences to the extracts: The concentration ranges are different to the extracts. Epipyrones (**1**-**3**) are exuded generally in high concentrations (between 0.23 – 2.00 mM; see **fig. 4.43**). Acetosellin (**4**) levels are much lower (between 0.00 – 0.09 mM; see **fig. 4.42**). Even under optimal production conditions for acetosellin (**4**), concentrations of epipyrones (**1**-**3**) are higher in the droplets.
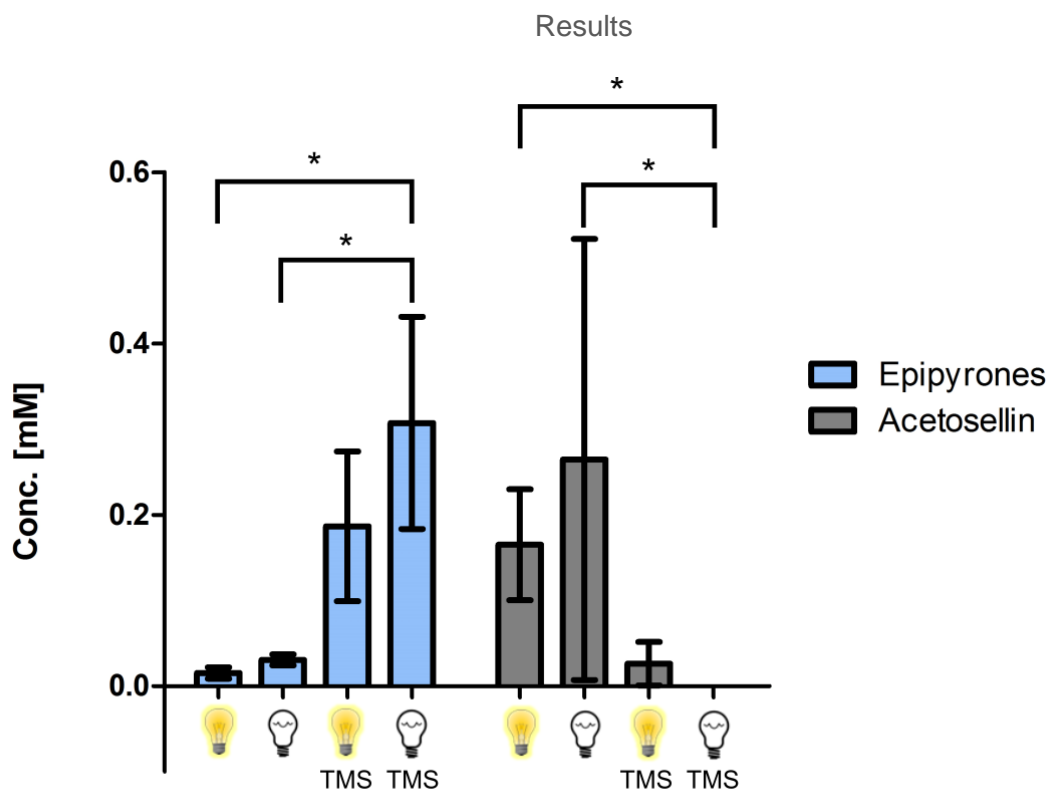
Fig. 4.41: Concentrations of the main metabolites – epipyrones (**1-3**) and acetosellin (**4**) – per Liter Czapek-Dox medium, from 3 replicate cultivations, together with the standard error of the mean and significance (Mann-Whitney test; *: $p \leq 0.05$). For the extraction method see **section 3.6**. **TMS** = supplementation with trace metal solution. **Yellow light bulbs** indicate fermentation under continuous illumination with white light, while **colorless light bulbs** indicate fermentation in darkness.

In general, levels of **1-3** are elevated compared to the extracts. In contrary, concentrations of **4** are lower in the guttation droplets than in the extracts under its optimal production conditions. This implies a mechanism or effect, which favors exudation of epipyrones (**1-3**) over acetosellin (**4**). Alternatively, the latter could have been reabsorbed into the hyphae (see **section 5.2** for possible reasons).

No profound differences could be found for the metabolite concentrations after 14 days compared to the concentrations after 28 days (see **fig. 4.42** and **4.43**). Taking into account the variability between replicate cultures, this observation shows that the concentration of epipyrones (**1-3**) and acetosellin (**4**) stays relatively constant throughout the cultivation period. Thus, the time point of droplet harvesting does not seem to be crucial for the analysis of the secondary metabolite content.
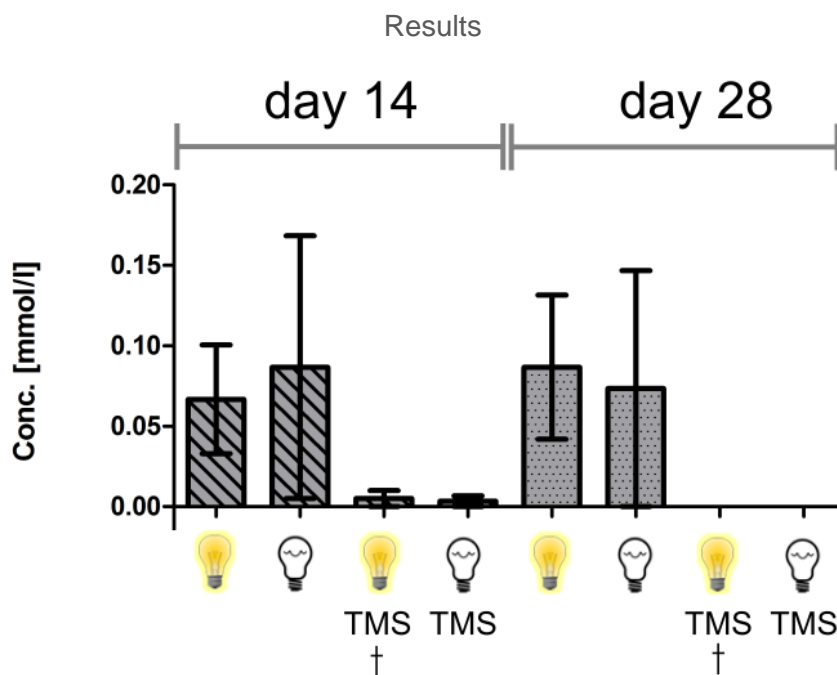
Fig. 4.42: Concentrations of acetosellin (**4**) in the guttation droplets from 3 replicate cultivations, together with the standard error of the mean and significance (Mann-Whitney test; *: $p \leq 0.05$). [†] For these cultures, the guttation droplets could only be collected twice because of insufficient production of droplets. **TMS** = supplementation with trace metal solution. **Yellow light bulbs** indicate fermentation under continuous illumination with white light, while **colorless light bulbs** indicate fermentation in darkness.
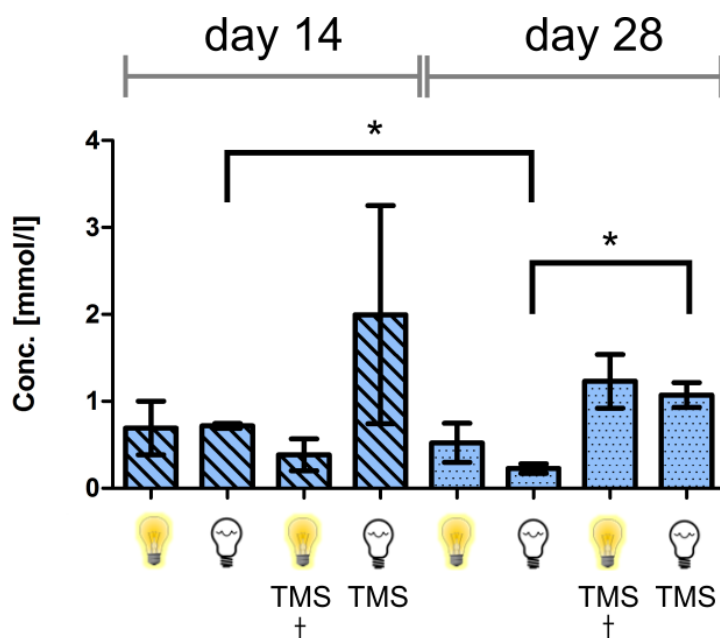
Fig. 4.43: Concentrations of epipyrones (**1-3**) in the guttation droplets from three replicate cultivations, together with the standard error of the mean and significance (Mann-Whitney test; *: $p \leq 0.05$). [†] For these cultures, the guttation droplets could only be collected twice because of insufficient production of droplets. **TMS** = supplementation with trace metal solution. **Yellow light bulbs** indicate fermentation under continuous illumination with white light, while **colorless light bulbs** indicate fermentation in darkness.

In order to get an idea about the influence of the two trace metals (Cu^{2+} and Zn^{2+}) for on secondary metabolism, an additional experiment was pursued: Five cultures of strain 749 were prepared on Czapek-Dox agar with supplementation of only one trace metal, either Cu^{2+} (CDA+Cu^{2+}) or Zn^{2+} (CDA+Zn^{2+}), respectively. The respective concentrations were identical to the concentrations in CDT medium (Czapek-Dox medium with trace metal supplementation, see **section 3.1.3** for details). Cultivation was carried out without illumination. For each experiment, CDA+Cu^{2+} and CDA+Zn^{2+}, the five cultures were pooled and extracted together.

Semi-quantitative comparison of the MS data with data from Czapek-Dox agar (CDA) and Czapek-Dox agar with trace metal solution (CDT) shows a remarkable difference for the two major metabolites (see **fig. 4.44** and **fig. 4.45**). Compared to simple CDA, Zn^{2+}-supplementation abolishes acetosellin (**4**) production, while Cu^{2+} strongly increases acetosellin (**4**) biosynthesis. Addition of both ions together, as mentioned before, downregulates its production.

The observations for epipyrones (**1**-**3**) are different. The selected ion chromatogram (see **fig. 8.98** in the appendix) presumably shows the isomers of the *C*-glycosyl- and polyenic moiety. This results in a complicated peak pattern, which could not completely be analyzed during this thesis. The data suggest, however, that the supplementation of neither Cu^{2+} nor Zn^{2+} alone is sufficient to upregulate production of epipyrones (**1**-**3**) to a degree, which was observed with both metals in combination. Surprisingly, even cultivation without any metal content is superior in this respect. Additionally, no guttation droplets (for Zn^{2+}) or only minute amounts (for Cu^{2+}; 13 µL total volume) could be harvested.
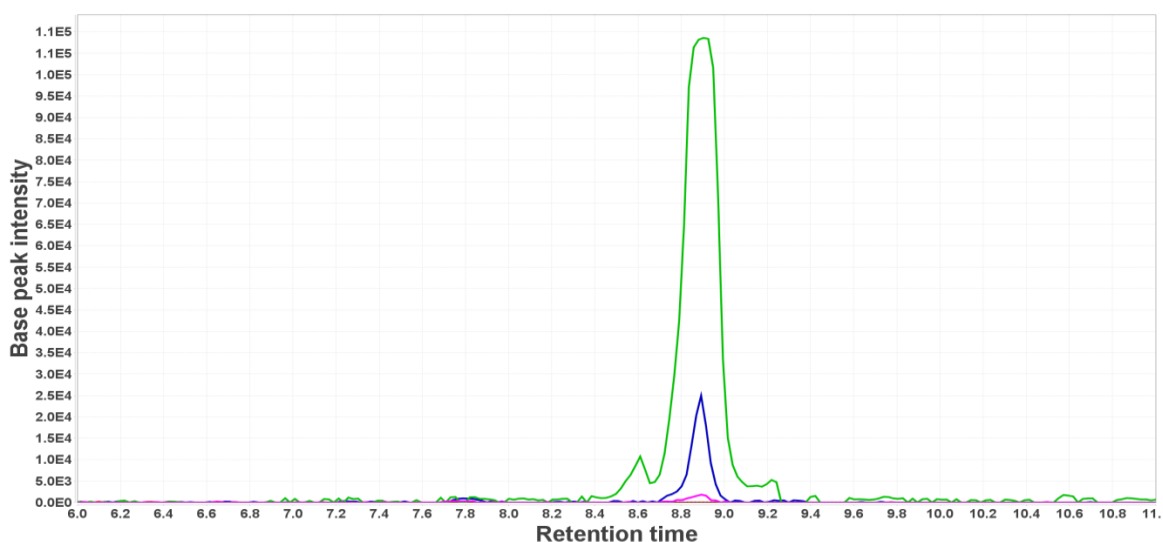
Fig. 4.44: Selected ion chromatogram of different culture extracts from strain 749, showing the mass of acetosellin (**4**) (*m/z* 395.1489 [M+H]$^+$, the selected range was 395.140-395.156). Analysis was performed using LC-HR-ESI-MS system C (see **section 3.3.2**). Colored lines represent following extracts (CDA = Czapek-Dox agar, CDT = Czapek-Dox agar with trace metal solution, all cultivations carried out under darkness under the same conditions): **blue:** CDA; **red (baseline):** CDA+Zn^{2+}; **green:** CDA+Cu^{2+}; **pink:** CDT

Taken together, the results show that *Epicoccum nigrum* strain 749 reacts sensitively on trace metal content and illumination by differentially controlling the production of epipyrones (**1**-**3**) and acetosellin (**4**), respectively. The differences are also reflected by the phenotype, specifically by culture morphology, pigmentation and guttation pattern. Strikingly, not only the production of secondary metabolites seems to be tightly regulated: The concentration of the aforementioned metabolites in the guttation droplets diverges from the pattern observed for the extracts. The reason is not clear, but it might also be an active regulation process. This will be further discussed later (see **section 5.2**).

The metabolites found in the guttation droplets render these fluids interesting targets for the quick and cost-efficient chemical analysis of fungal secondary metabolism. The workup process for LC-MS measurements is very simple and high metabolite concentrations facilitate the evaluation. Nevertheless, not every metabolite found in extracts could be clearly identified in the guttation droplets and this study could not show, whether specific secondary metabolites (*e.g.,* apolar compounds) are not exuded at all. Future studies could address these questions. Furthermore, the ecological reasons for the intense secretion of specific natural products as droplets onto the mycelium would be fruitful research subjects.

5 DISCUSSION

5.1 CHEMICAL STRUCTURES AND BIOACTIVITIES

5.1.1 EPIPYRONES (1-3)

C-glycosylated secondary metabolites are quite rare in fungi, even more so when the *C*-glycosyl moiety is attached to a pyrone functionality. This renders epipyrones (**1-3**) highly distinctive and intriguing molecules. In terms of biosynthesis, epipyrones (**1-3**) are probably polyketide-derived compounds (see **fig. 5.1**). The pyronepolyene backbone would thus be constructed by 12 acetate units and 4 methylation reactions, of which one methyl group would be oxidized to a carboxyl group. Following the cyclization of the 2-pyrone (= α-pyrone) moiety, glycosylation would occur at position 3, which is a typical position due to its high electron density [217]. Glycosylation reactions are carried out by glycosyltransferases using nucleoside diphosphate sugars as donor [218].
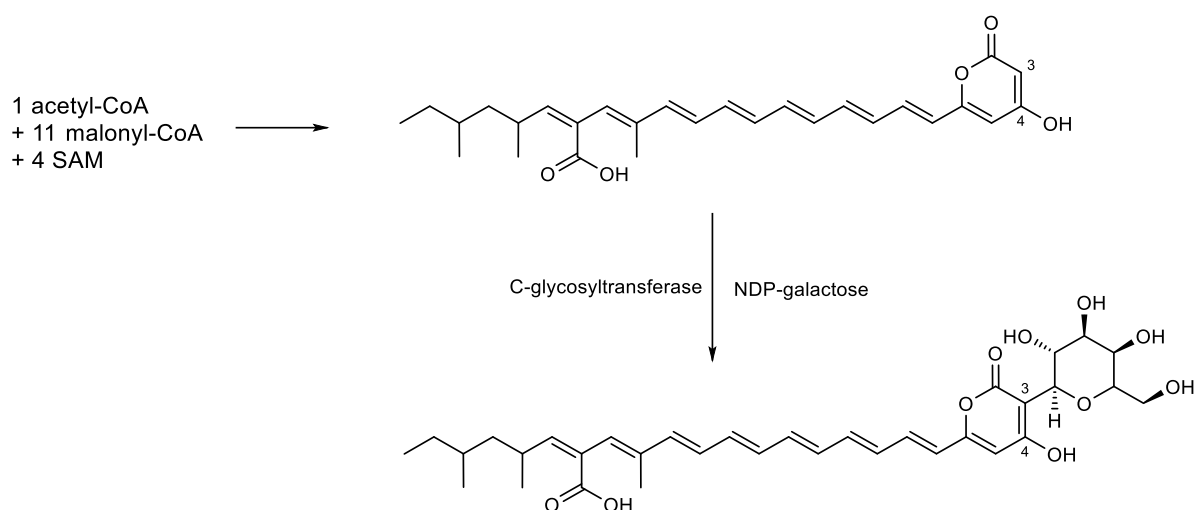
Fig. 5.1: Putative schematic path to epipyrones biosynthesis, exemplified for epipyrone A (**1**). NDP-galactose = nucleoside diphosphate linked to a galactose unit; SAM = S-adenosyl methionine.

Epipyrones (**1-3**) are not the only compounds of this class from *E. nigrum*. As can be seen from **fig. 5.2**, two more isomers were described, *i.e.,* ´compound 1´ (named as in the patent by Villas-Boas et al., where it was described) [219] and orevactaene [220].

The distinctive feature of the specific isomers lies in the *C*-glycosylated 2-pyrone motif. In orevactaene the glycosyl moiety is rearranged to form a pyran partial structure with the hydroxy function at C-4 of the 2-pyrone ring. In ´compound 1´ the 2-pyrone gives way to a bicyclic highly oxygenated ring system, which might be seen as an artefact from oxidation of orevactaene.

epipyrone A (1)

´compound 1´
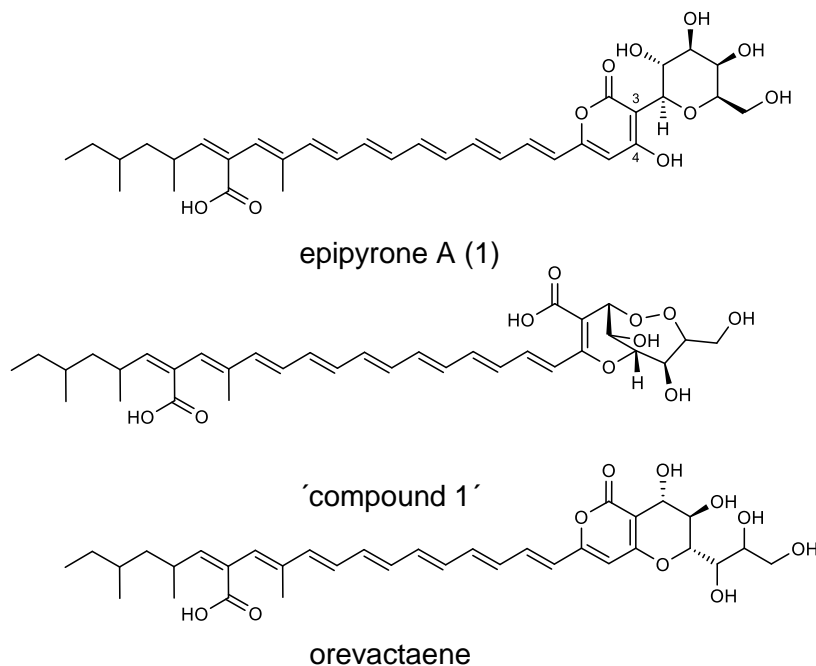
orevactaene

Fig. 5.2: Comparison of two further pyronepolyene *C*-glycosides from *E. nigrum* with epipyrone A (**1**), which were published before: Orevactaene and ´compound 1´.

Apart from that, only a few cases of *C*-glycosylated secondary metabolites from fungi could be found via literature search, particularly concerning 2- or 4-pyrones with an unsaturated side chain: While 2-pyrones and polyenes occur widely in nature [221–224], the *C*-glycosyl partial structure is highly distinctive. *C*-glycosides have mainly been described in plants, where phenolic secondary metabolites are often glycosylated to yield *O*-/ *N*-/ *S*-/ or *C*-glycosides [225,226]. The aglycones usually are flavonoids, anthranoids or gallic acid derivatives. A number of *C*-glycosylated natural products were also reported in bacteria and even in insects or mammals [227].

Concerning fungi, **fig. 5.3** shows the examples, which were found for *C*-glycosides with a backbone similar to that of epipyrones (**1-3**). Despite extensive literature search, no bacterial or fungal pyronepolyenes with a fully conjugated side chain connected to a *C*-glycosylated 2-pyrone moiety could be found. Instead, in all of the shown cases, the olefinic chain is partly saturated and a deoxy sugar forms the glycosyl unit.
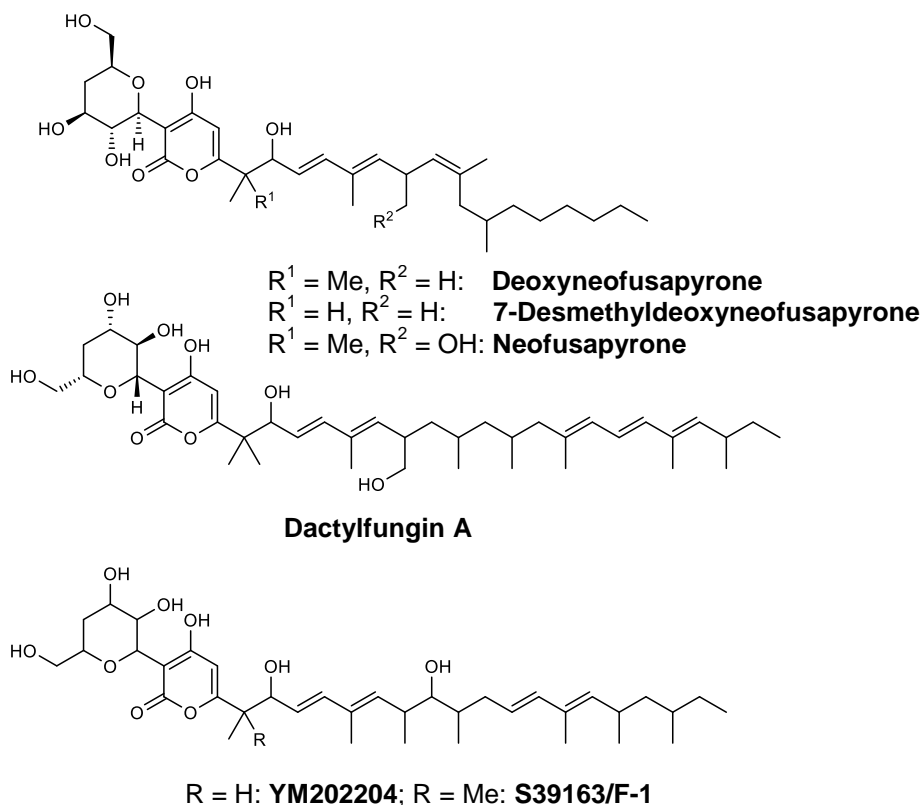
Fig. 5.3: Structures of *C*-glycosylated 2-pyrones with an unsaturated side chain:

Neofusapyrones (deoxyneofusapyrone; 7-desmethyldeoxyneofusapyrone and neofusapyrone; from *Fusarium* sp. FH-146 and *Verticillium dahlia*e, both Hypocreales) [228,229]

Dactylfungin A (found in *Dactylaria parvispora*, Helotiales) [230]

YM202204 (R = H) and **S39163/F-1** (R = Me) (found in *Phoma* sp. Q60596, Pleosporales) [231,232].

Much more examples can be found for 2-pyrones with an unsaturated side chain, which lack a glycosyl unit. **Fig. 5.4** only shows a few of them, with leptomycin A being a bacterial metabolite from a *Streptomyces* strain. From these examples, the high degree of functionalization of the side chain can be seen (regarding the degree of unsaturation, oxygenation and methylation pattern).

An interesting fact about both – glycosylated and non-glycosylated compounds – is that they often exert antifungal activity, usually without showing significant inhibition of bacteria and no or low cytotoxicity (*i.e.*, neofusapyrone, fusapyrone, desmethyldeoxyneofusapyrone, dactylfungin A, YM-202204, S39163/F-1, leptomycins [175,219,229–231,233–235]). This is specifically true for epipyrones (1-3, see **section 4.6.3.2** for bioactivities): Antifungal activity was described before against phytopathogens (*i.e., Botrytis cinerea* and *Lecanicillium muscarium* [175]) and observed during this study mainly for ascomycetes, specifically those belonging to Arthrodermataceae (´dermatophytes´).
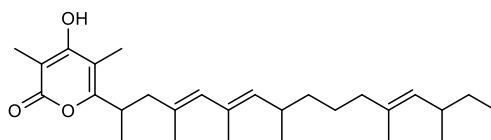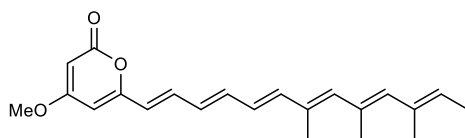
Alternapyrone

Citreomontanine
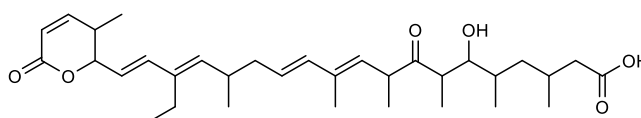
Leptomycin A

Fig. 5.4: Structures of 2-pyrones with an unsaturated side chain:

Alternapyrone (isolated from *Alternaria solani*, Pleosporales) [17,236]

Citreomontanine (found in *Penicillium* sp. CR07, Eurotiales) [237,238]

Leptomycin A (found in *Streptomyces* sp. ATS1287, Actinomycetales, Bacteria) [235]

Additionally, epipyrones (**1-3**) did not exhibit cytotoxic effects on different human cell lines, nor did they show antibacterial activities. Instead, potent effects on specific cellular human targets were noticed: The strongest activities were observed against specific cysteine and serine proteases (see **section 4.6.3**), followed by inhibition of human cerebroside sulfotransferase (hCST) and a minor activity at the nuclear receptor PPARγ. Inhibition of NF-κB (IC_{50} = 50 µM), Influenza virus H1N1 (101.3 µM) and telomerase (67 µM) have been described for epipyrones (**1-3**) before [176]. For the isomers ´compound 1´ and orevactaene (see **fig. 5.3**), antifungal and anti-HIV-activity (inhibition of binding of the regulatory protein Rev to RRE, IC_{50} = 3.6 µM) are known, respectively [219,220].

Taken together, our data suggest that epipyrones (**1-3**) selectively inhibit specific serine and cysteine proteases but still show considerable affinity towards other targets. These multiple activities could be the consequence of at least one common mechanism.

One explanation for the pleiotropic effects could be the amphiphilic structure, with a hydrophilic *C*-glycosyl unit and the apolar alkylic moiety, which lies beside the carboxylic acid group. Indeed, the herein described studies on the interaction of epipyrones (**1-3**) with a model membrane (see **section 4.6.6**) confirm the amphiphilic character of epipyrones (**1-3**) at physiological pH. The adsorption onto the membrane surface could be important at least at high compound concentrations: Compounds with phenolic structures or amphiphilic

character have been shown to interact with cell membranes and protein surfaces, thereby exerting different effects like modification of enzyme activities, perturbation of membrane structure and membrane fluidity or agglomeration of proteins [239–243].

In vivo, epipyrones (**1**-**3**) could also act as antioxidants, since polyenic substances can easily be oxidized under physiological conditions [243]. Antioxidant activity is also one explanation for the antifungal activity. Since reactive oxygen species (ROS) are crucial for differentiation processes in fungi, antioxidants are able to hamper the development of fungi [138,244,245]. Additionally, antioxidant activity is an important factor for the fungus to counteract abiotic stress factors. The herein reported strain 749 was isolated from a marine alga. The high salt concentration in marine environments leads to oxidative stress and is counteracted by various organisms through production of antioxidant compounds or enzymes [246–248]. This role is also supported by the upregulation of epipyrones-production under high salinity of the medium, which was shown during this work (see **section 4.3.1**). The 2-pyrone moiety confers an additional cue on possible modes of action mainly against serine and cysteine proteases: These partial structures are able to undergo transesterification reactions with nucleophilic residues (*e.g.,* alcohol or thiol residues of serine and cysteine) at the active site of enzymes like serine proteases and thus act as suicide inhibitors [249].

However, the proposed modes of action remain to be proven and would be interesting subjects for future studies. The same is true for the ecological significance of epipyrones´-production. In any case, since *E. nigrum* produces epipyrones (**1**-**3**) in high amounts and the production is tightly regulated (*i.e.,* by trace metals and light or osmotic stress), the production must be highly important for the survival of the producing fungus.

5.1.2   ACETOSELLIN (4)

The results given in **sections 4.4.4.3** and **4.4.4.4** strengthen the hypothesis that two separate polyketide units lead to the formation of acetosellin (**4**). Similar findings for other azaphilonoids lending support to the conclusions will be considered herein. Finally, a hypothetical biosynthetic scheme will be discussed in this section.

5.1.2.1   BIOSYNTHESIS OF OTHER AZAPHILONOID METABOLITES

Labeling studies on ochrephilone from *Penicillium multicolor* built the starting point for the theory of acetosellin (**4**) being formed by condensation of two polyketide-derived chains by Plitzko (**fig. 5.5**) [184,193]. However, structural similarity is more obvious between acetosellin (**4**) and the azaphilonoid pigments derived from *Monascus* spp. (Monascus azaphilone pigments = MAzPs): In the case of monascorubrin, monascoflavin and PP-V, the condensation of a hexaketide – forming the azaphilonoid core structure - with an acyclic pentaketide chain was proposed [177,192,199,250]. Any one of them showed a comparable incorporation pattern through feeding of ^{13}C- or ^{14}C-labeled acetate as precursor.

acetosellin

ochrephilone

monascorubrin

monascoflavin

PP-V
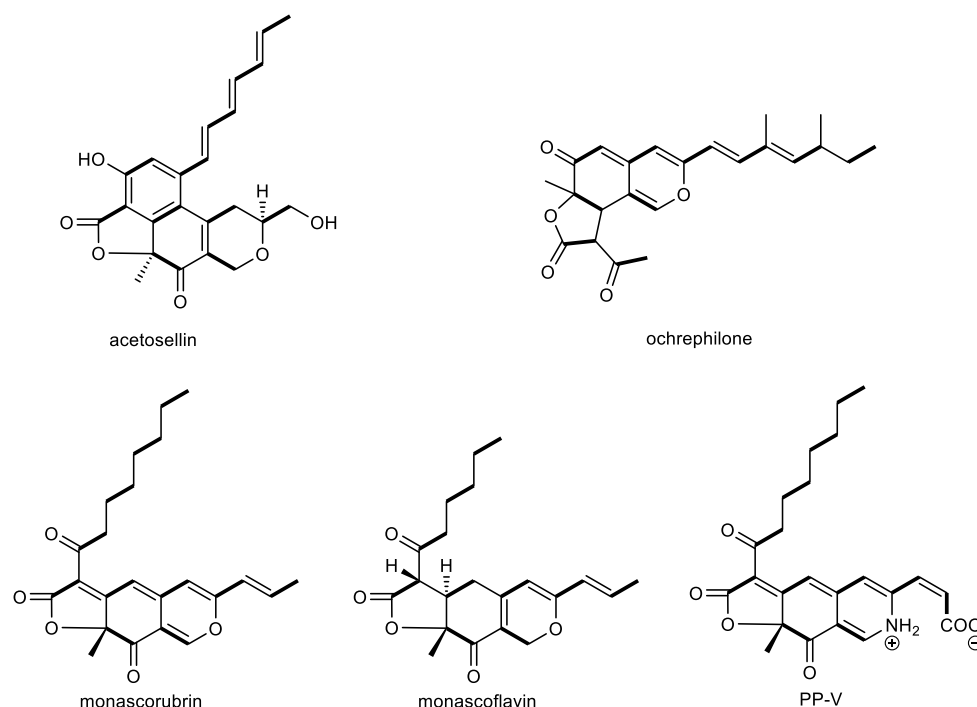
Fig. 5.5: Acetosellin (**4**) from *E. nigrum*, together with azaphilones isolated from *Monascus* spp. (monascorubrin, monascoflavin, PP-V) and *Penicillium multicolor* (ochrephilone). They show high structural similarity and a similar pattern of acetate incorporation after labeling studies. For details see text.

More recent findings on the genetic level outline that biosynthetic gene clusters (BGCs) - harboring polyketide synthase (PKS) and fatty acid synthase (FAS) genes as well as tailoring enzymes - are responsible for the formation of MAzPs [200,201]. The azaphilone partial structure is synthesized by a non-reducing fungal polyketide synthase with a reductive release domain (NR-fPKS-R) [202,251,252]. The acyclic tail, a 3-oxo-fatty-acyl chain, is provided by a canonical fatty acid synthase, called MpFAS2.

Interestingly, data from Balakrishnan et al. obtained with *M. purpureus* [252] indicate that this FAS is dedicated solely to secondary metabolite synthesis and the deletion mutant did not show an altered cellular fatty acid content. Additional genes (outside of the BGC) coding for FASs were found, which were hypothesized to take part in primary metabolism. In *Aspergillus nidulans*, a similar combined PKS-FAS gene cluster was analyzed before. This is responsible for the production of the carcinogenic xanthone derivative sterigmatocystin [253]. Brown et al. proved the FAS to be responsible for the supply of a hexanoyl starter unit. Like in *M. purpureus*, deletion of the regarding FAS gene seemingly did affect neither production of long-chain fatty acids for primary metabolism nor growth of the regarding strain.

Before the hexa- and the pentaketide units can be joined to form the azaphilonoid core structure, a crucial oxygenation reaction takes place: AzaH (in *Aspergillus niger*, or the homologue MppF in *Monascus purpureus*) - a monooxygenase - dearomatizes the 2-methyl orcinaldehyde partial structures of the hexaketide unit (see **fig. 5.6**). Thereby, the typical pyran-quinone partial structure is formed [202,251].

Esterification of the MpFAS2 product with the newly formed tertiary alcohol of the hexaketide unit can now be undertaken with the help of the acyltransferase MppB (see **fig. 5.6).** Knockout mutants of the genes coding for MpFAS2 or MppB, consequently, are incapable of producing *Monascus* azaphilone pigments. Formation of the γ-lactone moiety finally leads to the production of monascorubrin.

Azaphilonoid compounds forming a lactone moiety with an extended side chain also occur in other fungal genera: Compounds like the bulgarialactones (**fig. 5.7**) isolated from the wood-inhabiting ascomycete *Bulgaria inquinans* (Bulgariaceae) [254,255] and the pitholides isolated from the invertebrate-derived fungus *Pithomyces* sp. (Didymellaceae) [256] are examples for this subgroup with a linear tricyclic core structure. Angular azaphilones have also been isolated, *e.g.,* the deflectins from *Aspergillus deflectus* (Aspergillaceae) [257].
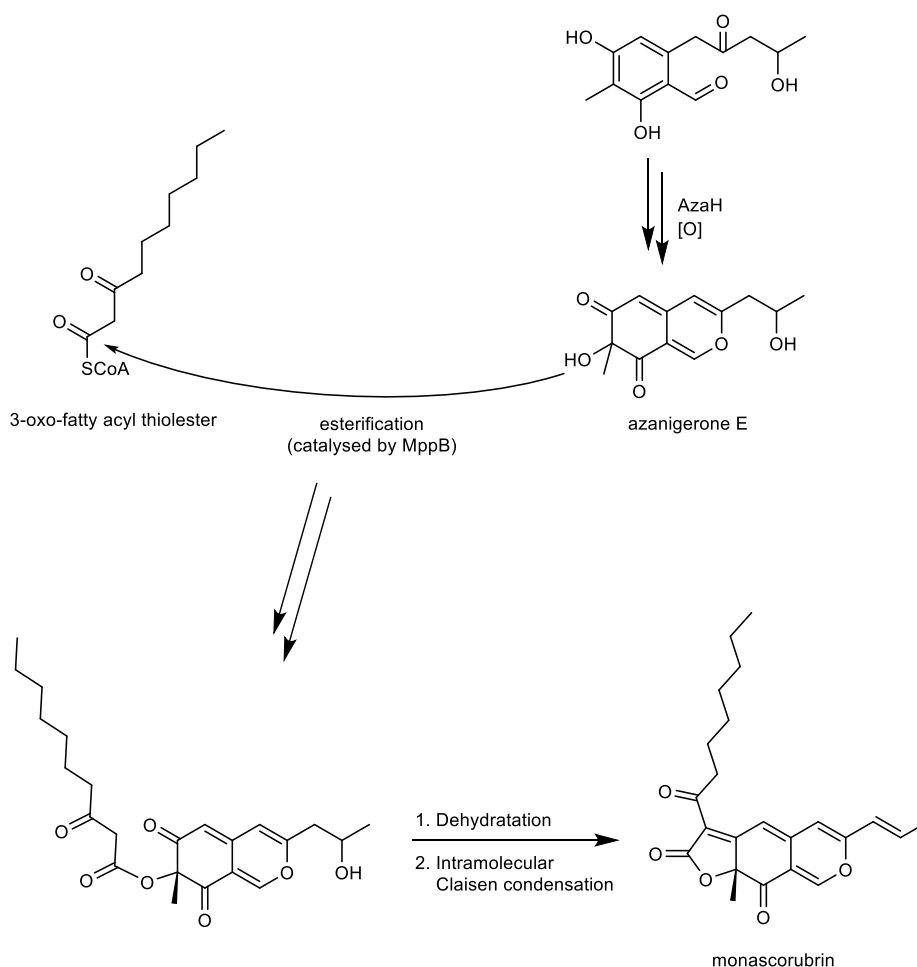
Fig. 5.6: Biosynthetic origin of monascorubrin as proposed by Balakrishnan et al. [251].

In the case of the bulgarialactones A-D, the side chain harbors a conjugated trienic partial structure and a vinylogous carboxylic acid function, which renders the side chain highly similar compared to epicocconone (**8**). The distinctive feature of the bulgarialactones is the isobutyl end group, which is replaced by a methyl group in epicocconone (**8**).

A remarkable feature, shared by acetosellin (**4**) and bulgarialactone D, is the reduced pyran moiety. Acetosellin (**4**), however, is the only known metabolite of that kind with an additional aromatic ring supposedly formed by another intramolecular condensation. This raises the question why an azaphilonoid compound of this type was not observed in cultures of *B. inquinans*, although the formation of bulgarialactone-derived congeners with an aromatic ring would be conceivable.

Both features – the aromatic moiety and the partially reduced pyran moiety – would make for interesting subjects of future investigations: None of the aforementioned studies did address

the biosynthesis or reaction leading to such a structure. A hypothesis on the mechanism will be provided in the following section.

Epicocconone

Acetosellin

Pitholide A

Bulgarialactone A: R = H
Bulgarialactone B: R = OH

Bulgarialactone C

Bulgarialactone D

Deflectin 1b
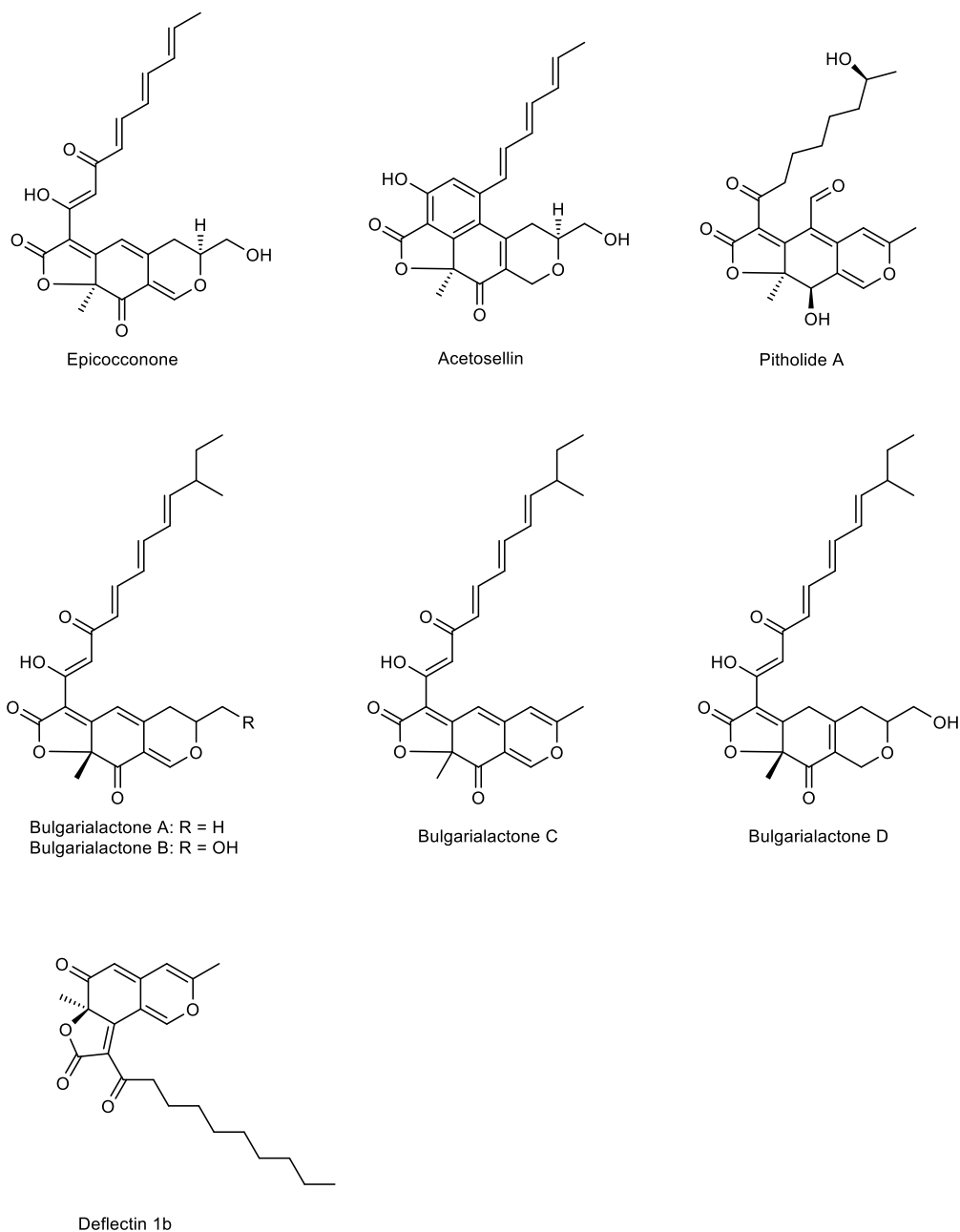
Fig. 5.7: Structures of different azaphilones with an extended side chain attached to a γ-lactone moiety: bulgarialactones A-C, isolated from *Bulgaria inquinans* [254] and bulgarialactone D, isolated from *B. inquinans* ICRM-184 [255]. Pitholide A, isolated from a *Pithomyces* sp. [256]. Deflectin 1b from *Aspergillus deflectus* [257].

5.1.2.2 HYPOTHETICAL SCHEME FOR THE BIOSYNTHESIS OF ACETOSELLIN (**4**)

Based on the findings mentioned above, following hypothesis on the biosynthesis of acetosellin (**4**) is proposed (see **fig. 5.8**):

As in the case of azanigerones and the MAzPs [202,251,252], two separate units would form the starting point - a pentaketide and an acyclic hexaketide. However, a hypothetical BGC would most probably not encompass a FAS as in the case of the MAzPs, but instead two different PKS genes as for azanigerones: The functionalities of the linear side chain cannot be introduced by a canonical FAS [203]. Instead, the programming of a PKS would allow for generation of the observed substitution pattern. In this case, a highly reducing PKS (HR-PKS) could synthesize the triene partial structure during the first three cycles under aid of the following three domains: KR (ketoreductase), DH (dehydratase), ER (enoylreductase). The following two steps would add the β-ketoacid functionality.

Contrary to the hexaketide, the pentaketide could be formed in a similar manner as was shown for azanigerones, by a non-reducing PKS (NR-PKS) [202]. The methyl group at C-8 most likely originates from the action of a C-methyl transferase (CMeT), which uses S-adenosyl methionine as a cofactor. CMeT enzymes usually act, while the nascent polyketide chain is attached to the acyl carrier protein (ACP). The methylene group in α-position of the thiolester is methylated after the elongation step [203]. However, whether the oxidation at C-17 – leading to the hydroxymethylene function – takes place during the chain elongation or later by the action of tailoring enzymes, is not clear.

Following the chain elongation, the first cyclization leads to a 3-methyl orcinaldehyde moiety, which is then dearomatized by a monoxygenase. The resulting tertiary alcohol is crucial for the synthesis of the lactone moiety later on.

In the next step, pyran-ring formation could be achieved via acetal formation. Finally, C-3 is reduced, ending up with the ultimate precursor for the esterification reaction.

The esterification and following Knoevenagel condensation of both ketide units would lead to the putative precursor epicocconone (**8**), a metabolite also reported for *E. nigrum* [258]. Based on the consideration that a precursor-product relationship between epicocconone (**8**) and acetosellin (**4**) is apparent [184], the last step of acetosellin (**4**) biosynthesis would be another cyclization, leading to the aromatic ring and therefore the final product. The driving force could be an oxidoreductase with NADPH as a cofactor. In *Monascus purpureus* YY-1, genes for oxidoreductases were identified. The authors attribute the gene products to pyran-

ring reduction of the monascin precursor [200]. However, in the case of *M. purpureus*, reduction does not induce a further cyclization step. This is probably due to a lack of an electrophilic function in the alkylic side chain.

Taken together, a biosynthetic pathway as shown in **fig. 5.8** seems conceivable. But since the genome of *E. nigrum* is not known and no other putative precursors have been isolated, the exact biosynthetic sequence remains elusive. Furthermore, epicocconone (**8**) is still to be proven as the direct precursor of acetosellin (**4**), as it could not be isolated during this project. This may owe to the fact that the cultures were extracted at room temperature during this study: During the first study on epicocconone (**8**), parts of the cultivation and extraction reportedly were carried out at +4°C [258].

Finally, compound **7** most probably is derived from acetosellin (**4**) by oxidation of the terminal double bond to yield the epoxide, which could be hydrolyzed (see **fig. 5.9**). This leads to the question, whether the oxidation is induced enzymatically or spontaneously in- or outside the cell. Oxidation reactions leading to the formation of epoxides at double bonds of polyenes are widespread in nature, specifically in carotenoids. Spontaneous (non-enzymatic) and enzymatic epoxidation were observed and are an important part of the antioxidant function of carotenoids in plants [243,259].

The characteristic masses of **7** were observed in crude extracts of strain 749 growing on CDA medium, as well as in guttation droplets of strain 749 on the same substrate. Nevertheless, the abiotic or biosynthetic origin remains to be elusive.

Fig. 5.8: Proposed biosynthetic route to acetosellin (**4**) via epicocconone (**8**) following the condensation of two polyketide-derived chains (named **A** and **B**). This scheme is based on findings from MAzPs and azanigerone [194,200,202,251], combined with labeling results obtained during the present study. However, none of the biosynthetic steps has been proven in *E. nigrum*. SAM = S-adenosyl methionine, NADPH = nicotinamide adenine dinucleotide phosphate (reduced form).

Fig. 5.9: Proposed route for the oxidation of acetosellin (**4**) at the terminal double bond via a hypothetical epoxide to yield the vicinal diol (**7**). It is currently not known, whether the oxidation is mediated by an enzyme or happens spontaneously in or outside the cell.

5.1.2.3   BIOLOGICAL EVALUATION AND POSSIBLE APPLICATIONS IN THE FUTURE

Past investigations showed that the class of azaphilones in general is highly diverse in terms of structure as well as biological activities. They were found to show antimicrobial and cytotoxic effects, anti-inflammatory, antioxidant activities as well as inhibition of different enzymes and the growth of tumor cells [177,178]. Thus, metabolites from *Monascus* spp., such as those shown in **Fig. 5.2**, were reported to show anti-inflammatory effects [260,261].

Bulgarialactones A and B were found to show activities against *Bacillus brevis*, *B. subtilis* and *Micrococcus luteus* as well as being nematicidal [254]. Bulgarialactone D is strongly active against *Staphylococcus aureus* [178].

The pitholides have not been reported to show biological activities [256], whereas the deflectins showed antibacterial effects against gram-positive and –negative bacteria, the authors also mention a weak antifungal activity [257].

In two reports, from Nasini et al. and Talontsi et al. [182,183], antimicrobial activity for acetosellin (**4**) was mentioned. Both describe weak or moderate activity towards gram-positive bacteria. Antifungal activity was not found.

During this study, antimicrobial activity could not be attributed to acetosellin (**4**), though a panel of 30 microbes was tested. Neither yeasts, nor gram-positive or –negative bacteria were inhibited. Additionally, no cytotoxic effect was found in HEK cells at a concentration of 30 µM. Testing against different cysteine and serine proteases did also not show an inhibitory activity at a concentration of 20 µM.

No clear answer can be given for the discrepancy of activities. However, details on the test procedure have only been described by Talontsi et al., but not by Nasini et al.

Furthermore, it became apparent during the work on acetosellin (**4**) that it easily degrades during the chromatographic process. Purification of the compound under aid of HPLC was hampered by its instability. Obviously, quick isolation and purification procedures – *e.g.,* flash chromatography – under mild conditions are necessary to yield sufficient amounts of a pure product. Exclusion of light would be preferable, but is difficult to maintain, especially for bioactivity testing.

5.1.3   OTHER POLYKETIDES

Compound **10** (see **fig. 5.10**) was hypothesized by Abdell-Lateff [208] to be a simple condensation product of a pentaketide chain. Compounds **9**, **11** and **12**, as well as paeciloside A presumably originate from a well-known building block (**fig. 5.11**): 5-methylorsellinic acid, which is a polyketide-derived phenolic metabolite [262]. While orsellinic acid and its derivatives occur widely in fungi [262,263] and lichens [264–266], methylation at C-5 is less common. Nevertheless, 5-methylorsellinic acid was found to be the precursor in the biosynthesis of mycophenolic acid (see **fig. 5.11**), which was the lead structure for the development of mycophenolate-mofetil, an important immunosuppressive drug [267].

9

10

11

12
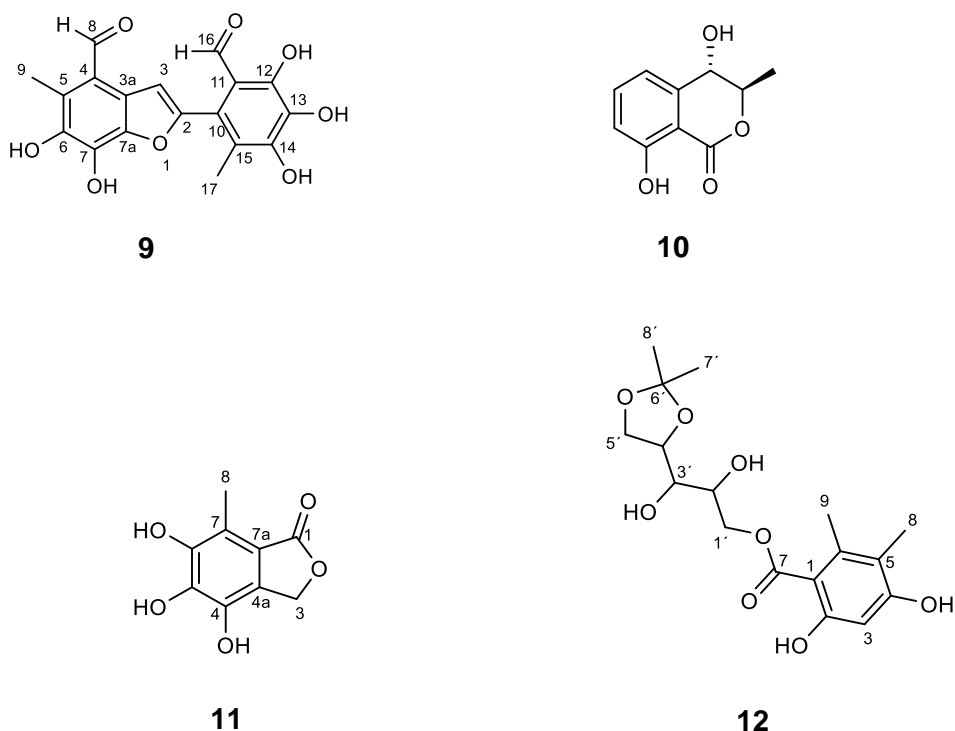
Fig. 5.10: Structures of epicoccolide B (**9**), (3R,4S)-4-hydroxymellein (**10**), epicoccone (**11**) and 1F4-1-6 (**12**).

The second putative building block, involved in biosynthesis of compound **12** and paeciloside A is derived from a pentitol (see **fig. 5.12**). Pentitols are part of the intermediary (primary) metabolism, which are produced in large amounts by fungi as storage metabolites [268,269]. Xylitol and D-arabinitol – both are pentitols – were found in fungi and are mainly produced by conversion of D-glucose in the pentose phosphate pathway [270,271]. In paeciloside A, the pentitol unit was identified as D-arabinitol, which matches the above mentioned distribution of this specific polyol in fungi. Unfortunately, the exact nature of the polyol-precursor of compound **12** could not be identified, since an attempt to elucidate its absolute configuration of compound **12** resulted in the loss of the compound. However, the acetonide substructure of compound **12** is most likely an artefact from the VLC fractionation process, during which acetone was used.
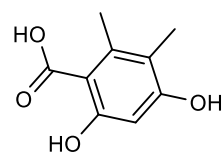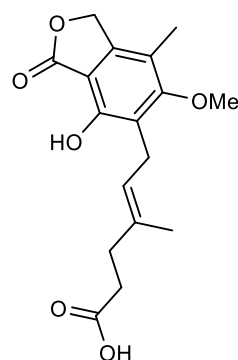
Fig. 5.11: Comparison of the structures of 5-methylorsellinic acid, mycophenolic acid, 1F4-1-6 (**12**) and paeciloside A.

Based on the biosynthetic studies undertaken for mycophenolic acid [267], a biosynthetic scheme is proposed for 1F4-1-6 (**12**) and epicoccone (**11**). Methylation probably takes place during chain elongation by S-adenosyl methionine (SAM). Subsequent cyclization leads to formation of 5-methylorsellinic acid. A following esterification reaction with a pentitol would finally lead to production of compound **12**. The final precursor for compound **11** was hypothesized to be flavipin [183], a dialdehyde found originally in *Aspergillus flavipes* and later in *E. nigrum*.
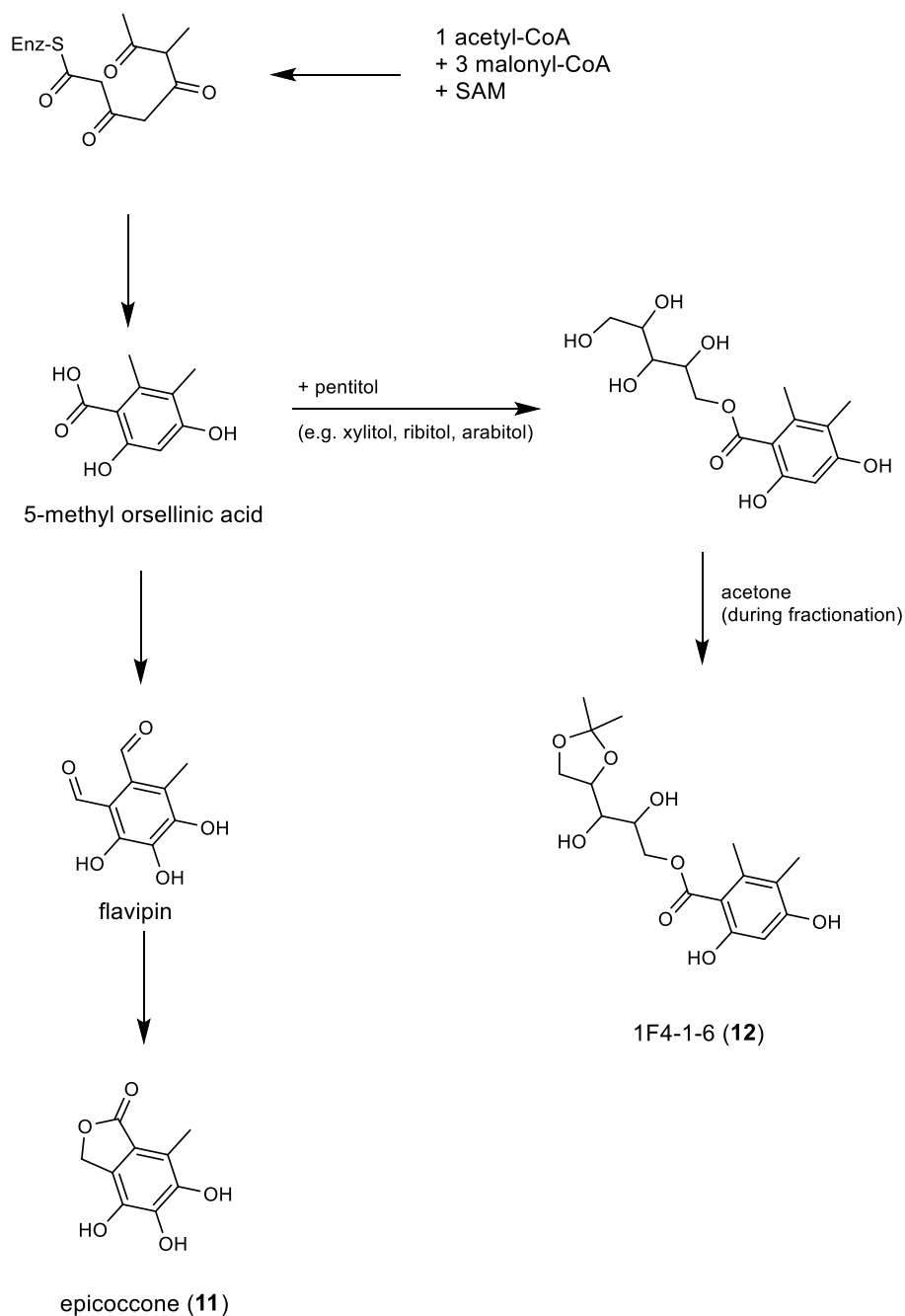
Fig. 5.12: Possible biosynthetic route to epicoccone (**11**) and 1F4-1-6 (**12**).

5.1.4 ISOPRENOIDS - TRICINONOIC ACID AND EPICARONIC ACID

Despite epicaronic acid (**13**) being a new metabolite, similar secondary metabolites have been described before, *e.g.,* the sesquiterpenoid phellilin A, isolated from the mycelium of *Phellinus linteus* (Hymenochaetaceae, Basidiomycota, **fig. 5.13**). The key difference to **13** is the ring closure between C-8 and C-13, resulting in a cyclopentane partial structure [272].
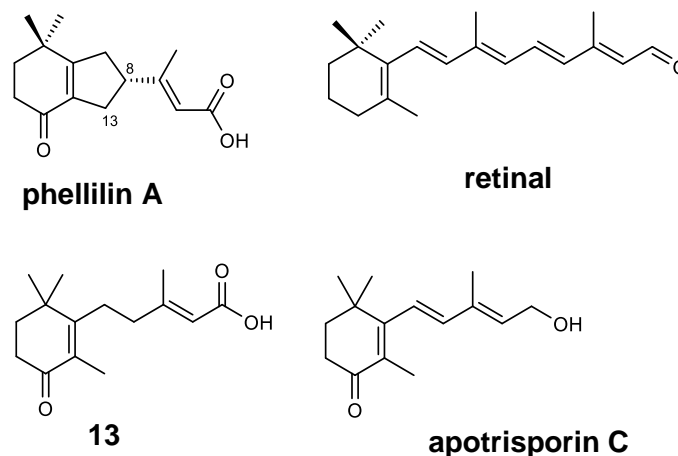
Fig. 5.13: Structure of phellilin A, isolated from *Phellinus linteus* as described in [272], retinal [273] and apotrisporin C [274], compared to compound **13**.

From the viewpoint of biosynthesis, compound **13** likely is an apocarotenoid. Thus, synthesis by oxidative degradation of a carotenoid can be assumed. The production of carotenoids was repeatedly described for *E. nigrum* [275–277]. Apocarotenoids are widely distributed in plants and fungi, functioning as pollinator attractants, fruit or vegetable flavors, antifungal compounds and as regulatory or sexual hormones [278].

In two genera of the former phylum Zygomycota, *i.e.*, *Phycomyces* (Mucoromycotina) and *Mortierella* (Mortierellomycotina), the trisporoids were found to act as sex hormones [279,280]. Byproducts of trisporoid formation – apotrisporins (see **fig. 5.13**) – are believed to serve as regulators for sex hormone production [274].

Furthermore, apocarotenoid production in plants was proven to be induced by infection with mycorrhizal symbionts. Thus, they are probably involved in the regulation of mycorrhizal symbioses [281]. Even retinal (see **fig. 5.13**), which is known to be the basis of human vision, was found in the Ascomycota, *e.g., Fusarium fujikuroi* [273].

However, the ecological role and biosynthesis of compound **13** have not been subjects of further investigations, yet. A possible biosynthetic route (see **fig. 5.14**) could follow a similar scheme as for the trisporoids [282]. It would start with oxidative cleavage of β-carotene (**step I**), which has already been isolated in *E. nigrum* before [276]. The product aldehyde could be further oxidized at C-4 and C-11 (**step II**). Finally the double bond at C-7/C-8 could undergo hydration (**step III**) to yield compound **13**.
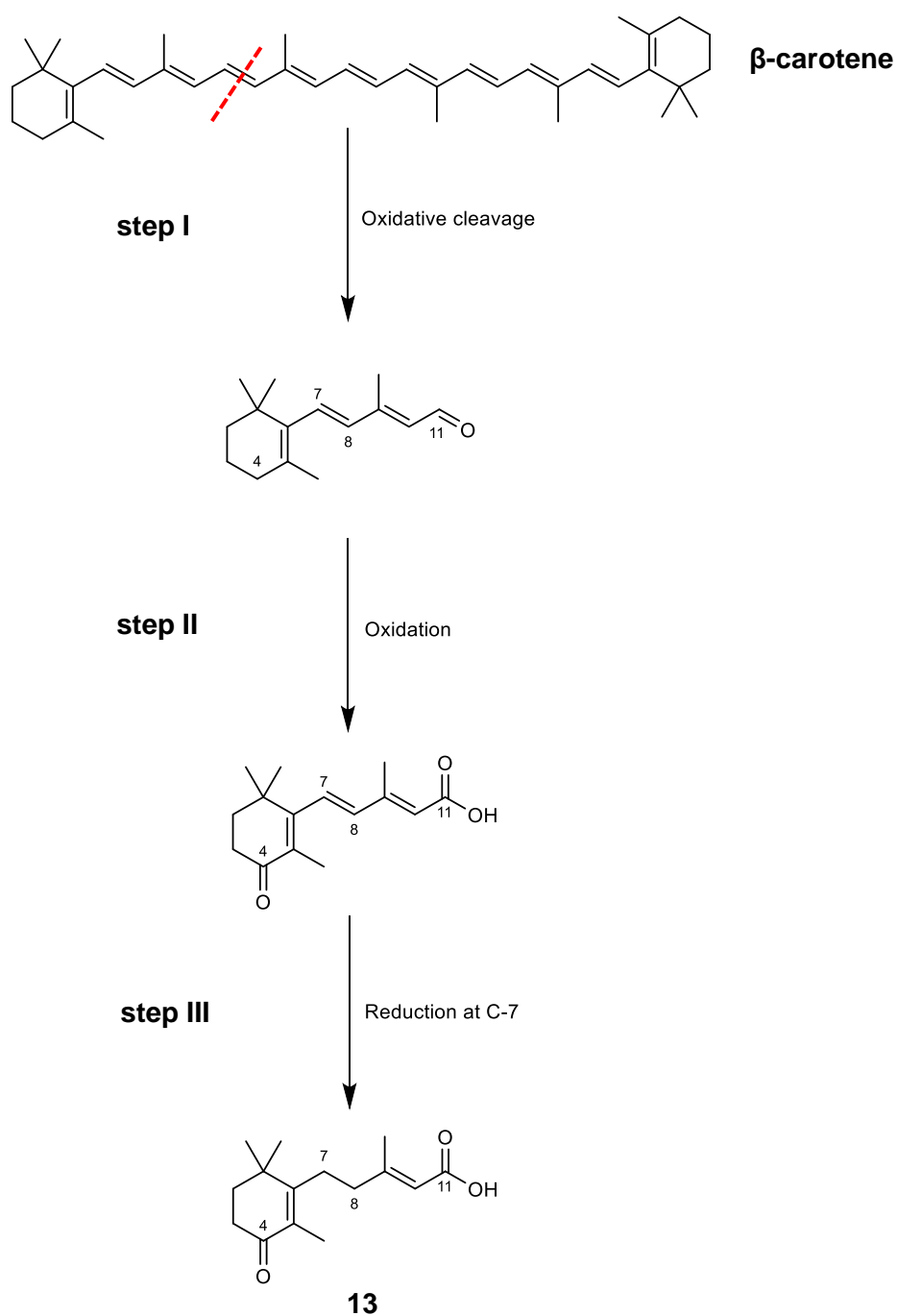
Fig. 5.14: Possible schematic biosynthetic route to epicaronic acid (**13**).

Finally, tricinonoic acid (**14**) is an irregular sesquiterpene, which supposedly emerged from oxidative cleavage of the regular sesquiterpene germacrene D (see **fig. 5.15**) [210].
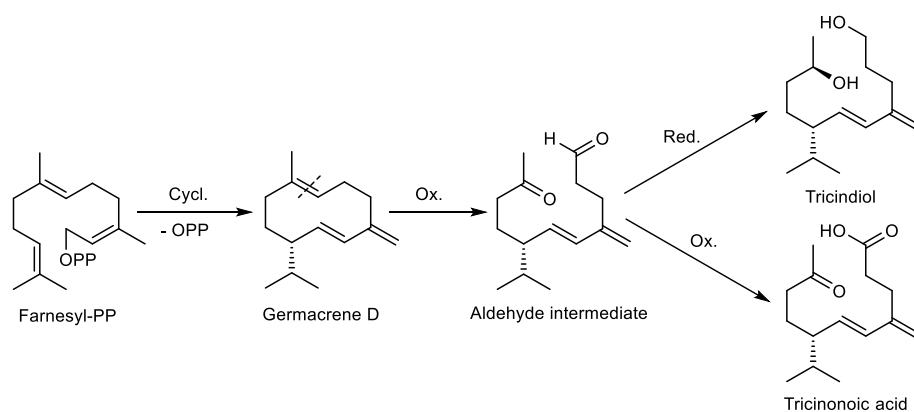
Fig. 5.15: Possible biosynthetic route to tricinonoic acid (**14**) and tricindiol according to Bashyal et al. [210].

5.1.5 BETA-CARBOLINES – ARTEFACTS FROM THE MEDIUM

Flazin (**15)** (**fig. 5.16**) is a highly fluorescent β-carboline alkaloid reported from marine *Streptomyces* spp. [212], Japanese sake, rice vinegar and soy sauce [283]. It was also reported in fruiting bodies of the basidiomycete *Suillus granulatus* by Tang et al. During their study, weak anti-HIV activity was found for flazin [284].
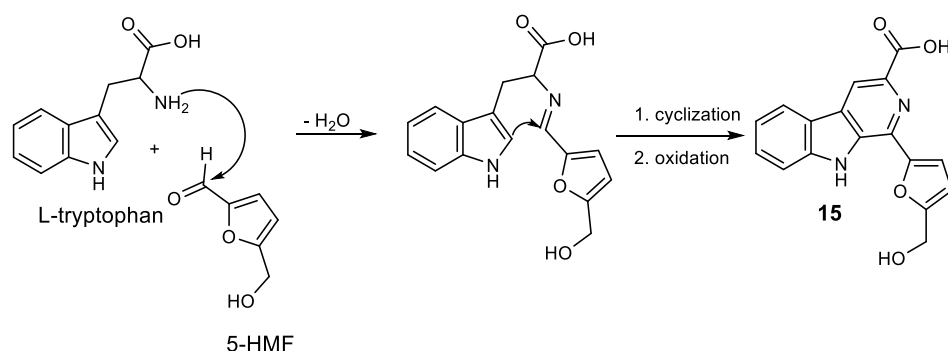
Fig. 5.16: Hypothetical reaction scheme for the formation of flazin from the supposed ingredient of malt extract L-tryptophan and the sugar artefact 5-hydroxymethylfurfural (5-HMF) under conditions of autoclaving.

Synthetic reactions of L-tryptophan and glucose led to the formation β-carboline alkaloids via Pictet-Spengler condensation [285] and derivatives of flazin could be synthesized in the laboratory using derivatives of L-tryptophan and 5-hydroxymethylfurfural (5-HMF) as reactants [284]. Since 5-HMF was found during NMR analysis of autoclaved pure malt extract based medium in high concentration, the possibility of flazin being an artefact emerging from the reaction of the mentioned educts under conditions of autoclaving seems possible (**fig. 5.16**).

5.2 GUTTATION – PATTERNS OF PRODUCTION AND METABOLITE CONTENT

Though *E. nigrum* is a known producer of guttation droplets [286], their constituents have not been studied to the best of my knowledge. Moreover, the ecological significance and regulation of the secretion of secondary metabolites into guttation droplets have not been clearly proven in fungi [131,133].

During this study, a set of four different growth conditions – involving alteration of illumination and trace metal content – was used to assess the differential production of guttation droplets and their respective secondary metabolite content in *E. nigrum*. Firstly, Czapek-Dox agar (CDA) enhances secondary metabolism, compared to nutrient-rich media (*e.g.,* malt extract agar, see **section 4.2**). Second, depending on the trace metal supplementation and illumination, major differences in the concentrations of specific secondary metabolites were recognized in the fungal extract. Pure CDA and CDA supplemented with Cu^{2+} alone, lead to upregulation of acetosellin (**4**) production (see **fig. 4.41** and **4.44**). Acetosellin (**4**) is therefore proposed to be an antioxidant, which counteracts oxidative stress. Epipyrones (**1-3**) are synthesized mainly under supplementation with Cu^{2+} in combination with Zn^{2+} in darkness. Thus, the application of different trace metal ions and illumination for the control of fungal secondary metabolism was shown to be a useful tool in the fungus *E. nigrum* strain 749.

Regarding the guttation droplets, variation of the culture conditions resulted in enhanced production volumes on CDA without trace metal supplementation. Furthermore, the exudates harbor high concentrations of the main metabolites. Concentration levels of epipyrones (**1-3**) were even much higher than in the extracts, while acetosellin (**4**) showed decreased concentrations in the guttation droplets [mean values in the guttation fluids: for epipyrones (**1-3**) between 0.23 – 2.00 mM, for acetosellin (**4**) between 0.00 – 0.09 mM, see **fig. 4.42** and **4.43**]. Additionally, an effect of trace metals on the metabolite concentration was also shown for guttation droplets, while the effect of illumination is less pronounced. However, no significant effect of the time point of exudate harvesting (after 14 days or after 28 days) could be found. The generally high level of exuded epipyrones (**1-3**), as opposed to acetosellin (**4**), could imply the presence of regulatory processes, which control secretion and/or reabsorption of the regarding secondary metabolites.

These data clearly show that guttation droplets can be used for the qualitative analysis of fungal secondary metabolism during its cultivation. The effect of changed cultivation conditions is reflected by the analytic data for the guttation droplets, though with limitation, since epipyrones (**1-3**) were generally exuded in high concentrations. This, however, evens

out the differences found in the extracts to some extent. Thus, the data for the guttation droplets do not allow a precise prediction on the quantitative metabolite content in the fungal mycelium due to different rates of excretion for each metabolite.

Finally, the high concentrations of the main secondary metabolites in guttation droplets are noteworthy from an ecological standpoint. They are sufficient to exert biological effects upon other organisms, since inhibitory activity on different enzymes was detected for epipyrones (**1**-**3**) already in the micromolar range (see **section 4.6**). Consequently, a defensive role of the exuded metabolites can be assumed.

Possible roles of illumination and trace metal ions

The influence of light on developmental processes and metabolism in fungi has been studied in a wide range of fungi. Thus, different types of receptors were found for blue or UV-A light (white collar-1 receptors and cryptochromes, both FAD-dependent), green (type I rhodopsins, retinal-dependent) and red light (phytochromes, bilin-dependent) [25,287]. Interestingly, fungal secondary metabolism reacts differently on light. In this respect, *Aspergillus nidulans* is among the most thoroughly studied fungi. Depending on the illumination, *A. nidulans* differentially produces specific secondary metabolites. Under light, Bayram et al. [25] found that antioxidant pathways are upregulated (*e.g.,* catalase, superoxide dismutase, melanin) together with the production of certain secondary metabolites (*e.g.*, terrequinone, a bisindolylbenzoquinone). Additionally, asexual reproduction is induced.

In darkness, however, sexual reproduction prevails in *A. nidulans*. Differential upregulation of secondary metabolites was also observed (*e.g.*, polyketides like sterigmatocystin, emodin). The aim of such a differential production strategy could be to channel resources for the production of a single or just a few metabolites. Thus, high concentrations of a metabolite are accumulated in a short time [200].

The switch in secondary metabolism and sexual/asexual development is in part conferred by the trimeric *velvet complex* (consisting of the proteins VeA, VelB and LaeA). Illumination by red light leads to binding of the red light-receptor (FphA) to a VeA/VelB heterodimer. Thereby, the translocation of VeA/VelB into the nucleus and the following buildup of the velvet complex are inhibited. As a consequence, asexual sporulation and the production of different secondary metabolites are induced. During dark periods, the VeA/VelB complex is translocated into the nucleus, where it forms a trimer with the methyl transferase LaeA, which epigenetically activates a wide array of genes. Thus, sexual development and the production

of specific secondary metabolites is induced. These light dependent processes – light perception and signal forwarding through the velvet complex – are partly highly conserved among fungi [25,287–289].

This being said, only few information could be found in the literature regarding the reaction of *E. nigrum* on altered illumination. Former reports noted that asexual sporulation is enhanced under white or near UV-light, though the response was largely dependent on the specific strain. The growth rate of the mycelium did not respond to different intensities of white light [290,291]. In another study, the pronounced production of red pigments in darkness compared to white light was mentioned. However, the authors were not able to identify the pigment(s) [292].

In *E. nigrum* strain 749, the production of epipyrones (**1**-**3**) seems to be regulated not only by the substrate, but also by illumination. This compound is preferably produced in darkness. To the best of my knowledge, this is the first time that such a correlation is reported for *E. nigrum*. The observations are in accordance with the results obtained before from *A. nidulans*, that different secondary metabolites may be produced mostly upon specific conditions or life stages. Epipyrones (**1**-**3**) may primarily exert their function in darkness as antioxidant or antifungal compounds. Such a janus-faced role as antioxidant and defensive (highly bioactive) compound has been documented for a number of fungal mycotoxins or pathways (*e.g.*, trichothecenes, aflatoxins, lovastatin) [293–295].

Numerous studies were published on the role of different heavy metal ions on fungal physiology and metabolism. The same is true for the acquisition of trace metals through bioweathering of rocks by fungi [296]. However, the effect of trace metals on secondary metabolism was not studied as thoroughly. In general, insufficient supply with trace metals induces the formation of siderophores. These are able to bind different polyvalent metal cations [*e.g.*, Fe(III), Cu(II), Cr(III)] with high affinity. Structurally, they most often show hydroxamate moieties or phenolic structures [297]. High concentrations of heavy metals, in turn, have different implications: They can induce the secretion of enzymes and secondary metabolites around the fungal mycelium in high concentrations [296]. More interestingly, the positive effect of Zn^{2+}, Cu^{2+} and Fe^{3+} was shown on the production of mycotoxins, namely zearalenone and aflatoxin B1, by *Fusarium graminearum* and *A. flavus*, respectively [23,298]. Ding et al. elicited the production of a new meroterpenoid by addition of Co^{2+} to the culture medium of an *Aspergillus* sp. Remarkably, the strain was isolated from a marine hydrothermal vent [299].

During this study, $CuSO_4$ and $ZnSO_4$ were applied as trace metal solution. Low concentrations of Cu^{2+} are needed as cofactor in a number of fungal oxidoreductases like laccases and superoxide dismutases (SOD) [300]. On the other hand, free Cu^{2+} induces oxidative stress in cells of different organisms, *i.e.*, fungi and plants, probably due to lipid peroxidation and alteration of membrane permeability [300–302]. Thus, high concentrations of > 1 mM (depending on the fungus) exert toxic effects due to membrane leakage and alteration of enzyme function [303]. Already in physiological concentrations, it is also able to elicit the production of antioxidant enzymes and secondary metabolites. This is the case for the production of the (antioxidant) mycotoxin citrinin by *Penicillium verrucosum* [24]. Interestingly, upregulation of citrinin production implies downregulation of another mycotoxin, namely zearalenone.

In the marine-derived fungi *Aspergillus clavatus* and *A. sclerotiorum*, Jiang et al. were even able to elicit the production of secondary metabolites in a dose-dependent manner by increasing concentrations of copper in the medium [304]. The mentioned literature data give further hints on the regulation of secondary metabolism in *E. nigrum*: Since the production of acetosellin (**4**) is markedly increased by addition of Cu^{2+}, this could be a further hint to the hypothesis that it is an antioxidant metabolite. On the other hand, acetosellin (4) production was also elevated without the addition of trace metals. Thus, it could act as a metal chelating metabolite due to its phenolic structure, which lies in β-position to the keto group of a lactone moiety.

Similar to copper, the physiological role of Zn^{2+} also lies in its catalytic action in the active side of numerous enzymes, *e.g.*, Zn-SOD, aldolases, transcription factors (zinc finger proteins) or alcohol dehydrogenase [305]. Even a Zn-dependent polyketide cyclase was found in a bacterial polyketide synthase gene cluster [306]. High Zinc concentrations (> 2 mM, depending on the fungus) show toxic effects against different fungi probably due to oxidative stress and disruption of iron- and sulfur-metabolism [307,308]. Regarding the role of zinc for the production of the two main metabolites in *E. nigrum* strain 749, no hypothesis can be provided. Nevertheless, it seems clear that optimal production of epipyrones (**1**-**3**) requires zinc and copper.

To date, it is not clear, how and why *E. nigrum* strain 749 delegates its metabolic resources in the observed ways. This includes the question, why the fungal secondary metabolism reacts so sensitively on the addition of trace metals on CDA. This, however, could be explained with the employed agar medium. CDA is a minimal medium, *i.e.*, it contains a limited set of defined chemicals, partly in an unfavorable form (see **section 3.1.3** for details). In previous studies, a link was found between increasing nutrient availability and diminished metal toxicity [309–311]. Consequently, secondary metabolism is linked to nutrient depletion

or the absence of preferred nutrient sources in different fungi [200,312]. The unfavorable nutrient composition of this medium is also reflected by poor growth and strong secondary metabolism of *E. nigrum* on CDA medium during this study.

At the beginning of this study, malt extract agar was used as a nutrient-rich complex medium (see section 4.3.1) in order to assess the secondary metabolism of *E. nigrum*. On this medium, the secondary metabolism and its trace metal-dependent shift was not as pronounced as with CDA. This could be a sign that the unfavorable nutrient composition of CDA hampers the ability of the fungus to balance its metabolism. As a consequence, the fungus could delegate a huge part of its resources to its secondary metabolism at the expense of its primary metabolism. A correlation of nutrient depletion in the medium and strongly upregulated secondary metabolism was found for Monascus purpureus. Cultivation under carbon starvation resulted in a strong production of azaphilonoid pigments [200].

Interestingly, unfavorable nutrient composition and nutrient depletion are believed to be the rule rather than the exception in nature [10,309,313–315]. In other words, the seemingly extreme reaction of *E. nigrum* on the applied culture conditions on CDA could give a hint on its metabolism in the natural environment.

Guttation droplets

The herein described metabolite concentrations in the guttation droplets (see **section 4.7**) lead to the question, how the fungus exudes such high concentrations of secondary metabolites. Literature data suggest that either the secretion of secondary metabolites is regulated by the fungus and may thus be achieved by an active transport mechanism, *i.e.,* exocytosis or by membrane transporters. In this scenario, the osmotic pressure - exerted by the secreted compounds - could lead to additional water outflow from the cytoplasm. This view may be reflected by the observation in *Oudemansiella melanotricha* (syn. *Xerula melanotricha*, Agaricales, Basidiomycota) that the plasma membrane below the cell wall is strongly folded at the sites of guttation. Thus, an increase of the surface for transmembrane transporters for the exudation process might be achieved. Interestingly, through electron microscopy the presence of channels in the cell wall was observed, through which the exudate can be released from the periplasmic space [316]. However, a folded plasma membrane does not exclude the possibility of a pressure-driven process (see below). Furthermore, the involvement of active transporters was only shown for secretion of secondary or primary metabolites by fungi into the medium or inside of glands from plants [124,125,317].

A study by Kikuchi et al. gives a hint on the possible involvement of aquaporins in the secretion processes: In the fungus *Rhizophagus clarus* (Glomeromycota), translocation of solutes - *i.e.,* polyphosphates - from the fungal hyphae to plant roots was found to be mediated by aquaporins. They facilitate water flow through the membrane and thus generate a mass flow of the cytoplasm, partially facilitated by tubular vacuoles. Polyphosphate can in this way be transported along the *source-sink* gradient and secreted by specific transporters, which are found adjacent to the aquaporins [318]. A source-sink relation due to transpiration is most likely also the driving force behind guttation in plants, which usually form guttation droplets at the leaf margin. Such a gradient could even help to explain the spatial distribution of guttation droplets in *E. nigrum*: Excretion of water or cytoplasmic contents could force an intrahyphal mass flow in direction of the guttation spot (see below).

The most convincing hypothesis on the guttation mechanism seems a pressure-driven outflow through the plasma membrane, which is one of the theories for guttation in plants. In this case, different solutes and water would pass the membrane directly without a translocator [319]. The increasing turgor pressure would be conveyed by the central vacuole. Further support for this hypothesis comes from the fact that mature or central parts of the fungal mycelium (*i.e.,* near the point of inoculation) are often highly vacuolated [320,321]. Guttation in *E. nigrum* strain 749 preferably occurred in aged parts of the mycelium.

Finally, three mechanisms would be conceivable for the secretion process:

(1) Aquaporins together with additional transporters might help to secrete different solutes. MFS (major facilitator superfamily) or ABC (ATP-binding cassette) transporters are amongst the transmembrane proteins, which could aid in this process. Their involvement in secretion/ excretion processes was proven for several fungal secondary metabolites (*e.g.*, gliotoxin, trichothecenes) [124,322,323]. However, the weakness of this explanation lies in the wide range of compounds, which were found in guttation droplets of plants and fungi.

(2) A vesicle-mediated secretion or exocytosis (granulocrine release). The involvement of specialized vesicles was proposed for exocytosis of aflatoxins in *A. parasiticus* [125].

(3) Increased permeability of the plasma membrane could lead to the diffusion of solutes and water through the plasma membrane. This explanation would be in accordance with the chemical diversity observed in guttation fluids in the literature. However, no evidence could be found for this type of secretion for fungal exudates.

The fact that acetosellin (**4**) concentration is comparatively low in the guttation droplets could be explained by two different mechanisms: It could be either reabsorbed into the cell after secretion. This possibility was already proven for citrinin, which can be reabsorbed and

degraded by the producing fungus [324]. Alternatively, secretion could be hampered due to its higher lipophilicity compared to epipyrones (**1**-**3**) [calculated log D values at pH 7: log D(epipyrones) = -1.38; log D(acetosellin) = 6.35; calculation performed by ACD/Labs Version 11.02 (©1994-2016 ACD/Labs)]. Low polarity could lead to stronger binding to cell structures, *e.g.*, the plasma membrane [243]. Furthermore, it could be stored in other compartments than epipyrones (**1**-**3**). Finally, the latter could be the preferred substrate for special transporters, e.g. MFS- or ABC-transporters (see above).

Assuming the hypothesis of a source-sink gradient, the question remains, why the guttation droplets are mainly formed in central or aged parts of the mycelium: Production of large guttation droplets was recognized in the center of the mycelium on Czapek-Dox agar without trace metal supplementation. On all media, guttation was not observed at the growing edge of the mycelium, but only in central regions with high pigmentation. Following the abovementioned data, this could be explained by two phenomena: First, by the high vacuolation in hyphae during idiophase or senescence, coupled with cytoplasmic streaming in this direction; second, by intense production of secondary metabolites in the secretion spots. Both – advanced developmental stages and secondary metabolism – are correlated to oxidative stress [295,325,326]. High secondary metabolite content in the mycelium, in turn, was linked by Figueroa et al. with guttation droplet production in *P. restrictum* [136].

An increased membrane permeability in the central mycelial portions, leading to guttation, could be explained with oxidative stress. It was proven to increase the permeability of the plasma membrane through lipid peroxidation and to cause electrolyte leakage [327–329]. A pressure-driven filtration process – *i.e.,* eccrine release – could thus be facilitated. Nevertheless, on medium with Cu^{2+} supplementation, which is supposed to impose oxidative stress on cells, only small amounts of guttation droplets were observed. This makes it more complex to link oxidative stress and spatial distribution of the droplets.

The content of specific primary and secondary metabolites in guttation droplets from plants [135,330], bacteria [129] and fungi [133,136,331–335] was investigated in just a few studies. This is surprising since their analysis can be achieved in a straightforward manner. Nevertheless, different studies confirm the data from this work regarding the presence of secondary metabolites in guttation droplets. Sun et al. and Aliferis et al. studied primary metabolites in *Suillus bovinus* (Boletales, Basidiomycota) and simple phenolic metabolites in *Rhizoctonia solani* (asexual form of *Thanatephorus cucumeris*, Cantharellales, Basidiomycota), respectively [119,335]. Their results showed that guttation droplets in these species contain a wide array of primary metabolites, *e.g.*, sugars, amino acids, sugar

alcohols and fatty acids. *R. solani* even exudes different organic acids, mostly phenolic substances, like ferulic acid, ellagic acid, gallic acid. Antioxidant activity was also published for exudates from *S. bovinus*, though they have not been characterized chemically [132].

Regarding secondary metabolites, mainly *Penicillium* spp. were studied due to the ample amount of exudates, which they regularly produce in axenic culture. Also, their specific coloration is an important taxonomic feature [286]. Thus Wang et al. showed in a study on *Penicillium citreonigrum* that guttation droplets can be a prolific source of secondary metabolites, among them azaphilones and meroterpenoids [331]. They also showed that epigenetic modifiers can be used to increase the number of secondary metabolites in the fungus and consequently in the droplets. These studies lend support to the observation that in *E. nigrum* strain 749 different secondary metabolites were found, while the complex chromatograms even suggest the presence of a wide array of non-identified metabolites. The complexity also reflects the wide spectrum of secondary metabolites, which have been found in *E. nigrum* in this work and before [336].

Further support for the remarkable concentration of epipyrones (**1-3**) found in guttation droplets (see **fig. 4.42** and **4.43** in **section 4.7**) during this work comes from following studies. Both analyzed the mycotoxin concentration in exudates. In the first study, the concentrations of ochratoxins A and B in *Penicillium nordicum* and *P. verrucosum* (both Aspergillaceae, Eurotiales) were shown to be significantly higher than in the underlying mycelium and culture medium [133]. Ochratoxins are highly nephrotoxic isocoumarin derivatives, which are often found in staples [337]. In another study, Gareis et al. assessed guttation droplets from different strains of *Stachybotrys chartarum* (Stachybotryaceae, Hypocreales) for their mycotoxin concentration and bioactivity. Using mass spectrometry and an MTT-assay, they found that the droplets are highly cytotoxic due to their content in different trichothecenes, *i.e.,* sesquiterpenes containing an epoxy function [334].

Thus, it can be concluded that guttation droplets are an important means for the exudation of highly bioactive substances. Also, data from this study and from the aforementioned work on *P. nordicum* show that guttation might just be one side of a two-sided secretion strategy, since the main metabolites were also found in the medium. The ecological relevance is also underpinned by the work of Figueroa et al. They reported on the identification of different polyhydroxyanthraquinones in exudates of *P. restrictum* [136]. Interestingly, these compounds exhibited inhibitory activity on the quorum sensing of methicillin-resistant *Staphylococcus aureus* (MRSA), which gives a hint on their ecological potential. They could also link the production of guttation droplets to high local concentrations of the mentioned metabolites by MS-Imaging.

These studies clearly show that exudates probably have a significant impact on the surrounding microbiota and on fungivores. The high concentration of epipyrones (**1**-**3**) and other secondary metabolites could thus be seen as a means to control the microbial community structure and maybe even to defend the fungus against fungivory. The latter was shown for guttation droplets of *A. nidulans*, which act to deter collembolans (syn. springtails, *Folsomia candida*) from feeding on the fruiting bodies [137].

Further studies on the regulation of secondary metabolism in *E. nigrum*, especially on genome and transcription level, could give more insights into the underlying mechanisms of guttation and its ecological roles. Electron microscopy and MS-imaging could also serve as powerful tools for the understanding of guttation and its correlation with secondary metabolism.

6   SUMMARY

Members of the kingdom of fungi belong to one of the most diverse life forms on earth. This is also reflected by the ability of these organisms to synthesize a huge array of secondary metabolites with unusual scaffolds and potent bioactivities. The latter also explain the application of many fungal products in therapy, *e.g.*, lovastatin, cyclosporine A, mycophenolic acid.

In order to find new chemical entities for medicinal use, increasingly remote or inaccessible areas are explored for yet not investigated fungal species or strains. Therefore, two marine-derived strains of *Epicoccum nigrum* – strain 749 and strain 800 – were chosen as target organisms for this work. They were subjected to different culture conditions in order to elicit the production of bioactive natural products.

In this way, a total of 12 compounds, mostly of polyketide origin, but with different scaffolds were isolated and identified based on the extensive use of a range of analytical techniques, especially NMR spectroscopy. Three of them are new chemical entities, *i.e.*, 5´,6´-dihydroxyacetosellin, 1F4-1-6, epicaronic acid, and one, *i.e.*, tricinonoic acid was not found in *E. nigrum* before.

The unusual structure of acetosellin suggested, that its biosynthesis may proceed via the condensation of two separate polyketide-derived moieties, a biosynthetic peculiarity that is rarely seen in nature. In order to verify this hypothesis, *E. nigrum* cultures were incubated with ^{13}C-labeled sodium acetate, and the resulting labeling pattern of the respective metabolite analyzed by NMR. The results indeed proved that acetosellin is the product of two separate polyketide synthases. These are postulated to synthesize a bicyclic core and an acyclic polyketide unit, which subsequently are condensated to form the unique naphthoquinone part of this metabolite.
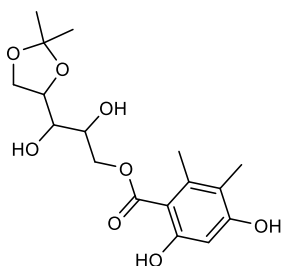
1F4-1-6
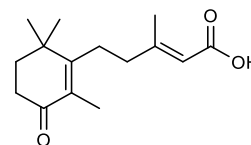
Epicaronic acid
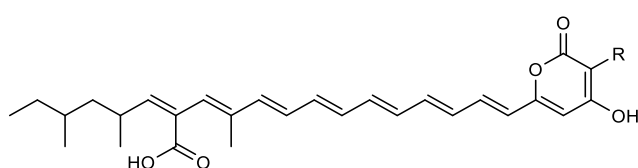
R = 1-*C*-(β-galactopyranosyl): Epipyrone A

R = 1-*C*-(α-galactofuranosyl): Epipyrone B

R = 1-*C*-(β-galactofuranosyl): Epipyrone C
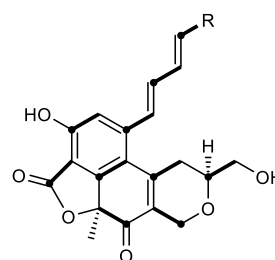
R =   **Acetosellin**
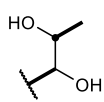
R =   **5´-6´-Dihydroxy-acetosellin**

Figure 6.1: Structures of metabolites isolated from *E. nigrum*. For acetosellin, the acetate units as analyzed by incubation with [1-^{13}C]acetate are shown in bold with bold dots indicating incorporated ^{13}C-1-atoms from [1-^{13}C]acetate.

The bioactivities of these natural products were foremost assessed against human enzymatic targets. Thus, epipyrones were proven to be the first inhibitors of human cerebroside sulfotransferase (hCST), an enzyme implicated in the lysosomal storage disease metachromatic leukodystrophy, with an IC$_{50}$ of 61.4 µM. Even though this activity is rather weak, this molecule can in future studies serve as a lead structure for the development of more potent inhibitors. Of special interest is also, that epipyrones exert potent and selective effects on cysteine- and serine-proteases, namely human leukocyte elastase (HLE) with an IC$_{50}$ of 4.63 µM, cathepsin S (IC$_{50}$ = 6.61 µM) and cathepsin K (IC$_{50}$ = 11.4 µM). Interestingly, trypsin, chymotrypsin, as well as cathepsins B and L were not inhibited, showing that there is a high degree of selectivity. The *C*-glycosyl moiety of epipyrones is an extraordinary chemical feature of these compounds, but also responsible for the chemical interconversions between epipyrones A-C. The glycosyl part of epipyrones was thus semi-synthetically

modified by acetylation, yielding a chemically stable tetra-, and a triacetate as major products. These, however, showed markedly diminished potency toward the aforementioned enzymes.

During cultivation, *E. nigrum* strain 749 forms guttation droplets, *i.e.*, exudates. This is highly dependent on growth conditions, *e.g.*, the addition of trace metals and illumination. Not only the production of guttation droplets is influenced, but also the type and concentration of secondary metabolites. In order to shed light on the regulation of this process, the levels of the major secondary metabolites – epipyrones and acetosellin – were analyzed in the guttation droplets and compared to those in extracts from the mycelium and cultivation medium. Thus, trace metal addition, *i.e.*, Cu^{2+} and Zn^{2+}, led to a pronounced production of epipyrones, of which the concentration is even more elevated, when the culture is not illuminated. Under optimal conditions, the concentration of epipyrones is 0.31 mM (per Liter medium) in the mycelium and medium extracts and 2.0 mM in the droplets. In contrast, acetosellin was best synthesized without trace metals. Acetosellin levels in the guttation droplets were always much lower than those for epipyrones, i.e. <0.09 mM.

In conclusion, *E. nigrum* is a producer of promising enzyme inhibitors, which may serve as the basis for the development of drug candidates. The herein described results concerning biosynthesis and differential production of secondary metabolites will support future studies with the respective compounds.

7   REFERENCES

1. Newman, D. J.; Cragg, G. M. Natural Products as Sources of New Drugs from 1981 to 2014. *J. Nat. Prod.* **2016**, *79*, 629–661.

2. Kellenberger, E.; Hofmann, A.; Quinn, R. J. Similar interactions of natural products with biosynthetic enzymes and therapeutic targets could explain why nature produces such a large proportion of existing drugs. *Nat. Prod. Rep.* **2011**, *28*, 1483–1492.

3. Brahmachari, G. Natural Products in Drug Discovery: Impacts and Opportunities - An Assessment. In *Bioactive natural products: opportunities and challenges in medicinal chemistry*; World Scientific Publishing Co. Pte. Ltd.: Singapore, 2011; pp. 1–199.

4. Blackwell, M. The Fungi: 1, 2, 3 ... 5.1 million species? *Am. J. Bot.* **2011**, *98*, 426–438.

5. Stajich, J. E.; Berbee, M. L.; Blackwell, M.; Hibbett, D. S.; James, T. Y.; Spatafora, J. W.; Taylor, J. W. Primer–The Fungi. *Curr. Biol. CB* **2009**, *19*, R840–R845.

6. Müller, K. Pharmaceutically relevant metabolites from lichens. *Appl. Microbiol. Biotechnol.* **2001**, *56*, 9–16.

7. Gueidan, C.; Villaseñor, C. R.; de Hoog, G. S.; Gorbushina, A. A.; Untereiner, W. A.; Lutzoni, F. A rock-inhabiting ancestor for mutualistic and pathogen-rich fungal lineages. *Stud. Mycol.* **2008**, *61*, 111–119.

8. Kogej, T.; Wheeler, M. H.; Lanisnik Rizner, T.; Gunde-Cimerman, N. Evidence for 1,8-dihydroxynaphthalene melanin in three halophilic black yeasts grown under saline and non-saline conditions. *FEMS Microbiol. Lett.* **2004**, *232*, 203–209.

9. Ottow, J. C. G. Böden als Lebensräume. In *Mikrobiologie von Böden*; Springer-Lehrbuch; Springer Berlin Heidelberg: Berlin, Heidelberg, 2011; pp. 1–28.

10. Garbeva, P.; Hol, W. H. G.; Termorshuizen, A. J.; Kowalchuk, G. A.; de Boer, W. Fungistasis and general soil biostasis – A new synthesis. *Soil Biol. Biochem.* **2011**, *43*, 469–477.

11. Adrio, J. L.; Demain, A. L. Fungal biotechnology. *Int. Microbiol.* **2003**, *6*, 191–199.

12. Ghorai, S.; Banik, S. P.; Verma, D.; Chowdhury, S.; Mukherjee, S.; Khowala, S. Fungal biotechnology in food and feed processing. *Food Res. Int.* **2009**, *42*, 577–587.

13. Bennett, J. W. Mycotechnology: the role of fungi in biotechnology. *J. Biotechnol.* **1998**, *66*, 101–107.

14. Fávaro, L. C. de L.; de Melo, F. L.; Aguilar-Vildoso, C. I.; Araújo, W. L. Polyphasic Analysis of Intraspecific Diversity in *Epicoccum nigrum* Warrants Reclassification into Separate Species. *PLoS ONE* **2011**, *6*, 1–18.

15. Brakhage, A. A. Regulation of fungal secondary metabolism. *Nat. Rev. Microbiol.* **2012**, *11*, 21–32.

16. Benoit, I.; Culleton, H.; Zhou, M.; DiFalco, M.; Aguilar-Osorio, G.; Battaglia, E.; Bouzid, O.; Brouwer, C. P. J. M.; El-Bushari, H. B. O.; Coutinho, P. M.; Gruben, B. S.; Hildén, K. S.; Houbraken, J.; Barboza, L. A. J.; Levasseur, A.; Majoor, E.; Mäkelä, M. R.; Narang, H.-M.; Trejo-Aguilar, B.; van den Brink, J.; vanKuyk, P. A.; Wiebenga, A.; McKie, V.; McCleary, B.;

Tsang, A.; Henrissat, B.; de Vries, R. P. Closely related fungi employ diverse enzymatic strategies to degrade plant biomass. *Biotechnol. Biofuels* **2015**, *8*, 1–14.

17. Hoffmeister, D.; Keller, N. P. Natural products of filamentous fungi: enzymes, genes, and their regulation. *Nat. Prod. Rep.* **2007**, *24*, 393–416.

18. Guyon, K.; Balagué, C.; Roby, D.; Raffaele, S. Secretome analysis reveals effector candidates associated with broad host range necrotrophy in the fungal plant pathogen Sclerotinia sclerotiorum. *Bmc Genomics* **2014**, *15*, 1–18.

19. Frisvad, J. C.; Andersen, B.; Thrane, U. The use of secondary metabolite profiling in chemotaxonomy of filamentous fungi. *Mycol. Res.* **2008**, *112*, 231–240.

20. Frisvad, J. C. Media and Growth Conditions for Induction of Secondary Metabolite Production. *Fungal Second. Metab.* **2012**, *944*, 47–58.

21. Fuchser, J.; Zeeck, A. Secondary Metabolites by Chemical Screening, 34.–Aspinolides and Aspinonene/Aspyrone Co-Metabolites, New Pentaketides Produced by Aspergillus ochraceus. *Liebigs Ann.* **1997**, *1997*, 87–95.

22. Bode, H. B.; Bethe, B.; Höfs, R.; Zeeck, A. Big Effects from Small Changes: Possible Ways to Explore Nature's Chemical Diversity. *ChemBioChem* **2002**, *3*, 619–627.

23. Cuero, R.; Ouellet, T. Metal ions modulate gene expression and accumulation of the mycotoxins aflatoxin and zearalenone. *J. Appl. Microbiol.* **2005**, *98*, 598–605.

24. Schmidt-Heydt, M.; Stoll, D.; Schütz, P.; Geisen, R. Oxidative stress induces the biosynthesis of citrinin by *Penicillium verrucosum* at the expense of ochratoxin. *Int. J. Food Microbiol.* **2015**, *192*, 1–6.

25. Bayram, Ö.; Feussner, K.; Dumkow, M.; Herrfurth, C.; Feussner, I.; Braus, G. H. Changes of global gene expression and secondary metabolite accumulation during light-dependent *Aspergillus nidulans* development. *Fungal Genet. Biol.* **2016**, *87*, 30–53.

26. Marmann, A.; Aly, A.; Lin, W.; Wang, B.; Proksch, P. Co-Cultivation—A Powerful Emerging Tool for Enhancing the Chemical Diversity of Microorganisms. *Mar. Drugs* **2014**, *12*, 1043–1065.

27. Kornienko, A.; Evidente, A.; Vurro, M.; Mathieu, V.; Cimmino, A.; Evidente, M.; van Otterlo, W. A. L.; Dasari, R.; Lefranc, F.; Kiss, R. Toward a Cancer Drug of Fungal Origin. *Med. Res. Rev.* **2015**, *35*, 937–967.

28. Alvarado, J. J.; Nemkal, A.; Sauder, J. M.; Russell, M.; Akiyoshi, D. E.; Shi, W.; Almo, S. C.; Weiss, L. M. Structure of a microsporidian methionine aminopeptidase type 2 complexed with fumagillin and TNP-470. *Mol. Biochem. Parasitol.* **2009**, *168*, 158–167.

29. Selvakumar, P.; Lakshmikuttyamma, A.; Dimmock, J. R.; Sharma, R. K. Methionine aminopeptidase 2 and cancer. *Biochim. Biophys. Acta BBA - Rev. Cancer* **2006**, *1765*, 148–154.

30. Microsporidiosis - Treatment information http://www.cdc.gov/dpdx/microsporidiosis/tx.html.

31. Kicia, M.; Wesolowska, M.; Kopacz, Z.; Jakuszko, K.; Sak, B.; Květonová, D.; Krajewska, M.; Kváč, M. Prevalence and molecular characteristics of urinary and intestinal microsporidia infections in renal transplant recipients. *Clin. Microbiol. Infect.* **2016**, *22*, 462.e5-462.e9.

32. Nakamura, I.; Yoshimura, S.; Masaki, T.; Takase, S.; Ohsumi, K.; Hashimoto, M.; Furukawa, S.; Fujie, A. ASP2397: a novel antifungal agent produced by *Acremonium persicinum* MF-347833. *J. Antibiot. (Tokyo)* **2016**, 1–7.

33. Nakamura, I.; Ohsumi, K.; Yoshikawa, K.; Kanasaki, R.; Masaki, T.; Takase, S.; Hashimoto, M.; Fujie, A.; Nakai, T.; Matsumoto, S.; Takeda, S.; Akamatsu, S.; Uchida, S.; Maki, K. ASP2397: A Novel Natural Product with Potent Fungicidal Activity against *Aspergillus* spp. (1) - A New Mode of Action and In Vitro Activity. In *54th Interscience Conference on Antimicrobial Agents and Chemotherapy*; Washington D.C., 2014.

34. Vical - Products - VL-2397 Antifungal. http://www.vical.com/products/VL-2397/default.aspx (accessed Sep 24, 2016).

35. Nakamura, I.; Nakai, T.; Matsumoto, S.; Takeda, S.; Akamatsu, S.; Uchida, S.; Koide, Y.; Mitori, H.; Noto, T.; Maki, K. ASP2397: A Novel Natural Product with Potent Fungicidal Activity against *Aspergillus* spp. (2) - In Vivo activity against *A. fumigatus*. In *54th Interscience Conference on Antimicrobial Agents and Chemotherapy*; Washington D.C., 2014.

36. Osherov, N.; Kontoyiannis, D. P. The anti-*Aspergillus* drug pipeline: Is the glass half full or empty? *Med. Mycol.* **2016**, 1–7.

37. Casieri, L.; Ait Lahmidi, N.; Doidy, J.; Veneault-Fourrey, C.; Migeon, A.; Bonneau, L.; Courty, P.-E.; Garcia, K.; Charbonnier, M.; Delteil, A.; Brun, A.; Zimmermann, S.; Plassard, C.; Wipf, D. Biotrophic transportome in mutualistic plant–fungal interactions. *Mycorrhiza* **2013**, *23*, 597–625.

38. Haq, I. U.; Zhang, M.; Yang, P.; van Elsas, J. D. The Interactions of Bacteria with Fungi in Soil. In *Advances in Applied Microbiology*; Elsevier, 2014; Vol. 89, pp. 185–215.

39. Bianciotto, V.; Bandi, C.; Minerdi, D.; Sironi, M.; Tichy, H. V.; Bonfante, P. An obligately endosymbiotic mycorrhizal fungus itself harbors obligately intracellular bacteria. *Appl. Environ. Microbiol.* **1996**, *62*, 3005–3010.

40. Bauchop, T. Rumen anaerobic fungi of cattle and sheep. *Appl. Environ. Microbiol.* **1979**, *38*, 148–158.

41. Klepzig, K. D.; Moser, J. C.; Lombardero, F. J.; Hofstetter, R. W.; Ayres, M. P. Symbiosis and competition: complex interactions among beetles, fungi, and mites. **2001**.

42. Currie, C. R.; Scott, J. A.; Summerbell, R. C.; Malloch, D. Fungus-growing ants use antibiotic-producing bacteria to control garden parasites. *Nature* **1999**, *398*, 701–704.

43. Moore, D.; Robson, G. D.; Trinci, A. P. J. *21st century guidebook to fungi*; Cambridge University Press: Cambridge ; New York, 2011.

44. Bouarab, K.; Potin, P.; Correa, J.; Kloareg, B. Sulfated oligosaccharides mediate the interaction between a marine red alga and its green algal pathogenic endophyte. *Plant Cell* **1999**, *11*, 1635–1650.

45. Trémouillaux-Guiller, J.; Rohr, T.; Rohr, R.; Huss, V. A. Discovery of an endophytic alga in *Ginkgo biloba*. *Am. J. Bot.* **2002**, *89*, 727–733.

46. Stone, J. K.; Polishook, J. D.; White, J. F. Endophytic fungi. *Biodivers. Fungi Elsevier Acad. Press Burlingt.* **2004**, 241–270.

47. Bacon, C. W.; White, J. F. Functions, mechanisms and regulation of endophytic and epiphytic microbial communities of plants. *Symbiosis* **2015**, *68*, 87–98.

48. Richardson, M. D.; Chapman, G. W.; Hoveland, C. S.; Bacon, C. W. Sugar Alcohols in Endophyte-Infected Tall Fescue Under Drought. *Crop Sci.* **1992**, *32*, 1060–1061.

49. Waller, F.; Achatz, B.; Baltruschat, H.; Fodor, J.; Becker, K.; Fischer, M.; Heier, T.; Hückelhoven, R.; Neumann, C.; von Wettstein, D.; Franken, P.; Kogel, K. H. The endophytic fungus *Piriformospora indica* reprograms barley to salt-stress tolerance, disease resistance, and higher yield. *Proc. Natl. Acad. Sci. U. S. A.* **2005**, *102*, 13386–13391.

50. Johnson, L. J.; de Bonth, A. C. M.; Briggs, L. R.; Caradus, J. R.; Finch, S. C.; Fleetwood, D. J.; Fletcher, L. R.; Hume, D. E.; Johnson, R. D.; Popay, A. J.; Tapper, B. A.; Simpson, W. R.; Voisey, C. R.; Card, S. D. The exploitation of epichloae endophytes for agricultural benefit. *Fungal Divers.* **2013**, *60*, 171–188.

51. White, J. F.; Torres, M. S. Is plant endophyte-mediated defensive mutualism the result of oxidative stress protection? *Physiol. Plant.* **2010**, *138*, 440–446.

52. Schardl, C. L.; Florea, S.; Pan, J.; Nagabhyru, P.; Bec, S.; Calie, P. J. The epichloae: alkaloid diversity and roles in symbiosis with grasses. *Curr. Opin. Plant Biol.* **2013**, *16*, 480–488.

53. Aly, A. H.; Debbab, A.; Proksch, P. Fungal endophytes - secret producers of bioactive plant metabolites. *Pharm.- Int. J. Pharm. Sci.* **2013**, *68*, 499–505.

54. Soliman, S. S. M.; Greenwood, J. S.; Bombarely, A.; Mueller, L. A.; Tsao, R.; Mosser, D. D.; Raizada, M. N. An Endophyte Constructs Fungicide-Containing Extracellular Barriers for Its Host Plant. *Curr. Biol.* **2015**, *25*, 2570–2576.

55. Heinig, U.; Scholz, S.; Jennewein, S. Getting to the bottom of Taxol biosynthesis by fungi. *Fungal Divers.* **2013**, *60*, 161–170.

56. El-Elimat, T.; Raja, H. A.; Graf, T. N.; Faeth, S. H.; Cech, N. B.; Oberlies, N. H. Flavonolignans from *Aspergillus iizukae* , a Fungal Endophyte of Milk Thistle (*Silybum marianum*). *J. Nat. Prod.* **2014**, *77*, 193–199.

57. Milic, N.; Milosevic, N.; Suvajdzic, L.; Zarkov, M.; Abenavoli, L. New therapeutic potentials of milk thistle (*Silybum marianum*). *Nat. Prod. Commun.* **2013**, 1801–1810.

58. Richards, T. A.; Jones, M. D. M.; Leonard, G.; Bass, D. Marine Fungi: Their Ecology and Molecular Diversity. *Annu. Rev. Mar. Sci.* **2012**, *4*, 495–522.

59. Zhang, T.; Wang, N.-F.; Zhang, Y.-Q.; Liu, H.-Y.; Yu, L.-Y. Diversity and Distribution of Aquatic Fungal Communities in the Ny-Ålesund Region, Svalbard (High Arctic): Aquatic Fungi in the Arctic. *Microb. Ecol.* **2016**, *71*, 543–554.

60. Webster, J.; Weber, R. *Introduction to fungi*; Cambridge University Press: Cambridge, UK; New York, 2007.

61. Manohar, C. S.; Raghukumar, C. Fungal diversity from various marine habitats deduced through culture-independent studies. *FEMS Microbiol. Lett.* **2013**, *341*, 69–78.

62. Pang, K.-L.; Jones, E. B. G. Phylogenetic Diversity of Fungi in the Sea including the Opisthosporidia. In *Biology of Microfungi*; Li, D.-W., Ed.; Springer International Publishing: Cham, 2016; pp. 267–283.

63. Jones, E. B. G. Fifty years of marine mycology. *Fungal Divers.* **2011**, *50*, 73–112.

64. Flewelling, A. J.; Johnson, J. A.; Gray, C. A. Isolation and bioassay screening of fungal endophytes from North Atlantic marine macroalgae. *Bot. Mar.* **2013**, *56*.

65. Rateb, M. E.; Ebel, R. Secondary metabolites of fungi from marine habitats. *Nat. Prod. Rep.* **2011**, *28*, 290.

66. Newman, D.; Cragg, G. Drugs and Drug Candidates from Marine Sources: An Assessment of the Current "State of Play." *Planta Med.* **2016**, *82*, 775–789.

67. Jin, L.; Quan, C.; Hou, X.; Fan, S. Potential Pharmacological Resources: Natural Bioactive Compounds from Marine-Derived Fungi. *Mar. Drugs* **2016**, *14*, 76.

68. Yamazaki, Y.; Tanaka, K.; Nicholson, B.; Deyanat-Yazdi, G.; Potts, B.; Yoshida, T.; Oda, A.; Kitagawa, T.; Orikasa, S.; Kiso, Y.; Yasui, H.; Akamatsu, M.; Chinen, T.; Usui, T.; Shinozaki, Y.; Yakushiji, F.; Miller, B. R.; Neuteboom, S.; Palladino, M.; Kanoh, K.; Lloyd, G. K.; Hayashi, Y. Synthesis and Structure–Activity Relationship Study of Antimicrotubule Agents Phenylahistin Derivatives with a Didehydropiperazine-2,5-dione Structure. *J. Med. Chem.* **2012**, *55*, 1056–1071.

69. Fenical, W.; Jensen, P. R.; Cheng, X. C. Halimide, a cytotoxic marine natural product, and derivatives thereof. US Patent 6,069,146. 2000.

70. Singh, A. V.; Bandi, M.; Raje, N.; Richardson, P.; Palladino, M. A.; Chauhan, D.; Anderson, K. C. A novel vascular disrupting agent plinabulin triggers JNK-mediated apoptosis and inhibits angiogenesis in multiple myeloma cells. *Blood* **2011**, *117*, 5692–5700.

71. Assessment of Docetaxel + Plinabulin Compared to Docetaxel + Placebo in Patients With Advanced NSCLC With at Least One Measurable Lung Lesion https://clinicaltrials.gov/ct2/show/NCT02504489?term=plinabulin&rank=2 (accessed Sep 25, 2016).

72. Zech, Isabell Substratreduktionstherapie der Metachromatischen Leukodystrophie: Expression der Cerebrosid-Sulfotransferase und Etablierung einer hochdurchsatzfähigen Aktivitätsbestimmung. Dissertation, Universität Bonn: Bonn, 2013.

73. Yaghootfam, A.; Sorkalla, T.; Häberlein, H.; Gieselmann, V.; Kappler, J.; Eckhardt, M. Cerebroside Sulfotransferase Forms Homodimers in Living Cells. *Biochemistry (Mosc.)* **2007**, *46*, 9260–9269.

74. Honke, K.; Yamane, M.; Ishii, A.; Kobayashi, T.; Makita, A. Purification and characterization of 3′-phosphoadenosine-5′-phosphosulfate: GalCer sulfotransferase from human renal cancer cells. *J. Biochem. (Tokyo)* **1996**, *119*, 421–427.

75. Biffi, A.; Lucchini, G.; Rovelli, A.; Sessa, M. Metachromatic leukodystrophy: an overview of current and prospective treatments. *Bone Marrow Transplant.* **2008**, *42*, S2–S6.

76. Takahashi, T.; Suzuki, T. Role of sulfatide in normal and pathological cells and tissues. *J. Lipid Res.* **2012**, *53*, 1437–1450.

77. Gieselmann, V.; Krägeloh-Mann, I. Metachromatic Leukodystrophy – An Update. *Neuropediatrics* **2010**, *41*, 1–6.

78. Kuchař, L.; Ledvinová, J.; Hřebíček, M.; Myšková, H.; Dvořáková, L.; Berná, L.; Chrastina, P.; Asfaw, B.; Elleder, M.; Petermöller, M.; Mayrhofer, H.; Staudt, M.; Krägeloh-Mann, I.; Paton, B. C.; Harzer, K. Prosaposin deficiency and saposin B deficiency (activator-deficient metachromatic leukodystrophy): Report on two patients detected by analysis of urinary sphingolipids and carrying novel PSAP gene mutations. *Am. J. Med. Genet. A* **2009**, *149A*, 613–621.

79. Siri, L.; Rossi, A.; Lanza, F.; Mazzotti, R.; Costa, A.; Stroppiano, M.; Gaiero, A.; Cohen, A.; Biancheri, R.; Filocamo, M. A novel homozygous splicing mutation in PSAP gene causes metachromatic leukodystrophy in two Moroccan brothers. *neurogenetics* **2014**, *15*, 101–106.

References

80. Multicenter Study of HGT-1110 Administered Intrathecally in Children With Metachromatic Leukodystrophy (MLD) (IDEAMLD) https://clinicaltrials.gov/ct2/show/NCT01510028 (accessed Jul 22, 2016).

81. Biffi, A.; Montini, E.; Lorioli, L.; Cesani, M.; Fumagalli, F.; Plati, T.; Baldoli, C.; Martino, S.; Calabria, A.; Canale, S.; Benedicenti, F.; Vallanti, G.; Biasco, L.; Leo, S.; Kabbara, N.; Zanetti, G.; Rizzo, W. B.; Mehta, N. A. L.; Cicalese, M. P.; Casiraghi, M.; Boelens, J. J.; Del Carro, U.; Dow, D. J.; Schmidt, M.; Assanelli, A.; Neduva, V.; Di Serio, C.; Stupka, E.; Gardner, J.; von Kalle, C.; Bordignon, C.; Ciceri, F.; Rovelli, A.; Roncarolo, M. G.; Aiuti, A.; Sessa, M.; Naldini, L. Lentiviral Hematopoietic Stem Cell Gene Therapy Benefits Metachromatic Leukodystrophy. *Science* **2013**.

82. Platt, F. M.; Jeyakumar, M. Substrate reduction therapy. *Acta Paediatr.* **2008**, *97*, 88–93.

83. Pastores, G. M. Miglustat: substrate reduction therapy for lysosomal storage disorders associated with primary central nervous system involvement. *Recent Patents CNS Drug Discov.* **2006**, *1*, 77–82.

84. Warnock, D. G.; Bichet, D. G.; Holida, M.; Goker-Alpan, O.; Nicholls, K.; Thomas, M.; Eyskens, F.; Shankar, S.; Adera, M.; Sitaraman, S.; Khanna, R.; Flanagan, J. J.; Wustman, B. A.; Barth, J.; Barlow, C.; Valenzano, K. J.; Lockhart, D. J.; Boudes, P.; Johnson, F. K. Oral Migalastat HCl Leads to Greater Systemic Exposure and Tissue Levels of Active α-Galactosidase A in Fabry Patients when Co-Administered with Infused Agalsidase. *PLOS ONE* **2015**, *10*, 1–17.

85. Germain, D. P.; Giugliani, R.; Hughes, D. A.; Mehta, A.; Nicholls, K.; Barisoni, L.; Jennette, C. J.; Bragat, A.; Castelli, J.; Sitaraman, S.; Lockhart, D. J.; Boudes, P. Safety and pharmacodynamic effects of a pharmacological chaperone on α-galactosidase A activity and globotriaosylceramide clearance in Fabry disease: report from two phase 2 clinical studies. *Orphanet J. Rare Dis.* **2012**, *7*, 1–11.

86. Miyake, Y.; Ebata, M. Inhibition of *β*-Galactosidase by Galactostatin, Galactostatin-lactam, and 1-Deoxygalactostatin. *Agric. Biol. Chem.* **1988**, *52*, 1649–1654.

87. Di Cera, E. Serine proteases. *IUBMB Life* **2009**, *61*, 510–515.

88. Puente, X. S.; Sánchez, L. M.; Gutiérrez-Fernández, A.; Velasco, G.; López-Otín, C. A genomic view of the complexity of mammalian proteolytic systems. *Biochem. Soc. Trans.* **2005**, *33*, 331–334.

89. Rawlings, N. D.; Barrett, A. J.; Finn, R. Twenty years of the *MEROPS* database of proteolytic enzymes, their substrates and inhibitors. *Nucleic Acids Res.* **2016**, *44*, D343–D350.

90. Page, M. J.; Di Cera, E. Serine peptidases: Classification, structure and function. *Cell. Mol. Life Sci.* **2008**, *65*, 1220–1236.

91. Buhling, F.; Groneberg, D.; Welte, T. Proteases and their role in chronic inflammatory lung diseases. *Curr. Drug Targets* **2006**, *7*, 751–759.

92. Antão, C. M.; Malcata, F. X. Plant serine proteases: biochemical, physiological and molecular features. *Plant Physiol. Biochem.* **2005**, *43*, 637–650.

93. Hedstrom, L. Serine Protease Mechanism and Specificity. *Chem. Rev.* **2002**, *102*, 4501–4524.

94. Löffler, G.; Mössner, J. Gastrointestinaltrakt. In *Biochemie und Pathobiochemie*; Heinrich, C. P.; Müller, M.; Graeve, L., Eds.; Springer Berlin Heidelberg: Berlin, Heidelberg, 2014; pp. 745–769.

References

95. Pham, C. T. N. Neutrophil serine proteases: specific regulators of inflammation. *Nat. Rev. Immunol.* **2006**, *6*, 541–550.

96. Verma, S.; Dixit, R.; Pandey, K. C. Cysteine Proteases: Modes of Activation and Future Prospects as Pharmacological Targets. *Front. Pharmacol.* **2016**, *7*.

97. Barrett, A. J.; Rawlings, N. D. Families and clans of cysteine peptidases. *Perspect. Drug Discov. Des.* **1996**, *6*, 1–11.

98. Konno, K.; Hirayama, C.; Nakamura, M.; Tateishi, K.; Tamura, Y.; Hattori, M.; Kohno, K. Papain protects papaya trees from herbivorous insects: role of cysteine proteases in latex: *Role of cysteine proteases in latex. Plant J.* **2004**, *37*, 370–378.

99. Turk, V.; Stoka, V.; Vasiljeva, O.; Renko, M.; Sun, T.; Turk, B.; Turk, D. Cysteine cathepsins: From structure, function and regulation to new frontiers. *Biochim. Biophys. Acta BBA - Proteins Proteomics* **2012**, *1824*, 68–88.

100. de Sousa, L. R. F.; Wu, H.; Nebo, L.; Fernandes, J. B.; da Silva, M. F. das G. F.; Kiefer, W.; Schirmeister, T.; Vieira, P. C. Natural products as inhibitors of recombinant cathepsin L of *Leishmania mexicana. Exp. Parasitol.* **2015**, *156*, 42–48.

101. Sun, Y.-L.; Zhang, X.-Y.; Zheng, Z.-H.; Xu, X.-Y.; Qi, S.-H. Three new polyketides from marine-derived fungus *Penicillium citrinum* SCSGAF 0167. *Nat. Prod. Res.* **2014**, *28*, 239–244.

102. Tabares, P.; Degel, B.; Schaschke, N.; Hentschel, U.; Schirmeister, T. Identification of the protease inhibitor miraziridine A in the Red sea sponge *Theonella swinhoei. Pharmacogn. Res.* **2012**, *4*, 63–66.

103. Zeng, G.-Z.; Pan, X.-L.; Tan, N.-H.; Xiong, J.; Zhang, Y.-M. Natural biflavones as novel inhibitors of cathepsin B and K. *Eur. J. Med. Chem.* **2006**, *41*, 1247–1252.

104. Zeng, G.-Z.; Tan, N.-H.; Hao, X.-J.; Mu, Q.-Z.; Li, R.-T. Natural inhibitors targeting osteoclast-mediated bone resorption. *Bioorg. Med. Chem. Lett.* **2006**, *16*, 6178–6180.

105. Patil, A. D.; Freyer, A. J.; Carte, B.; Taylor, P. B.; Johnson, R. K.; Faulkner, D. J. Haploscleridamine, a Novel Tryptamine-Derived Alkaloid from a Sponge of the Order Haploscleriда: An Inhibitor of Cathepsin K. *J. Nat. Prod.* **2002**, *65*, 628–629.

106. Neumann, K.; Kehraus, S.; Gutschow, M.; Konig, G. M. Cytotoxic and HLE-inhibitory tetramic acid derivatives from marine-derived fungi. *Nat. Prod. Commun.* **2009**, *4*, 347–354.

107. Almeida, C.; Hemberger, Y.; Schmitt, S. M.; Bouhired, S.; Natesan, L.; Kehraus, S.; Dimas, K.; Gütschow, M.; Bringmann, G.; König, G. M. Marilines A-C: Novel Phthalimidines from the Sponge-Derived Fungus *Stachylidium* sp. *Chem. - Eur. J.* **2012**, *18*, 8827–8834.

108. Grady, T.; Mah'Moud, M.; Otani, T.; Rhee, S.; Lerch, M. M.; Gorelick, F. S. Zymogen proteolysis within the pancreatic acinar cell is associated with cellular injury. *Am. J. Physiol. - Gastrointest. Liver Physiol.* **1998**, *275*, G1010–G1017.

109. Döring, G. The Role of Neutrophil Elastase in Chronic Inflammation. *Am. J. Respir. Crit. Care Med.* **1994**, *150*, S114–S117.

110. Ohbayashi, H. Neutrophil elastase inhibitors as treatment for COPD. *Expert Opin. Investig. Drugs* **2002**, *11*, 965–980.

111. Brömme, D.; Lecaille, F. Cathepsin K inhibitors for osteoporosis and potential off-target effects. *Expert Opin. Investig. Drugs* **2009**, *18*, 585–600.

112. Schmitz, J.; Li, T.; Bartz, U.; Gütschow, M. Cathepsin B Inhibitors: Combining Dipeptide Nitriles with an Occluding Loop Recognition Element by Click Chemistry. *ACS Med. Chem. Lett.* **2016**, *7*, 211–216.

113. Sudhan, D. R.; Siemann, D. W. Cathepsin L targeting in cancer treatment. *Pharmacol. Ther.* **2015**, *155*, 105–116.

114. Gupta, S.; Singh, R. K.; Dastidar, S.; Ray, A. Cysteine cathepsin S as an immunomodulatory target: present and future trends. *Expert Opin. Ther. Targets* **2008**, *12*, 291–299.

115. Lee-Dutra, A.; Wiener, D. K.; Sun, S. Cathepsin S inhibitors: 2004 – 2010. *Expert Opin. Ther. Pat.* **2011**, *21*, 311–337.

116. Schönefuß, A.; Wendt, W.; Schattling, B.; Schulten, R.; Hoffmann, K.; Stuecker, M.; Tigges, C.; Lübbert, H.; Stichel, C. Upregulation of cathepsin S in psoriatic keratinocytes: Cathepsin S in psoriatic keratinocytes. *Exp. Dermatol.* **2009**, *19*, e80–e88.

117. Van Hees, P. A. W.; Rosling, A.; Essén, S.; Godbold, D. L.; Jones, D. L.; Finlay, R. D. Oxalate and ferricrocin exudation by the extramatrical mycelium of an ectomycorrhizal fungus in symbiosis with *Pinus sylvestris*. *New Phytol.* **2006**, *169*, 367–378.

118. Schuster, M.; Martin-Urdiroz, M.; Higuchi, Y.; Hacker, C.; Kilaru, S.; Gurr, S. J.; Steinberg, G. Co-delivery of cell-wall-forming enzymes in the same vesicle for coordinated fungal cell wall formation. *Nat. Microbiol.* **2016**, *1*, 16149.

119. Sun, Y.-P.; Unestam, T.; Lucas, D. S.; Johanson, J. K.; Kenne, L.; Finlay, R. Exudation-reabsorption in a mycorrhizal fungus, the dynamic interface for interaction with soil and soil microorganisms. *Mycorrhiza* **1999**, *9*, 137–144.

120. Rangel-Castro, J. I.; Danell, E.; Pfeffer, P. E. A 13C-NMR study of exudation and storage of carbohydrates and amino acids in the ectomycorrhizal edible mushroom *Cantharellus cibarius*. *Mycologia* **2002**, *94*, 190–199.

121. McCotter, S. W.; Horianopoulos, L. C.; Kronstad, J. W. Regulation of the fungal secretome. *Curr. Genet.* **2016**, *62*, 533–545.

122. Casadevall, A.; Nosanchuk, J. D.; Williamson, P.; Rodrigues, M. L. Vesicular transport across the fungal cell wall. *Trends Microbiol.* **2009**, *17*, 158–162.

123. Schrettl, M.; Carberry, S.; Kavanagh, K.; Haas, H.; Jones, G. W.; O'Brien, J.; Nolan, A.; Stephens, J.; Fenelon, O.; Doyle, S. Self-Protection against Gliotoxin—A Component of the Gliotoxin Biosynthetic Cluster, GliT, Completely Protects *Aspergillus fumigatus* Against Exogenous Gliotoxin. *PLoS Pathog.* **2010**, *6*, e1000952.

124. Wang, D.-N.; Toyotome, T.; Muraosa, Y.; Watanabe, A.; Wuren, T.; Bunsupa, S.; Aoyagi, K.; Yamazaki, M.; Takino, M.; Kamei, K. GliA in *Aspergillus fumigatus* is required for its tolerance to gliotoxin and affects the amount of extracellular and intracellular gliotoxin. *Med. Mycol.* **2014**, *52*, 506–518.

125. Chanda, A.; Roze, L. V.; Linz, J. E. A Possible Role for Exocytosis in Aflatoxin Export in *Aspergillus parasiticus*. *Eukaryot. Cell* **2010**, *9*, 1724–1727.

126. Teijeira, F.; Ullán, R. V.; Guerra, S. M.; García-Estrada, C.; Vaca, I.; Martín, J. F. The transporter CefM involved in translocation of biosynthetic intermediates is essential for cephalosporin production. *Biochem. J.* **2009**, *418*, 113–124.

127. Andrade, A. C.; Van Nistelrooy, J. G. M.; Peery, R. B.; Skatrud, P. L.; De Waard, M. A. The role of ABC transporters from *Aspergillus nidulans* in protection against cytotoxic agents and in antibiotic production. *Mol. Gen. Genet. MGG* **2000**, *263*, 966–977.

128. Colotelo, N. Fungal exudates. *Can. J. Microbiol.* **1978**, *24*, 1173–1181.

129. Madhusudhan, D. N.; Mazhari, B. B. Z.; Dastager, S. G.; Agsar, D. Production and Cytotoxicity of Extracellular Insoluble and Droplets of Soluble Melanin by *Streptomyces lusitanus* DMZ-3. *BioMed Res. Int.* **2014**, *2014*, 1–11.

130. Singh, S.; Singh, T. N. Guttation 1: chemistry, crop husbandry and molecular farming. *Phytochem. Rev.* **2013**, *12*, 147–172.

131. Dörfelt, H.; Ruske, E. Leitbegriffe und Bildtafeln. In *Morphologie der Großpilze: mit 112 Farbbildtafeln, Glossar und Namensregister*; Dörfelt, H.; Ruske, E., Eds.; Springer Berlin Heidelberg: Berlin, Heidelberg, 2014; pp. 10–213.

132. Pereira, E.; Oliveira, I.; Baptista, P. Guttation droplets of the edible mushroom *Suillus bovinus* as a new source of natural antioxidants. *Sci. Hortic.* **2012**, *148*, 89–92.

133. Gareis, M.; Gareis, E.-M. Guttation droplets of *Penicillium nordicum* and *Penicillium verrucosum* contain high concentrations of the mycotoxins ochratoxin A and B. *Mycopathologia* **2007**, *163*, 207–214.

134. Unestam, T.; Sun, Y.-P. Extramatrical structures of hydrophobic and hydrophilic ectomycorrhizal fungi. *Mycorrhiza* **1995**, *5*, 301–311.

135. Goatley, J. L.; Lewis, R. W. Composition of guttation fluid from rye, wheat, and barley seedlings. *Plant Physiol.* **1966**, *41*, 373–375.

136. Figueroa, M.; Jarmusch, A. K.; Raja, H. A.; El-Elimat, T.; Kavanaugh, J. S.; Horswill, A. R.; Cooks, R. G.; Cech, N. B.; Oberlies, N. H. Polyhydroxyanthraquinones as Quorum Sensing Inhibitors from the Guttates of *Penicillium restrictum* and Their Analysis by Desorption Electrospray Ionization Mass Spectrometry. *J. Nat. Prod.* **2014**, *77*, 1351–1358.

137. Rohlfs, M. Fungal secondary metabolite dynamics in fungus-grazer interactions: novel insights and unanswered questions. *Front. Microbiol.* **2015**, *5*, 1–5.

138. Pandey, M. K.; Sarma, B. K.; Singh, D. P.; Singh, U. P. Biochemical investigations of sclerotial exudates of *Sclerotium rolfsii* and their antifungal activity. *J. Phytopathol.* **2007**, *155*, 84–89.

139. Jennings, D. H. The role of droplets in helping to maintain a constant growth rate of aerial hyphae. *Mycol. Res.* **1991**, *95*, 883–884.

140. Graw, J. Molekulare Struktur und Regulation eukaryotischer Gene. In *Genetik*; Graw, J., Ed.; Springer Berlin Heidelberg: Berlin, Heidelberg, 2010; pp. 271–325.

141. Schmidt-Stohn, G.; Oertel, B. DNA-Analysen in der Pilz-Taxonomie. *J. Journee Eur. Cortinaire* **2009**, *11*, 10–19.

142. Schoch, C. L.; Seifert, K. A.; Huhndorf, S.; Robert, V.; Spouge, J. L.; Levesque, C. A.; Chen, W.; Bolchacova, E.; Voigt, K.; Crous, P. W. Nuclear ribosomal internal transcribed spacer (ITS) region as a universal DNA barcode marker for Fungi. *Proc. Natl. Acad. Sci.* **2012**, *109*, 6241–6246.

143. White, T. J.; Bruns, T.; Lee, S.; Taylor, J. W. Amplification and direct sequencing of fungal ribosomal RNA genes for phylogenetics. *PCR Protoc. Guide Methods Appl.* **1990**, *18*, 315–322.

144. Metzker, M. L. Sequencing technologies — the next generation. *Nat. Rev. Genet.* **2010**, *11*, 31–46.

145. Kearse, M.; Moir, R.; Wilson, A.; Stones-Havas, S.; Cheung, M.; Sturrock, S.; Buxton, S.; Cooper, A.; Markowitz, S.; Duran, C.; Thierer, T.; Ashton, B.; Meintjes, P.; Drummond, A. Geneious Basic: An integrated and extendable desktop software platform for the organization and analysis of sequence data. *Bioinformatics* **2012**, *28*, 1647–1649.

146. Benson, D. A.; Karsch-Mizrachi, I.; Lipman, D. J.; Ostell, J.; Wheeler, D. L. GenBank. *Nucleic Acids Res.* **2004**, *33*, D34–D38.

147. Altschul, S. F.; Madden, T. L.; Schäffer, A. A.; Zhang, J.; Zhang, Z.; Miller, W.; Lipman, D. J. Gapped BLAST and PSI-BLAST: a new generation of protein database search programs. *Nucleic Acids Res.* **1997**, *25*, 3389–3402.

148. Tamura, K.; Nei, M. Estimation of the number of nucleotide substitutions in the control region of mitochondrial DNA in humans and chimpanzees. *Mol. Biol. Evol.* **1993**, *10*, 512–526.

149. Tamura, K.; Stecher, G.; Peterson, D.; Filipski, A.; Kumar, S. MEGA6: Molecular Evolutionary Genetics Analysis Version 6.0. *Mol. Biol. Evol.* **2013**, *30*, 2725–2729.

150. Perrot, S.; Dutertre-Catella, H.; Martin, C.; Warnet, J.-M.; Rat, P. A new nondestructive cytometric assay based on resazurin metabolism and an organ culture model for the assessment of corneal viability. *Cytometry* **2003**, *55A*, 7–14.

151. Shahan, T.; Siegel, P.; Sorenson, W.; Kuschner, W.; Lewis, D. A sensitive new bioassay for tumor necrosis factor. *J. Immunol. Methods* **1994**, *175*, 181—187.

152. Zapol'skii, V. A.; Namyslo, J. C.; Sergeev, G.; Brönstrup, M.; Gjikaj, M.; Kaufmann, D. E. Reinvestigation of the Nitration of Tri-chloroethene - Subsequent Reactions of the Products and Evaluation of Their Anti-microbial and Antifungal Activity: Reinvestigation of the Nitration of Trichloroethene. *Eur. J. Org. Chem.* **2015**, *2015*, 7763–7774.

153. Mehnaz, S.; Saleem, R. S. Z.; Yameen, B.; Pianet, I.; Schnakenburg, G.; Pietraszkiewicz, H.; Valeriote, F.; Josten, M.; Sahl, H.-G.; Franzblau, S. G.; Gross, H. Lahorenoic Acids A–C, *ortho*-Dialkyl-Substituted Aromatic Acids from the Biocontrol Strain *Pseudomonas aurantiaca* PB-St2. *J. Nat. Prod.* **2013**, *76*, 135–141.

154. Kremb, S.; Helfer, M.; Heller, W.; Hoffmann, D.; Wolff, H.; Kleinschmidt, A.; Cepok, S.; Hemmer, B.; Durner, J.; Brack-Werner, R. EASY-HIT: HIV Full-Replication Technology for Broad Discovery of Multiple Classes of HIV Inhibitors. *Antimicrob. Agents Chemother.* **2010**, *54*, 5257–5268.

155. Jungalwala, F. B.; Natowicz, M. R.; Chaturvedi, P.; Newburg, D. S. [11] Analysis of sulfatide and enzymes of sulfatide metabolism. In *Methods in Enzymology*; Academic Press, 2000; Vol. Volume 311, pp. 94–105.

156. Frizler, M.; Lohr, F.; Furtmann, N.; Kläs, J.; Gütschow, M. Structural Optimization of Azadipeptide Nitriles Strongly Increases Association Rates and Allows the Development of Selective Cathepsin Inhibitors. *J. Med. Chem.* **2011**, *54*, 396–400.

157. Frizler, M.; Lohr, F.; Lülsdorff, M.; Gütschow, M. Facing the gem-Dialkyl Effect in Enzyme Inhibitor Design: Preparation of Homocycloleucine-Based Azadipeptide Nitriles. *Chem. - Eur. J.* **2011**, *17*, 11419–11423.

158. Gütschow, M.; Pietsch, M.; Themann, A.; Fahrig, J.; Schulze, B. 2,4,5-Triphenylisothiazol-3(2-*H*)-one 1,1-dioxides as inhibitors of human leukocyte elastase. *J. Enzyme Inhib. Med. Chem.* **2005**, *20*, 341–347.

159. Sisay, M. T.; Steinmetzer, T.; Stirnberg, M.; Maurer, E.; Hammami, M.; Bajorath, J.; Gütschow, M. Identification of the First Low-Molecular-Weight Inhibitors of Matriptase-2. *J. Med. Chem.* **2010**, *53*, 5523–5535.

160. Sisay, M. T.; Hautmann, S.; Mehner, C.; König, G. M.; Bajorath, J.; Gütschow, M. Inhibition of Human Leukocyte Elastase by Brunsvicamides A–C: Cyanobacterial Cyclic Peptides. *ChemMedChem* **2009**, *4*, 1425–1429.

161. Tzameli, I.; Fang, H.; Ollero, M.; Shi, H.; Hamm, J. K.; Kievit, P.; Hollenberg, A. N.; Flier, J. S. Regulated Production of a Peroxisome Proliferator-activated Receptor- Ligand during an Early Phase of Adipocyte Differentiation in 3T3-L1 Adipocytes. *J. Biol. Chem.* **2004**, *279*, 36093–36102.

162. Ciocoiu, C. C.; Nikolić, N.; Nguyen, H. H.; Thoresen, G. H.; Aasen, A. J.; Hansen, T. V. Synthesis and dual PPARα/δ agonist effects of 1,4-disubstituted 1,2,3-triazole analogues of GW 501516. *Eur. J. Med. Chem.* **2010**, *45*, 3047–3055.

163. Gluzman, Y. SV40-transformed simian cells support the replication of early SV40 mutants. *Cell* **1981**, *23*, 175–182.

164. Hochard, A.; Oumata, N.; Bettayeb, K.; Gloulou, O.; Fant, X.; Durieu, E.; Buron, N.; Porceddu, M.; Borgne-Sanchez, A.; Galons, H.; Flajolet, M.; Meijer, L. Aftins increase amyloid-β42, lower amyloid-β38, and do not alter amyloid-β40 extracellular production in vitro: toward a chemical model of Alzheimer's disease? *J. Alzheimers Dis.* **2013**, *35*, 107–120.

165. Bettayeb, K.; Oumata, N.; Zhang, Y.; Luo, W.; Bustos, V.; Galons, H.; Greengard, P.; Meijer, L.; Flajolet, M. Small-molecule inducers of A-42 peptide production share a common mechanism of action. *FASEB J.* **2012**, *26*, 5115–5123.

166. Leclerc, S.; Garnier, M.; Hoessel, R.; Marko, D.; Bibb, J. A.; Snyder, G. L.; Greengard, P.; Biernat, J.; Wu, Y.-Z.; Mandelkow, E.-M.; Eisenbrand, G.; Meijer, L. Indirubins Inhibit Glycogen Synthase Kinase-3beta and CDK5/P25, Two Protein Kinases Involved in Abnormal Tau Phosphorylation in Alzheimer's Disease. *J. Biol. Chem.* **2001**, *276*, 251–260.

167. Schmitz, P. Der Einfluss von Cyr61 auf die Adhäsionsfunktion von Integrinen und dessen Hemmung durch Heparin als Beitrag für eine antimetastatische Wirkung. Dissertation, Rheinische Friedrich-Wilhelms-Universität Bonn, 2013.

168. Simonis, D. Untersuchung der Heparinwirkung an Adhäsionsrezeptoren mithilfe akustischer Biosensoren, Rheinische Friedrich-Wilhelms-Universität Bonn, 2009.

169. Reder-Christ, K.; Schmitz, P.; Bota, M.; Gerber, U.; Falkenstein-Paul, H.; Fuss, C.; Enachescu, M.; Bendas, G. A Dry Membrane Protection Technique to Allow Surface Acoustic Wave Biosensor Measurements of Biological Model Membrane Approaches. *Sensors* **2013**, *13*, 12392–12405.

170. Moore, D.; Robson, G. D.; Trinci, A. P. J. Natural classification of fungi. In *21st Century Guidebook to Fungi*; Cambridge University Press, 2000; pp. 41–82.

171. Zhang, Y.; Schoch, C. L.; Fournier, J.; Crous, P. W.; de Gruyter, J.; Woudenberg, J. H. C.; Hirayama, K.; Tanaka, K.; Pointing, S. B.; Spatafora, J. W.; Hyde, K. D. Multi-locus phylogeny of Pleosporales: a taxonomic, ecological and evolutionary re-evaluation. *Stud. Mycol.* **2009**, *64*, 85-102-S5.

172. Aveskamp, M. M.; de Gruyter, J.; Woudenberg, J. H. C.; Verkley, G. J. M.; Crous, P. W. Highlights of the Didymellaceae: A polyphasic approach to characterise Phoma and related pleosporalean genera. *Stud. Mycol.* **2010**, *65*, 1–60.

173. Chen, Q.; Jiang, J. R.; Zhang, G. Z.; Cai, L.; Crous, P. W. Resolving the Phoma enigma. *Stud. Mycol.* **2015**, *82*, 137–217.

174. Arenal, F.; Platas, G.; Martin, J.; Asensio, F.; Salazar, O.; Collado, J.; Vicente, F.; Basilio, A.; Ruibal, C.; Royo, I.; others Comparison of genotypic and phenotypic techniques for assessing the variability of the fungus *Epicoccum nigrum*. *J. Appl. Microbiol.* **2002**, *93*, 36–45.

175. Van Ginkel, R.; Selwood, A.; Wilkins, A. L.; Ford, S.; Calder, C. Anti-microbial compositions. Patent US2012/0108526 A1, 2012.

176. Peng, J.; Jiao, J.; Li, J.; Wang, W.; Gu, Q.; Zhu, T.; Li, D. Pyronepolyene C-glucosides with NF-κB inhibitory and anti-influenza A viral (H1N1) activities from the sponge-associated fungus *Epicoccum* sp. JJY40. *Bioorg. Med. Chem. Lett.* **2012**.

177. Gao, J.-M.; Yang, S.-X.; Qin, J.-C. Azaphilones: chemistry and biology. *Chem. Rev.* **2013**, *113*, 4755–4811.

178. Osmanova, N.; Schultze, W.; Ayoub, N. Azaphilones: a class of fungal metabolites with diverse biological activities. *Phytochem. Rev.* **2010**, *9*, 315–342.

179. Coghlan, D. R.; Mackintosh, J. A.; Karuso, P. Mechanism of Reversible Fluorescent Staining of Protein with Epicocconone. *Org. Lett.* **2005**, *7*, 2401–2404.

180. Wei, W.-G.; Yao, Z.-J. Synthesis Studies toward Chloroazaphilone and Vinylogous γ-Pyridones: Two Common Natural Product Core Structures. *J. Org. Chem.* **2005**, *70*, 4585–4590.

181. Lin, T. F.; Yakushijin, K.; Büchi, G. H.; Demain, A. L. Formation of water-soluble *Monascus* red pigments by biological and semi-synthetic processes. *J. Ind. Microbiol.* **1992**, *9*, 173–179.

182. G. Nasini Structure and absolute configuration of acetosellin, a new polyketide from a phytotoxic strain of *Cercosporella acetosella*. *Tetrahedron Lett.* **2002**.

183. Talontsi, F. M.; Dittrich, B.; Schüffler, A.; Sun, H.; Laatsch, H. Epicoccolides: Antimicrobial and Antifungal Polyketides from an Endophytic Fungus *Epicoccum* sp. Associated with *Theobroma cacao*. *Eur. J. Org. Chem.* **2013**, *2013*, 3174–3180.

184. Plitzko, I. Zur Biosynthese des Borrelidins sowie Isolierung und Strukturaufklärung von Sekundärmetaboliten aus marinen und terrestrischen Mikroorganismen. Dissertation, Niedersächsische Staats-und Universitätsbibliothek Göttingen, 2007.

185. Son, S.; Ko, S.-K.; Kim, J. W.; Lee, J. K.; Jang, M.; Ryoo, I.-J.; Hwang, G. J.; Kwon, M. C.; Shin, K.-S.; Futamura, Y.; Hong, Y.-S.; Oh, H.; Kim, B. Y.; Ueki, M.; Takahashi, S.; Osada, H.; Jang, J.-H.; Ahn, J. S. Structures and biological activities of azaphilones produced by *Penicillium* sp. KCB11A109 from a ginseng field. *Phytochemistry* **2016**, *122*, 154–164.

186. Nakanishi, K.; Schooley, D. A.; Koreeda, M.; Miura, I. General method for distinguishing threo and erythro isomers of certain alpha-glycols and related compounds. *J. Am. Chem. Soc.* **1972**, *94*, 2865–2867.

187. Allen, D. A.; Tomaso, A. E.; Priest, O. P.; Hindson, D. F.; Hurlburt, J. L. Mosher Amides: Determining the Absolute Stereochemistry of Optically-Active Amines. *J. Chem. Educ.* **2008**, *85*, 698–700.

188. Wagner, U.; Kratky, C. Structure Elucidation of Natural Compounds by X-Ray Crystallography. In *Progress in the Chemistry of Organic Natural Products 100*; Kinghorn, D. A.; Falk, H.; Kobayashi, J., Eds.; Springer International Publishing: Cham, 2015; pp. 1–75.

189. Birch, A. J.; Fitton, P.; Pride, E.; Ryan, A. J.; Smith, H.; Whalley, W. B. 923. Studies in relation to biosynthesis. Part XVII. Sclerotiorin, citrinin, and citromycetin. *J. Chem. Soc. Resumed* **1958**, 4576–4581.

190. Colombo, L.; Gennari, C.; Potenza, D.; Scolastico, C.; Aragozzini, F.; Merendi, C. Biosynthesis of citrinin and synthesis of its biogenetic precursors. *J. Chem. Soc. [Perkin 1]* **1981**, 2594–2597.

191. Hajjaj, H.; Klaébé, A.; Loret, M. O.; Goma, G.; Blanc, P. J.; François, J. Biosynthetic pathway of citrinin in the filamentous fungus *Monascus ruber* as revealed by 13C nuclear magnetic resonance. *Appl. Environ. Microbiol.* **1999**, *65*, 311–314.

192. Ogihara, J.; Kato, J.; Oishi, K.; Fujimoto, Y. Biosynthesis of PP-V, a monascorubramine homologue, by *Penicillium* sp. AZ. *J. Biosci. Bioeng.* **2000**, *90*, 678–680.

193. Seto, H.; Tanabe, M. Utilization of 13C-13C coupling in structural and biosynthetic studies. III. Ochrephilone-a new fungal metabolite. *Tetrahedron Lett.* **1974**, *15*, 651–654.

194. Balakrishnan, B.; Chandran, R.; Park, S.-H.; Kwon, H.-J. Delineating citrinin biosynthesis: Ctn-ORF3 dioxygenase-mediated multi-step methyl oxidation precedes a reduction-mediated pyran ring cyclization. *Bioorg. Med. Chem. Lett.* **2016**, *26*, 392–396.

195. Patakova, P. *Monascus* secondary metabolites: production and biological activity. *J. Ind. Microbiol. Biotechnol.* **2013**, *40*, 169–181.

196. Pascual-Ahuir, A.; Vanacloig-Pedros, E.; Proft, M. Toxicity Mechanisms of the Food Contaminant Citrinin: Application of a Quantitative Yeast Model. *Nutrients* **2014**, *6*, 2077–2087.

197. Chen, W.; He, Y.; Zhou, Y.; Shao, Y.; Feng, Y.; Li, M.; Chen, F. Edible Filamentous Fungi from the Species *Monascus*: Early Traditional Fermentations, Modern Molecular Biology, and Future Genomics. *Compr. Rev. Food Sci. Food Saf.* **2015**, *14*, 555–567.

198. Birch, A. J.; Cassera, A.; Fitton, P.; Holker, J. S. E.; Smith, H.; Thompson, G. A.; Whalley, W. B. 699. Studies in relation to biosynthesis. Part XXX. Rotiorin, monascin, and rubropunctatin. *J. Chem. Soc. Resumed* **1962**, 3583–3586.

199. Kurono, M.; Nakanishi, K.; Shindo, K.; Tada, M. Biosyntheses of Monascorubrin and Monascoflavin. *Chem. Pharm. Bull. (Tokyo)* **1963**, *11*, 359–362.

200. Yang, Y.; Liu, B.; Du, X.; Li, P.; Liang, B.; Cheng, X.; Du, L.; Huang, D.; Wang, L.; Wang, S. Complete genome sequence and transcriptomics analyses reveal pigment biosynthesis and regulatory mechanisms in an industrial strain, *Monascus purpureus* YY-1. *Sci. Rep.* **2015**, *5*, 8331.

201. Balakrishnan, B.; Karki, S.; Chiu, S.-H.; Kim, H.-J.; Suh, J.-W.; Nam, B.; Yoon, Y.-M.; Chen, C.-C.; Kwon, H.-J. Genetic localization and in vivo characterization of a *Monascus* azaphilone pigment biosynthetic gene cluster. *Appl. Microbiol. Biotechnol.* **2013**, *97*, 6337–6345.

202. Zabala, A. O.; Xu, W.; Chooi, Y.-H.; Tang, Y. Characterization of a Silent Azaphilone Gene Cluster from *Aspergillus niger* ATCC 1015 Reveals a Hydroxylation-Mediated Pyran-Ring Formation. *Chem. Biol.* **2012**, *19*, 1049–1059.

203. Cox, R. J. Polyketides, proteins and genes in fungi: programmed nano-machines begin to reveal their secrets. *Org. Biomol. Chem.* **2007**, *5*, 2010.

204. Vertesy, L.; Kurz, M.; Markus-Erb, A.; Toti, L. 2-Phenyl-benzofuran derivatives, method for the production thereof and their use. Patent CA2543629 A1, 2005.

205. Abdel-Lateff, A.; Fisch, K. M.; Wright, A. D.; Konig, G. M. A new antioxidant isobenzofuranone derivative from the algicolous marine fungus *Epicoccum* sp. *Planta Med.* **2003**, *69*, 831–834.

206. Devys, M.; Barbier, M.; Bousquet, J.-F.; Kollmann, A. Notes: Isolation of the New (-)-(3 R, 4S)-4-Hydroxymellein from the *Fungus Septoria* nodorum Berk. *Z. Fuer Naturforschung C* **1992**, *47*, 779–781.

207. Son, B. W. Biotransformation of Bioactive (–)-Mellein by a Marine Isolate of Bacterium *Stappia* sp. *J. Microbiol. Biotechnol.* **2010**, *20*, 985–987.

208. Abdel-Lateff, A. Secondary Metabolites of Marine-Derived Fungi: Natural Product Chemistry and Biological Activity. Dissertation, Universitäts-und Landesbibliothek Bonn, 2004.

209. Talontsi, F. M.; Kenla, T. J. N.; Dittrich, B.; Douanla-Meli, C.; Laatsch, H. Paeciloside A, a new antimicrobial and cytotoxic polyketide from *Paecilomyces* sp. strain CAFT156. *Planta Med.* **2012**, *78*, 1020–1023.

210. Bashyal, B. P.; Leslie Gunatilaka, A. A. Tricinonoic acid and tricindiol, two new irregular sesquiterpenes from an endophytic strain of *Fusarium tricinctum*. *Nat. Prod. Res.* **2010**, *24*, 349–356.

211. Igarashi, Y.; Hanafusa, T.; Gohda, F.; Peterson, S.; Bills, G. Species-level assessment of secondary metabolite diversity among *Hamigera* species and a taxonomic note on the genus. *Mycology* **2014**, *5*, 102–109.

212. Shaaban, M.; Schroder, D.; Shaaban, K. A.; Helmke, E.; Grun-Wollny, I.; Wagner-Dobler, I.; Laatsch, H. Flazin, perlolyrin, and other beta-carbolines from marine-derived Bacteria. *Rev. Latinoam. Quím.* **2007**, *35*, 58–67.

213. Irwin, J. J.; Sterling, T.; Mysinger, M. M.; Bolstad, E. S.; Coleman, R. G. ZINC: A Free Tool to Discover Chemistry for Biology. *J. Chem. Inf. Model.* **2012**, *52*, 1757–1768.

214. Hou, H.; Zhou, R.; Li, A.; Li, C.; Li, Q.; Liu, J.; Jiang, B. Citreoviridin inhibits cell proliferation and enhances apoptosis of human umbilical vein endothelial cells. *Environ. Toxicol. Pharmacol.* **2014**, *37*, 828–836.

215. Franck, B.; Gehrken, H.-P. Citreoviridins from *Aspergillus terreus*. *Angew. Chem. Int. Ed. Engl.* **1980**, *19*, 461–462.

216. Pieckenstain, F. L.; Bazzalo, M. E.; Roberts, A. M. I.; Ugalde, R. A. *Epicoccum purpurascens* for biocontrol of *Sclerotinia* head rot of sunflower. *Mycol. Res.* **2001**, *105*, 77–84.

217. Gutmann, A.; Nidetzky, B. Enzymatic *C*-glycosylation: Insights from the study of a complementary pair of plant O- and C-glucosyltransferases. *Pure Appl. Chem.* **2013**, *85*.

218. Dürr, C.; Hoffmeister, D.; Wohlert, S.-E.; Ichinose, K.; Weber, M.; von Mulert, U.; Thorson, J. S.; Bechthold, A. The Glycosyltransferase UrdGT2 Catalyzes Both C- and O-Glycosidic Sugar Transfers. *Angew. Chem. Int. Ed.* **2004**, *43*, 2962–2965.

219. Villas-Boas, S. G. Fungicidal compounds and methods of their use. Patent WO2011071396 A1, 2011.

220. Shu, Y.-Z.; Ye, Q.; Li, H.; Kadow, K. F.; Hussain, R. A.; Huang, S.; Gustavson, D. R.; Lowe, S. E.; Chang, L.-P.; Pirnik, D. M.; Kodukula, K. Orevactaene, a novel binding inhibitor of HIV-1 rev protein to Rev response element (RRE) from *Epicoccum nigrum* WC47880. *Bioorg. Med. Chem. Lett.* **1997**, *7*, 2295–2298.

221. Madden, K. S.; Mosa, F. A.; Whiting, A. Non-isoprenoid polyene natural products – structures and synthetic strategies. *Org Biomol Chem* **2014**, *12*, 7877–7899.

222. Schäberle, T. F. Biosynthesis of α-pyrones. *Beilstein J. Org. Chem.* **2016**, *12*, 571–588.

223. Thirsk, C.; Whiting, A. Polyene natural products. *J. Chem. Soc. [Perkin 1]* **2002**, 999–1023.

224. Cimermancic, P.; Medema, M. H.; Claesen, J.; Kurita, K.; Wieland Brown, L. C.; Mavrommatis, K.; Pati, A.; Godfrey, P. A.; Koehrsen, M.; Clardy, J.; Birren, B. W.; Takano, E.; Sali, A.; Linington, R. G.; Fischbach, M. A. Insights into Secondary Metabolism from a Global Analysis of Prokaryotic Biosynthetic Gene Clusters. *Cell* **2014**, *158*, 412–421.

225. Xiao, J.; Capanoglu, E.; Jassbi, A. R.; Miron, A. Advance on the Flavonoid *C* - glycosides and Health Benefits. *Crit. Rev. Food Sci. Nutr.* **2016**, *56*, S29–S45.

226. Wang, X. Structure, mechanism and engineering of plant natural product glycosyltransferases. *FEBS Lett.* **2009**, *583*, 3303–3309.

227. Hultin, P. G. Bioactive *C*-Glycosides from Bacterial Secondary Metabolism. *Curr. Top. Med. Chem.* **2005**, *5*, 1299–1331.

228. Hiramatsu, F.; Miyajima, T.; Murayama, T.; Takahashi, K.; Koseki, T.; Shiono, Y. Isolation and Structure Elucidation of Neofusapyrone from a Marine-derived *Fusarium* species, and Structural Revision of Fusapyrone and Deoxyfusapyrone. *J. Antibiot. (Tokyo)* **2006**, *59*, 704–709.

229. Honma, M.; Kudo, S.; Takada, N.; Tanaka, K.; Miura, T.; Hashimoto, M. Novel neofusapyrones isolated from *Verticillium dahliae* as potent antifungal substances. *Bioorg. Med. Chem. Lett.* **2010**, *20*, 709–712.

230. Xaio, J.-Z.; Kumazawa, S.; Yoshikawa, N.; Mikawa, T. Dactylfungins, novel antifungal antibiotics produced by *Dactylaria parvispora*. *J. Antibiot. (Tokyo)* **1993**, *46*, 48–55.

231. Nagai et al. YM-202204, a New Antifungal Antibiotic Produced by Marine Fungus *Phoma* sp. *J. Antibiot. (Tokyo)* **2002**, *55*, 1036–1041.

232. McGlacken, G. P.; Fairlamb, I. J. S. 2-Pyrone natural products and mimetics: isolation, characterisation and biological activity. *Nat. Prod. Rep.* **2005**, *22*, 369.

233. Altomare, C.; Pengue, R.; Favilla, M.; Evidente, A.; Visconti, A. Structure-Activity Relationships of Derivatives of Fusapyrone, an Antifungal Metabolite of *Fusarium semitectum*. *J. Agric. Food Chem.* **2004**, *52*, 2997–3001.

234. Tscherter, H.; Hofmann, H.; Ewald, R.; Dreyfuss, M. M. Antibiotic lactone compound. US Patent 4,753,959. 1988.

235. Hamamoto, T.; Seto, H.; Beppu, T. Leptomycins A and B, new antifungal antibiotics. II. Structure elucidation. *J. Antibiot. (Tokyo)* **1983**, *36*, 646–650.

References

236. Fujii, I.; Yoshida, N.; Shimomaki, S.; Oikawa, H.; Ebizuka, Y. An Iterative Type I Polyketide Synthase PKSN Catalyzes Synthesis of the Decaketide Alternapyrone with Regio-Specific Octa-Methylation. *Chem. Biol.* **2005**, *12*, 1301–1309.

237. Asai, T.; Luo, D.; Yamashita, K.; Oshima, Y. Structures and Biomimetic Synthesis of Novel α-Pyrone Polyketides of an Endophytic *Penicillium* sp. in *Catharanthus roseus. Org. Lett.* **2013**, *15*, 1020–1023.

238. Satre, M. The effect of asteltoxin and citreomontanine, two polyenic alpha-pyrone mycotoxins, on *Escherichia coli* adenosine triphosphatase. *Biochem. Biophys. Res. Commun.* **1981**, *100*, 267–274.

239. McGovern, S. L.; Helfand, B. T.; Feng, B.; Shoichet, B. K. A specific mechanism of nonspecific inhibition. *J. Med. Chem.* **2003**, *46*, 4265–4272.

240. Ingólfsson, H. I.; Thakur, P.; Herold, K. F.; Hobart, E. A.; Ramsey, N. B.; Periole, X.; de Jong, D. H.; Zwama, M.; Yilmaz, D.; Hall, K.; Maretzky, T.; Hemmings, H. C.; Blobel, C.; Marrink, S. J.; Koçer, A.; Sack, J. T.; Andersen, O. S. Phytochemicals Perturb Membranes and Promiscuously Alter Protein Function. *ACS Chem. Biol.* **2014**, *9*, 1788–1798.

241. Baell, J. B. Feeling Nature's PAINS: Natural Products, Natural Product Drugs, and Pan Assay Interference Compounds (PAINS). *J. Nat. Prod.* **2016**, *79*, 616–628.

242. Kopeć, W.; Telenius, J.; Khandelia, H. Molecular dynamics simulations of the interactions of medicinal plant extracts and drugs with lipid bilayer membranes. *FEBS J.* **2013**, *280*, 2785–2805.

243. Britton, G. Structure and properties of carotenoids in relation to function. *FASEB J.* **1995**, *9*, 1551–1558.

244. Georgiou, C. D.; Tairis, N.; Sotiropoulou, A. Hydroxyl radical scavengers inhibit sclerotial differentiation and growth in *Sclerotinia sclerotiorum* and *Rhizoctonia solani. Mycol. Res.* **2000**, *104*, 1191–1196.

245. Elad, Y. The use of antioxidants (free radical scavengers) to control grey mould (*Botrytis cinerea*) and white mould (*Sclerotinia sclerotiom*) in various crops. *Plant Pathol.* **1992**, *41*, 417–426.

246. Li, C.; Xu, Y.; Jiang, W.; Lv, X.; Dong, X. Effect of sodium chloride and cadmium on the growth, oxidative stress and antioxidant enzyme activities of *Zygosaccharomyces rouxii. J. Ocean Univ. China* **2014**, *13*, 460–466.

247. Marova, I.; Breierova, E.; Koci, R.; Friedl, Z.; Slovak, B.; Pokorna, J. Influence of exogenous stress factors on production of carotenoids by some strains of carotenogenic yeasts. *Ann. Microbiol.* **2004**, *54*, 73–86.

248. Qi, W.; Fan, Z.-C.; Wang, C.-L.; Hou, L.-H.; Liu, J.-F.; Cao, X.-H. Non-targeted metabolomic reveals the effect of salt stress on global metabolite of halotolerant yeast *Candida versatilis* and principal component analysis. *J. Ind. Microbiol. Biotechnol.* **2014**, *41*, 1553–1562.

249. Westkaemper, R. B.; Abeles, R. H. Novel inactivators of serine proteases based on 6-chloro-2-pyrone. *Biochemistry (Mosc.)* **1983**, *22*, 3256–3264.

250. Tam, W.-T. Characterization of polyketide synthases in *Penicillium marneffei*. Dissertation, University of Hong Kong, 2012.

251. Bijinu, B.; Suh, J.-W.; Park, S.-H.; Kwon, H.-J. Delineating *Monascus* azaphilone pigment biosynthesis: oxidoreductive modifications determine the ring cyclization pattern in azaphilone biosynthesis. *RSC Adv.* **2014**, *4*, 59405–59408.

252. Balakrishnan, B.; Kim, H.-J.; Suh, J.-W.; Chen, C.-C.; Liu, K.-H.; Park, S.-H.; Kwon, H.-J. *Monascus* azaphilone pigment biosynthesis employs a dedicated fatty acid synthase for short chain fatty acyl moieties. *J. Korean Soc. Appl. Biol. Chem.* **2014**, *57*, 191–196.

253. Brown, D. W.; Adams, T. H.; Keller, N. P. *Aspergillus* has distinct fatty acid synthases for primary and secondary metabolism. *Proc. Natl. Acad. Sci.* **1996**, *93*, 14873–14877.

254. Stadler, M.; Anke, H.; Dekermendjian, K.; Reiss, R.; Sterner, O.; Witt, R. Novel Bioactive Azaphilones from Fruit Bodies and Mycelial Cultures of the Ascomycete *Bulgaria inquinans* (Fr.). *Nat. Prod. Res.* **1995**, *7*, 7–14.

255. Musso, L.; Dallavalle, S.; Merlini, L.; Bava, A.; Nasini, G.; Penco, S.; Giannini, G.; Giommarelli, C.; De Cesare, A.; Zuco, V.; Vesci, L.; Pisano, C.; Dal Piaz, F.; De Tommasi, N.; Zunino, F. Natural and semisynthetic azaphilones as a new scaffold for Hsp90 inhibitors. *Bioorg. Med. Chem.* **2010**, *18*, 6031–6043.

256. Wang, G.-Y.-S.; Borgeson, B. M.; Crews, P. Pitholides A-D, polyketides from a marine tunicate-derived culture of *Pithomyces* sp. *Tetrahedron Lett.* **1997**, *38*, 8449–8452.

257. Anke, H.; Kemmer, T.; Höfle, G. Deflectins, new antimicrobial azaphilones from *Aspergillus deflectus*. *J. Antibiot. (Tokyo)* **1981**, *34*, 923–928.

258. Bell, P. J. L.; Karuso, P. Epicocconone, A Novel Fluorescent Compound from the Fungus *Epicoccum nigrum*. *J. Am. Chem. Soc.* **2003**, *125*, 9304–9305.

259. Jahns, P.; Latowski, D.; Strzalka, K. Mechanism and regulation of the violaxanthin cycle: The role of antenna proteins and membrane lipids. *Biochim. Biophys. Acta BBA - Bioenerg.* **2009**, *1787*, 3–14.

260. Akihisa, T.; Tokuda, H.; Ukiya, M.; Kiyota, A.; Yasukawa, K.; Sakamoto, N.; Kimura, Y.; Suzuki, T.; Takayasu, J.; Nishino, H. Anti-Tumor-Initiating Effects of Monascin, an Azaphilonoid Pigment from the Extract of *Monascus pilosus* Fermented Rice (Red-Mold Rice). *Chem. Biodivers.* **2005**, *2*, 1305–1309.

261. Akihisa, T.; Tokuda, H.; Yasukawa, K.; Ukiya, M.; Kiyota, A.; Sakamoto, N.; Suzuki, T.; Tanabe, N.; Nishino, H. Azaphilones, Furanoisophthalides, and Amino Acids from the Extracts of *Monascus pilosus* -Fermented Rice (Red-Mold Rice) and Their Chemopreventive Effects. *J. Agric. Food Chem.* **2005**, *53*, 562–565.

262. Jørgensen, S. H.; Frandsen, R. J. N.; Nielsen, K. F.; Lysøe, E.; Sondergaard, T. E.; Wimmer, R.; Giese, H.; Sørensen, J. L. Fusarium graminearum PKS14 is involved in orsellinic acid and orcinol synthesis. *Fungal Genet. Biol.* **2014**, *70*, 24–31.

263. Schroeckh, V.; Scherlach, K.; Nützmann, H.-W.; Shelest, E.; Schmidt-Heck, W.; Schuemann, J.; Martin, K.; Hertweck, C.; Brakhage, A. A. Intimate bacterial–fungal interaction triggers biosynthesis of archetypal polyketides in *Aspergillus nidulans*. *Proc. Natl. Acad. Sci.* **2009**, *106*, 14558–14563.

264. Nguyen, K.-H.; Chollet-Krugler, M.; Gouault, N.; Tomasi, S. UV-protectant metabolites from lichens and their symbiotic partners. *Nat. Prod. Rep.* **2013**, *30*, 1490–1508.

265. Xu, M.; Heidmarsson, S.; Olafsdottir, E. S.; Buonfiglio, R.; Kogej, T.; Omarsdottir, S. Secondary metabolites from cetrarioid lichens: Chemotaxonomy, biological activities and pharmaceutical potential. *Phytomedicine* **2016**, *23*, 441–459.

266. Shrestha, G.; St. Clair, L. L. Lichens: a promising source of antibiotic and anticancer drugs. *Phytochem. Rev.* **2013**, *12*, 229–244.

267. Regueira, T. B.; Kildegaard, K. R.; Hansen, B. G.; Mortensen, U. H.; Hertweck, C.; Nielsen, J. Molecular Basis for Mycophenolic Acid Biosynthesis in *Penicillium brevicompactum. Appl. Environ. Microbiol.* **2011**, *77*, 3035–3043.

268. El-Kady, I. A.; Moubasher, M. H.; Mostafa, M. E. Accumulation of sugar alcohols by filamentous fungi. *Folia Microbiol. (Praha)* **1995**, *40*, 481–486.

269. Lewis, D. H.; Smith, D. C. Sugar alcohols (polyols) in fungi and green plants. I. Distribution, physiology and metabolism. *New Phytol.* **1967**, *66,* 143–184.

270. Diano, A.; Bekker-Jensen, S.; Dynesen, J.; Nielsen, J. Polyol synthesis in *Aspergillus niger*: Influence of oxygen availability, carbon and nitrogen sources on the metabolism. *Biotechnol. Bioeng.* **2006**, *94*, 899–908.

271. Wong, B.; Murray, J. S.; Castellanos, M.; Croen, K. D. D-arabitol metabolism in *Candida albicans*: studies of the biosynthetic pathway and the gene that encodes NAD-dependent D-arabitol dehydrogenase. *J. Bacteriol.* **1993**, *175*, 6314–6320.

272. Huang, S.-C.; Kuo, P.-C.; Hwang, T.-L.; Chan, Y.-Y.; Chen, C.-H.; Wu, T.-S. Three novel sesquiterpenes from the mycelium of *Phellinus linteus. Tetrahedron Lett.* **2013**, *54*, 3332–3335.

273. Prado-Cabrero, A.; Scherzinger, D.; Avalos, J.; Al-Babili, S. Retinal Biosynthesis in Fungi: Characterization of the Carotenoid Oxygenase CarX from *Fusarium fujikuroi. Eukaryot. Cell* **2007**, *6*, 650–657.

274. Sutter, R. P. Apotrisporin-E: A new sesquiterpenoid isolated from *Phycomyces blakesleeanus* and *Blakeslea trispora. Exp. Mycol.* **1986**, *10,* 256–258.

275. Gribanovski-Sassu, O.; Foppen, F. H. The carotenoids of the fungus *Epicoccum nigrum* link. *Phytochemistry* **1967**, *6*, 907–909.

276. Gribanovski-Sassu, O.; Tuttobello, L.; Foppen, F. Carotenoids in some ultraviolet mutants of *Epicoccum nigrum* LINK. *Arch. Microbiol.* **1970**, *73*, 216–223.

277. Foppen, F.; Gribanovski-Sassu, O. Carotenogenesis in diphenylamine-treated *Epicoccum nigrum* LINK. *Biochim. Biophys. Acta BBA-Lipids Lipid Metab.* **1969**, *176*, 357–366.

278. Auldridge, M. E.; McCarty, D. R.; Klee, H. J. Plant carotenoid cleavage oxygenases and their apocarotenoid products. *Curr. Opin. Plant Biol.* **2006**, *9*, 315–321.

279. Schimek, C.; Kleppe, K.; Saleem, A.-R.; Voigt, K.; Burmester, A.; Wöstemeyer, J. Sexual reactions in Mortierellales are mediated by the trisporic acid system. *Mycol. Res.* **2003**, *107*, 736–747.

280. Polaino, S.; Gonzalez-Delgado, J. A.; Arteaga, P.; Herrador, M. M.; Barrero, A. F.; Cerdá-Olmedo, E. Apocarotenoids in the sexual interaction of *Phycomyces blakesleeanus. Org. Biomol. Chem.* **2012**, *10*, 3002.

281. Fester, T.; Hause, B.; Schmidt, D.; Halfmann, K.; Schmidt, J.; Wray, V.; Hause, G.; Strack, D. Occurrence and Localization of Apocarotenoids in Arbuscular Mycorrhizal Plant Roots. *Plant Cell Physiol.* **2002**, *43*, 256–265.

282. Avalos, J.; Carmen Limón, M. Biological roles of fungal carotenoids. *Curr. Genet.* **2015**, *61*, 309–324.

283. Nakatsuka, S.; Feng, B.-N.; Goto, T.; Kihara, K. Structures of flazin and YS, highly fluorescent compounds isolated from Japanese soy sauce. *Tetrahedron Lett.* **1986**, *27*, 3399–3402.

284. Tang, J.-G.; Wang, Y.-H.; Wang, R.-R.; Dong, Z.-J.; Yang, L.-M.; Zheng, Y.-T.; Liu, J.-K.; others Synthesis of analogues of flazin, in particular, flazinamide, as promising anti-HIV agents. *Chem. Biodivers.* **2008**, *5*, 447–460.

285. Rönner, B.; Lerche, H.; Bergmüller, W.; Freilinger, C.; Severin, T.; Pischetsrieder, M. Formation of Tetrahydro-β-carbolines and β-Carbolines during the Reaction of L-Tryptophan with D-Glucose. *J. Agric. Food Chem.* **2000**, *48*, 2111–2116.

286. Pitt, J. I.; Hocking, A. D. Primary Keys and Miscellaneous Fungi. In *Fungi and Food Spoilage*; Springer US: Boston, MA, 2009; pp. 53–143.

287. Fuller, K. K.; Loros, J. J.; Dunlap, J. C. Fungal photobiology: visible light as a signal for stress, space and time. *Curr. Genet.* **2015**, *61*, 275–288.

288. Bayram, O.; Krappmann, S.; Ni, M.; Bok, J. W.; Helmstaedt, K.; Valerius, O.; Braus-Stromeyer, S.; Kwon, N.-J.; Keller, N. P.; Yu, J.-H.; Braus, G. H. VelB/VeA/LaeA Complex Coordinates Light Signal with Fungal Development and Secondary Metabolism. *Science* **2008**, *320*, 1504–1506.

289. Bayram, Ö.; Braus, G. H. Coordination of secondary metabolism and development in fungi: the velvet family of regulatory proteins. *FEMS Microbiol. Rev.* **2012**, *36*, 1–24.

290. Kilpatrick, J.; Chilvers, G. Effects of light on sporulation in isolates of *Epicoccum purpurascens*. *Trans. Br. Mycol. Soc.* **1981**, *77*, 605–613.

291. Gribanovski-Sassu, O.; Foppen, F. H. Light and temperature effect on *Epicoccum nigrum*. *Phytochemistry* **1968**, *7*, 1605–1612.

292. Schol-Schwarz, M. B. The genus *Epicoccum* Link. *Trans. Br. Mycol. Soc.* **1959**, *42*, 149–173.

293. Reverberi, M.; Zjalic, S.; Ricelli, A.; Fabbri, A. A.; Fanelli, C. Oxidant/antioxidant balance in *Aspergillus parasiticus* affects aflatoxin biosynthesis. *Mycotoxin Res.* **2006**, *22*, 39–47.

294. Ponts, N.; Pinson-Gadais, L.; Verdal-Bonnin, M.-N.; Barreau, C.; Richard-Forget, F. Accumulation of deoxynivalenol and its 15-acetylated form is significantly modulated by oxidative stress in liquid cultures of *Fusarium graminearum*. *FEMS Microbiol. Lett.* **2006**, *258*, 102–107.

295. Miranda, R. U.; Gómez-Quiroz, L. E.; Mejía, A.; Barrios-González, J. Oxidative state in idiophase links reactive oxygen species (ROS) and lovastatin biosynthesis: Differences and similarities in submerged- and solid-state fermentations. *Fungal Biol.* **2013**, *117*, 85–93.

296. Gadd, G. M. Geomycology: biogeochemical transformations of rocks, minerals, metals and radionuclides by fungi, bioweathering and bioremediation. *Mycol. Res.* **2007**, *111*, 3–49.

297. Renshaw, J. C.; Robson, G. D.; Trinci, A. P. J.; Wiebe, M. G.; Livens, F. R.; Collison, D.; Taylor, R. J. Fungal siderophores: structures, functions and applications. *Mycol. Res.* **2002**, *106*, 1123–1142.

298. Cuero, R.; Ouellet, T.; Yu, J.; Mogongwa, N. Metal ion enhancement of fungal growth, gene expression and aflatoxin synthesis in *Aspergillus flavus*: RT-PCR characterization. *J. Appl. Microbiol.* **2003**, *94*, 953–961.

299. Ding, C.; Wu, X.; Auckloo, B.; Chen, C.-T.; Ye, Y.; Wang, K.; Wu, B. An Unusual Stress Metabolite from a Hydrothermal Vent Fungus *Aspergillus* sp. WU 243 Induced by Cobalt. *Molecules* **2016**, *21*, 1–11.

300. Griffith, G. W.; Easton, G. L.; Detheridge, A.; Roderick, K.; Edwards, A.; Worgan, H. J.; Nicholson, J.; Perkins, W. T. Copper deficiency in potato dextrose agar causes reduced pigmentation in cultures of various fungi. *FEMS Microbiol. Lett.* **2007**, *276*, 165–171.

301. Shuang Gui Tie Oxidative damage and antioxidant response caused by excess copper in leaves of maize. *Afr. J. Biotechnol.* **2012**, *11*.

302. Festa, R. A.; Thiele, D. J. Copper at the Front Line of the Host-Pathogen Battle. *PLoS Pathog.* **2012**, *8*, e1002887.

303. Abe, F.; Miura, T.; Nagahama, T.; Inoue, A.; Usami, R.; Horikoshi, K. Isolation of a highly copper-tolerant yeast, *Cryptococcus* sp., from the Japan Trench and the induction of superoxide dismutase activity by Cu2+. *Biotechnol. Lett.* **2001**, *23*, 2027–2034.

304. Jiang, W., Yuqian|Shen,Li|Wu,Xiaodan|Ye,Ying Stress-driven Discovery of Natural Products from Extreme Marine Environment-Kueishantao Hydrothermal Vent, a Case Study of Metal Switch Valve. *Curr. Org. Chem.* **2014**, *18*, 925–934.

305. Wilson, D.; Citiulo, F.; Hube, B. Zinc Exploitation by Pathogenic Fungi. *PLoS Pathog.* **2012**, *8*, e1003034.

306. Silvennoinen, L.; Sandalova, T.; Schneider, G. The polyketide cyclase RemF from *Streptomyces resistomycificus* contains an unusual octahedral zinc binding site. *FEBS Lett.* **2009**, *583*, 2917–2921.

307. Pagani, M. A.; Casamayor, A.; Serrano, R.; Atrian, S.; Ariño, J. Disruption of iron homeostasis in *Saccharomyces cerevisiae* by high zinc levels: a genome-wide study. *Mol. Microbiol.* **2007**, *65*, 521–537.

308. Savi, G. D.; Bortoluzzi, A. J.; Scussel, V. M. Antifungal properties of Zinc-compounds against toxigenic fungi and mycotoxin. *Int. J. Food Sci. Technol.* **2013**, *48*, 1834–1840.

309. Ramsay, L. M.; Sayer, J. A.; Gadd, G. M. Stress responses of fungal colonies towards toxic metals. In *The fungal colony*; Gow, N. A. R.; Robson, G. D.; Gadd, G. M., Eds.; Cambridge University Press, 1999; pp. 178–200.

310. Fomina, M.; Ritz, K.; Gadd, G. M. Nutritional influence on the ability of fungal mycelia to penetrate toxic metal-containing domains. *Mycol. Res.* **2003**, *107*, 861–871.

311. Baldrian, P.; Gabriel, J. Effect of heavy metals on the growth of selected wood-rotting basidiomycetes. *Folia Microbiol. (Praha)* **1997**, *42*, 521–523.

312. Brzonkalik, K.; Herrling, T.; Syldatk, C.; Neumann, A. The influence of different nitrogen and carbon sources on mycotoxin production in *Alternaria alternata*. *Int. J. Food Microbiol.* **2011**, *147*, 120–126.

313. Dobbs, C. G.; Hinson, W. H. A Widespread Fungistasis in Soils. *Nature* **1953**, *172*, 197–199.

314. Lockwood, J. L. Fungistasis in soil. *Biol. Rev.* **1977**, *52*, 1–43.

315. Lynch, J. M. Limits to Microbial Growth in Soil. *Microbiology* **1982**, *128*, 405–410.

316. Dörfelt, H.; Schröder, M.-B. Untersuchungen zur submikroskopischen Struktur von *Xerula melanotricha*. *Nova Hedwig.* **1981**, *35*, 435–452.

317. Kobayashi, H. Ion Secretion via Salt Glands in Poaceae. *Jpn. J. Plant Sci.* **2008**, *1*, 1–8.

318. Kikuchi, Y.; Hijikata, N.; Ohtomo, R.; Handa, Y.; Kawaguchi, M.; Saito, K.; Masuta, C.; Ezawa, T. Aquaporin-mediated long-distance polyphosphate translocation directed towards the host in arbuscular mycorrhizal symbiosis: application of virus-induced gene silencing. *New Phytol.* **2016**, *211*, 1202–1208.

319. Sonnewald, U. Physiology of Metabolism. In *Strasburger's Plant Sciences*; Springer Berlin Heidelberg: Berlin, Heidelberg, 2013; pp. 239–409.

320. Veses, V.; Richards, A.; Gow, N. A. Vacuoles and fungal biology. *Curr. Opin. Microbiol.* **2008**, *11*, 503–510.

321. Shoji, J.-Y.; Arioka, M.; Kitamoto, K. Possible involvement of pleiomorphic vacuolar networks in nutrient recycling in filamentous fungi. *Autophagy* **2006**, *2*, 226–227.

322. Del Sorbo, G.; Schoonbeek, H.; De Waard, M. A. Fungal Transporters Involved in Efflux of Natural Toxic Compounds and Fungicides. *Fungal Genet. Biol.* **2000**, *30*, 1–15.

323. Alexander, N. J.; McCormick, S. P.; Hohn, T. M. TRI12, a trichothecene efflux pump from *Fusarium sporotrichioides*: gene isolation and expression in yeast. *Mol. Gen. Genet. MGG* **1999**, *261*, 977–984.

324. Barber, J.; Chapman, A. C.; Howard, T. D.; Tebb, G. Recycling of polyketides by fungi: the degradation of citrinin by *Penicillium citrinum. Appl. Microbiol. Biotechnol.* **1988**, *29*, 387–391.

325. Koman, V.; Betina, V.; Baráth, Z. Fatty acid, lipid and cyanein production by *Penicillium cyaneum. Arch. Für Mikrobiol.* **1969**, *65*, 172–180.

326. Betina, V. Differentiation and secondary metabolism in some prokaryotes and fungi. *Folia Microbiol. (Praha)* **1995**, *40*, 51–67.

327. Itri, R.; Junqueira, H. C.; Mertins, O.; Baptista, M. S. Membrane changes under oxidative stress: the impact of oxidized lipids. *Biophys. Rev.* **2014**, *6*, 47–61.

328. Ohsumi, Y.; Kitamoto, K.; Anraku, Y. Changes induced in the permeability barrier of the yeast plasma-membrane by cupric ion. *J. Bacteriol.* **1988**, *170*, 2676–2682.

329. Avery, S. V.; Howlett, N. G.; Radice, S. Copper toxicity towards *Saccharomyces cerevisiae*: dependence on plasma membrane fatty acid composition. *Appl. Environ. Microbiol.* **1996**, *62*, 3960–3966.

330. Koulman, A.; Lane, G. A.; Christensen, M. J.; Fraser, K.; Tapper, B. A. Peramine and other fungal alkaloids are exuded in the guttation fluid of endophyte-infected grasses. *Phytochemistry* **2007**, *68*, 355–360.

331. Wang, X.; Sena Filho, J. G.; Hoover, A. R.; King, J. B.; Ellis, T. K.; Powell, D. R.; Cichewicz, R. H. Chemical Epigenetics Alters the Secondary Metabolite Composition of Guttate Excreted by an Atlantic-Forest-Soil-Derived *Penicillium citreonigrum. J. Nat. Prod.* **2010**, *73*, 942–948.

332. Sprecher, E. Über die Stoffausscheidung bei Pilzen. I. *Arch. Für Mikrobiol.* **1960**, *38*, 114–155.

333. Sprecher, E. Über die Stoffausscheidung bei Pilzen II. *Arch. Microbiol.* **1961**, *38*, 299–325.

334. Gareis, M.; Gottschalk, C. *Stachybotrys* spp. and the guttation phenomenon. *Mycotoxin Res.* **2014**, *30*, 151–159.

335. Aliferis, K. A.; Jabaji, S. Metabolite Composition and Bioactivity of *Rhizoctonia solani* Sclerotial Exudates. *J. Agric. Food Chem.* **2010**, *58*, 7604–7615.

336. da Silva Araújo, F. D.; de Lima Fávaro, L. C.; Araújo, W. L.; de Oliveira, F. L.; Aparicio, R.; Marsaioli, A. J. Epicolactone - Natural Product Isolated from the Sugarcane Endophytic Fungus *Epicoccum nigrum*. *Eur. J. Org. Chem.* **2012**, *2012*, 5225–5230.

337. Kück, U.; Nowrousian, M.; Hoff, B.; Engh, I. *Schimmelpilze*; 3rd ed.; Springer Berlin Heidelberg: Berlin, Heidelberg, 2009.

8   APPENDIX

The resulting genetic sequences of the herein described fungal strains:

- *E. nigrum* **strain 749:**

TGTACTTTTGGACGTCGTCGTTATGAGTGCAAAGCGCGAGATGTACTGCGCTCCGAAATCAATACGCCGGCT
GCCAATTGTTTTAAGGCGAGTCTACACGCAGAGGCGAGACAAACACCCAACACCAAGCAGAGCTTGAAGGTA
CAAATGACGCTCGAACAGGCATGCCCCATGGAATACCAAGGGGCGCAATGTGCGTTCAAAGATTCGATGATT
CACTGAATTCTGCAATTCACACTACTTATCGCATTTCGCTGCGTTCTTCATCGATGCCAGAACCAAGAGATCC
GTTGTTGAAAGTTGTAACTATTATGTTTTTTCAGACGCTGATTGCAACTGCAAAGGGTTTGAATGTTGTCCAAT
CGGCGGGCGGACCCGCCGAGGAAACGAAGGTACTCAAAAGACATGGGTAAGAGGTAGCAGACCGAAGTCT
ACAAACTCTAGGTAATGATCCTTCCGCAGGTTC

- *E. nigrum* **strain 800:**

TGTACTTTTGGACGTCGTCGTTGTGAGTGCAAAGCGCGAGATGTACTGCGCTCCGAAATCAATACGCCGGCT
GCCAATTGTTTTAAGGCGAGTCTACACGCAGAGGCGAGACAAACACCCAACACCAAGCAGAGCTTGAAGGTA
CAAATGACGCTCGAACAGGCATGCCCCATGGAATACCAAGGGGCGCAATGTGCGTTCAAAGATTCGATGATT
CACTGAATTCTGCAATTCACACTACTTATCGCATTTCGCTGCGTTCTTCATCGATGCCAGAACCAAGAGATCC
GTTGTTGAAAGTTGTAACTATTATGTTTTTTCAGACGCTGATTGCAACTGCAAAGGGTTTGAATGTTGTCCAAT
CGGCGGGCGGACCCGCCGAGGAAACGAAGGTACTCAAAAGACATGGGTAAGAGGTAGCAGACCGAAGTCT
ACAAACTCTAGGTAATGATCCTTCCGCAGGTTCA

Further sequences used for the phylogenetic tree:

- *Gliomastix murorum* **strain 469**

ACCTGCGGAGGGATCATTACCGAGTTGCAAAACTCCCAAACCCACTGTGAACCAATACCACTGTTGCTTCGG
CGGACACGCCCCGGGCGCACCTCCTCAGGGGGGTGTGCCCCGGAACCAGGCGCCCGCCGGGGGGACCGAA
ACCTCTGTATTTACCATTTGAGTACTCTGAGTGTGATTTACAAAATCAAAATTAAAACTTTCAACAACGGATCT
CTTGGCTCTAGCATCGATGAAGAACGCAGCGAAATGCGATAAGTAATGCGAATTGCAGAATTCAGTGAATCA
TCGAATCTTTGAACGCACATTGCGCCCGCCAGTATTCTGGCGGGCATGCCTGTCTGAGCGTCGTTTCGACCC
TCGCGCCCGGCTTCTGTCGGGGGCGGTGTTGGGGATCGGCCACACCCTTTACTGGGCGGCCGTCCCCTAA
ATCCAGTGGCGACCACGCTGTAGCCTCCCCTGCGTAGTACTAAAACCACCTCGCAGGCGGAGAGCGGTGCG
GCCCGCCGTAAAACCCCCCAACTT

- *Phoma betae* **strain 815**

CCGTAGGTGAACCTGCGGAAGGATCATTACCAATATGAAAGCGGGTGGGGAGCCACAGAAGTTGGGGCCCT
CGTGGCTCTACTTCTGCCCCATCTGTCTGAATATTCACCCATGTCTTTTGCGTACCCATTGTTTCCTTGGCGG
GCTTGCCCGCCAACAGGACATTATTAAACCTTTTGTAATTGCAGTCAGCGTCAGAAATAACTTAATAGTTACAA
CTTTCAACAACGGATCTCTTGGTTCTGGCATCGATGAAGAACGCAGCGAAATGCGATAAGTAGTGTGAATTG
CAGAATTCAGTGAATCATCGAATCTTTGAACGCACATTGCGCCCCCTTGGTATTCCATGGGGCATGCCTGTTC
GAGCGTCATTTGTACCCTCAAGCTCTGCTTGGTGTTGGGTGTTTGTCTCTTCCGGGAGACTCGCCTCAAAAC

AATTGGCAGCCGGCATATTGGTATCGGAGCGCAGCACAAGTCGCGCTTCTGTCCATATTTGTTGGCATCCAG
CAAGACC

- ***Phoma exigua* (syn. *Boeremia exigua*) strain PB5**

CCGTAGGTGAACCTGCGGAAGGATCATTACCTAGAGTTGTAGGCTTTGCCTACCATCTCTTACCCATGTCTTT
TGAGTACCTTCGTTTCCTCGGCGGGTCCGCCCGCCGATTGGACAAACTTAAACCCTTTGTAATTGAAATCAG
CGTCTGAAAAAACATAATAGTTACAACTTTCAACAACGGATCTCTTGGTTCTGGCATCGATGAAGAACGCAGC
GAAATGCGATAAGTAGTGTGAATTGCAGAATTCAGTGAATCATCGAATCTTTGAACGCACATTGCGCCCCTTG
GTATTCCATGGGGCATGCCTGTTCGAGCGTCATTTGTACCTTCAAGCTCTGCTTGGTGTTGGGTGTTTGTCTC
GCCTTTGCGTGTAGACTCGCCTTAAAACAATTGGCAGCCGGCGTATTGATTTCGGAGCGCAGTACATCTCGC
GCTTTGCACTCATAACGACGACGTCCAAAAAGTAC

Additional sequences of different *Epicoccum nigrum* strains taken from GenBank for assembly of the phylogeny (GenBank accession numbers are given):

JX402194.1, JX402182.1, JX402191.1, KF164404.1, KC305160.1, KF574877.1, KC222840.1, KC568289.1

Tab. 8.1a: Inhibitory activity on neutrophil elastase (HLE, see **section 3.5.4** for the method) of a crude extract from *E. nigrum* strain 749 grown on MES (malt extract agar with artificial sea water) under continuous illumination with white light. Activity is given as residual activity in %. Number of replicates N = 4. SD = standard deviation, abs/min = Absorption of the cleaved chromophore/minute.

Conc. [µg/ml]	Abs/min.	SD	N	Rest activity [%]
0	0,0057	0,0005	4	100,00
2	0,0044	0,0007	4	77,19
4	0,0034	0,0009	4	59,65
6	0,0027	0,0007	4	47,37
8	0,0024	0,0006	4	42,11
10	0,0019	0,0004	4	33,33

Tab. 8.1b: Data as for Tab. 8.1a, extract from *E. nigrum* strain 749 grown on MEA (malt extract agar).

Conc. [µg/ml]	Abs/min.	SD	N	Rest activity [%]
0	0,0081	-	8	100,00
2	0,0036	0,0004	4	44,44
4	0,0025	0,0005	4	30,86
6	0,0016	0,0003	4	19,75
8	0,0012	0,0003	4	14,81
10	0,0008	0,0003	4	9,88
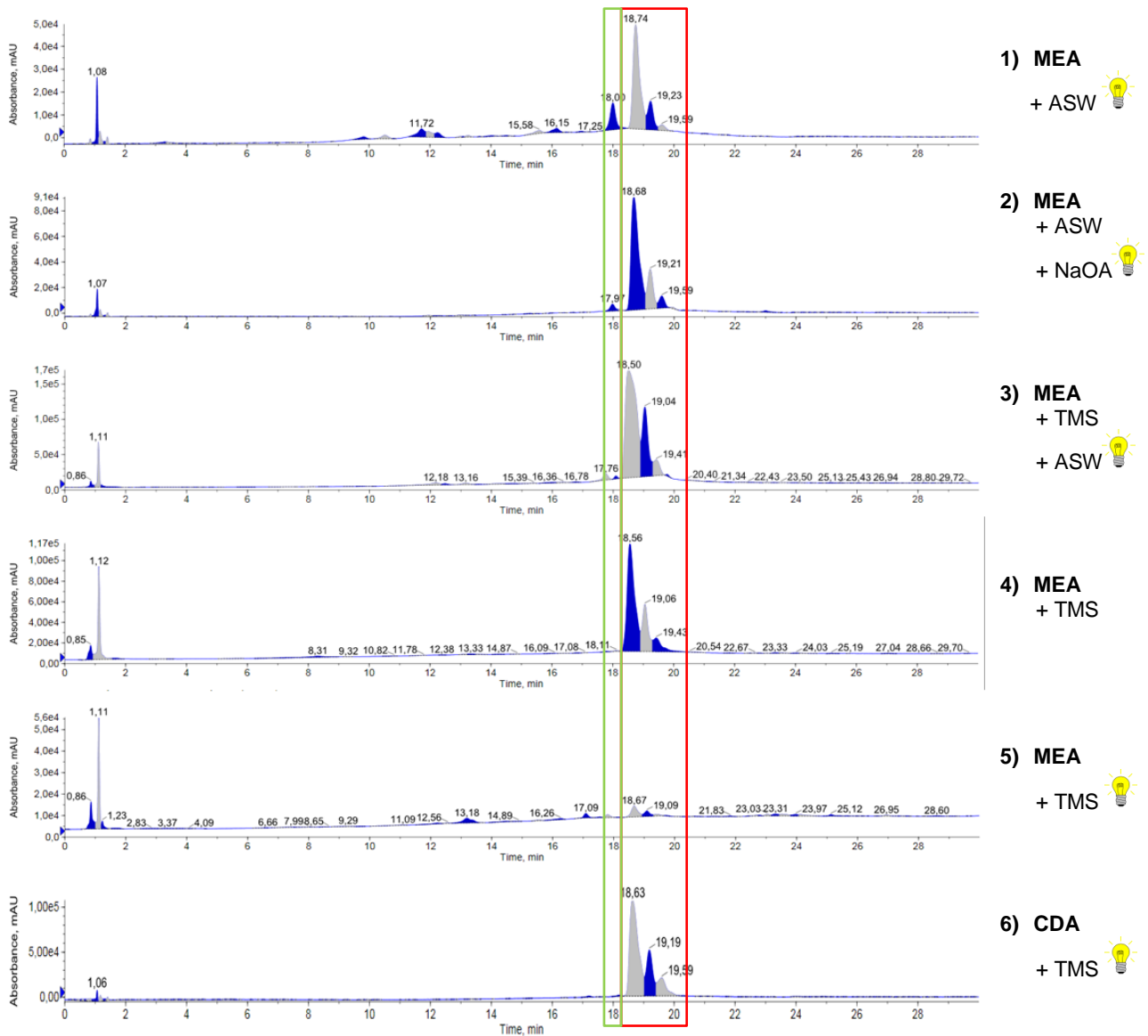
Fig. 8.1: Comparison of the TWC (total wavelength count) from LC-MS runs of crude extracts from *E. nigrum* **strain 749** (for the method see section 3.3.2). The red rectangle indicates the time frame, in which epipyrones (**1**-**3**) elute, the green rectangle highlights acetosellin-derived peaks. Lightbulbs indicate continuous illumination with white light. MEA = malt extract agar; ASW = artificial sea water; CDA = Czapek-Dox agar; TMS = trace metal solution.
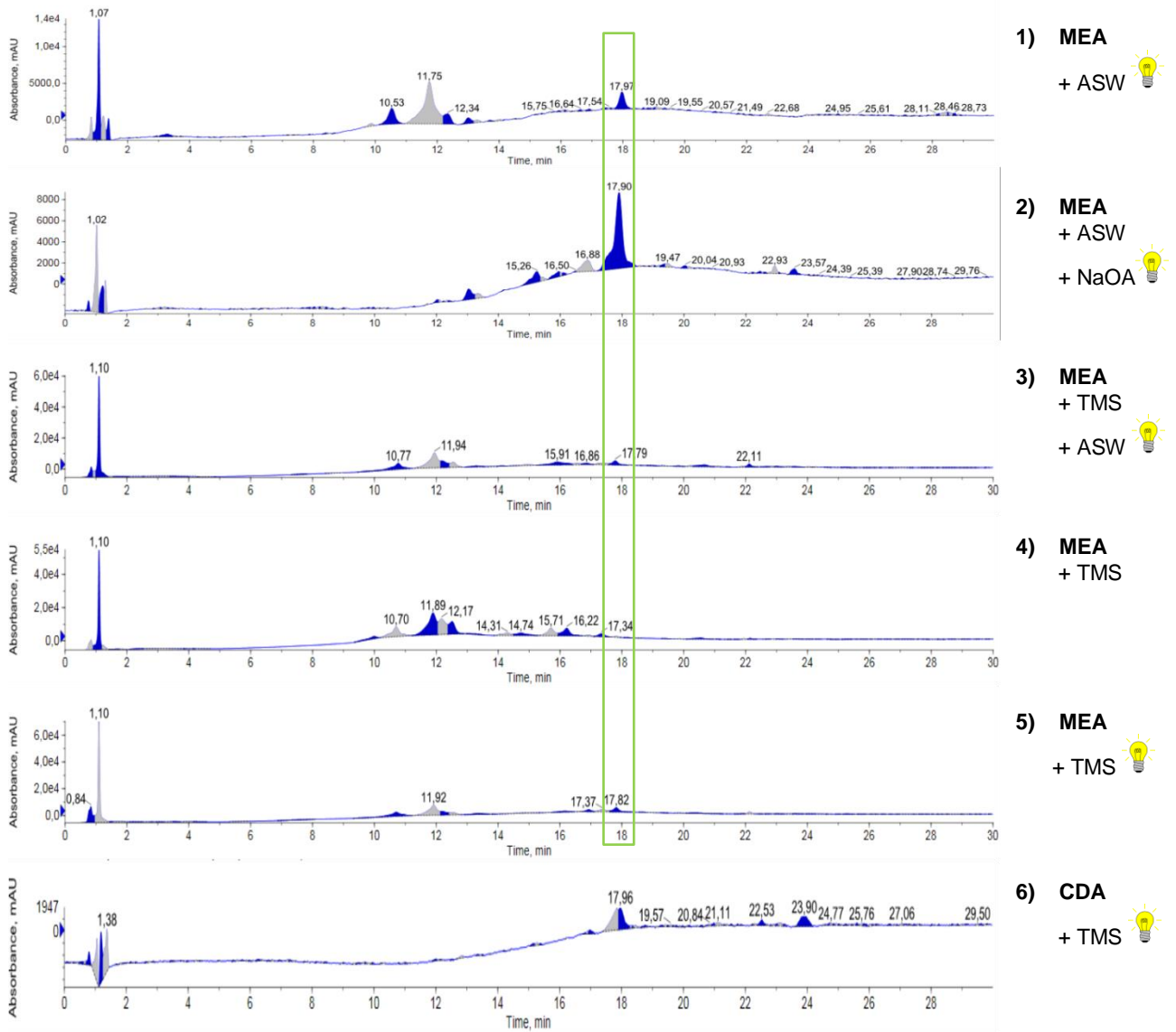
Fig. 8.2: Comparison of the TWC (total wavelength count) from LC-MS runs of crude extracts from *E. nigrum* **strain 800** (for the method see section 3.3.2). The green rectangle indicates the time, at which acetosellin elutes (on CDA with TMS, no acetosellin was detected). Lightbulbs indicate continuous illumination with white light. MEA = malt extract agar; ASW = artificial sea water; CDA = Czapek-Dox agar.

[1]
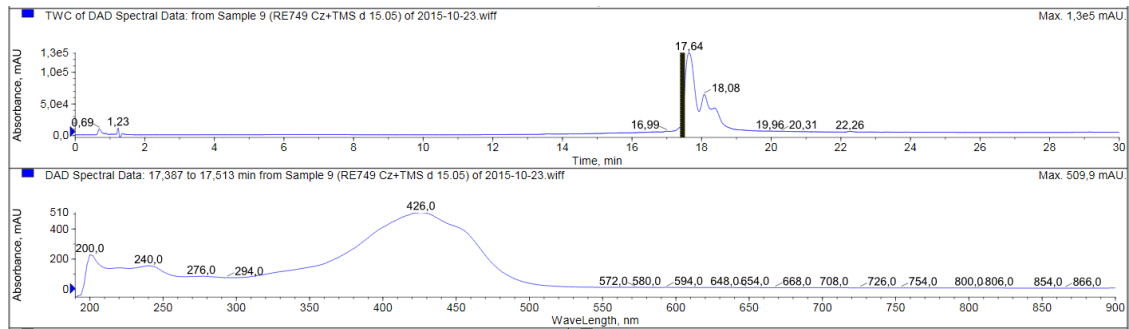
[2]
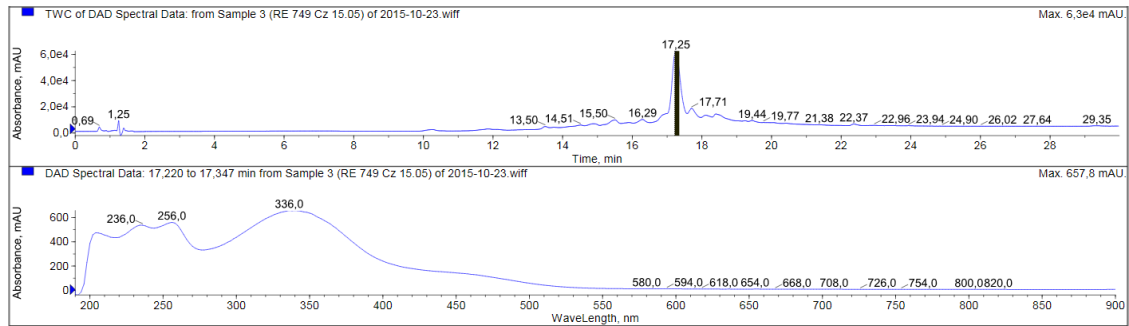
Fig. 8.3: Comparison of the composition of two extracts from *E. nigrum* strain 749 on:

[1] CDA (Czapek-Dox agar), under continuous illumination with white light.

[2] CDT (Czapek-Dox agar with trace metal solution), grown in darkness.

Shown are the UV-data (TWC and the selected UV-spectrum of the respective main metabolite) obtained during an LC-ESI-MS run.
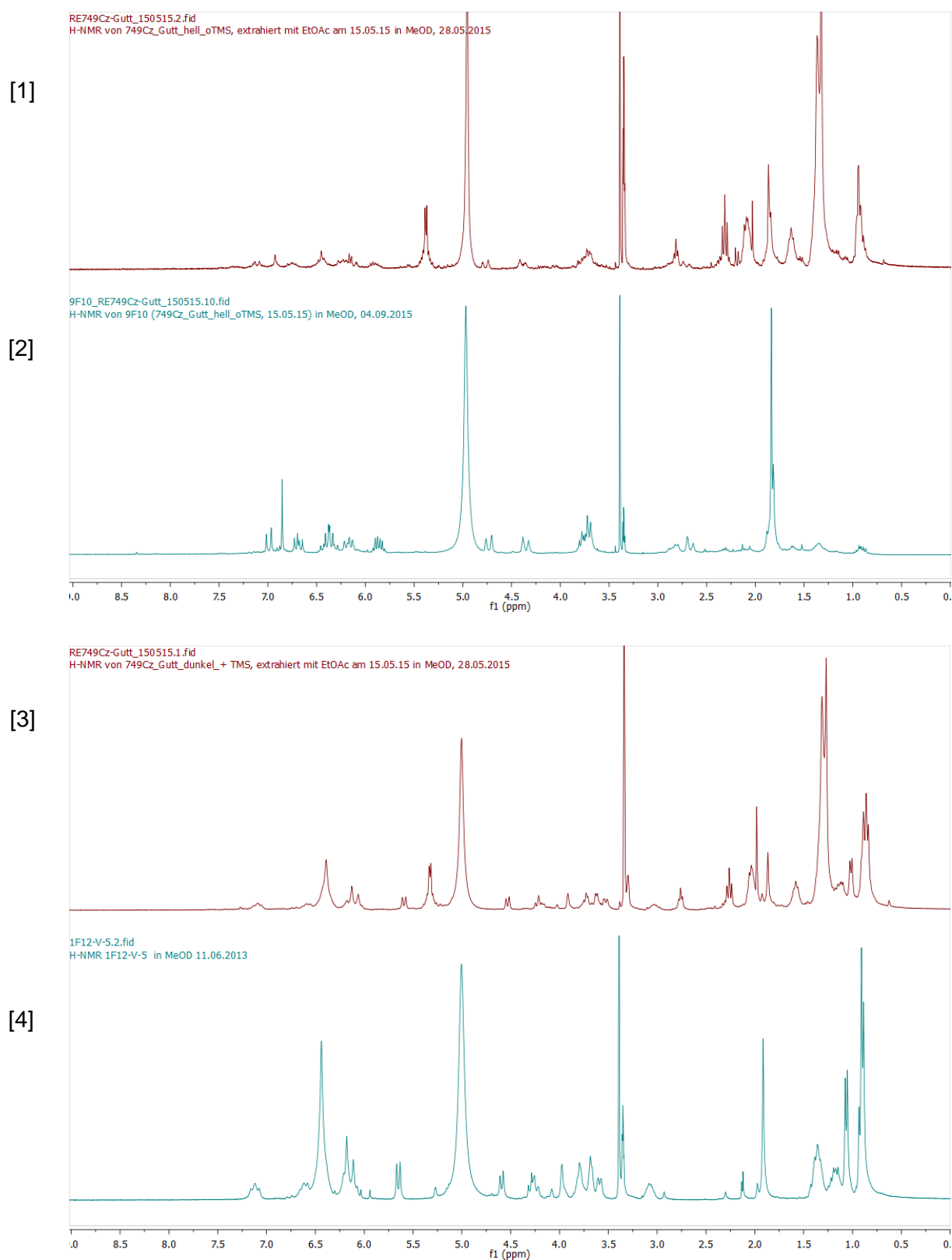
Fig. 8.4: Comparison of the ^{1}H-NMR experiments of (in MeOH-d_4 and recorded at 300 MHz):

[1] *E. nigrum* strain 749 grown on CDA (Czapek-Dox agar), under continuous illumination.

[2] Acetosellin (**4**)

[3] *E. nigrum* strain 749 grown on CDT in darkness (Czapek-Dox agar with trace metal solution).

[4] Epipyrones (**1-3**)

1F12-V-5.2.1.1r
H-NMR 1F12-V-5 in MeOD 11.06.2013
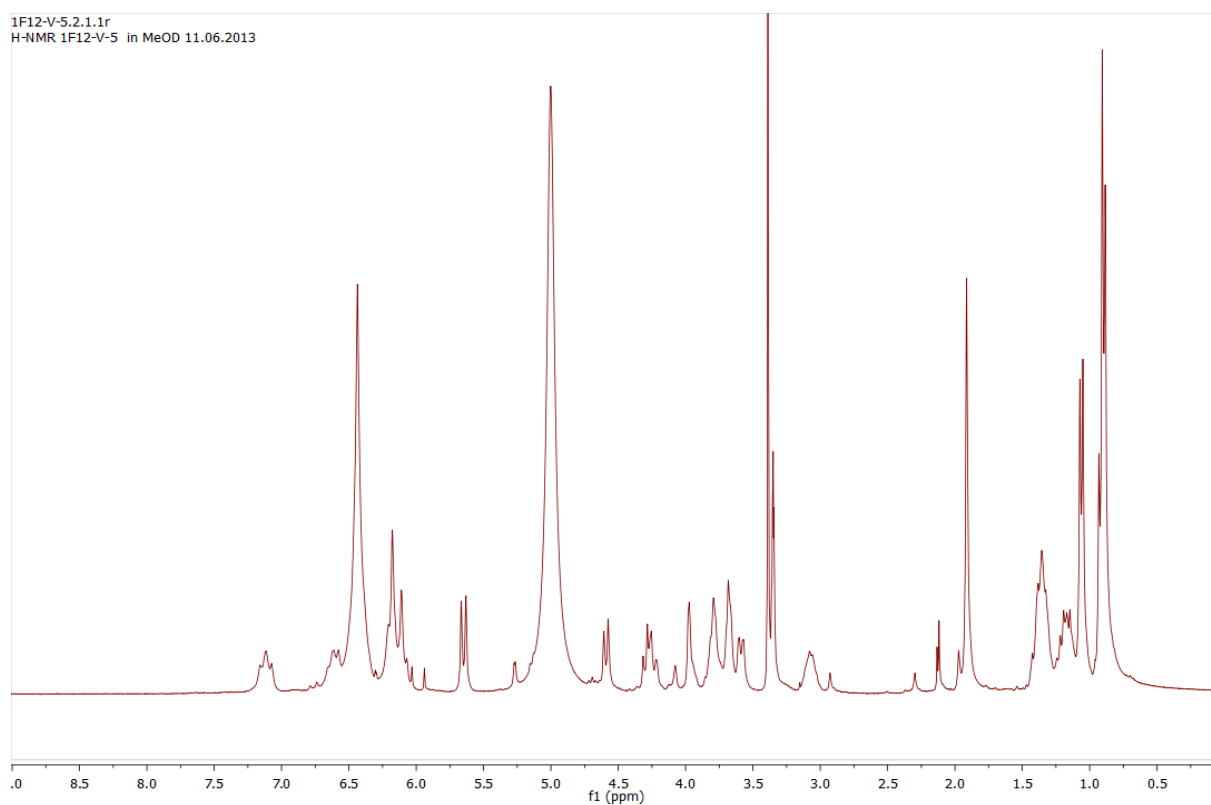
Fig. 8.5: ^{1}H-NMR of epipyrones (**1-3**) in MeOH-d_4, measured at 300 MHz.

1F12-V-5.20.1.1r
C-NMR 1F12-V-5 in MeOD 05.06.2013
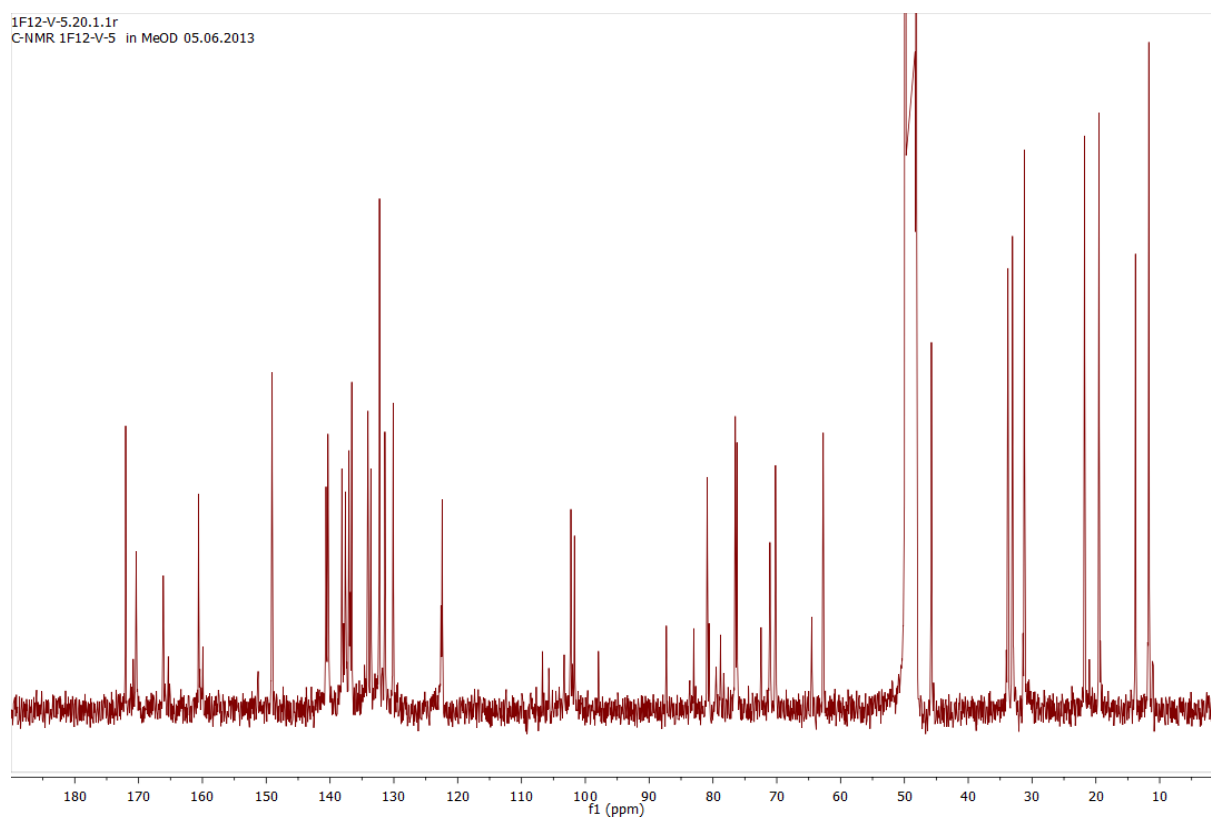
Fig. 8.6: ^{13}C-NMR of epipyrones (**1-3**) in MeOH-d_4, measured at 75 MHz.
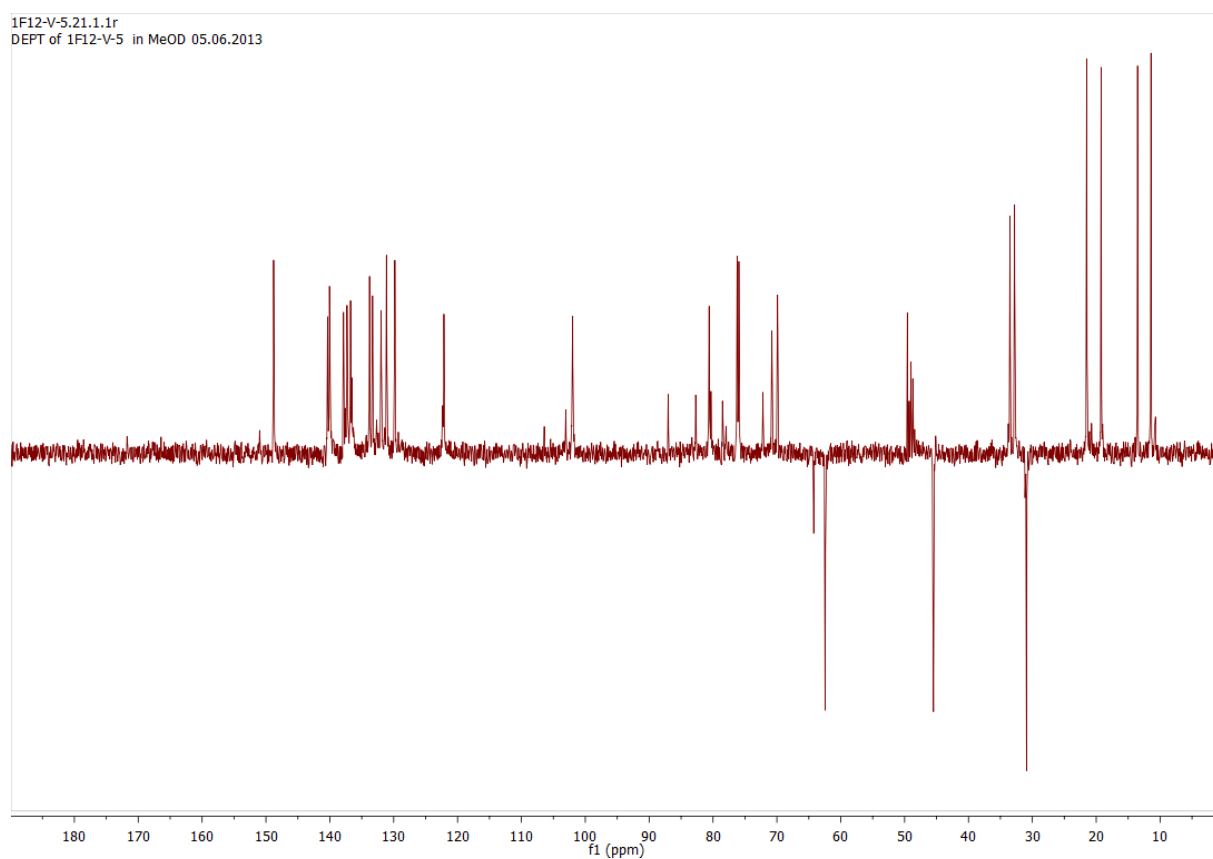
Fig. 8.7: DEPT-135 of epipyrones (**1**-**3**) in MeOH-d_4.
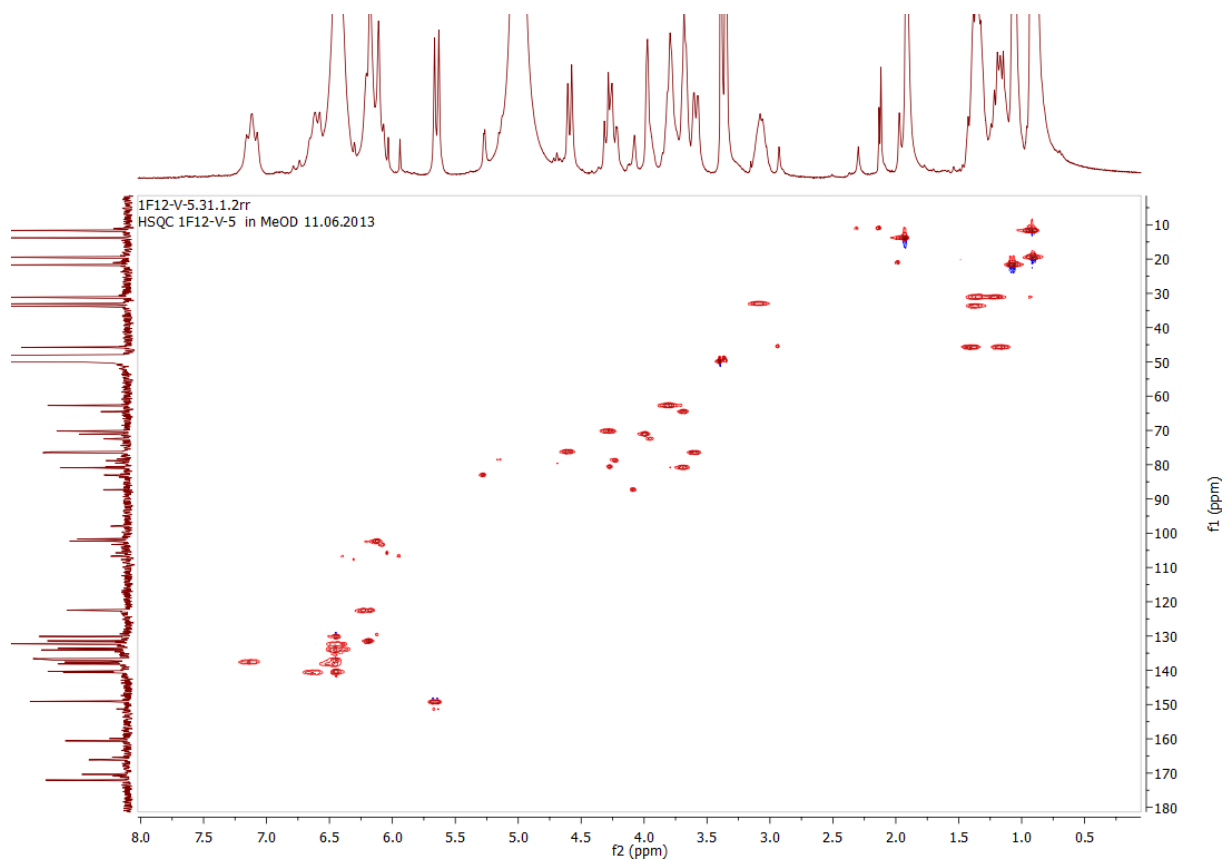
Fig. 8.8: HSQC of epipyrones (**1**-**3**) in MeOH-d_4, measured at 300 MHz.
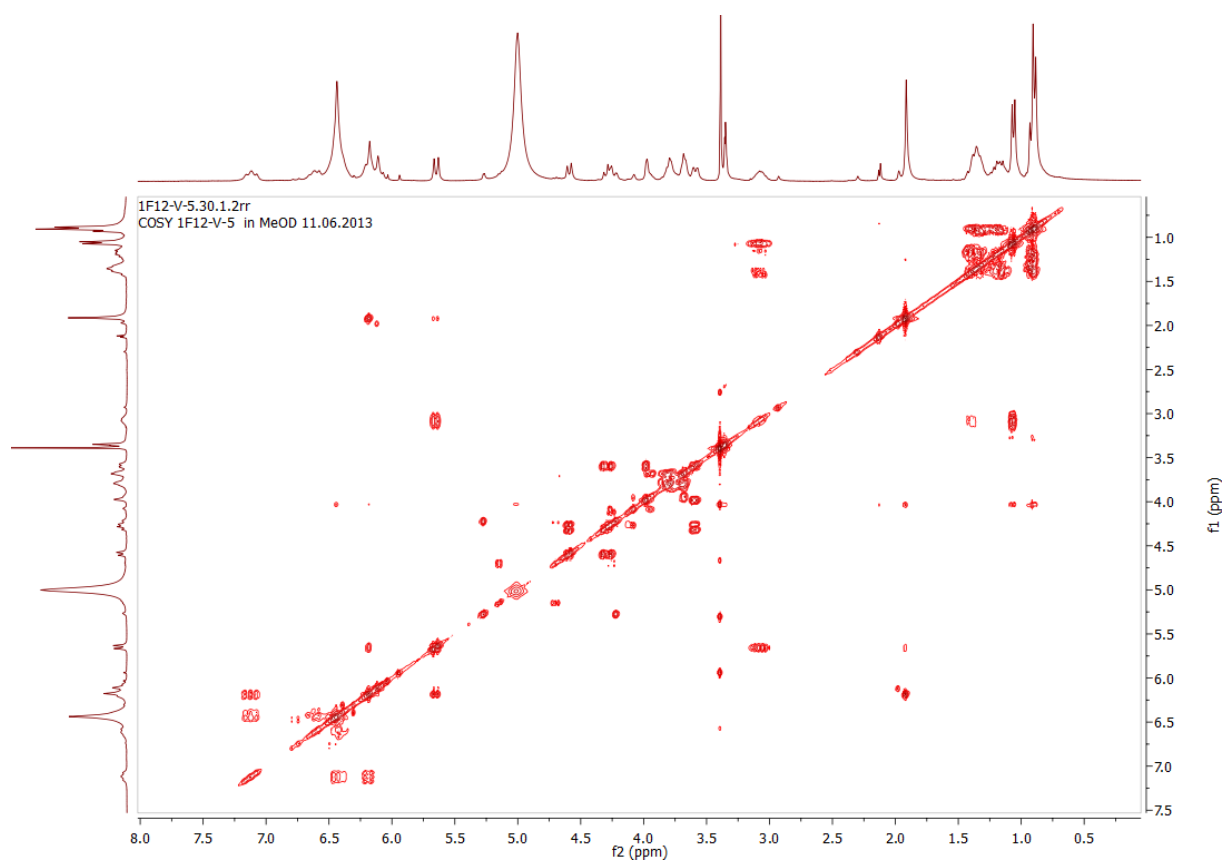
Fig. 8.9: COSY of epipyrones (**1-3**) in MeOH-d_4, measured at 300 MHz.
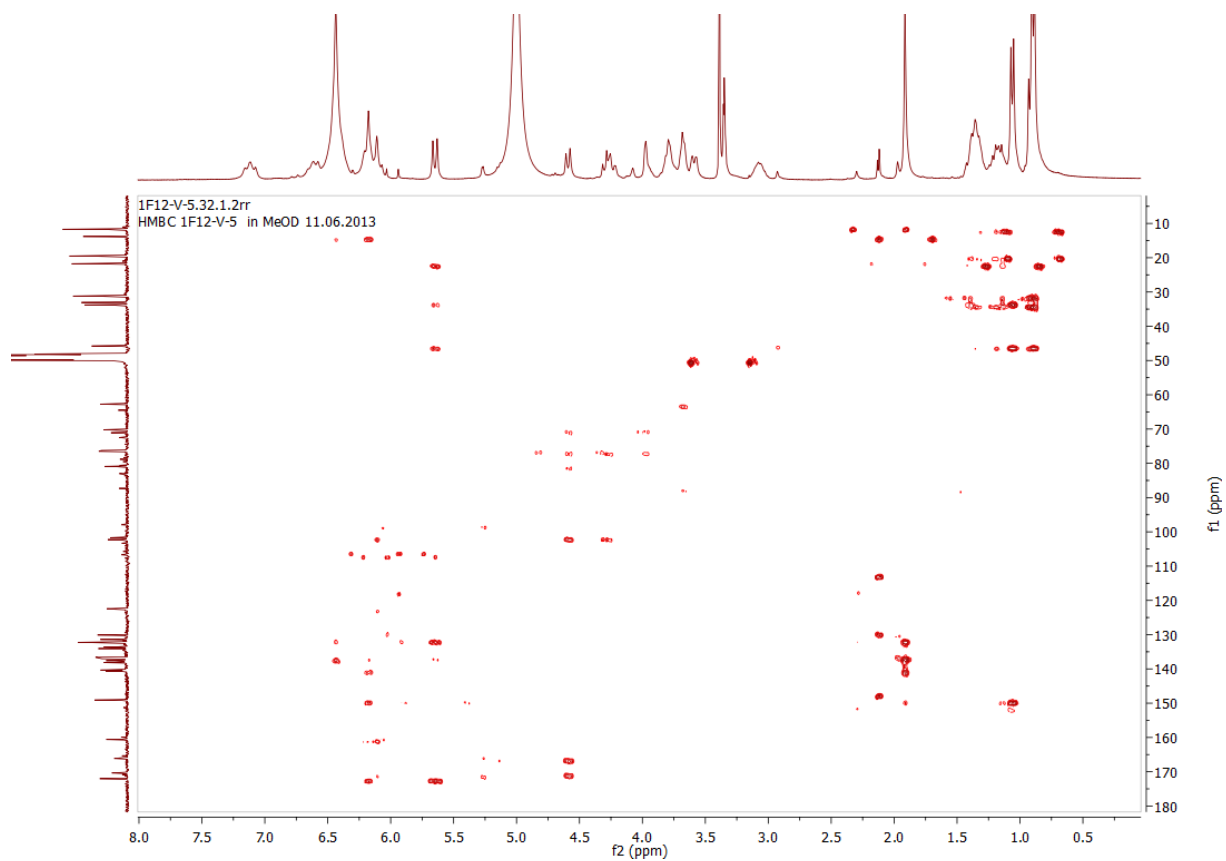
Fig. 8.10: HMBC of epipyrones (**1-3**) in MeOH-d_4, measured at 300 MHz.
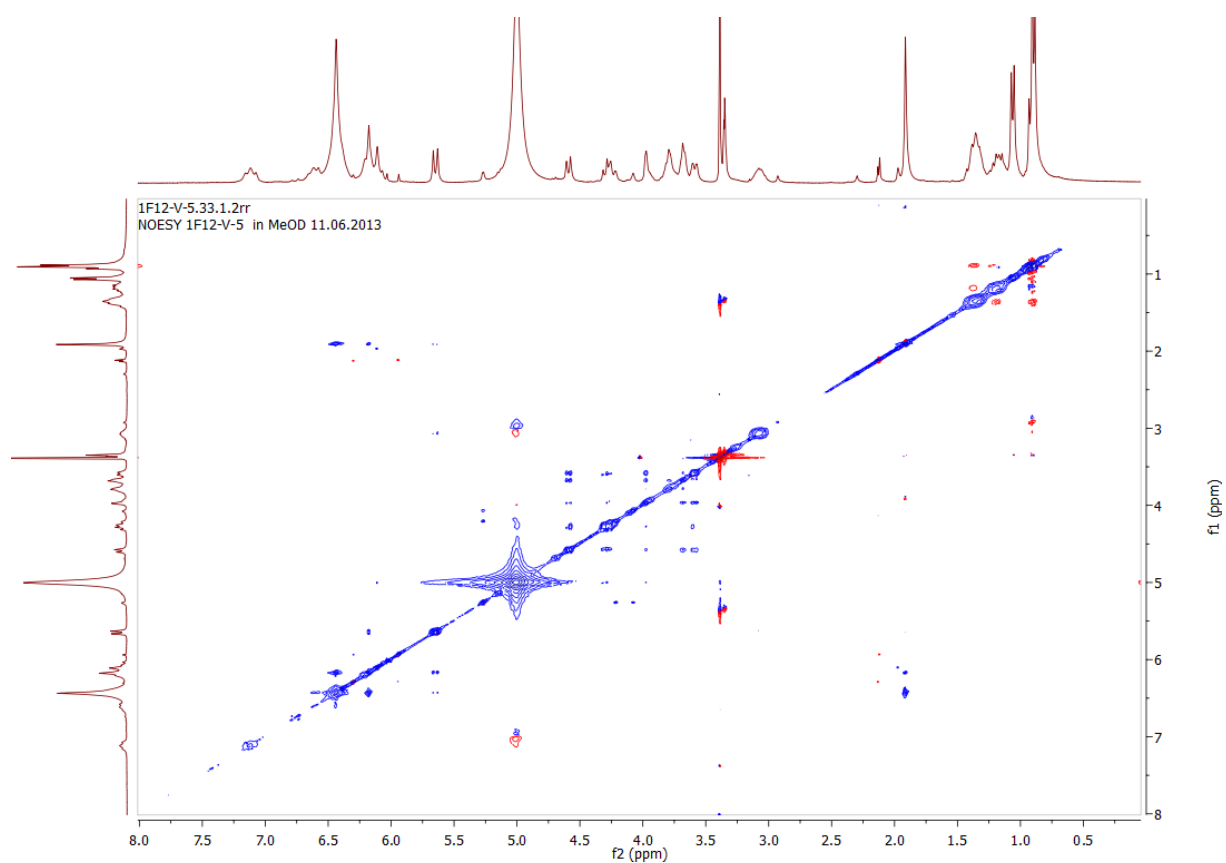
Fig. 8.11: NOESY of epipyrones (**1-3**) in MeOH-d_4, measured at 300 MHz.
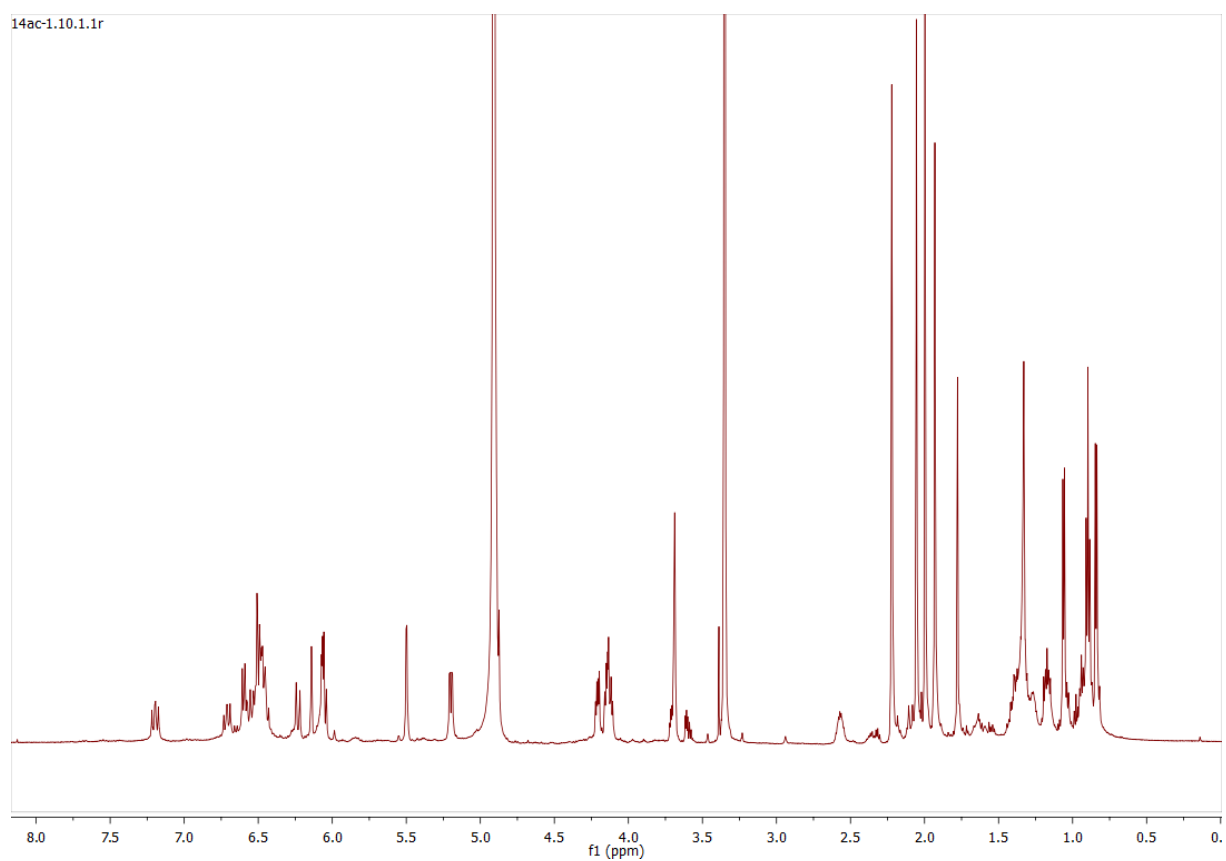
Fig. 8.12: ^{1}H-NMR of epipyrone tetraacetate (**5**) in MeOH-d_4, measured at 600 MHz.

14Ac-1-600er.20.1.1r
C-NMR 1F12-V-4ac-1 in MeOD 28.07.2014
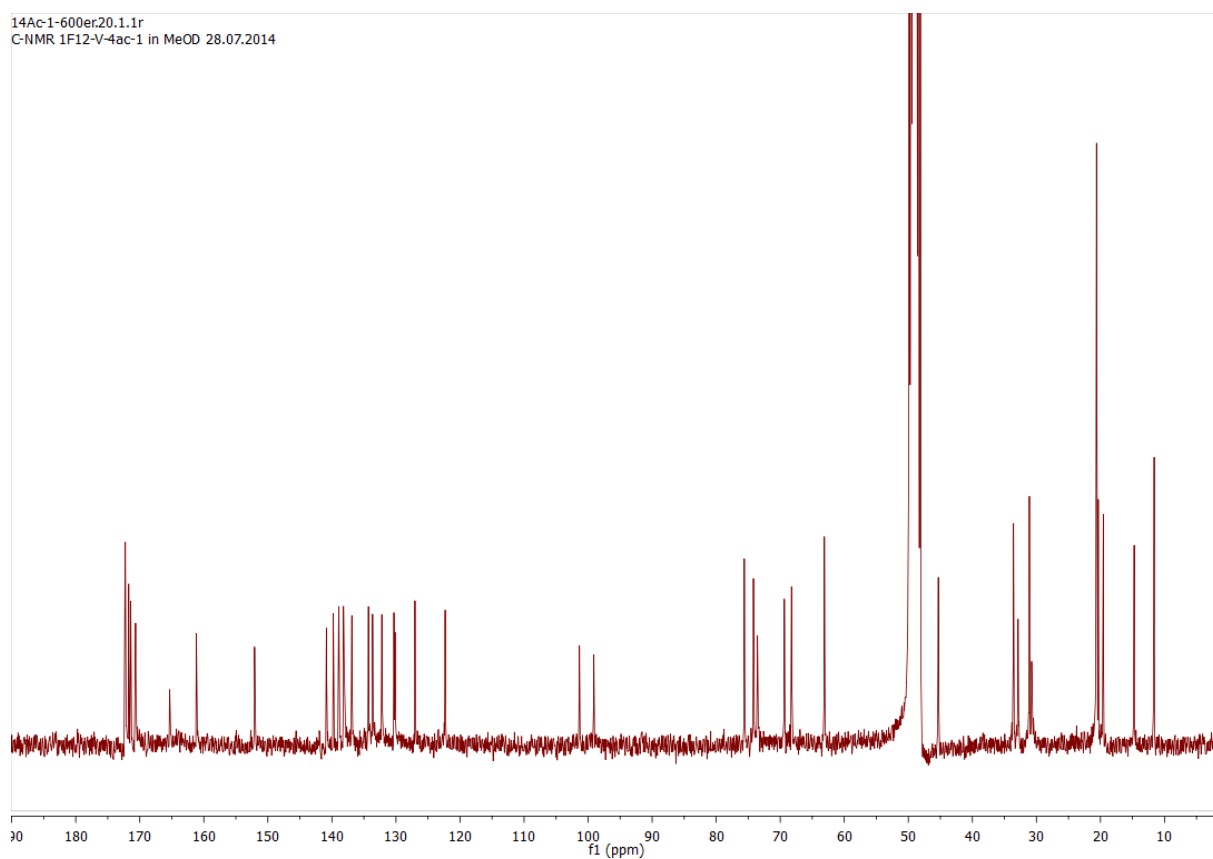
Fig. 8.13: ^{13}C-NMR of epipyrone tetraacetate (**5**) in MeOH-d_4, measured at 150 MHz.

1F12-V-4ac-1.21.1.1r
DEPT von 1F12-V-4ac-1 in MeOD 29.07.2014
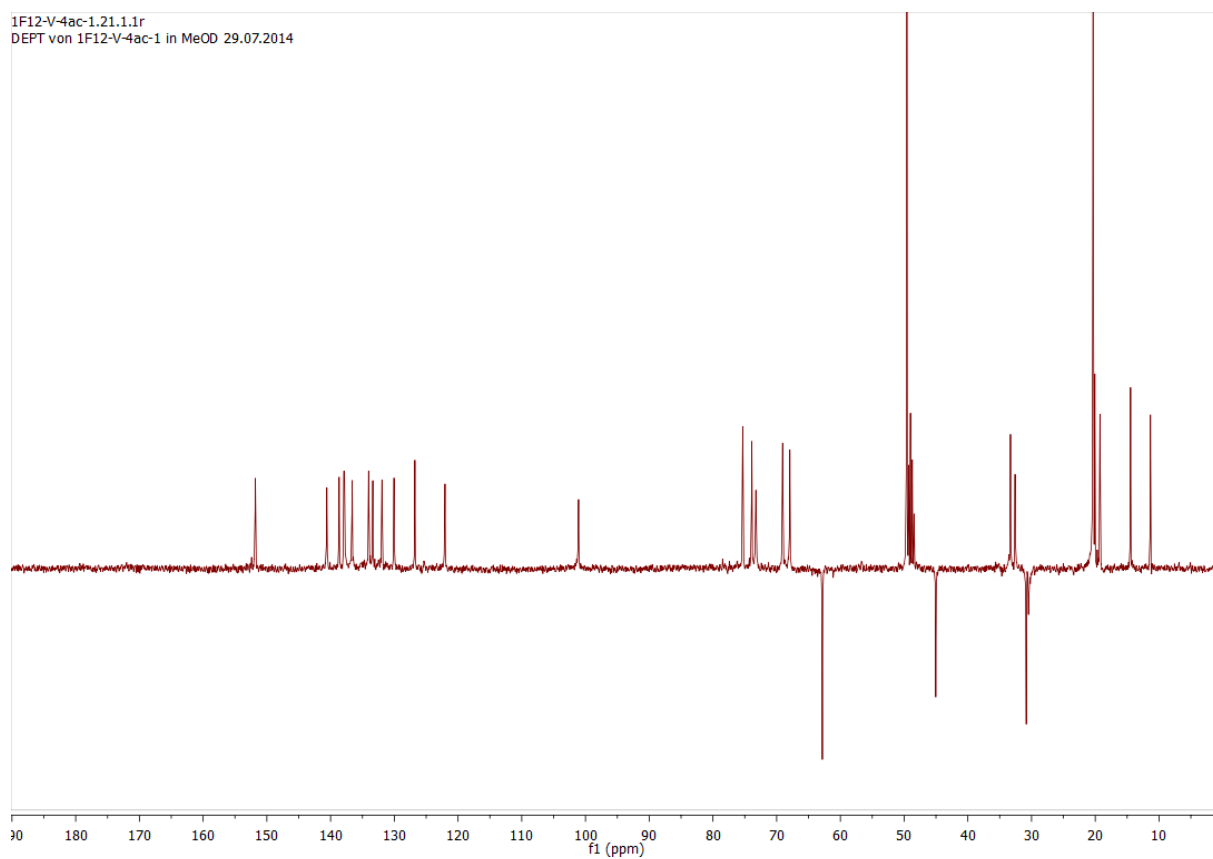
Fig. 8.14: DEPT-135 of epipyrone tetraacetate (**5**) in MeOH-d_4.
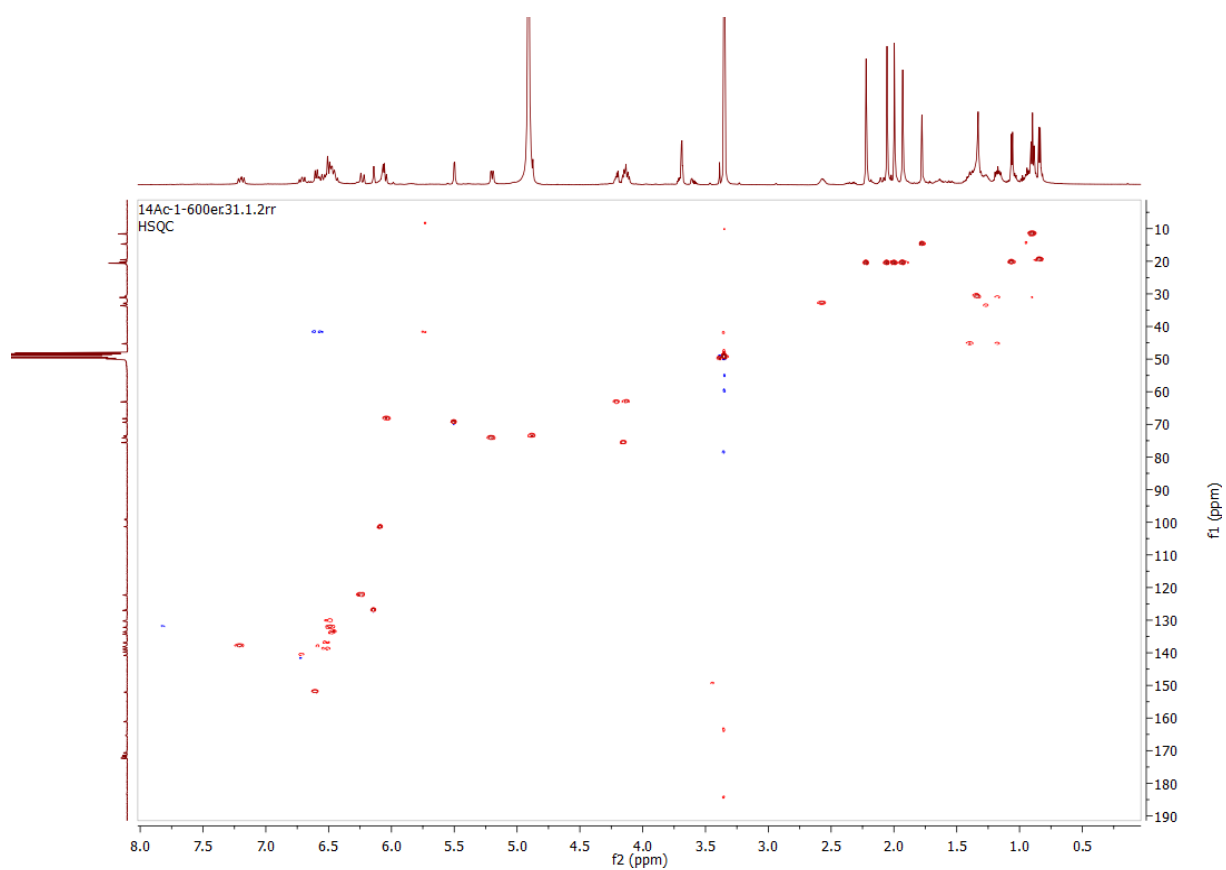
Fig. 8.15: HSQC of epipyrone tetraacetate (**5**) in MeOH-d_4, measured at 600 MHz.
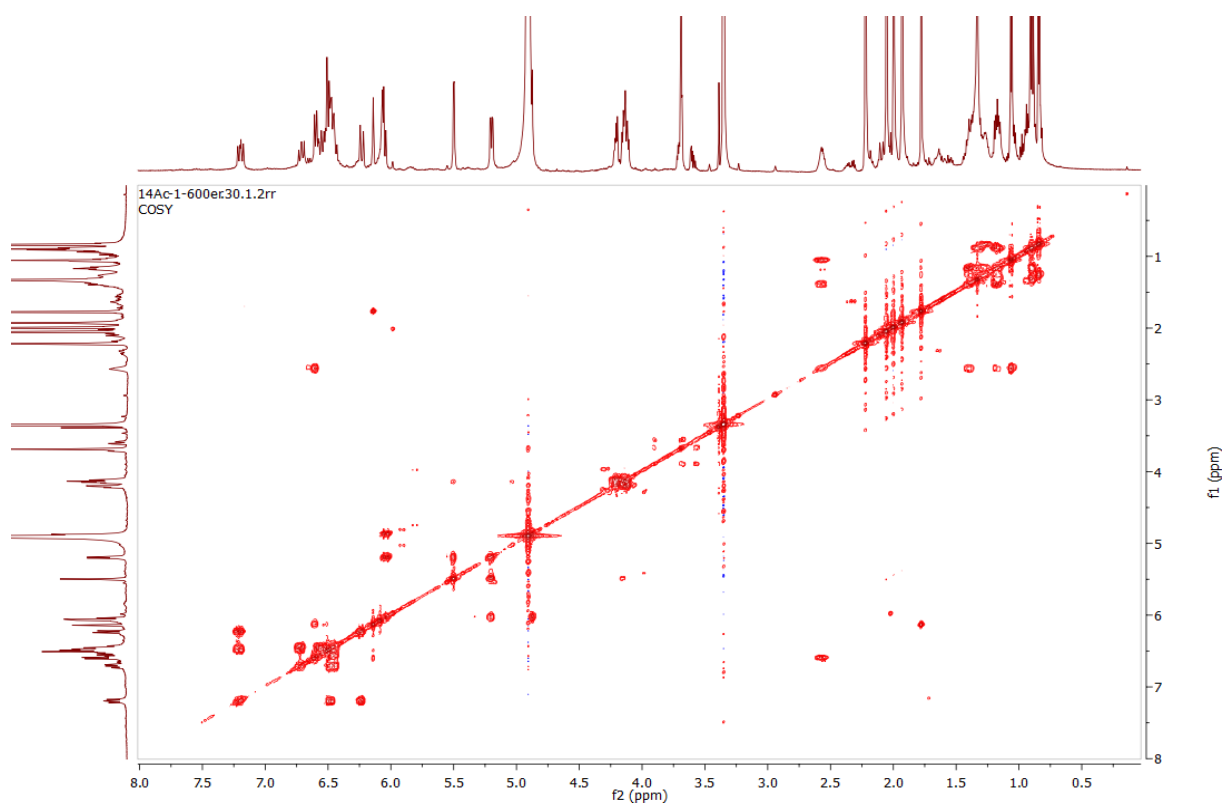
Fig. 8.16: COSY of epipyrone tetraacetate (**5**) in MeOH-d_4.
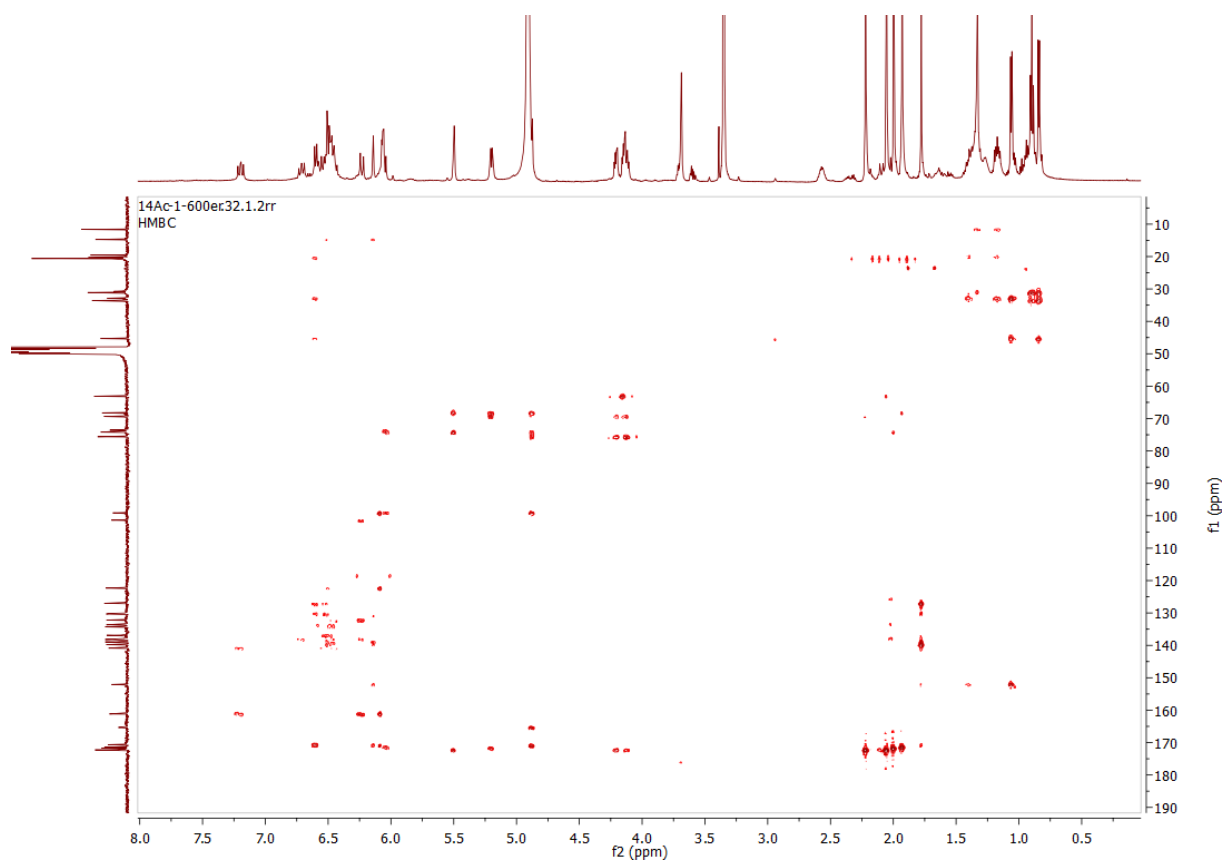
Fig. 8.17: HMBC of epipyrone tetraacetate (**5**) in MeOH-d_4, measured at 600 MHz.
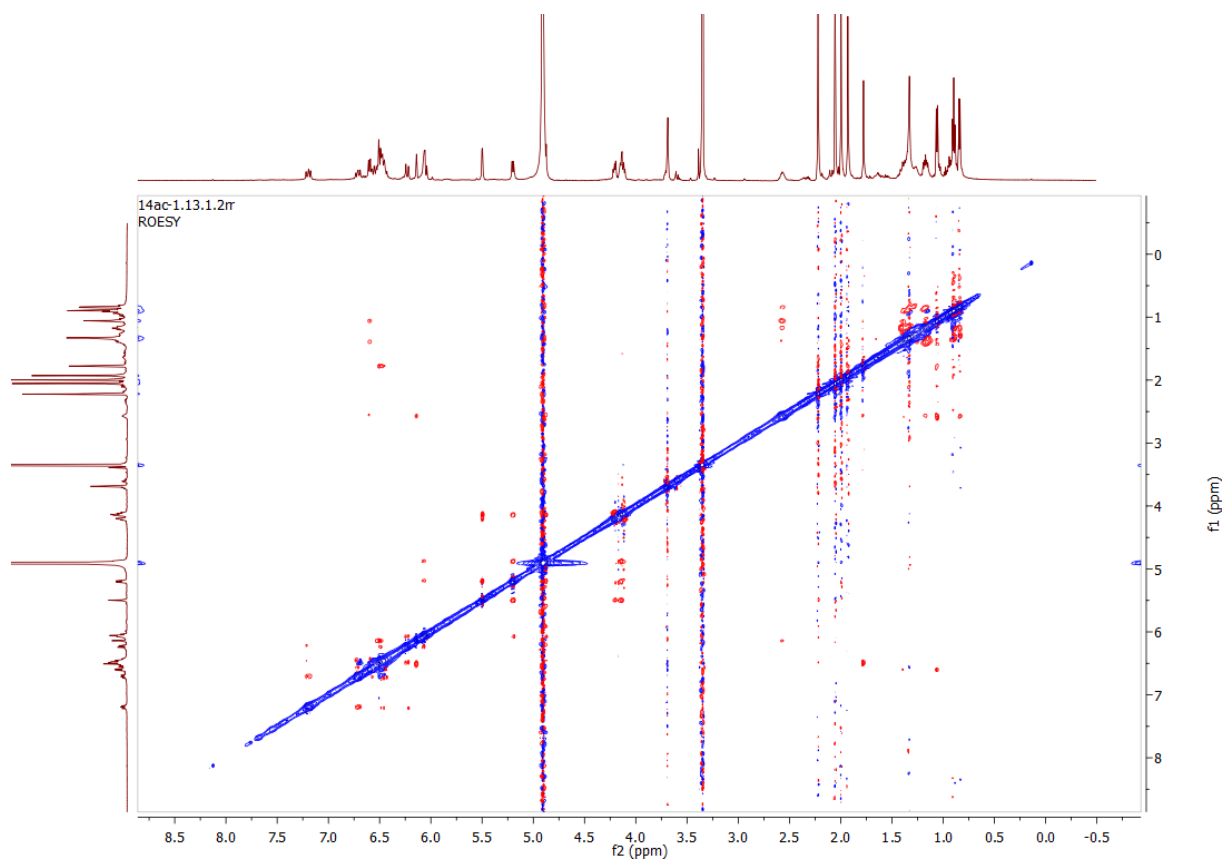
Fig. 8.18: ROESY of epipyrone tetraacetate (**5**) in MeOH-d_4, measured at 600 MHz.
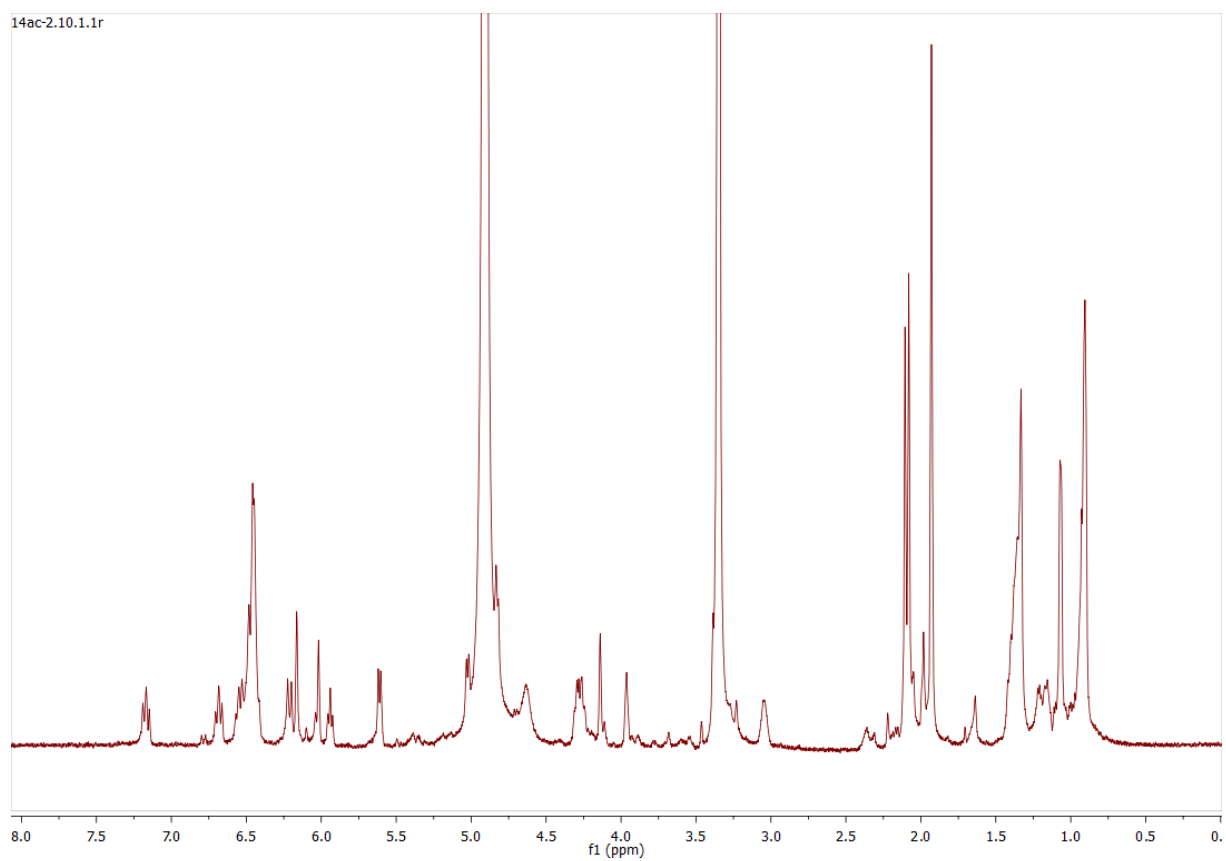
Fig. 8.19: ^{1}H-NMR of epipyrone triacetate (**6**) in MeOH-d_4, measured at 600 MHz.
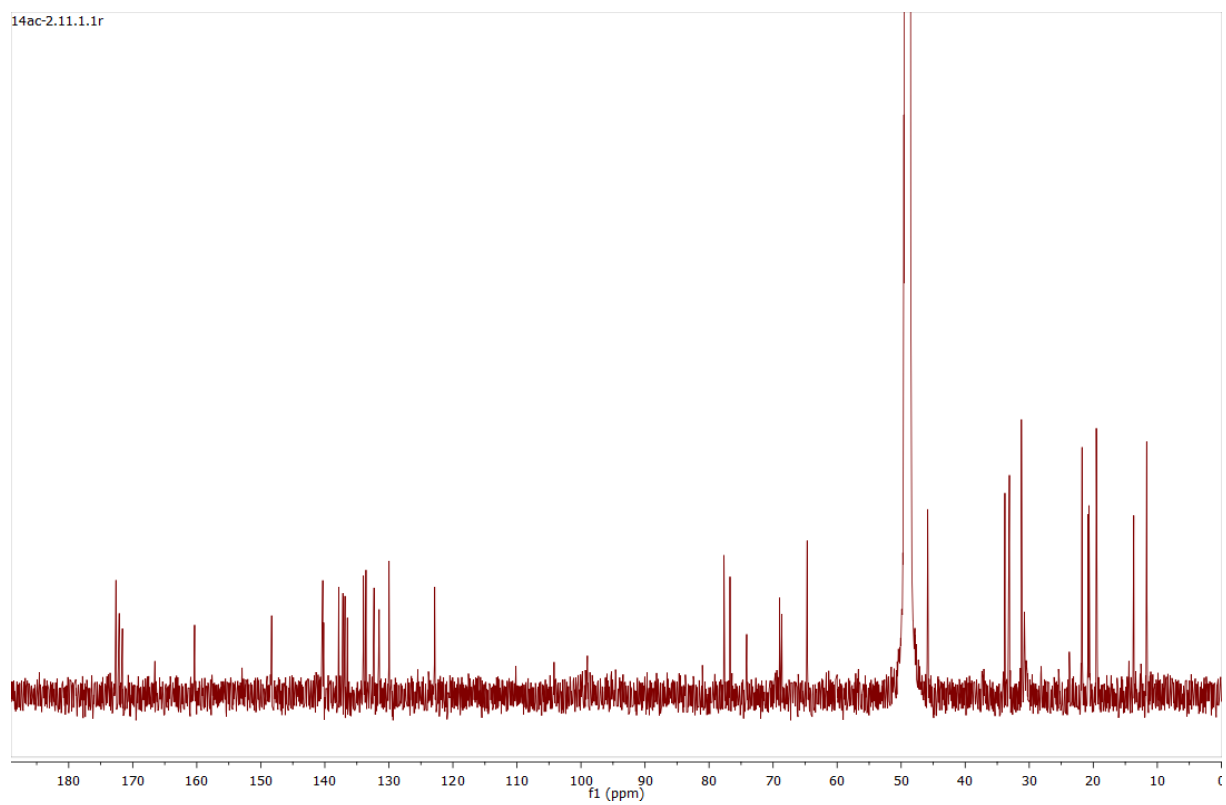
Fig. 8.20: ^{13}C-NMR of epipyrone triacetate (**6**) in MeOH-d_4, measured at 150 MHz.

14ac-2.17.1.1r
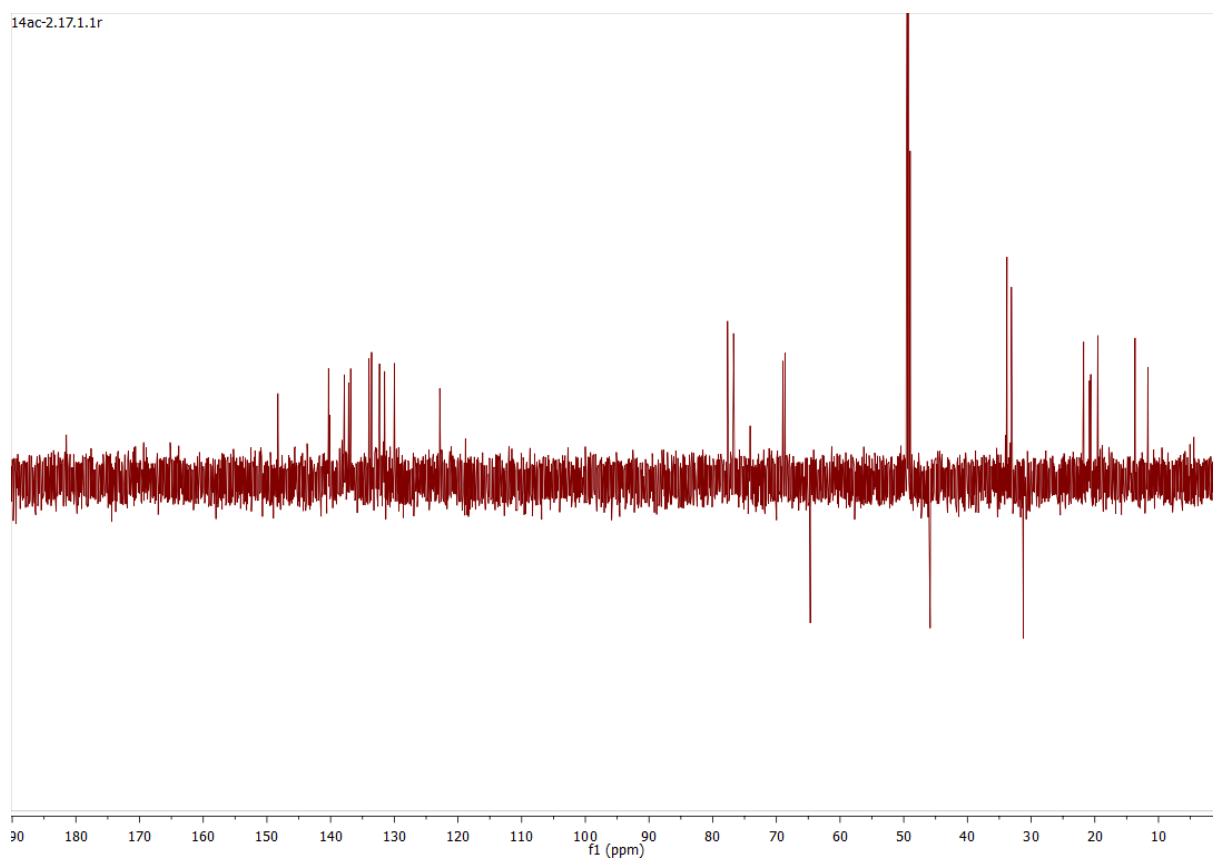
Fig. 8.21: DEPT-135 of epipyrone triacetate (**6**) in MeOH-d_4.
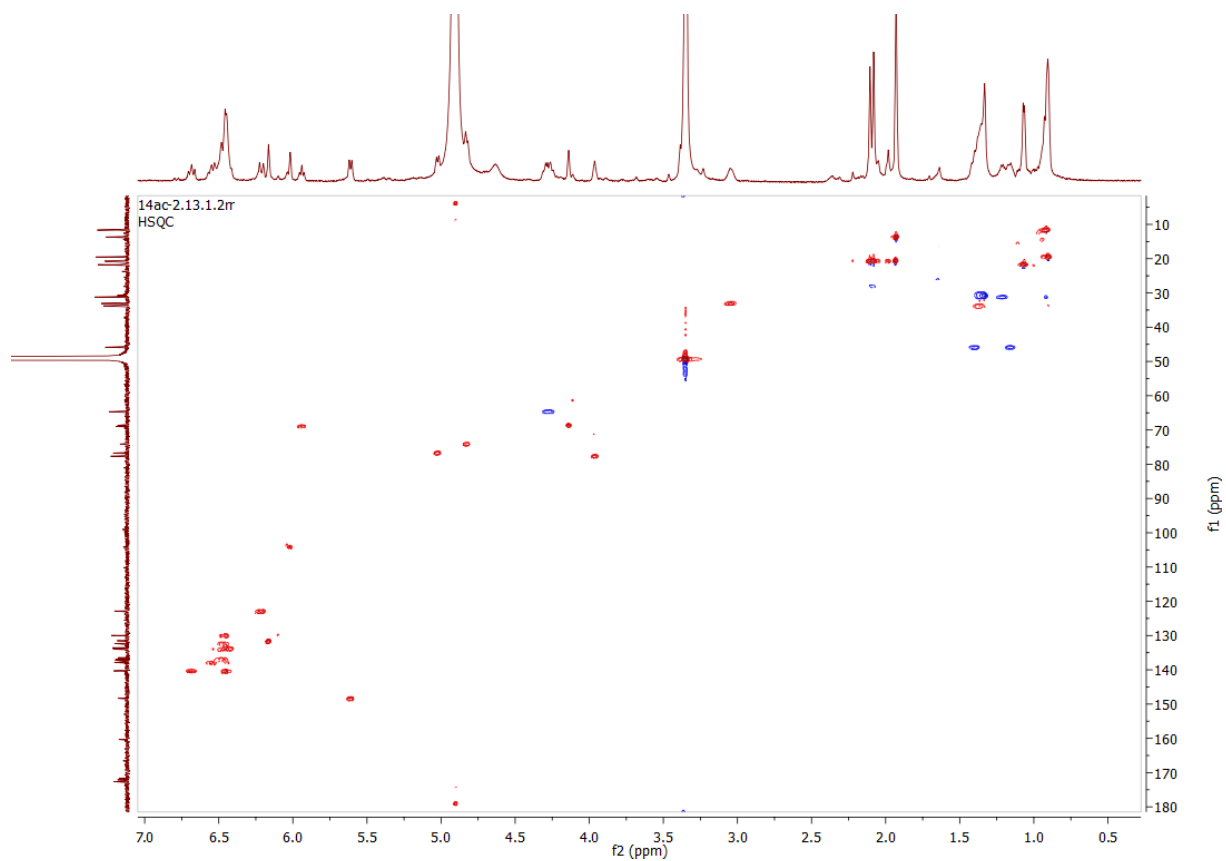
Fig. 8.22: HSQC of epipyrone triacetate (**6**) in MeOH-d_4, measured at 600 MHz.
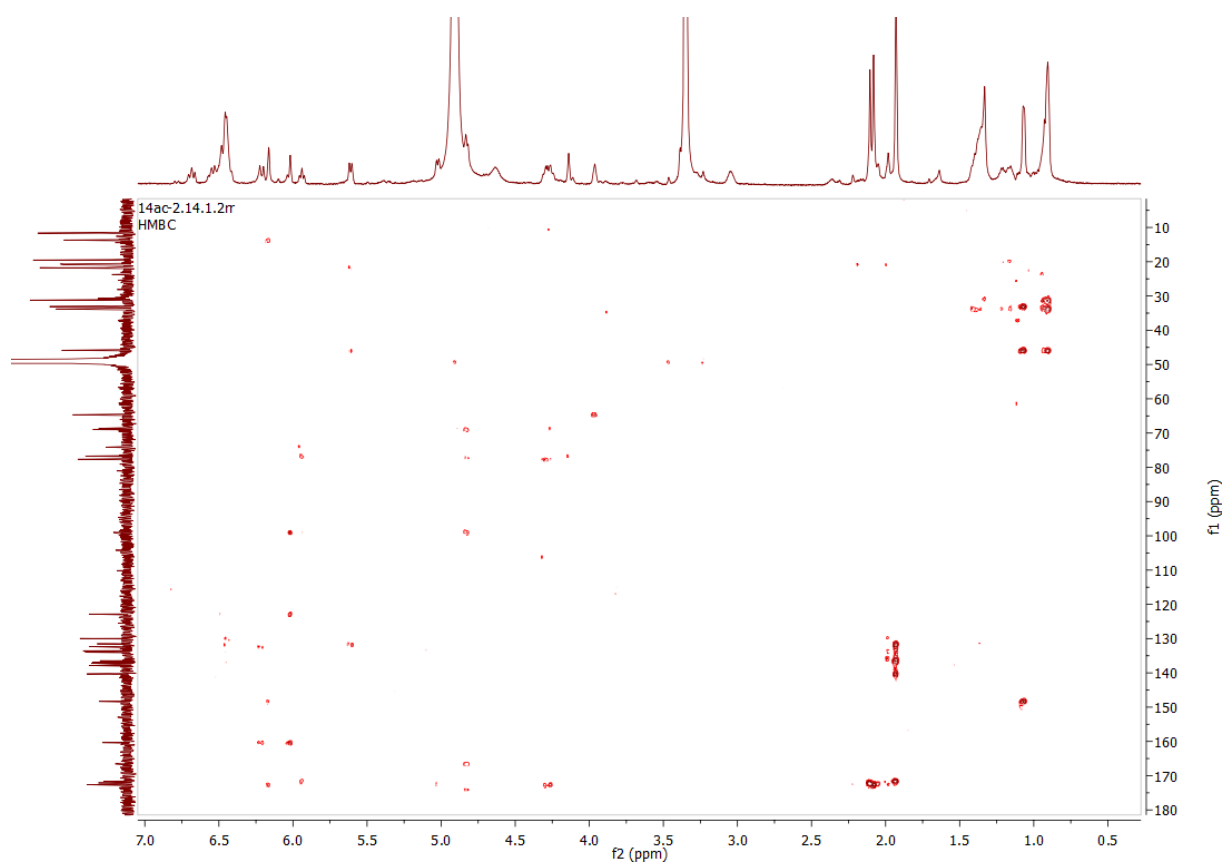
Fig. 8.23: HMBC of epipyrone triacetate (**6**) in MeOH-*d₄*, measured at 600 MHz.
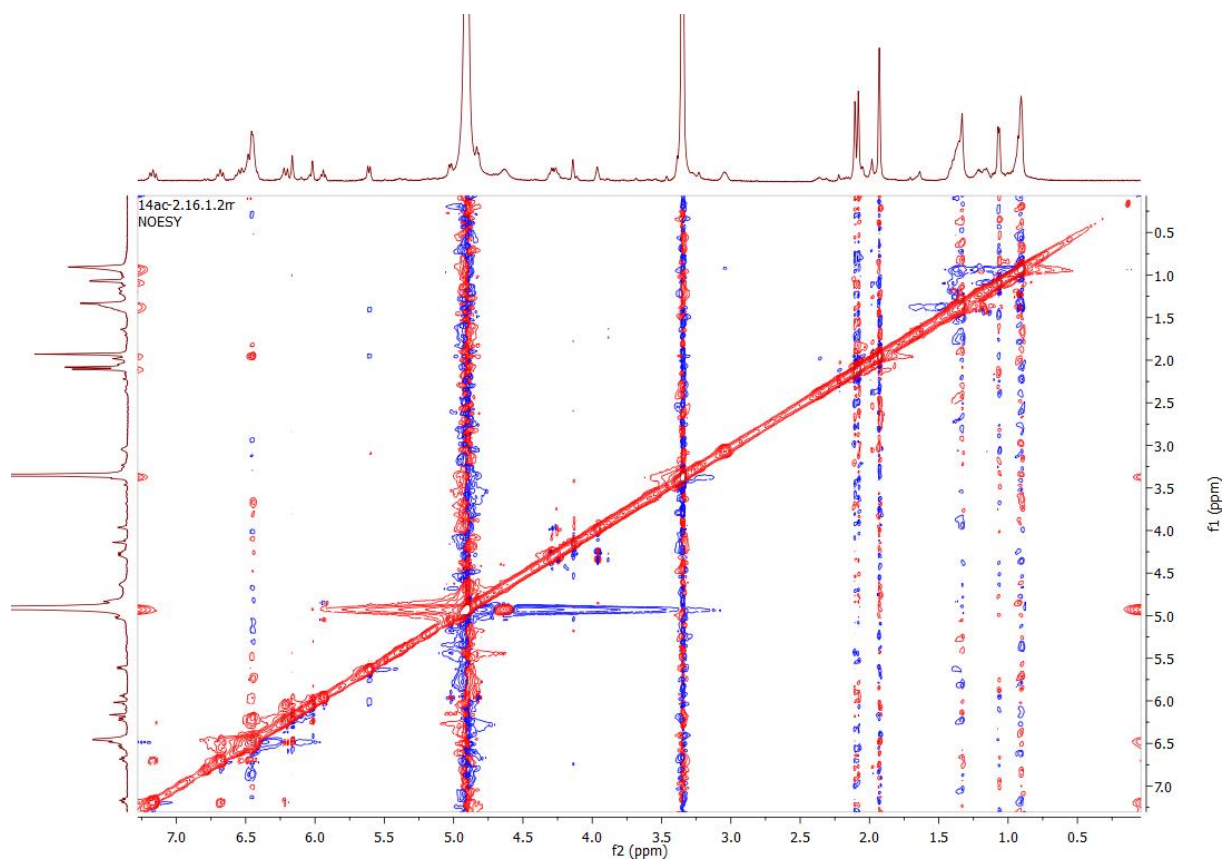
Fig. 8.24: NOESY of epipyrone triacetate (**6**) in MeOH-*d₄*, measured at 600 MHz.
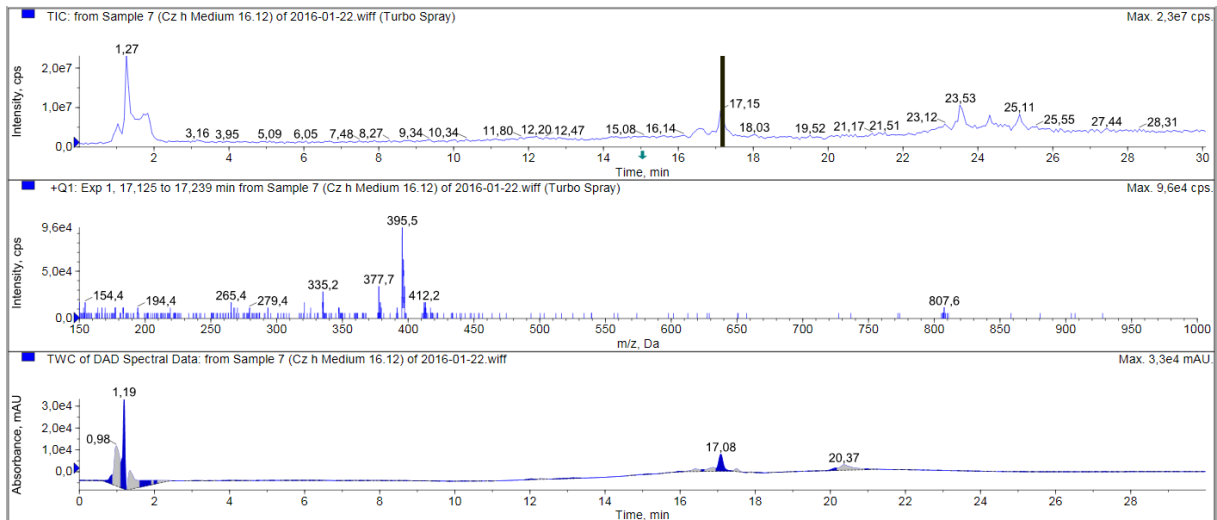
Fig. 8.25: LC-ESI-MS experiment of a crude extract made from the agar medium. The mycelium of *E. nigrum* strain 749, grown on Czapek-Dox agar with continuous illumination, was separated from the medium prior to the extraction. As can be deduced from retention time and mass (t_R = 17.15 min; *m/z* = 412; 395; 377), acetosellin (**4**) was found to be exuded into the medium.
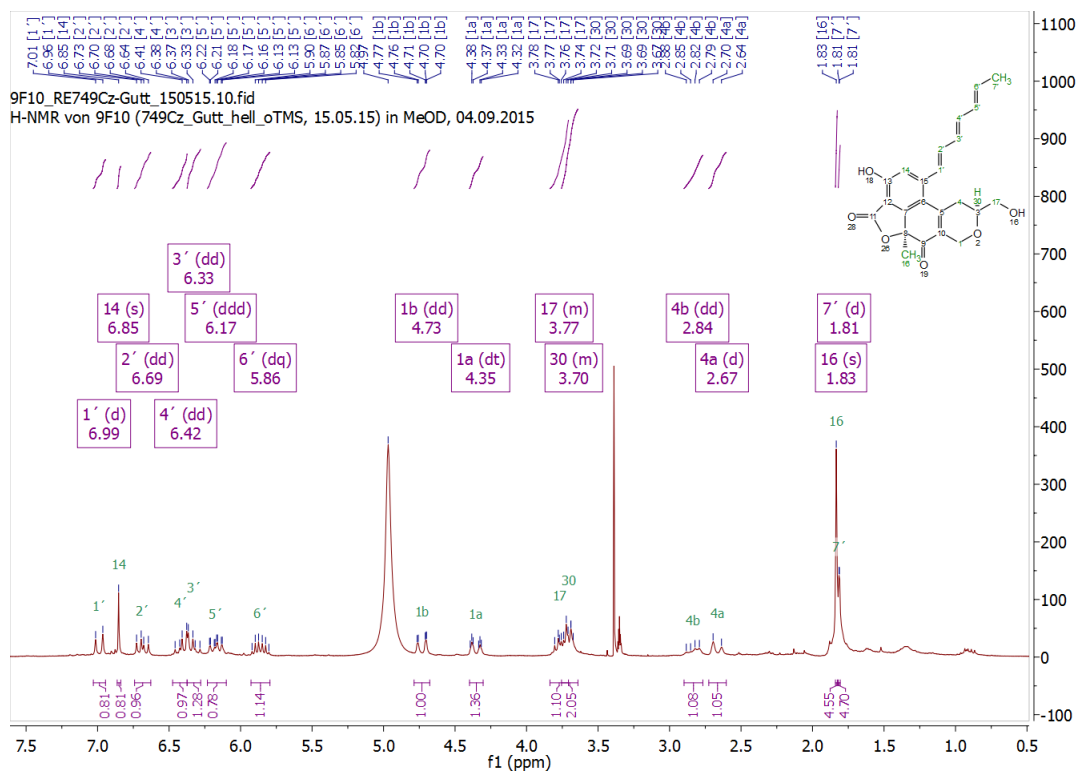
Fig. 8.26: ^{1}H-NMR of acetosellin (**4**) in MeOH-d_4, measured at 300 MHz.
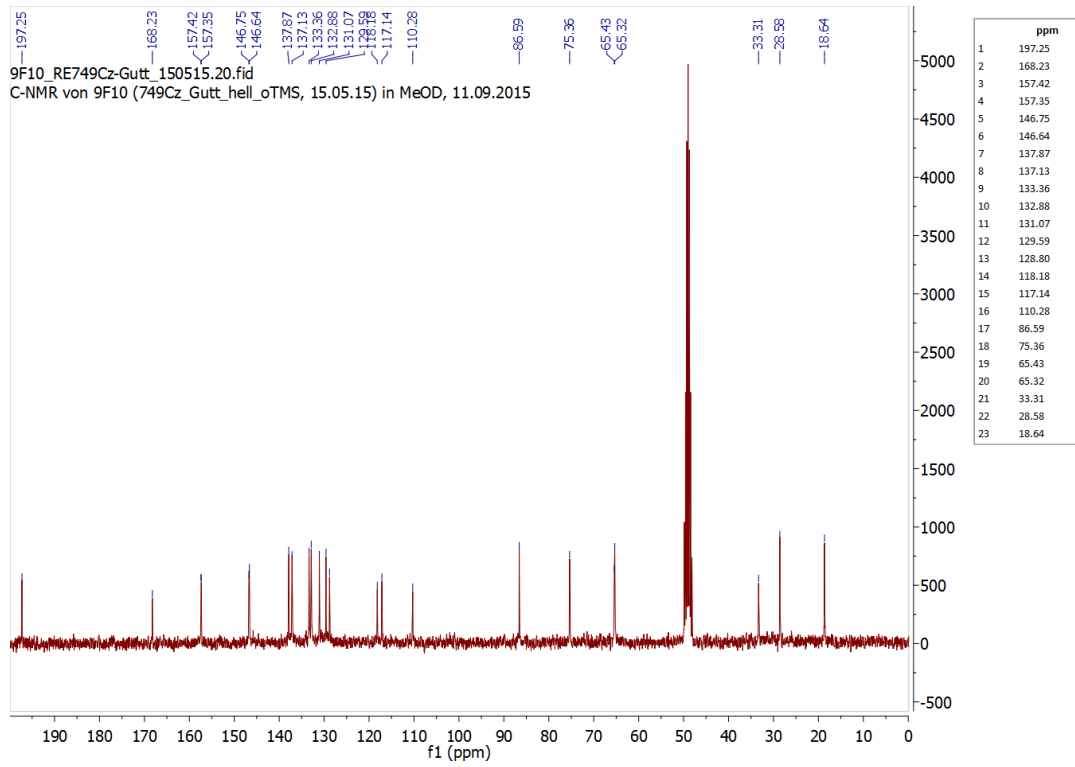
Fig. 8.27: ^{13}C-NMR of acetosellin (**4**) in MeOH-d_4, measured at 75 MHz.
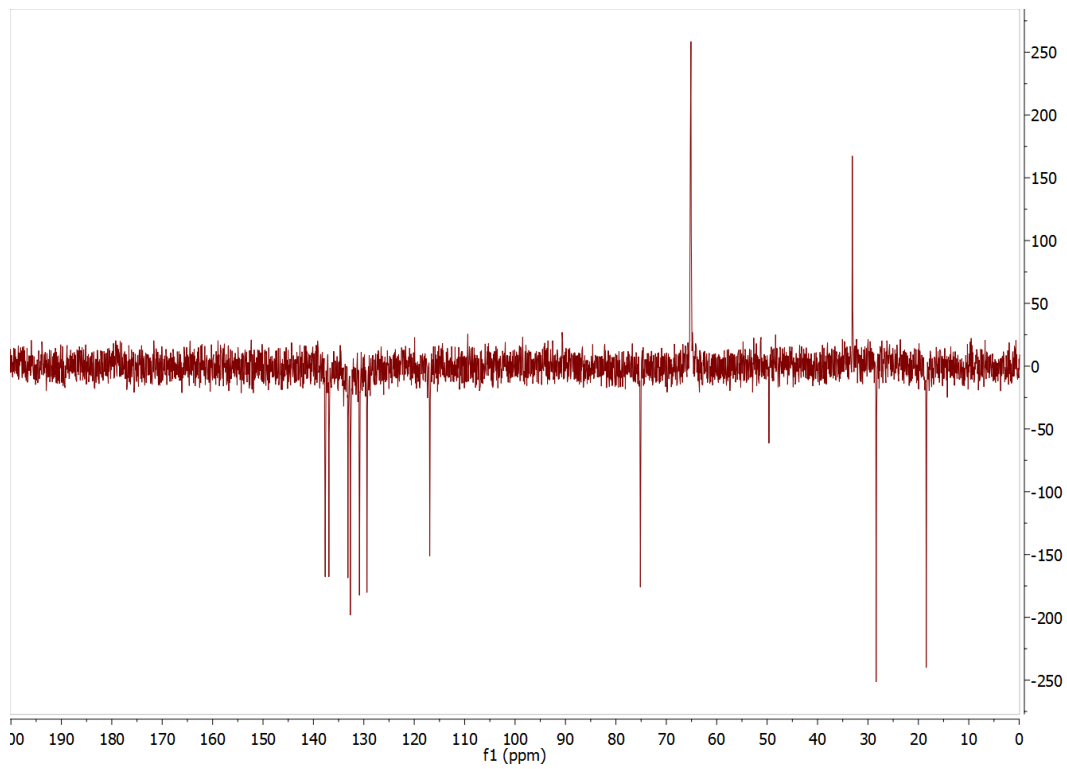
Fig. 8.28: DEPT-135 of acetosellin (**4**) in MeOH-d_4, measured at 75 MHz.
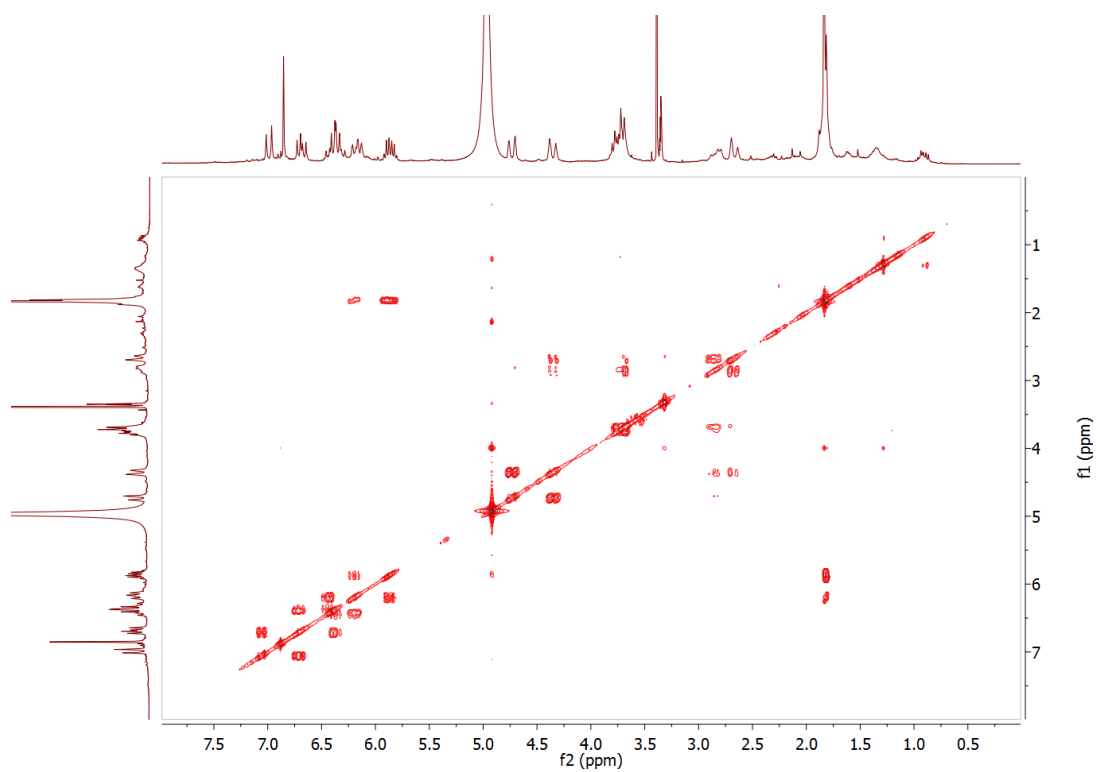
Fig. 8.29: COSY of acetosellin (**4**) in MeOH-d_4.
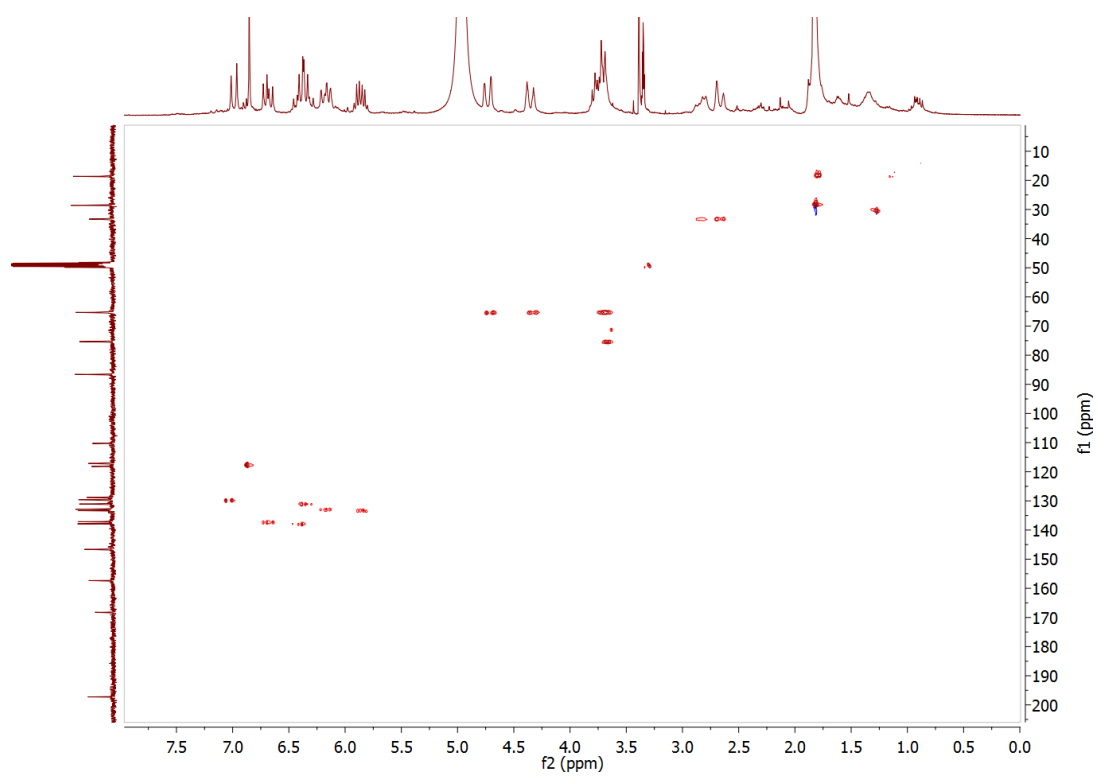
Fig. 8.30: HSQC of acetosellin (**4**) in MeOH-d_4.
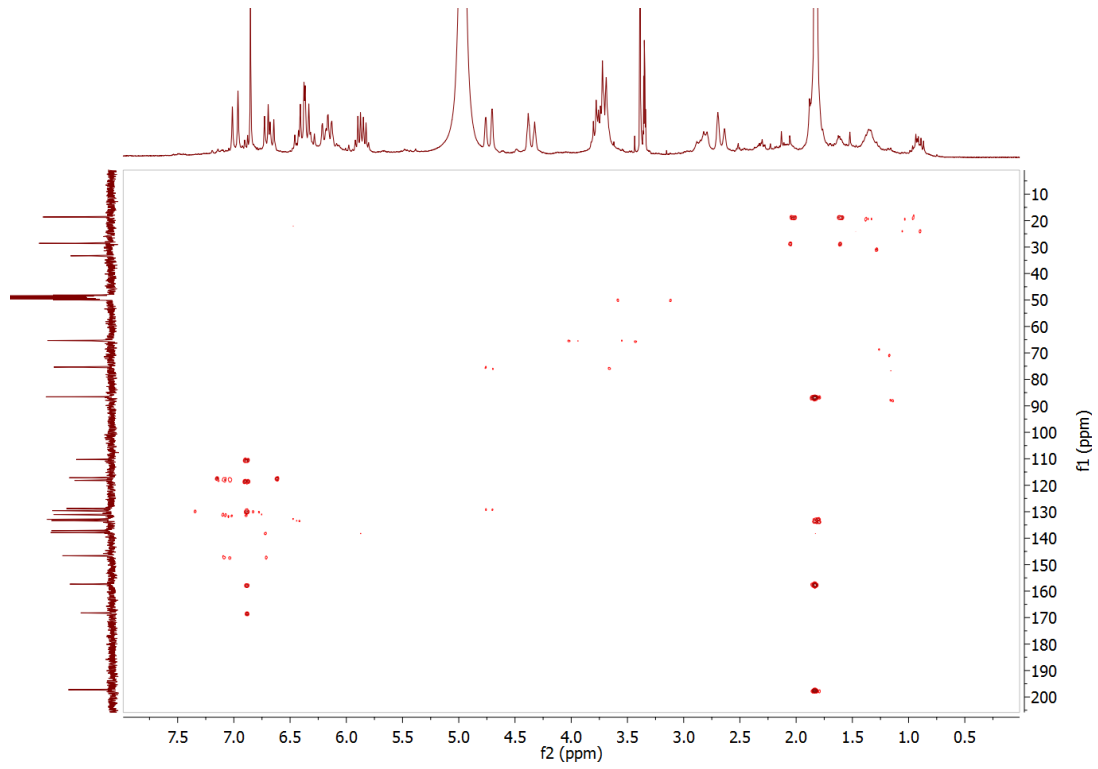
Fig. 8.31: HMBC of acetosellin (**4**) in MeOH-*d₄*.
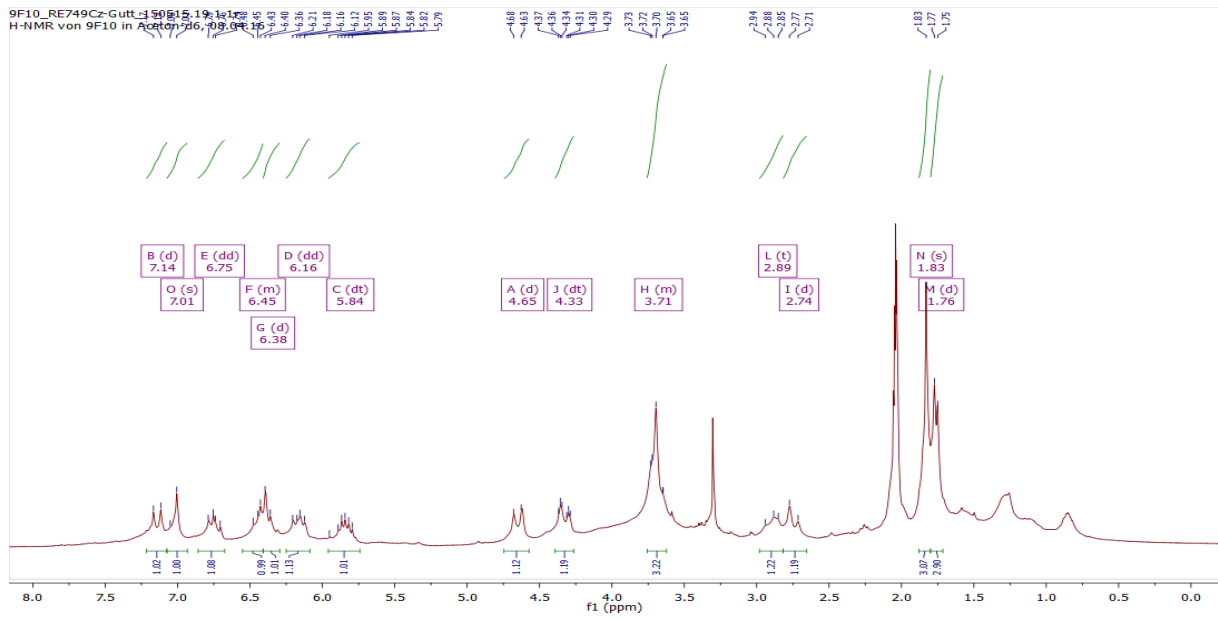
Fig. 8.32: ¹H-NMR of acetosellin (**4**) in acetone-*d₆*, measured at 300 MHz.

9F10_RE749Cz-Gutt_150515.29.fid
H-NMR von 9F10 (749Cz_Gutt_hell_oTMS, 15.05.15) in MeOD, 04.09.2015
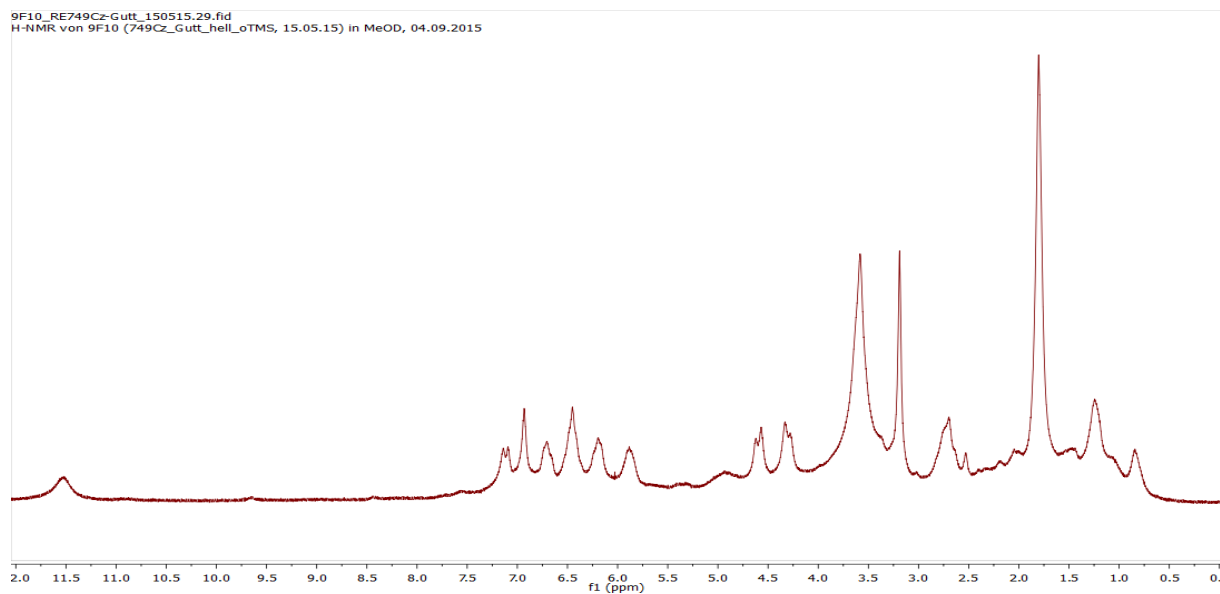
Fig. 8.33: ^{1}H-NMR of acetosellin (**4**) in DMSO-d_6, measured at 300 MHz.
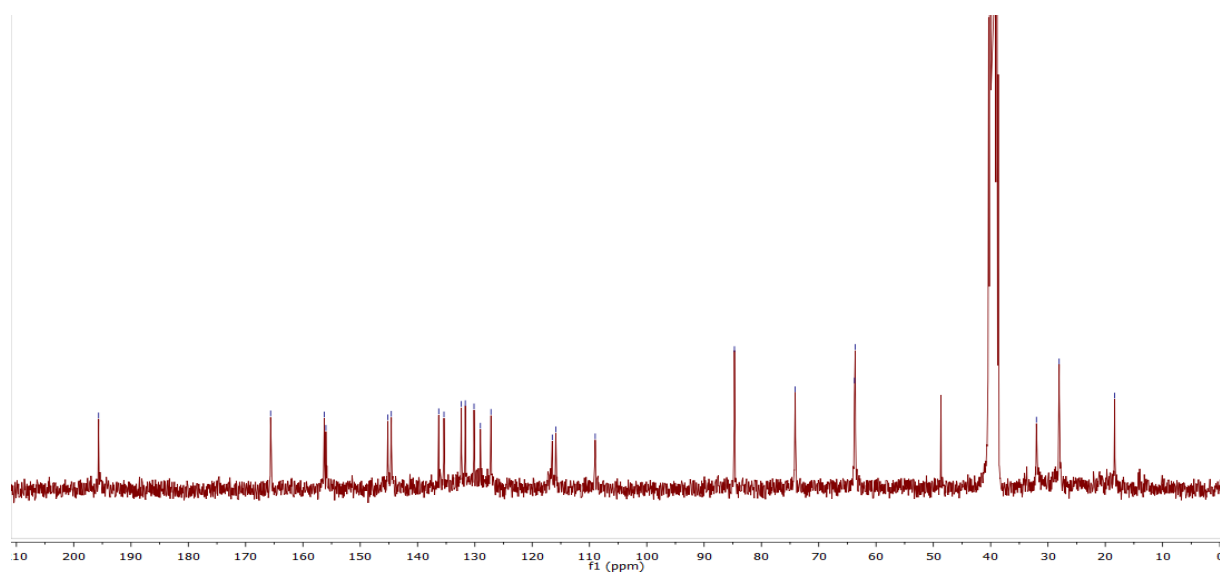
Fig. 8.34: ^{13}C-NMR of acetosellin (**4**) in DMSO-d_6, measured at 75 MHz.
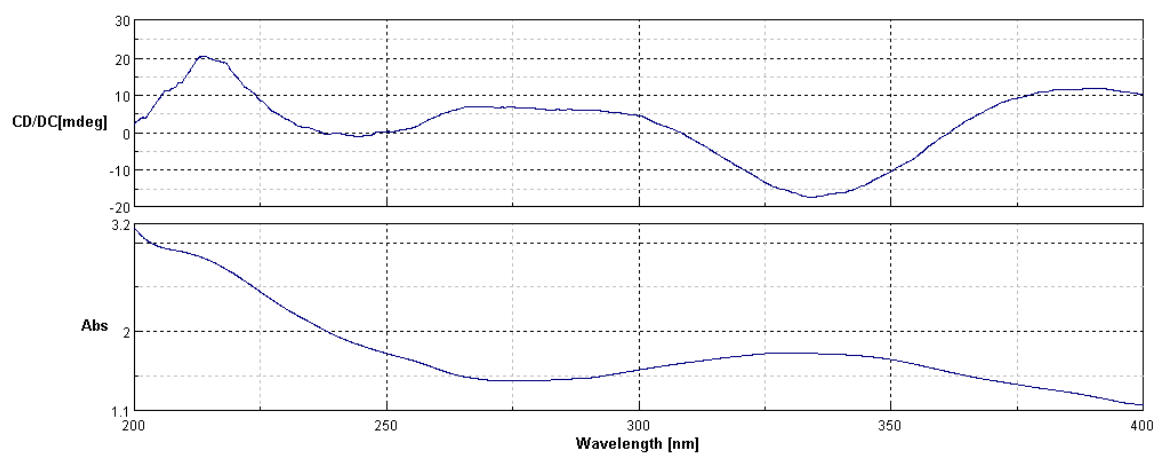
Fig. 8.35: CD spectrum of acetosellin in MeOH.
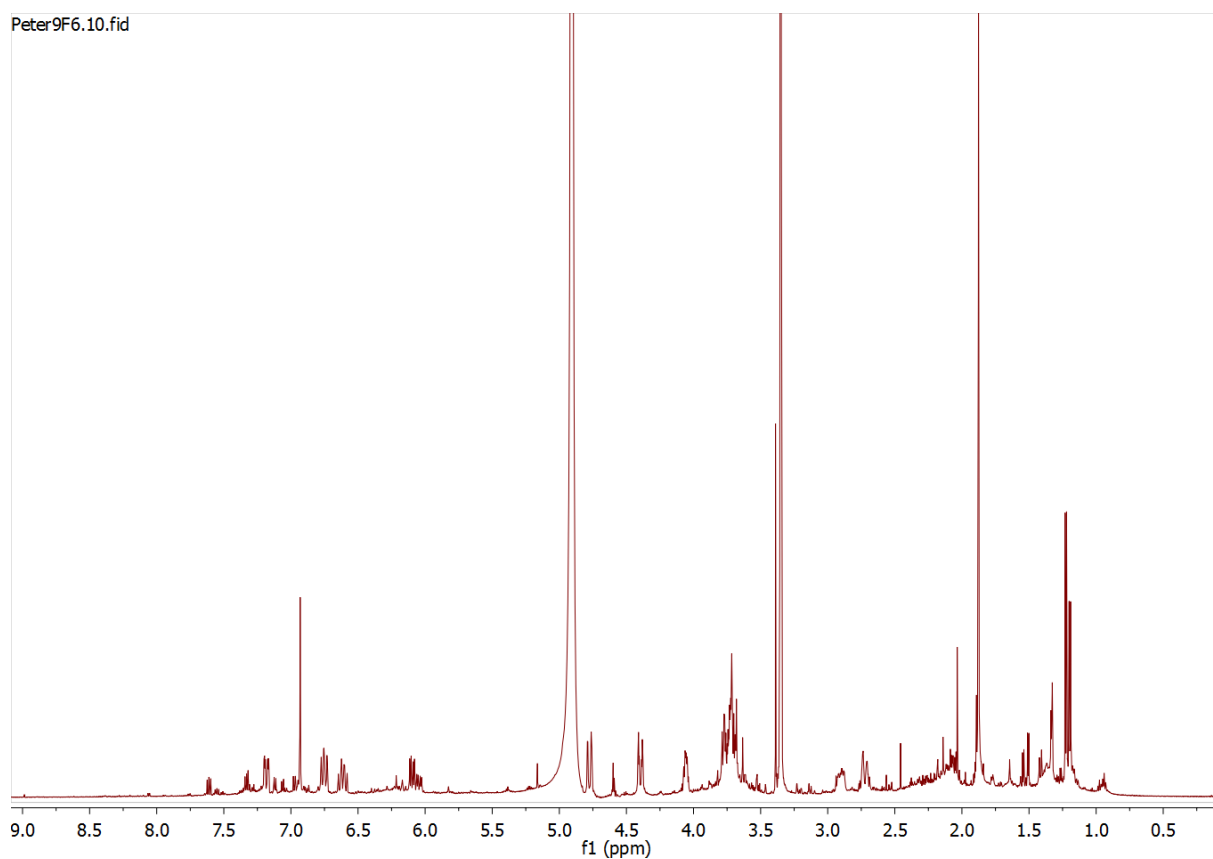
Fig. 8.36: ^{1}H-NMR of 5´,6´-dihydroxyacetosellin (**7**) in MeOH-d_4 at 600 MHz.
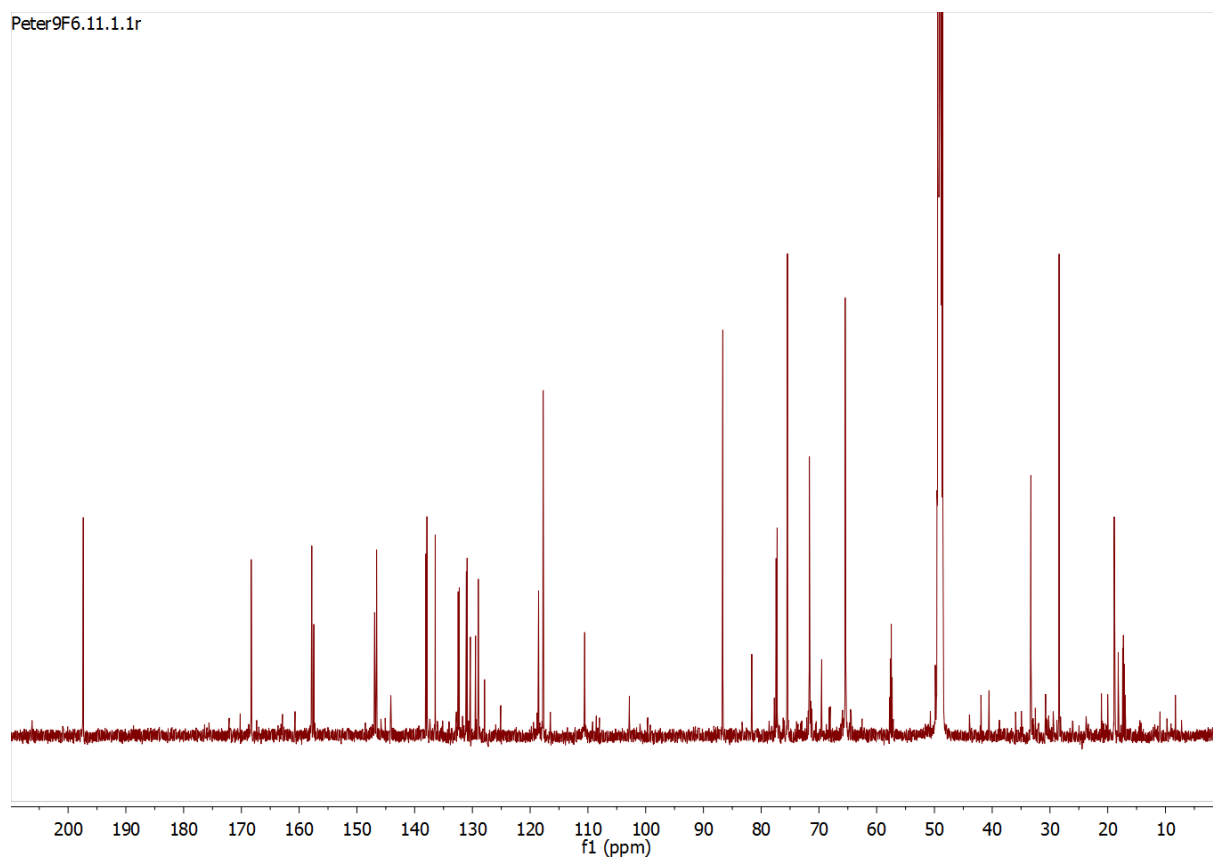
Fig. 8.37: ^{13}C-NMR of 5´,6´-dihydroxyacetosellin (**7**) in MeOH-d_4 at 125 MHz.
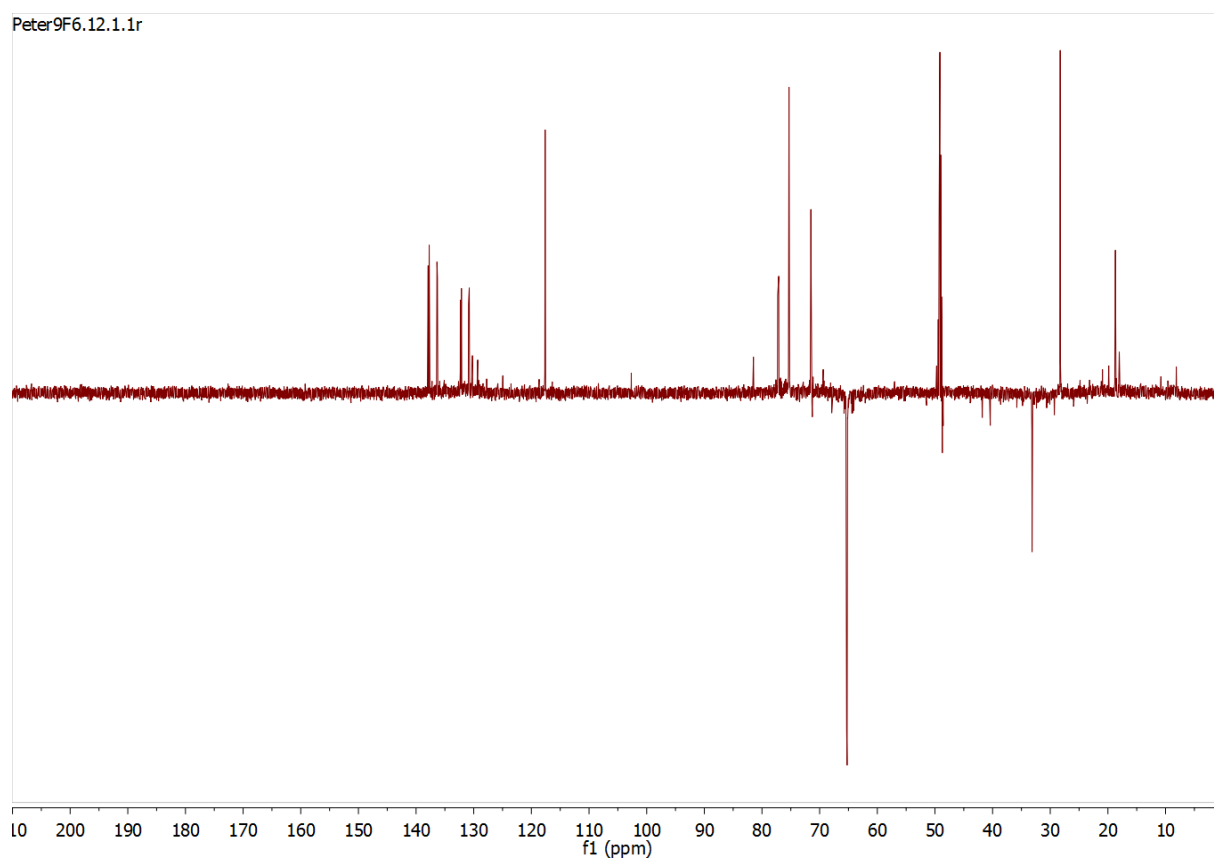
Fig. 8.38: DEPT-135 of 5´,6´-dihydroxyacetosellin (**7**) in MeOH-d_4 at 600 MHz.
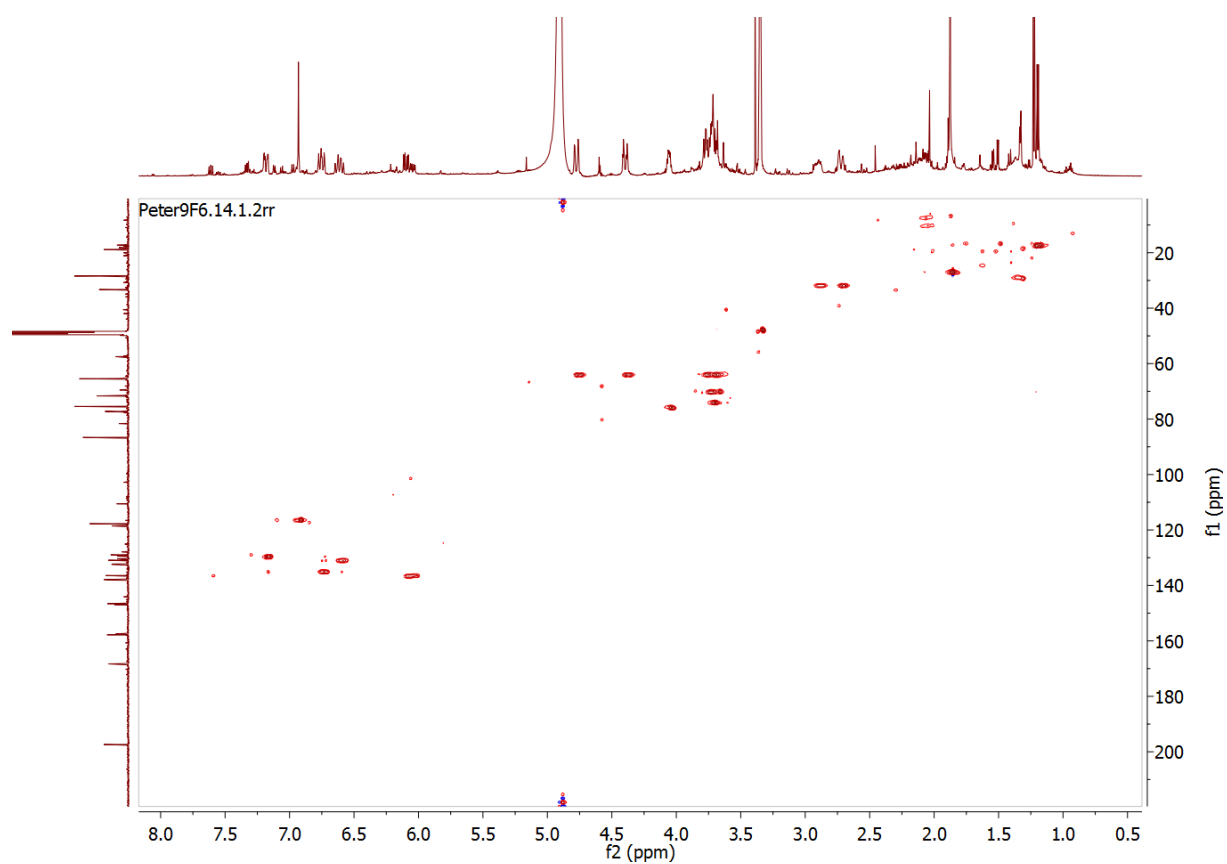
Fig. 8.39: HSQC of 5´,6´-dihydroxyacetosellin (**7**) in MeOH-d_4 at 600 MHz.
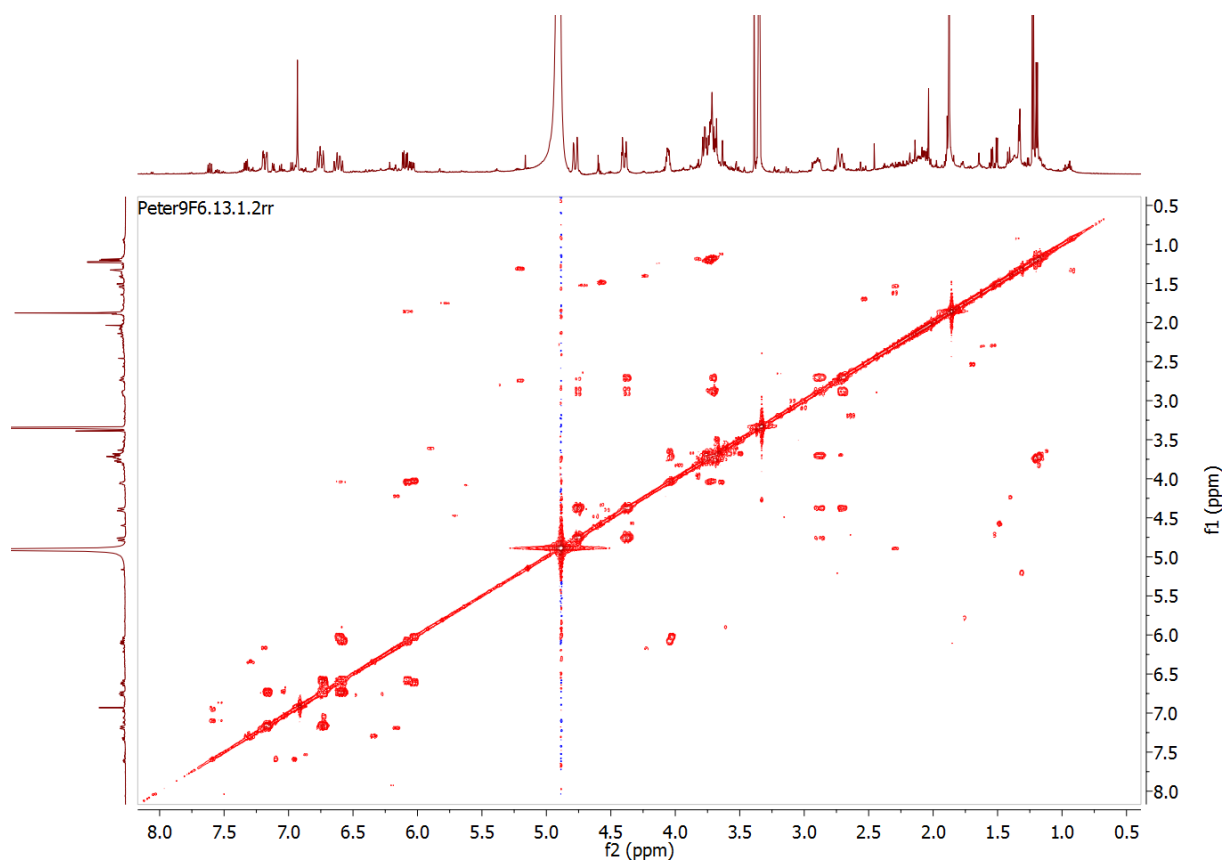
Fig. 8.40: COSY of 5´,6´-dihydroxyacetosellin (**7**) in MeOH-d_4 at 600 MHz.
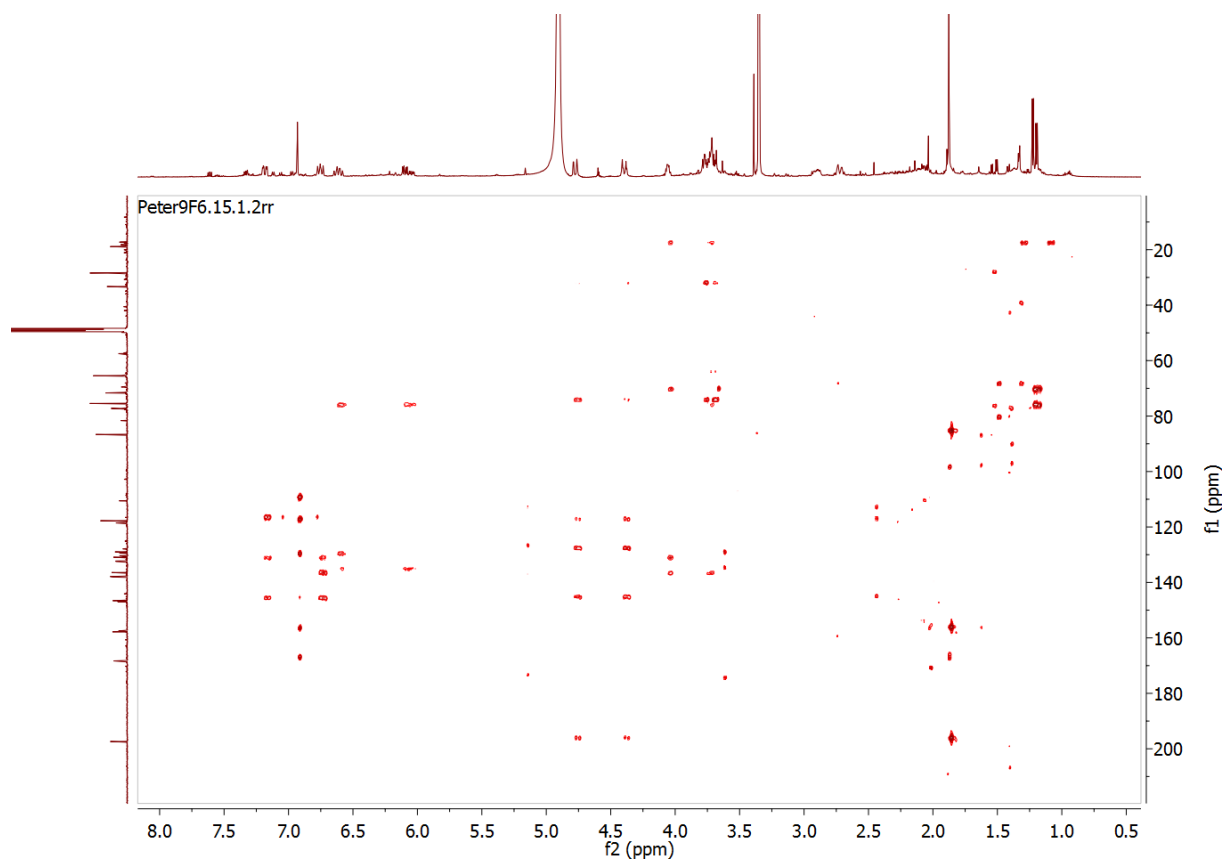
Fig. 8.41: HMBC of 5´,6´-dihydroxyacetosellin (**7**) in MeOH-d_4 at 600 MHz.
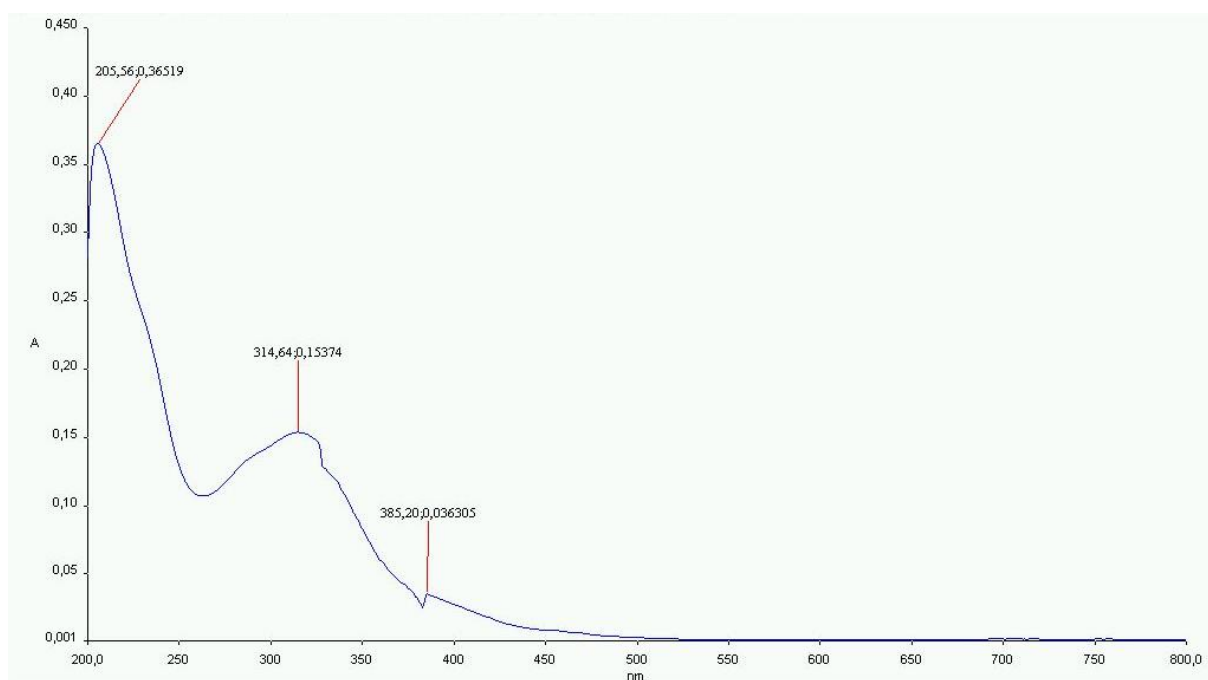
Fig. 8.42: UV-spectrum of 5´,6´-dihydroxyacetosellin (**7**) in MeOH.
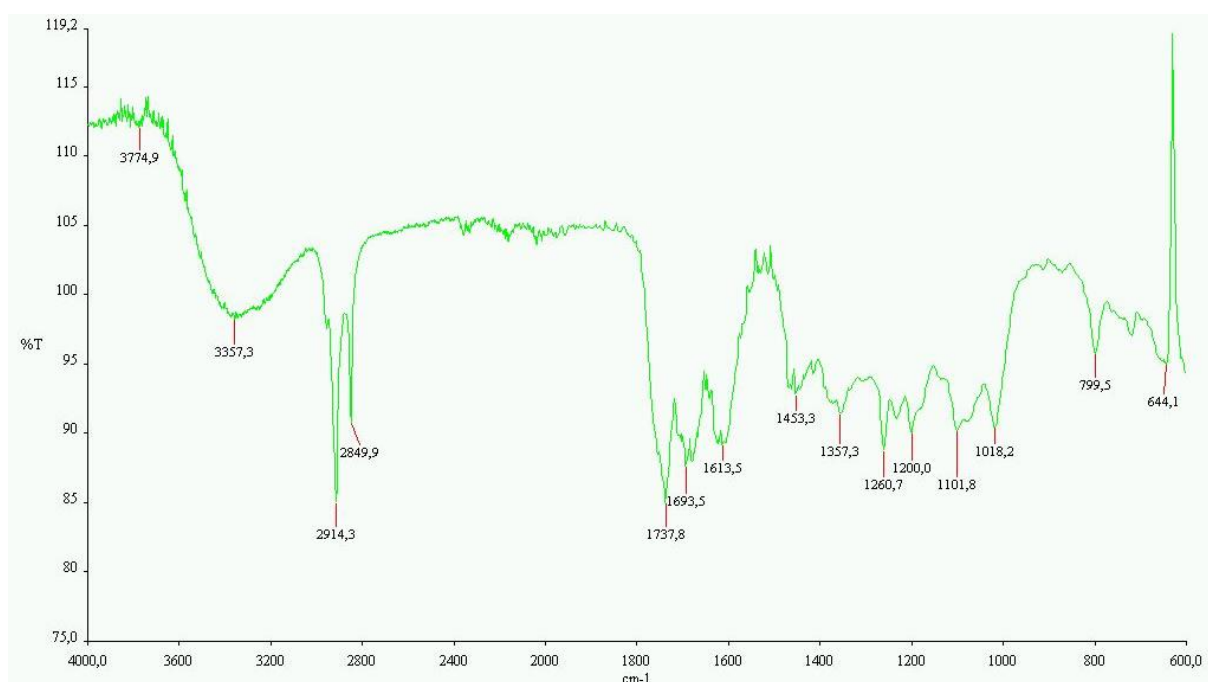
Fig. 8.43: IR-spectrum of 5´,6´-dihydroxyacetosellin (**7**) in MeOH.
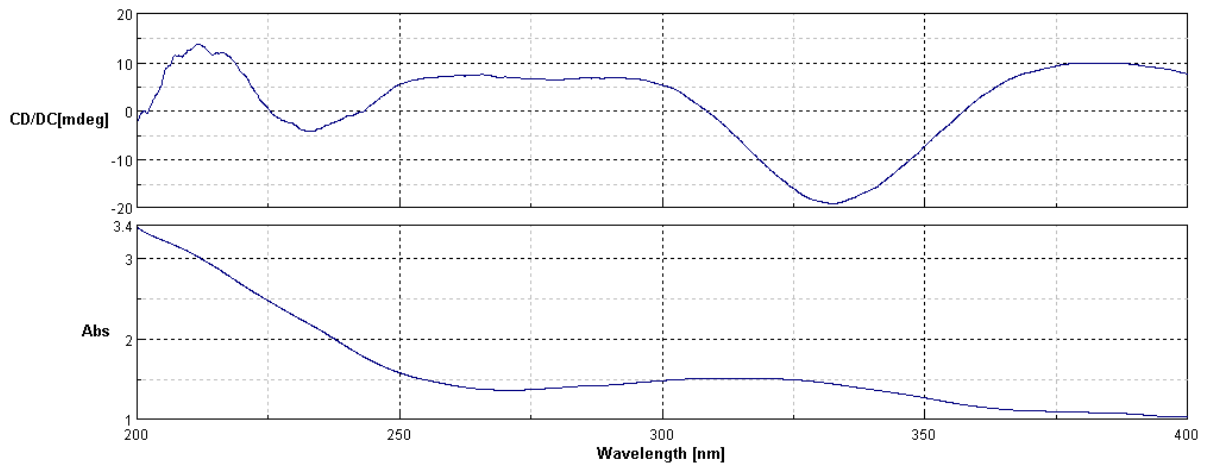
Fig. 8.44: CD spectrum of 5´,6´-dihydroxyacetosellin in MeOH.
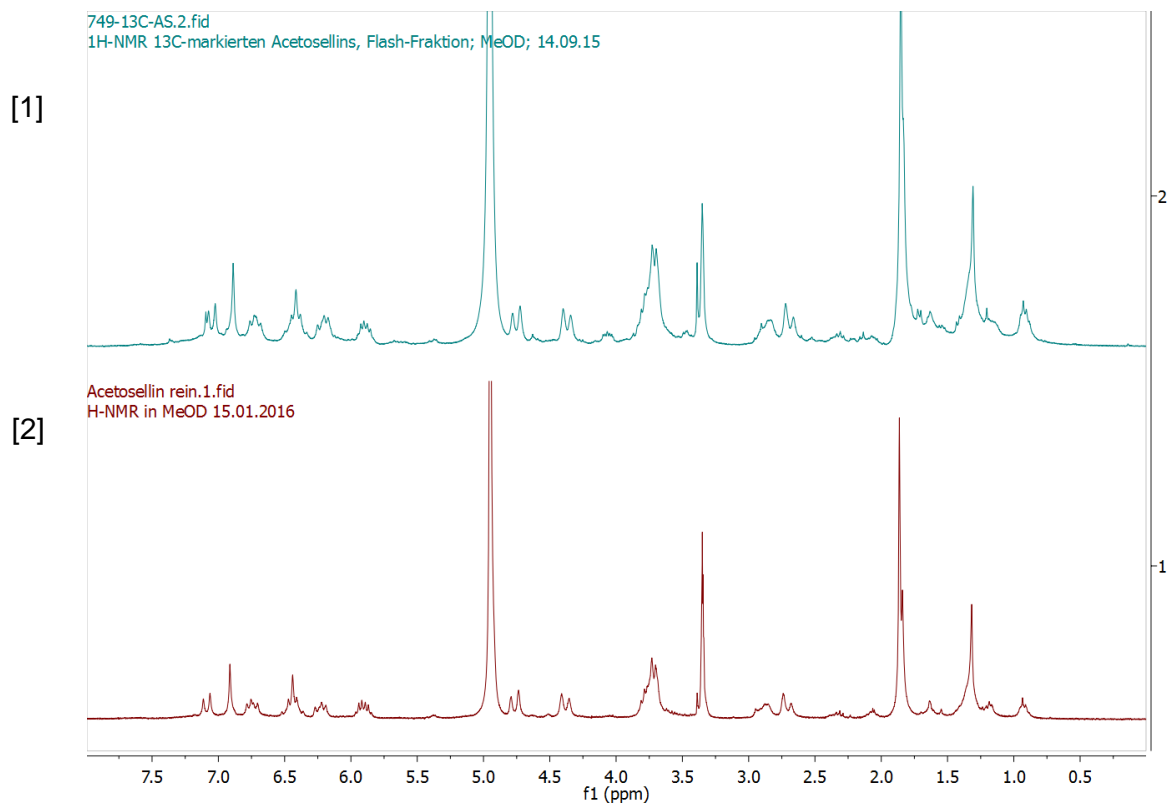
Fig. 8.45: Comparison of ^{1}H-NMR spectra from ^{13}C-labeled acetosellin ([1]) and unlabeled ([2]) acetosellin (**4**) in MeOH-d_4.
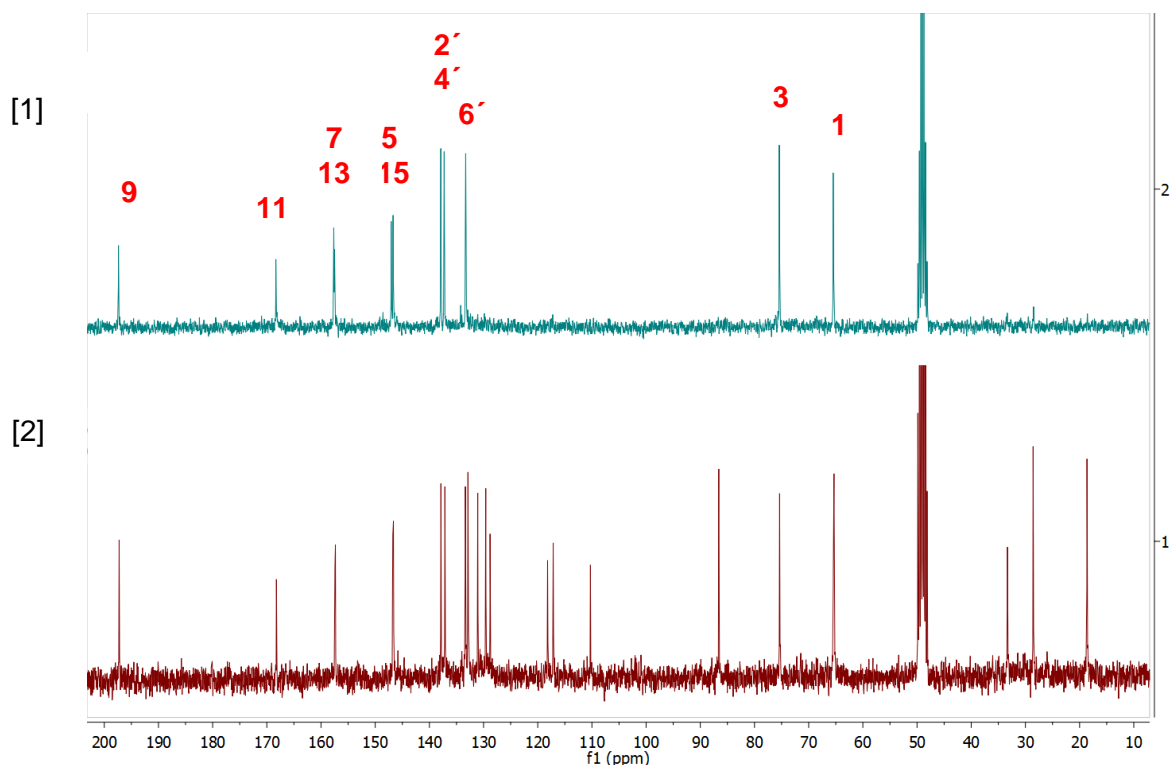
Fig. 8.46: Comparison of ^{13}C-NMR spectra from ^{13}C-labeled acetosellin ([1]) and unlabeled ([2]) acetosellin (**4**) in MeOH-d_4. Signals are marked following the numbering in **fig. 4.16**.
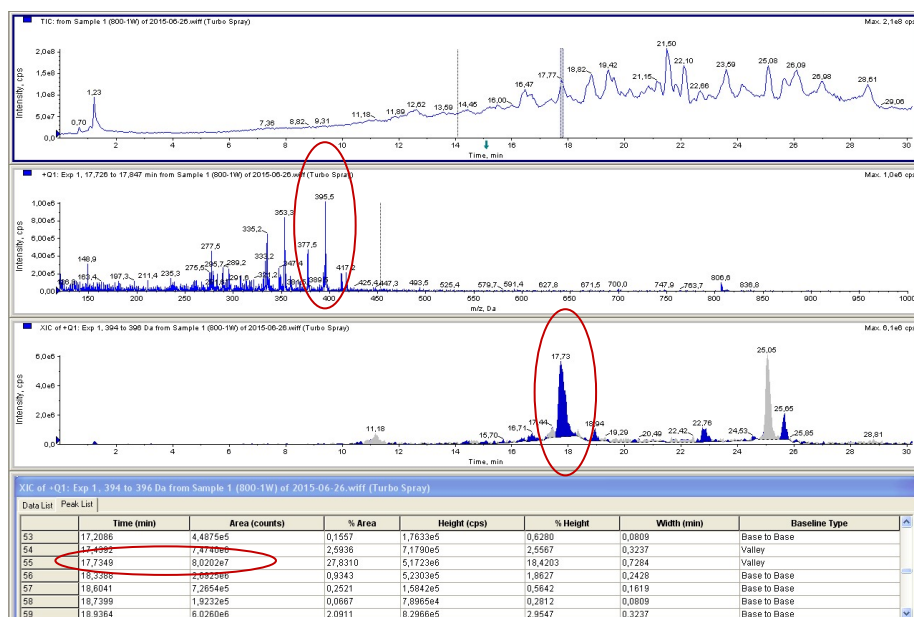
Fig. 8.47: LC-ESI-MS data sheet for a crude extract of *E. nigrum* strain 800 cultivated on MEN medium (malt extract agar supplemented with NaOAc and artificial sea water) under continuous illumination. Extraction was carried out after **one** week of cultivation using EtOAc.
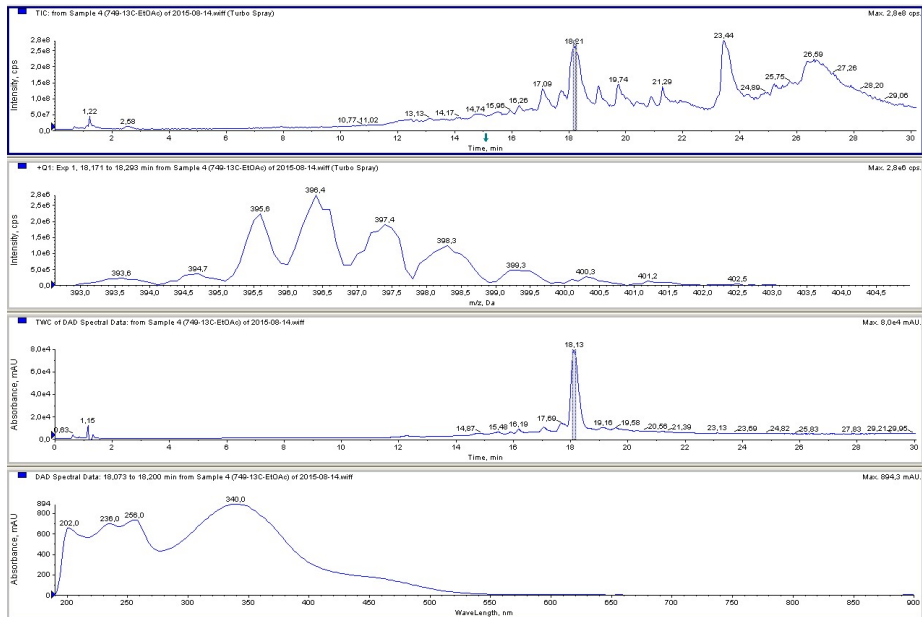
Fig. 8.48: LC-ESI-MS data sheet for the crude extract of the [^{13}C]-labeled culture of *E. nigrum* strain 749 showing the total ion chromatogram (TIC), the isotopic pattern of [^{13}C]-enriched acetosellin (**4**), the total wavelength chromatogram (TWC) and the DAD spectral data for acetosellin (**4**) (from top to bottom).
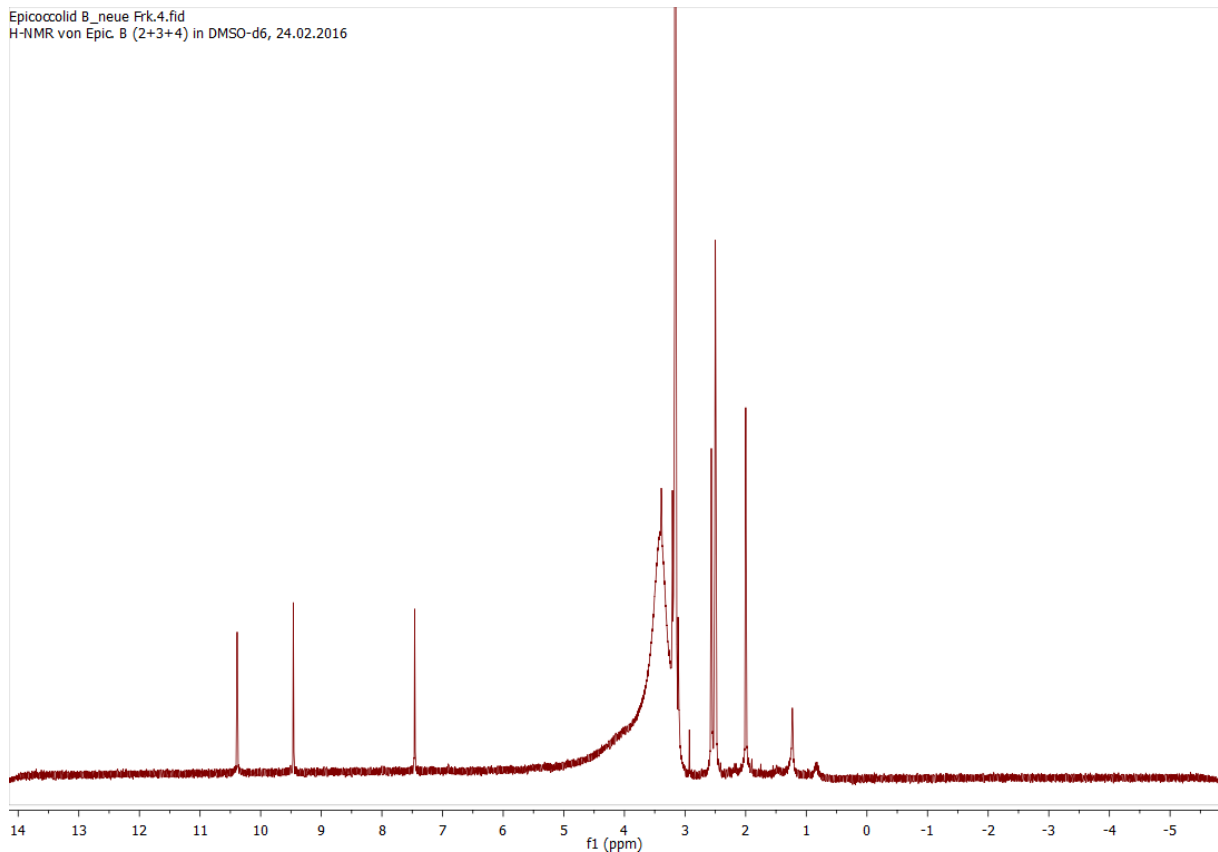
Fig. 8.49: ^{1}H-NMR of epicoccolide B (**9**) in DMSO-d_6.
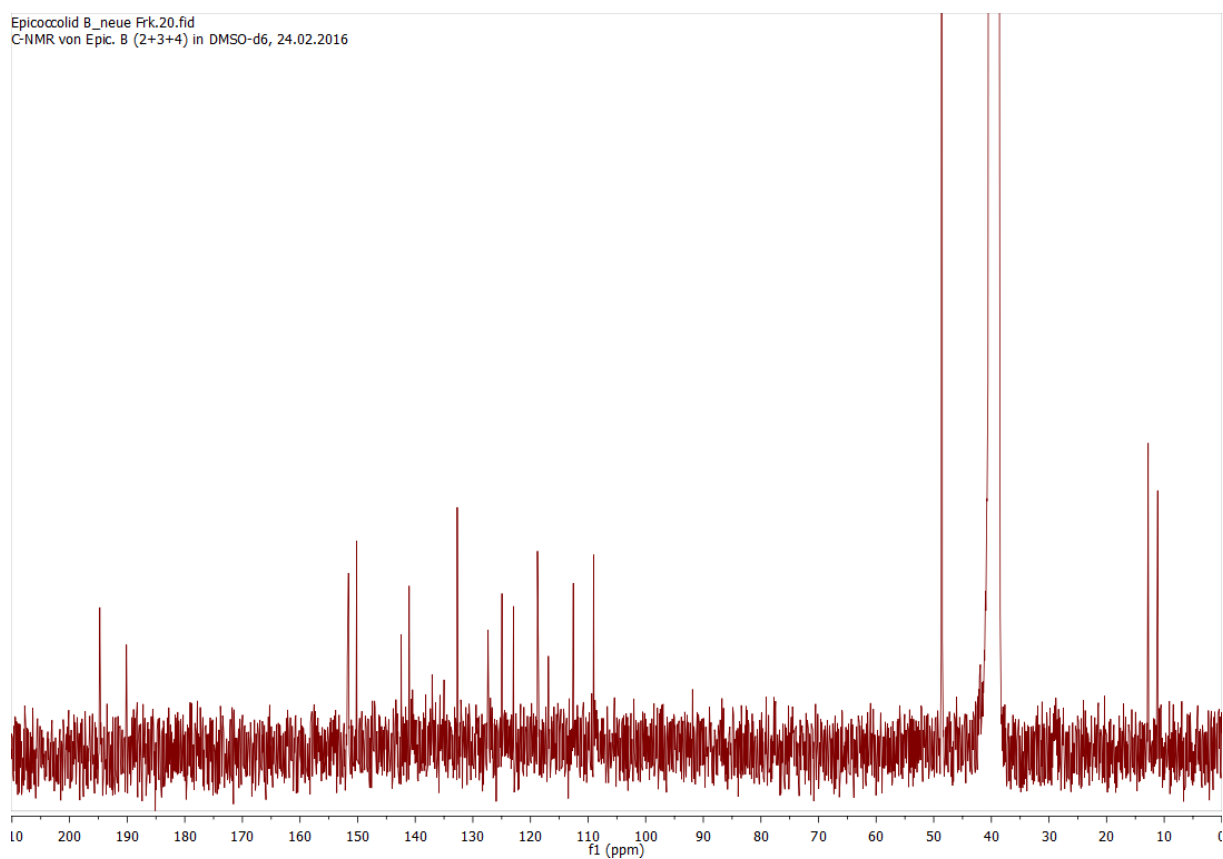
Fig. 8.50: ^{13}C-NMR of epicoccolide B (**9**) in DMSO-d_6.
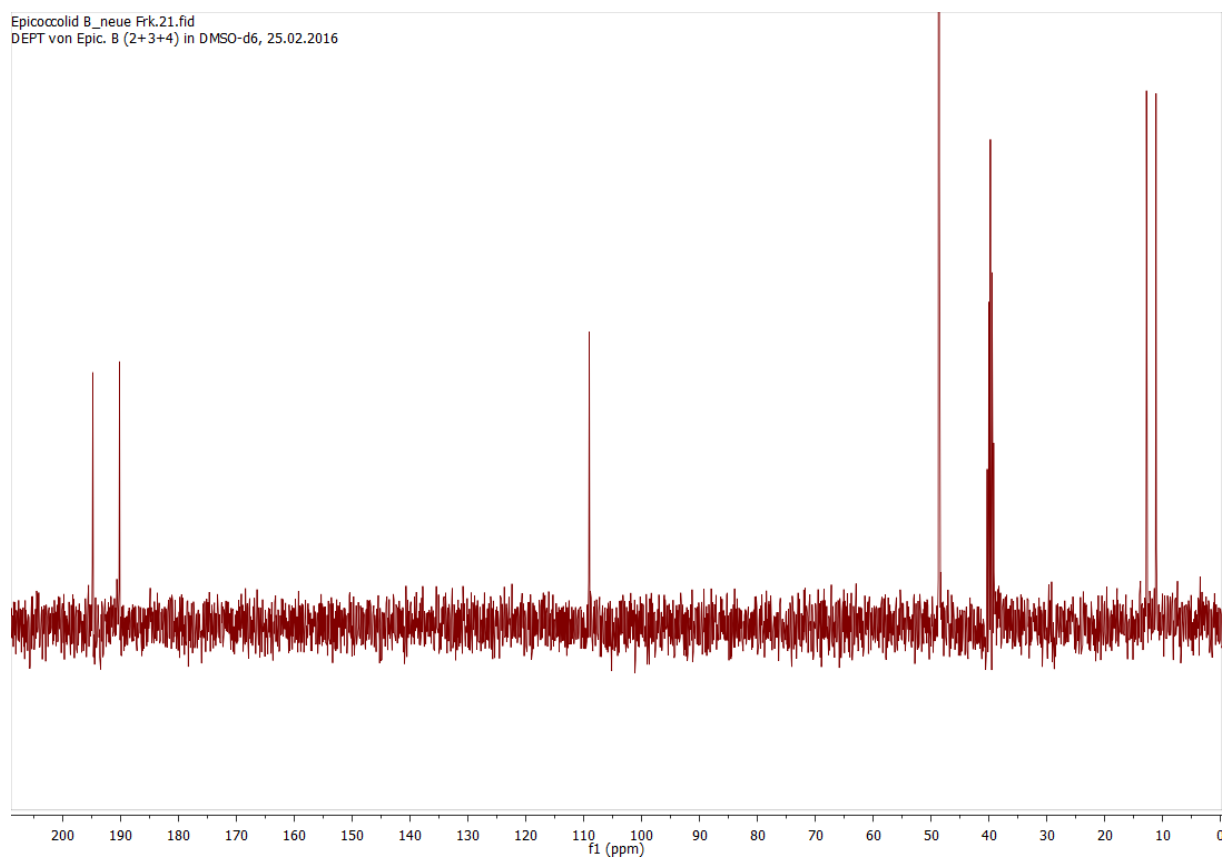
Fig. 8.51: DEPT-135 of epicoccolide B (**9**) in DMSO-d_6.
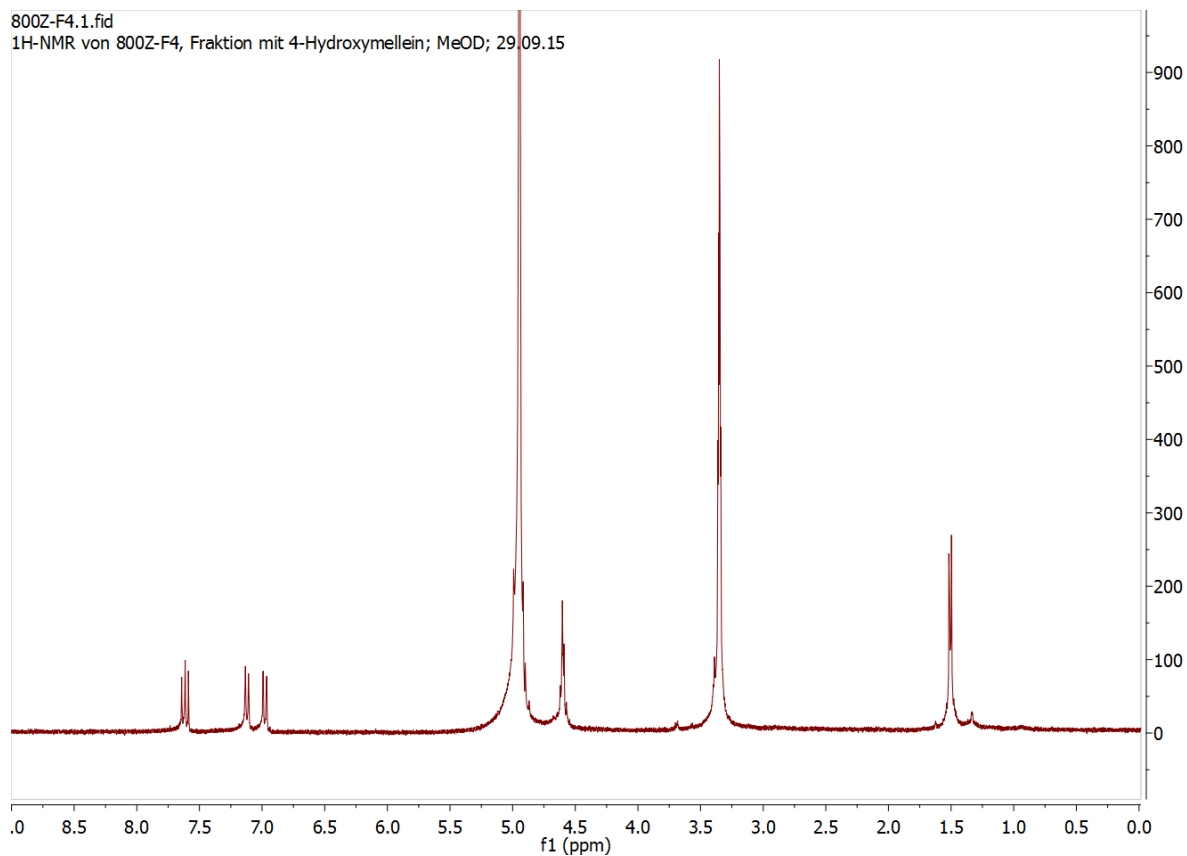
Fig. 8.52: ^{1}H-NMR of (3*R*,4*S*)-4-hydroxymellein (**10**) in MeOH-*d*$_4$.
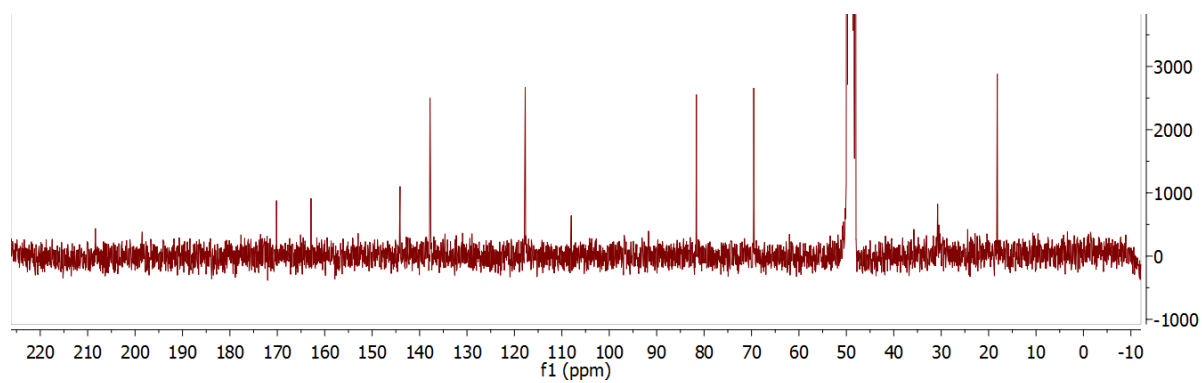
Fig. 8.53: ^{13}C-NMR of (3*R*,4*S*)-4-hydroxymellein (**10**) in MeOH-*d*$_4$.
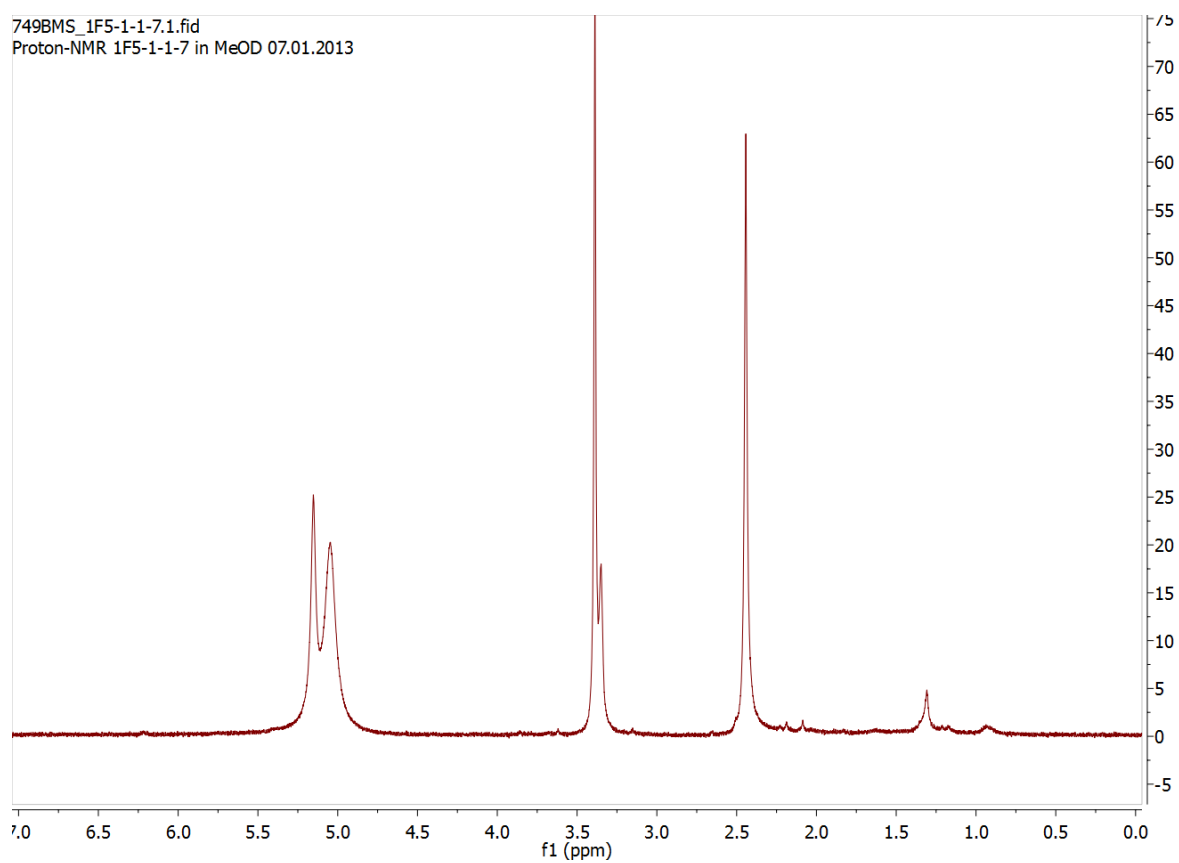
Fig. 8.54: ^{1}H-NMR of epicoccone (**11**) in MeOH-d_4.
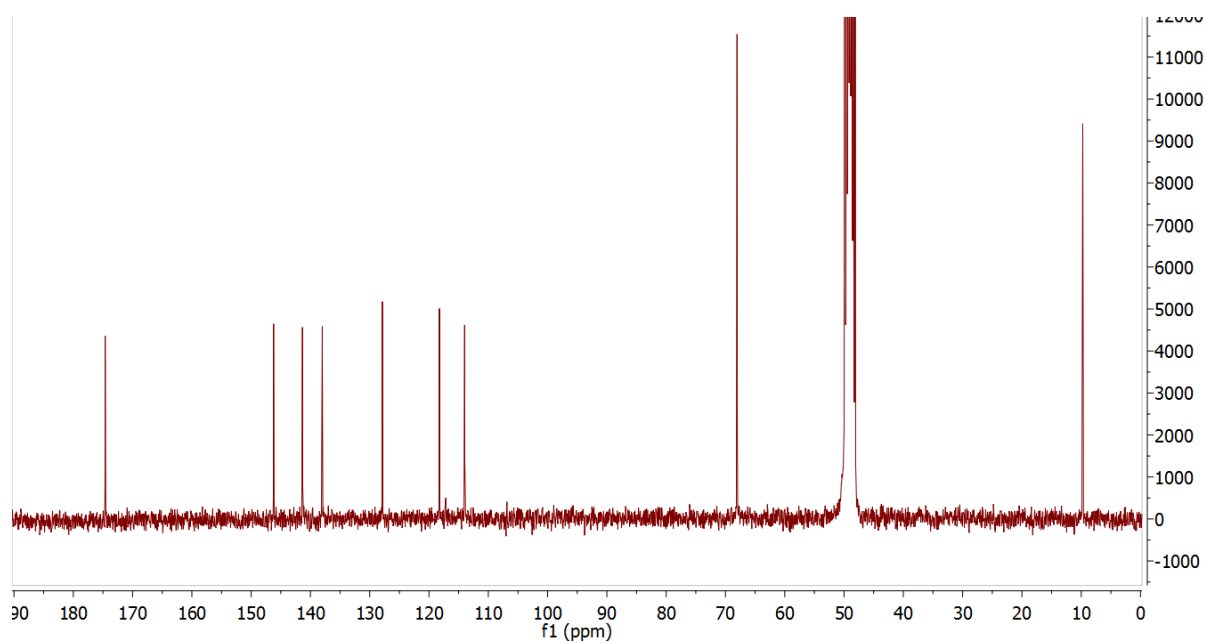
Fig. 8.55: ^{13}C-NMR of epicoccone (**11**) in MeOH-d_4.

749BMS_1F5-1-1-x.21.fid
DEPT-NMR 1F5-1-1-7 in MeOD 08.01.2013
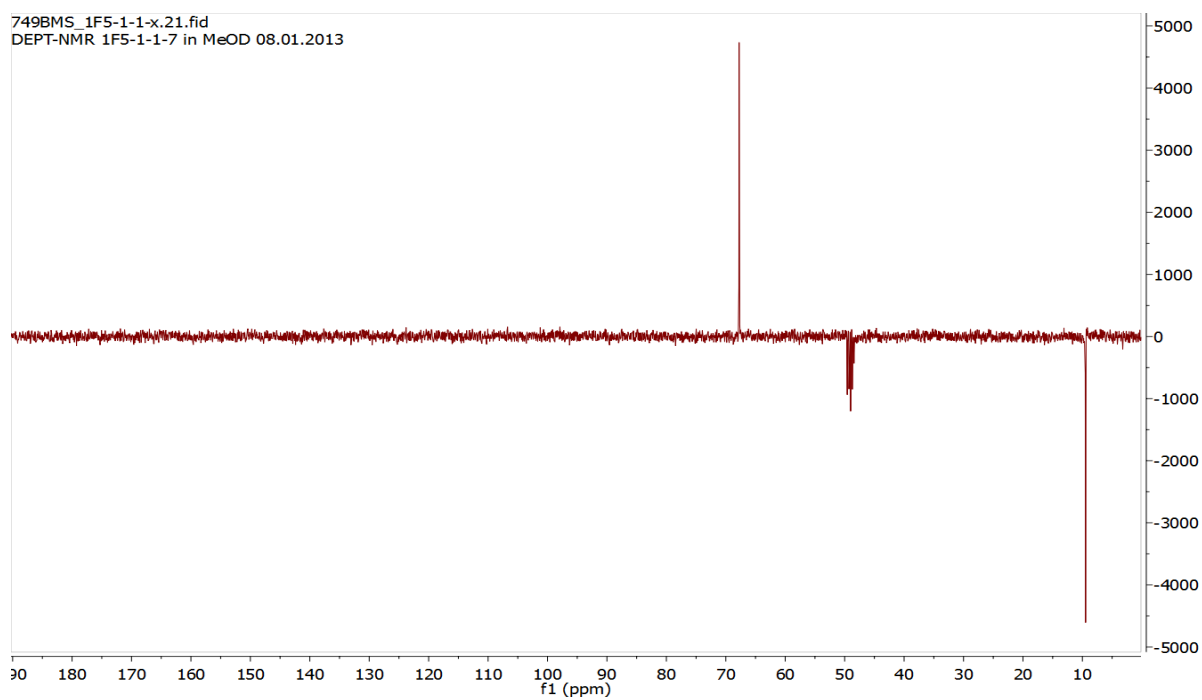
Fig. 8.56: DEPT-135 of epicoccone (**11**) in MeOH-d_4.

749 1F4-1-6.1.1.1r
A proton NMR 749 1F4-1-6 in MeOD 20.04.2012
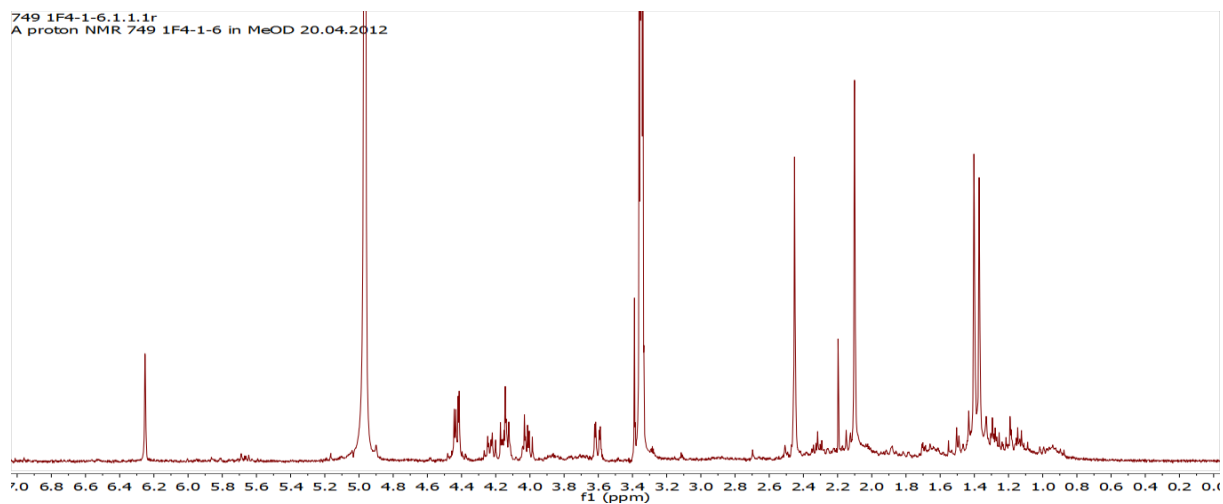
Fig. 8.57: ^{1}H-NMR of 1F4-1-6 (**12**) in MeOH-d_4.
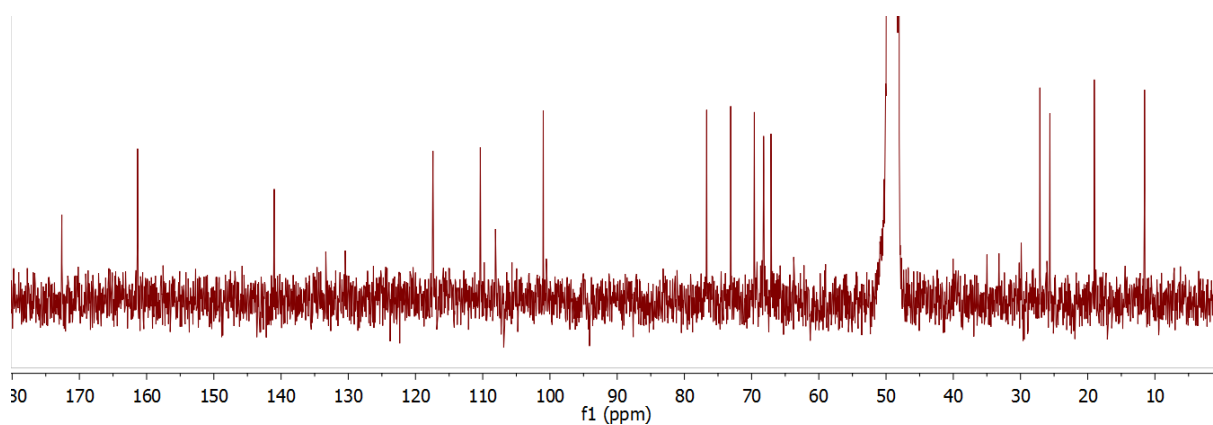
Fig. 8.58: ^{13}C-NMR of 1F4-1-6 (**12**) in MeOH-d_4.
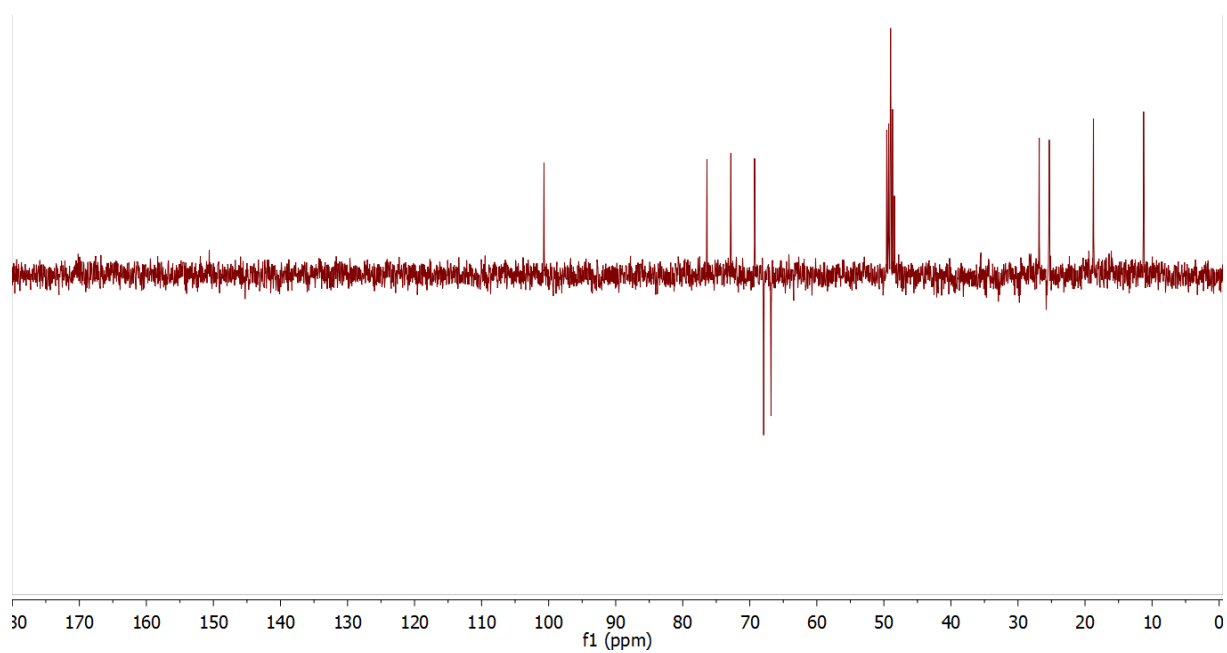
Fig. 8.59: DEPT-135 of 1F4-1-6 (**12**) in MeOH-d_4.
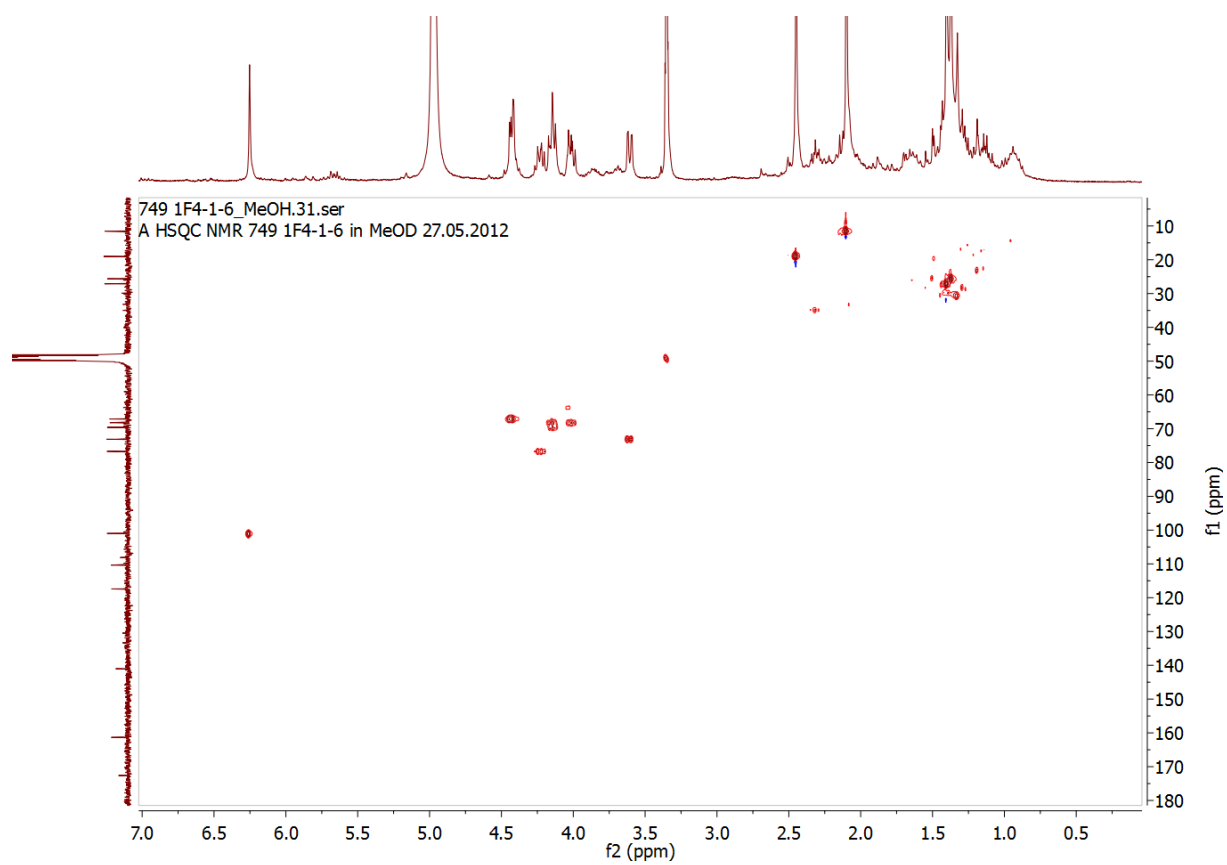
Fig. 8.60: HSQC of 1F4-1-6 (**12**) in MeOH-d_4.
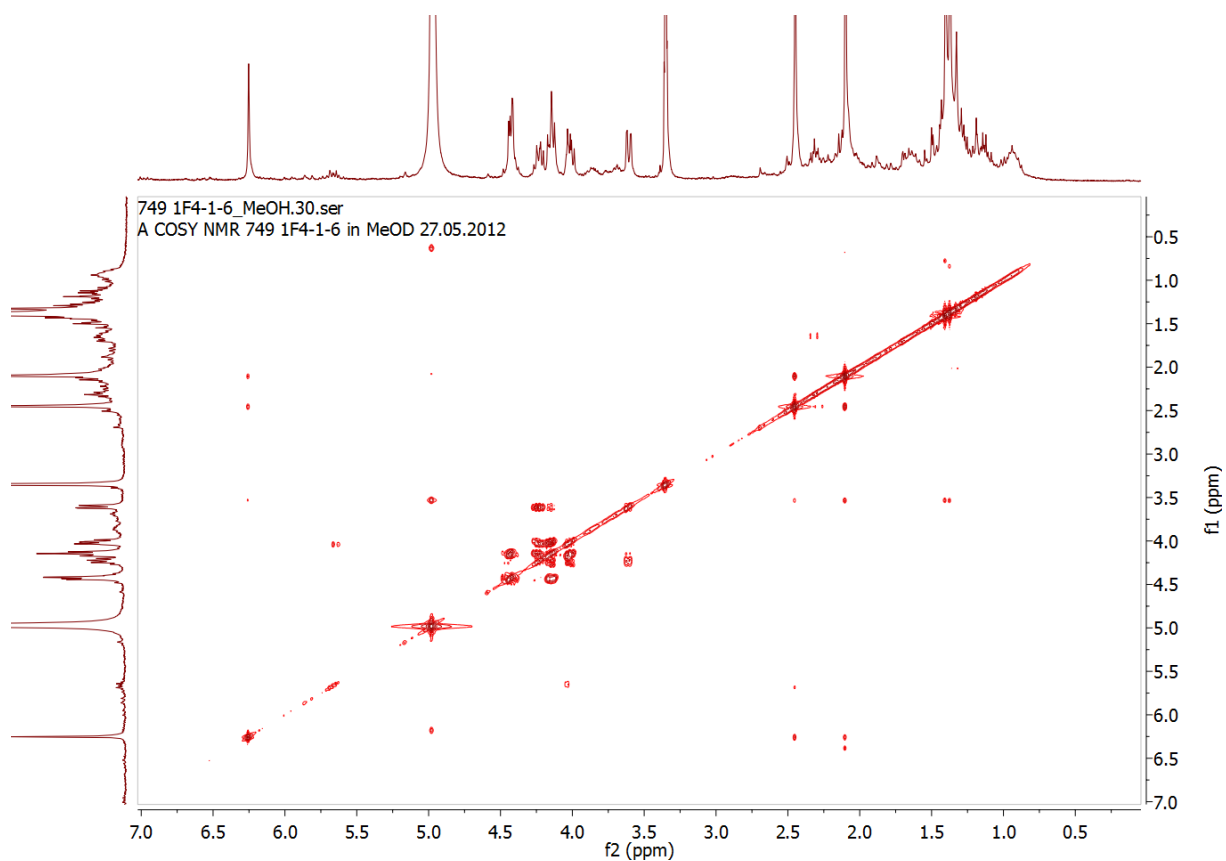
Fig. 8.61: COSY of 1F4-1-6 (**12**) in MeOH-d_4.
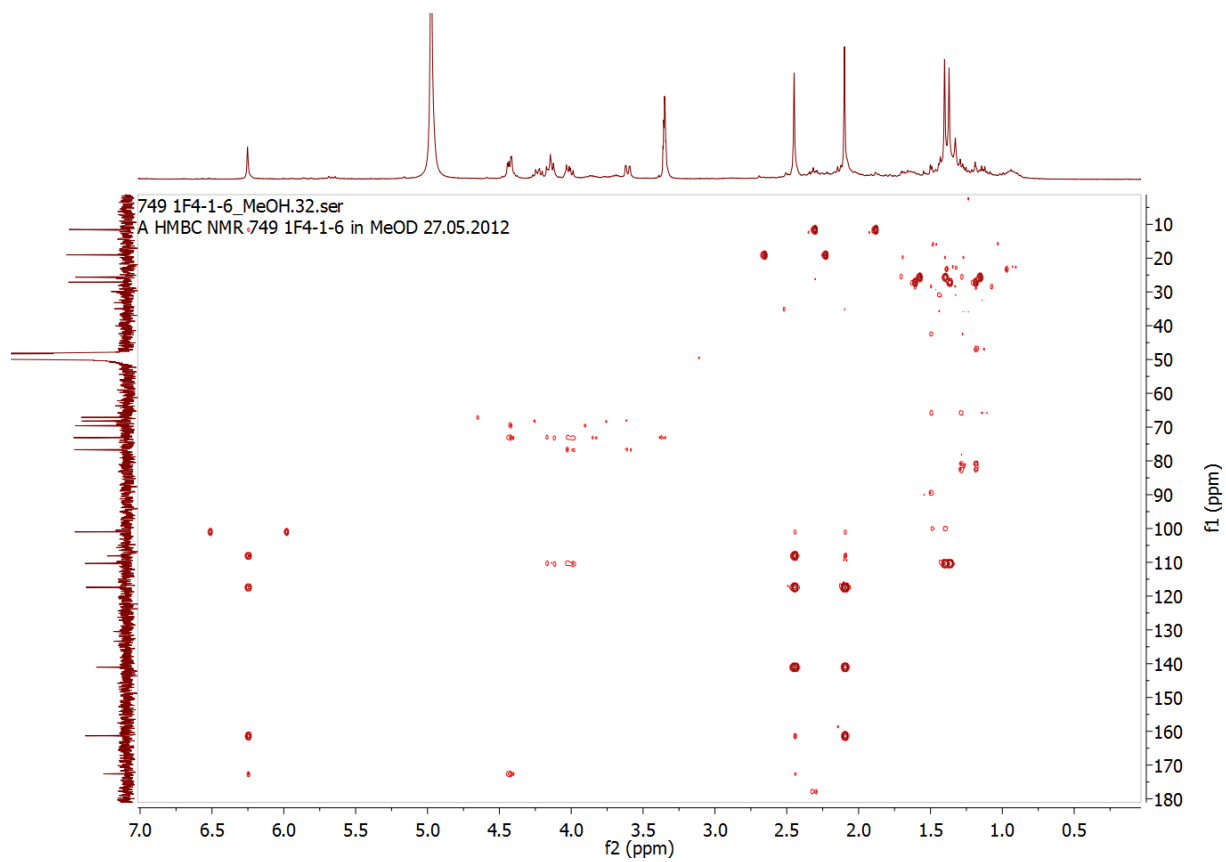
Fig. 8.62: HMBC of 1F4-1-6 (**12**) in MeOH-d_4.

749-1F4-1-6 Aceton.1.fid
1 H NMR in Aceton
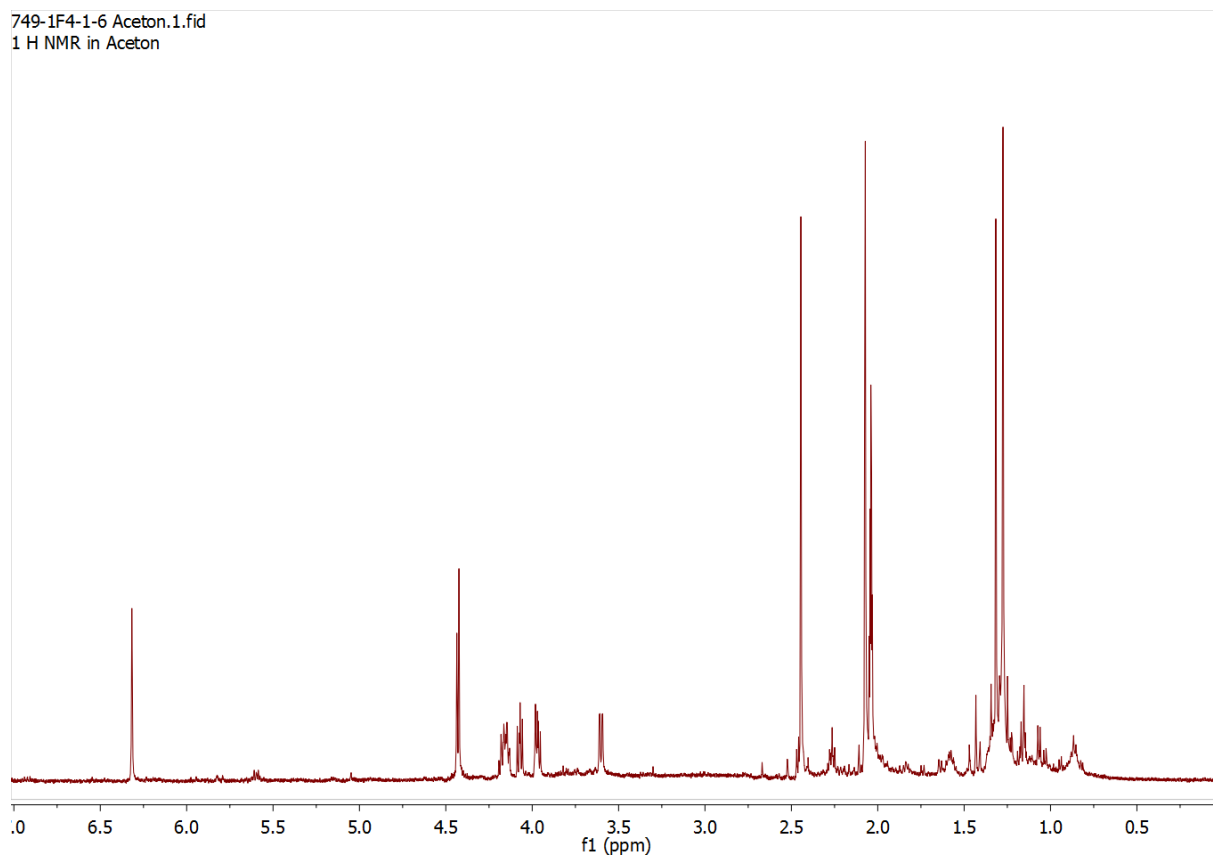
Fig. 8.63: ^{1}H-NMR of 1F4-1-6 (**12**) in acetone-d_6.

749-1F4-1-6 Aceton.20.fid
carbon spectrum of
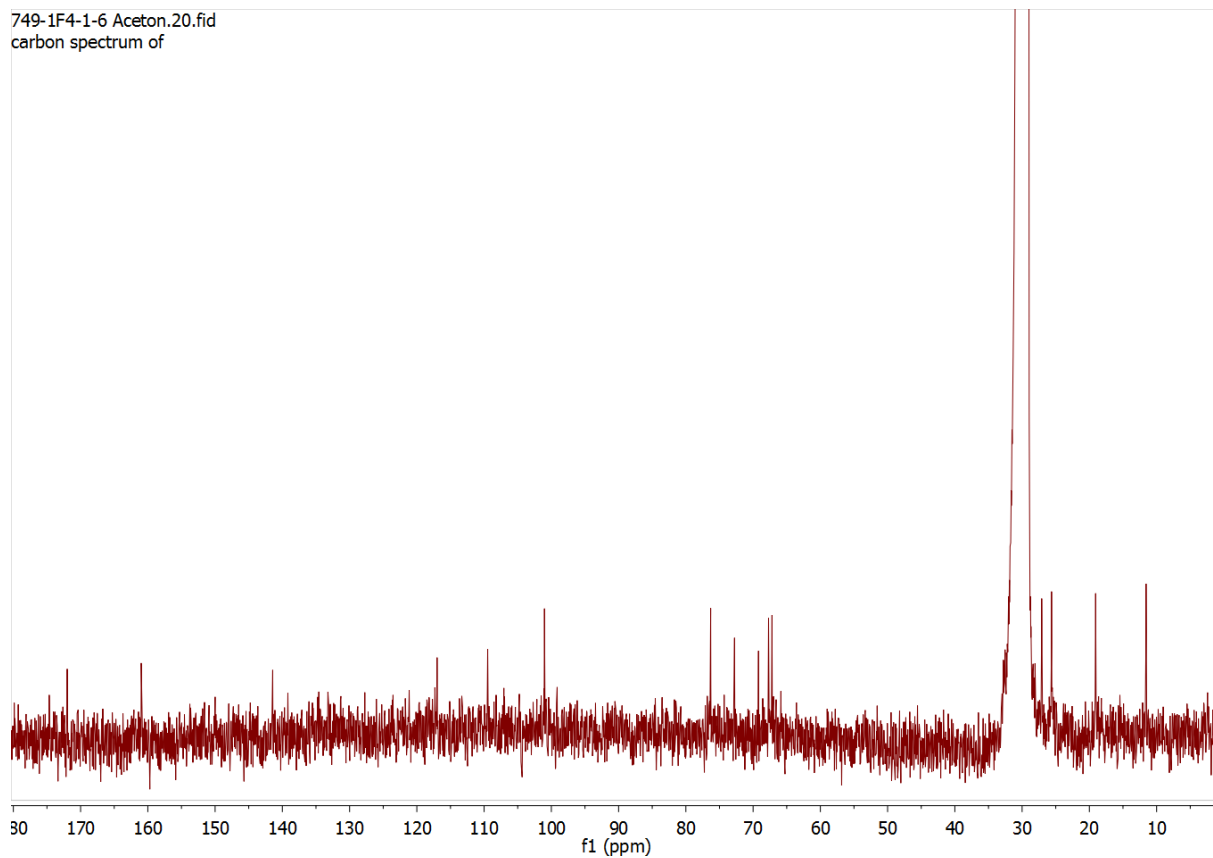
Fig. 8.64: ^{13}C-NMR of 1F4-1-6 (**12**) in acetone-d_6.
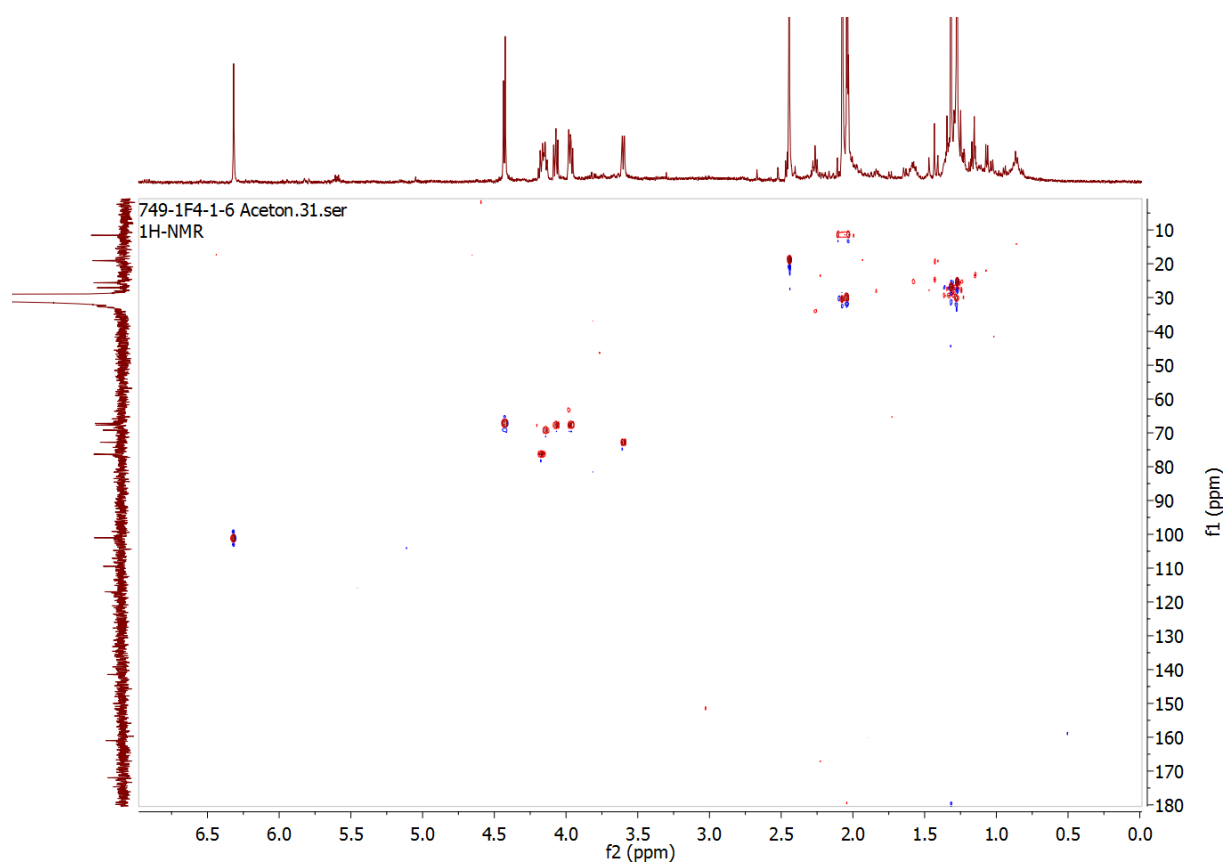
Fig. 8.65: HSQC of 1F4-1-6 (**12**) in acetone-d_6.
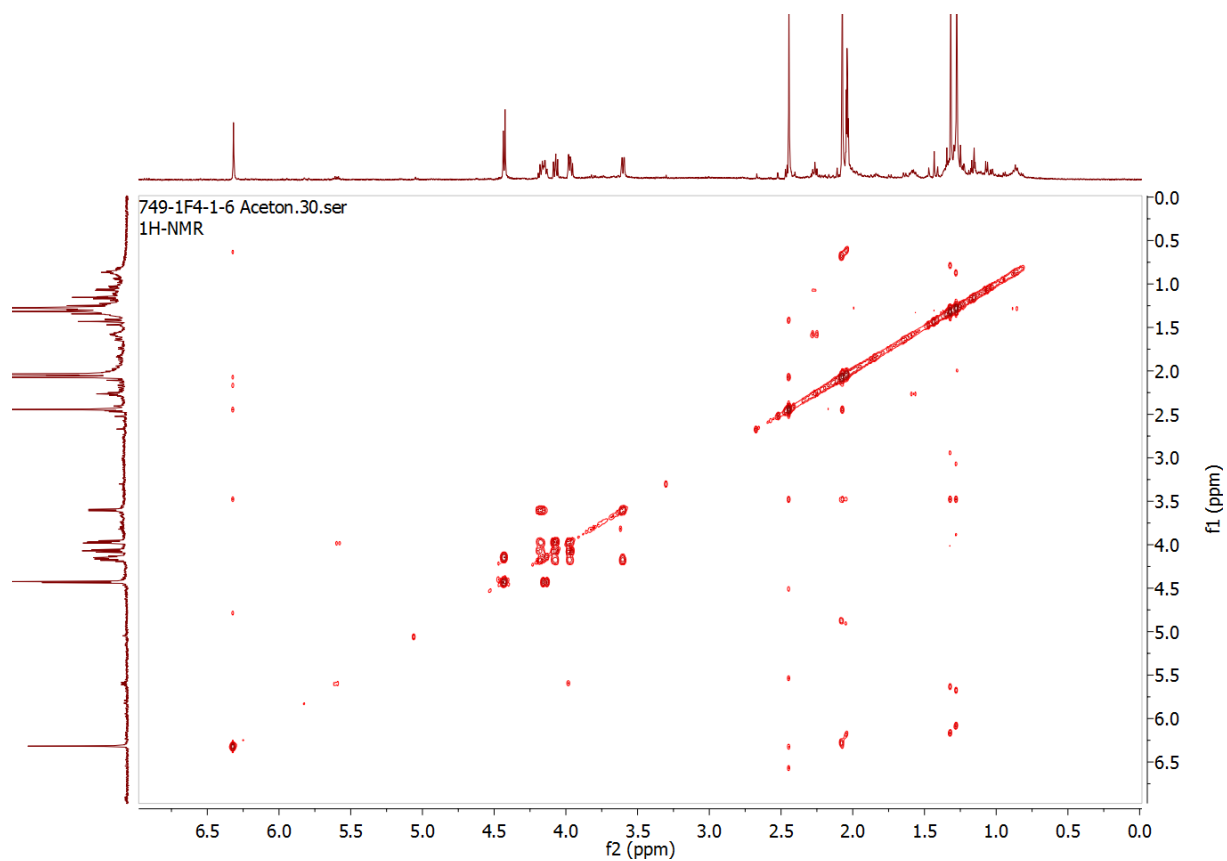
Fig. 8.66: COSY of 1F4-1-6 (**12**) in acetone-d_6.
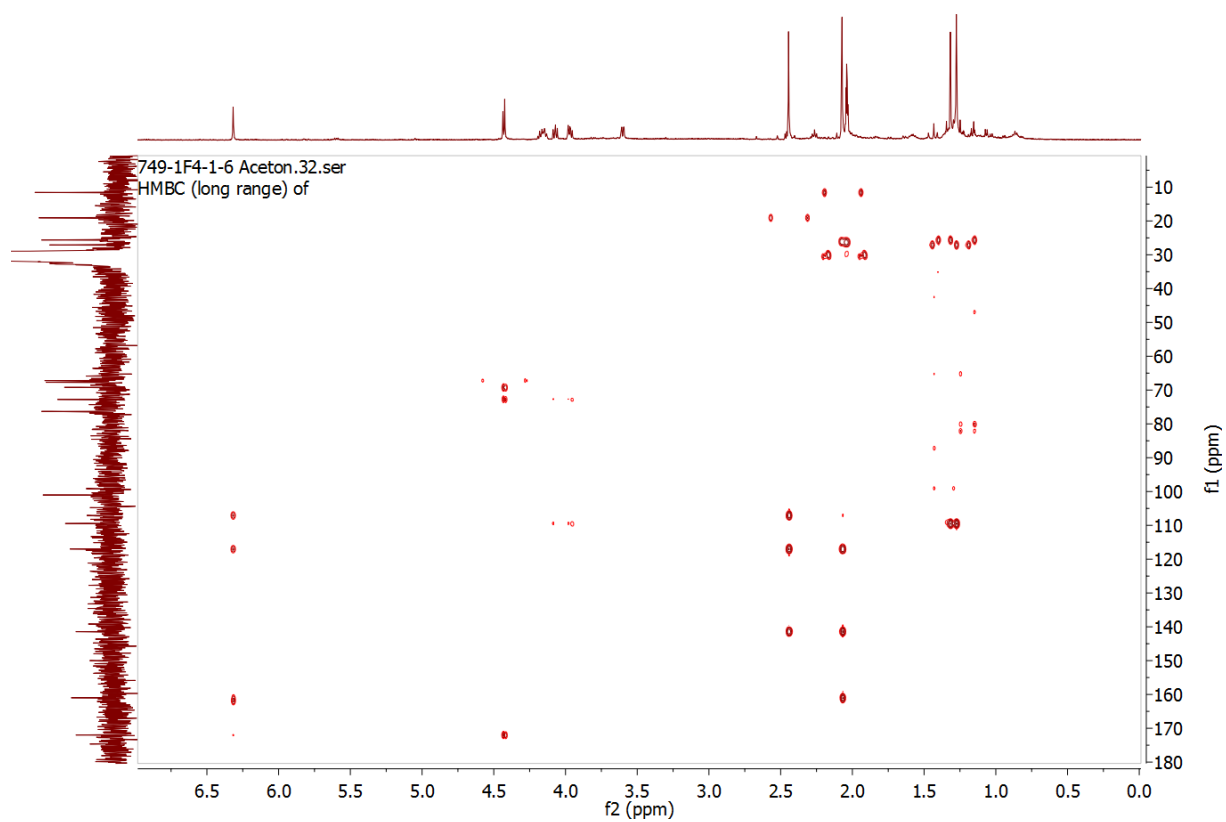
Fig. 8.67: HMBC of 1F4-1-6 (**12**) in acetone-d_6.
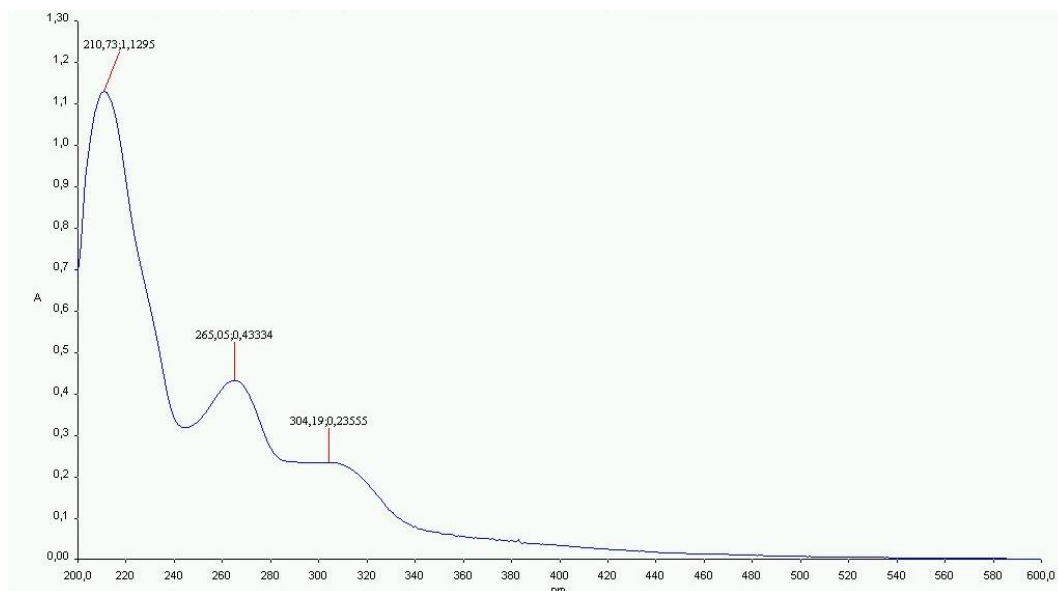
Fig. 8.68: UV-spectrum of 1F4-1-6 (**12**) in MeOH.
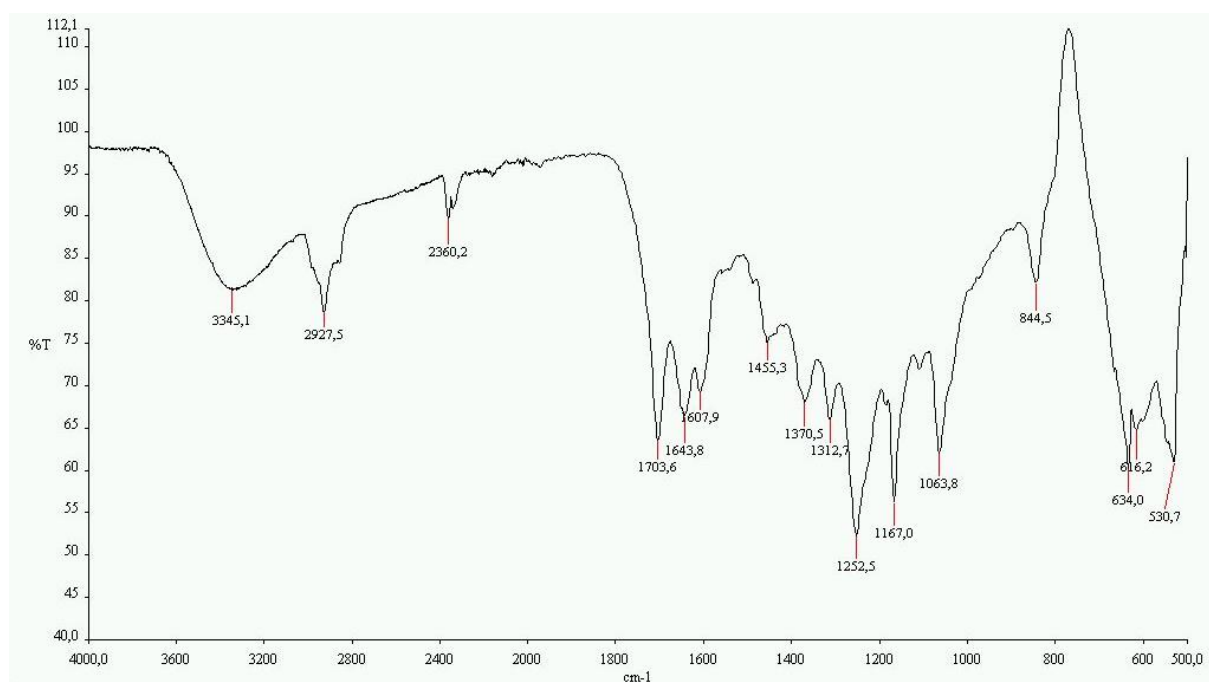
Fig. 8.69: IR-spectrum of 1F4-1-6 (**12**).
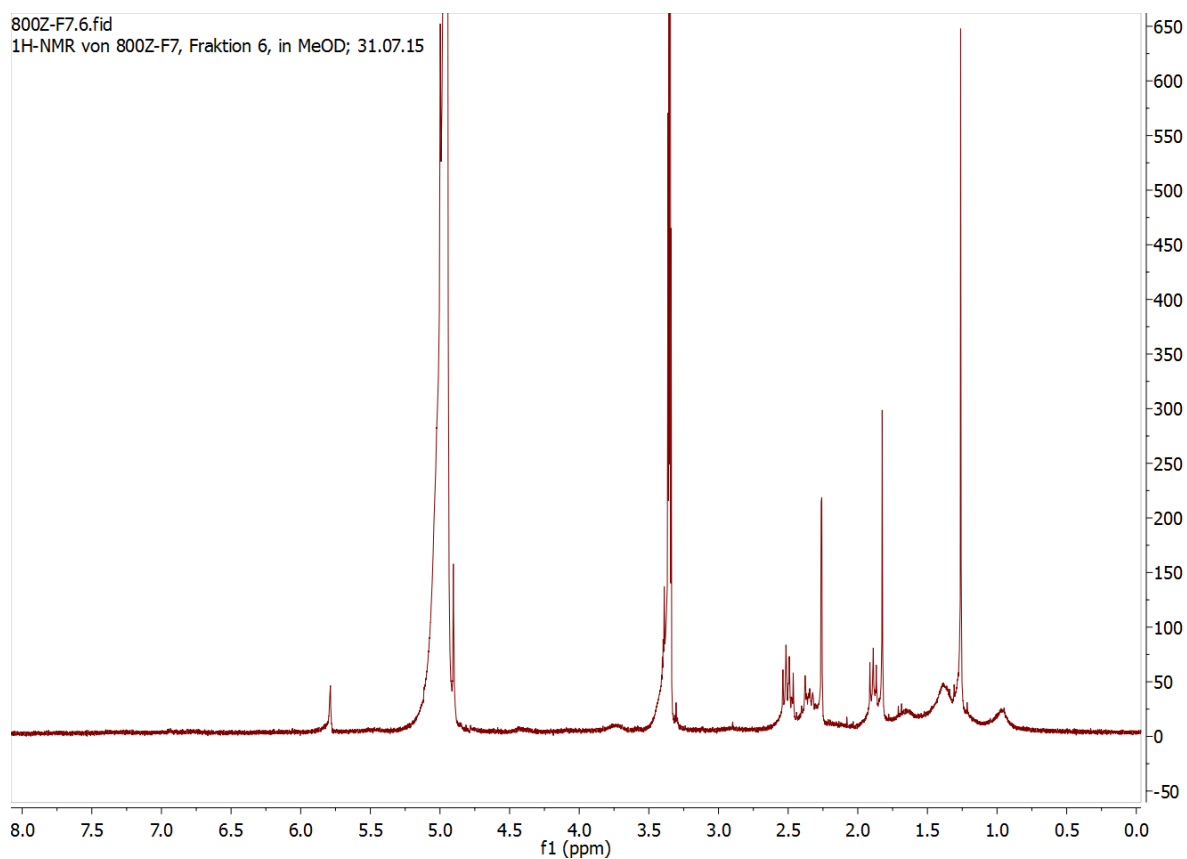
Fig. 8.70: ^{1}H-NMR of epicaronic acid (**13**) in MeOH-d_4.
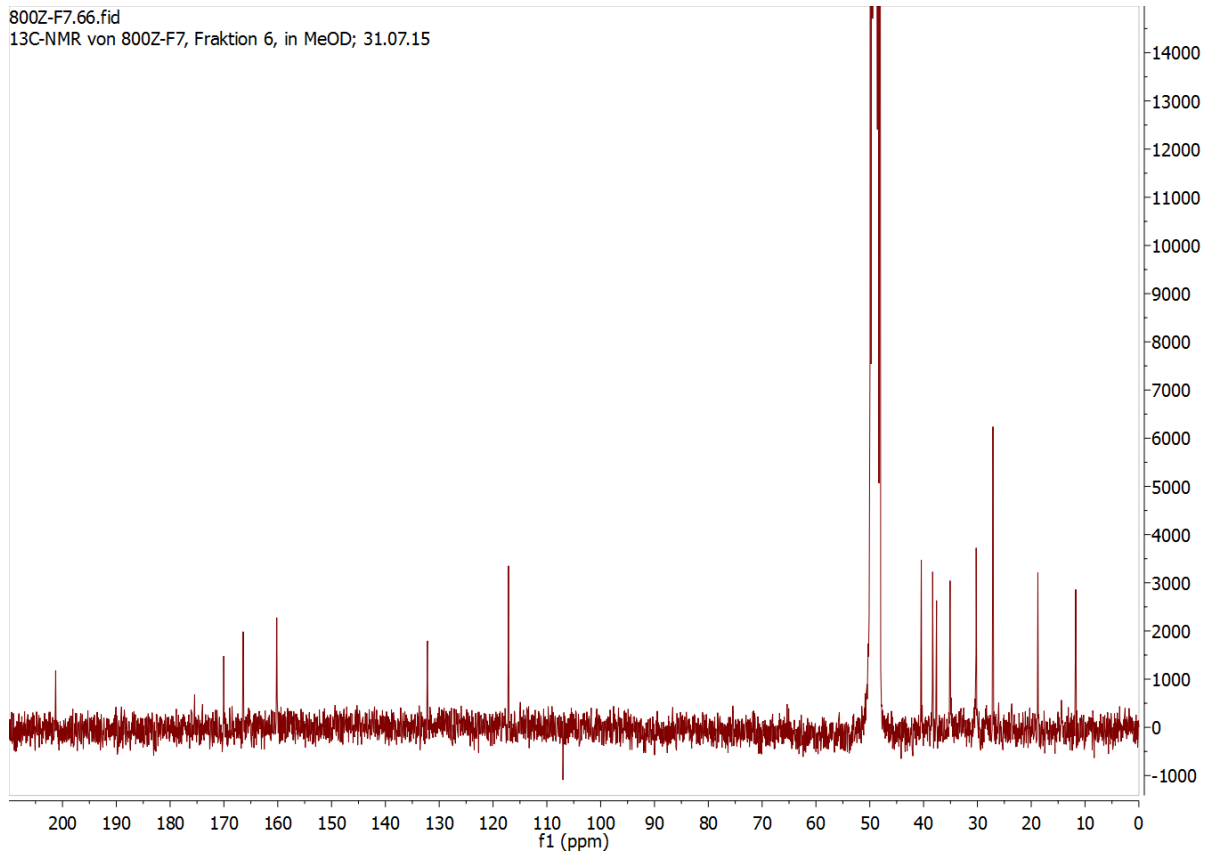
Fig. 8.71: ^{13}C-NMR of epicaronic acid (**13**) in MeOH-d_4.
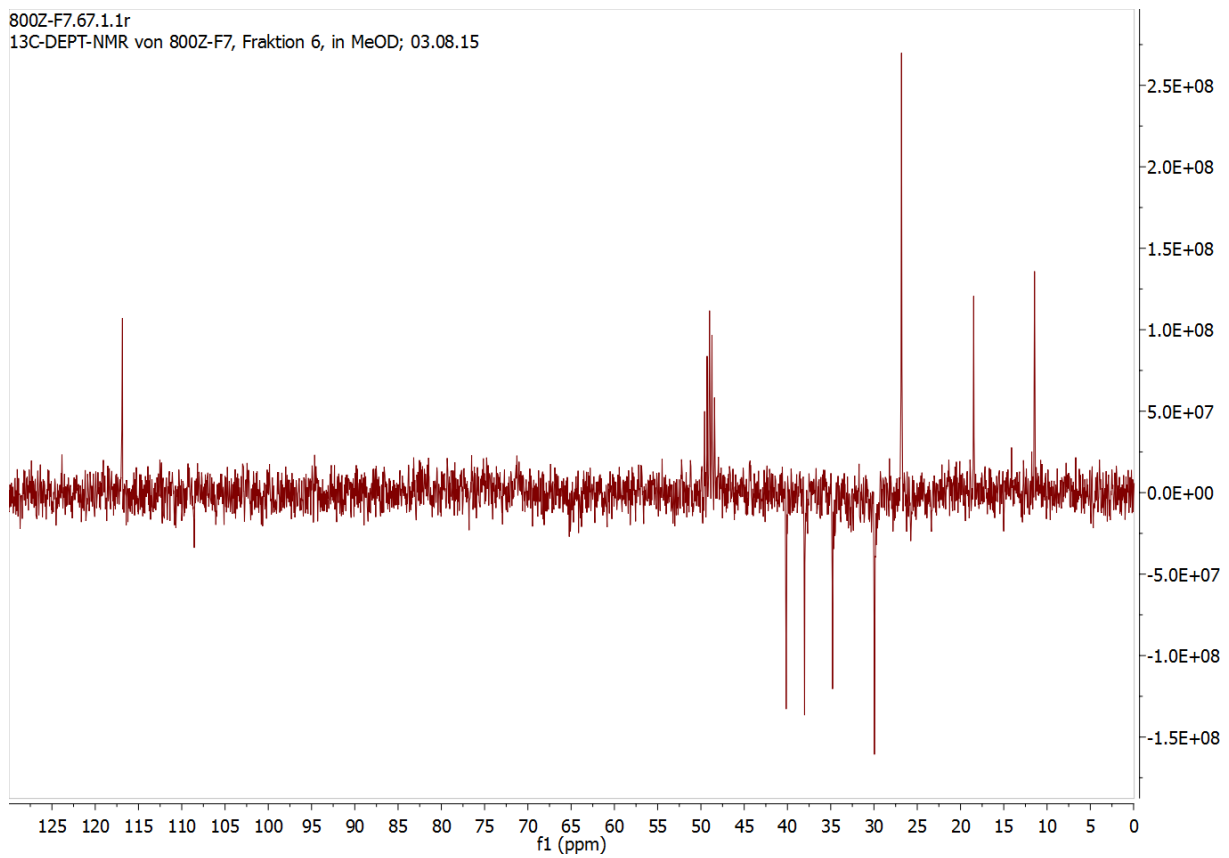
Fig. 8.72: DEPT-135 of epicaronic acid (**13**) in MeOH-d_4.
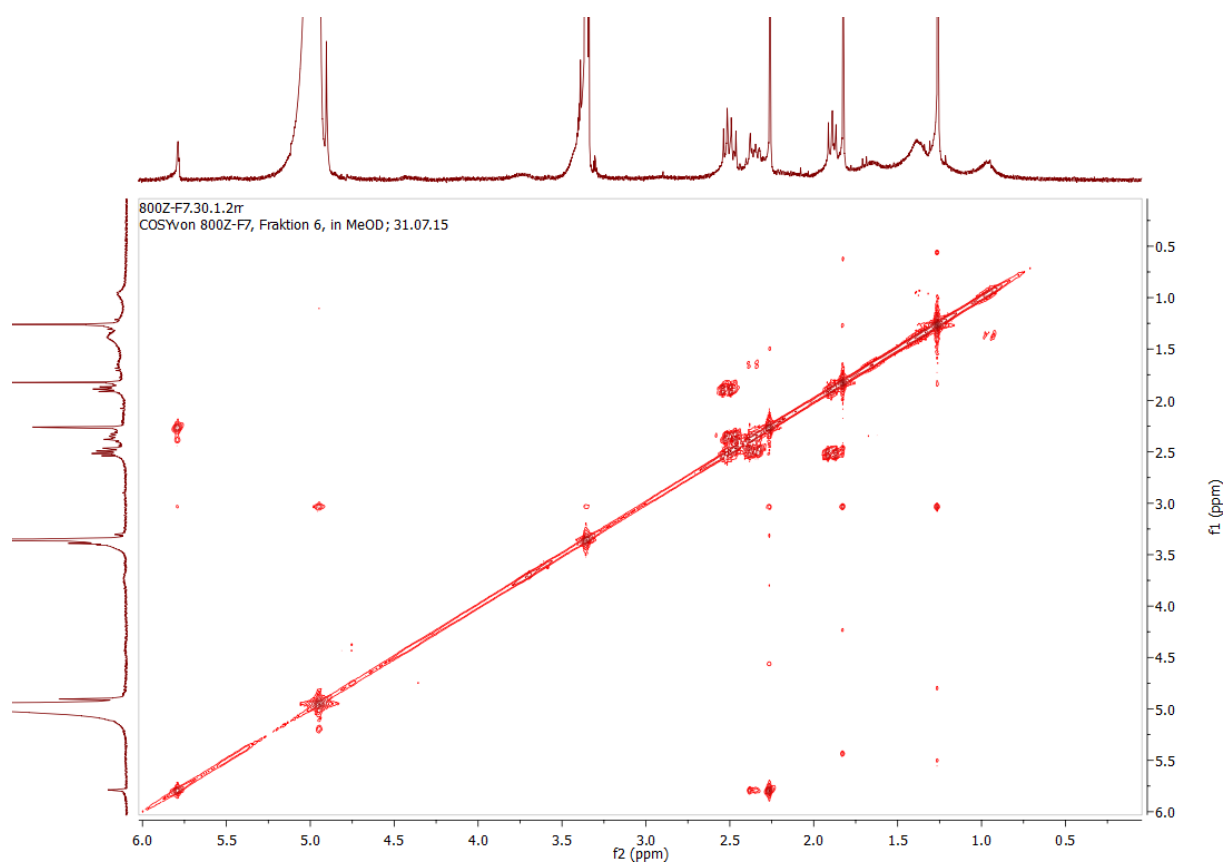
Fig. 8.73: COSY of epicaronic acid (**13**) in MeOH-d_4.
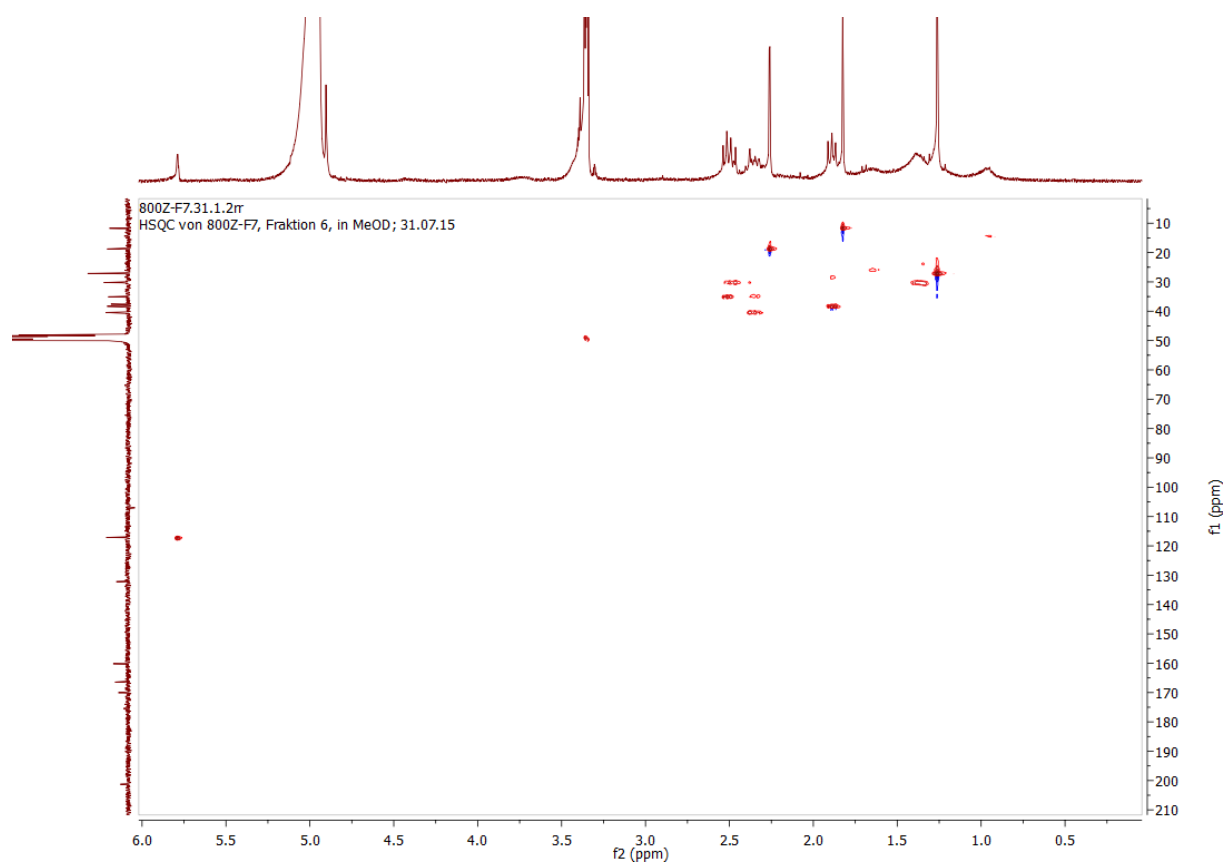
Fig. 8.74: HSQC of epicaronic acid (**13**) in MeOH-d_4.
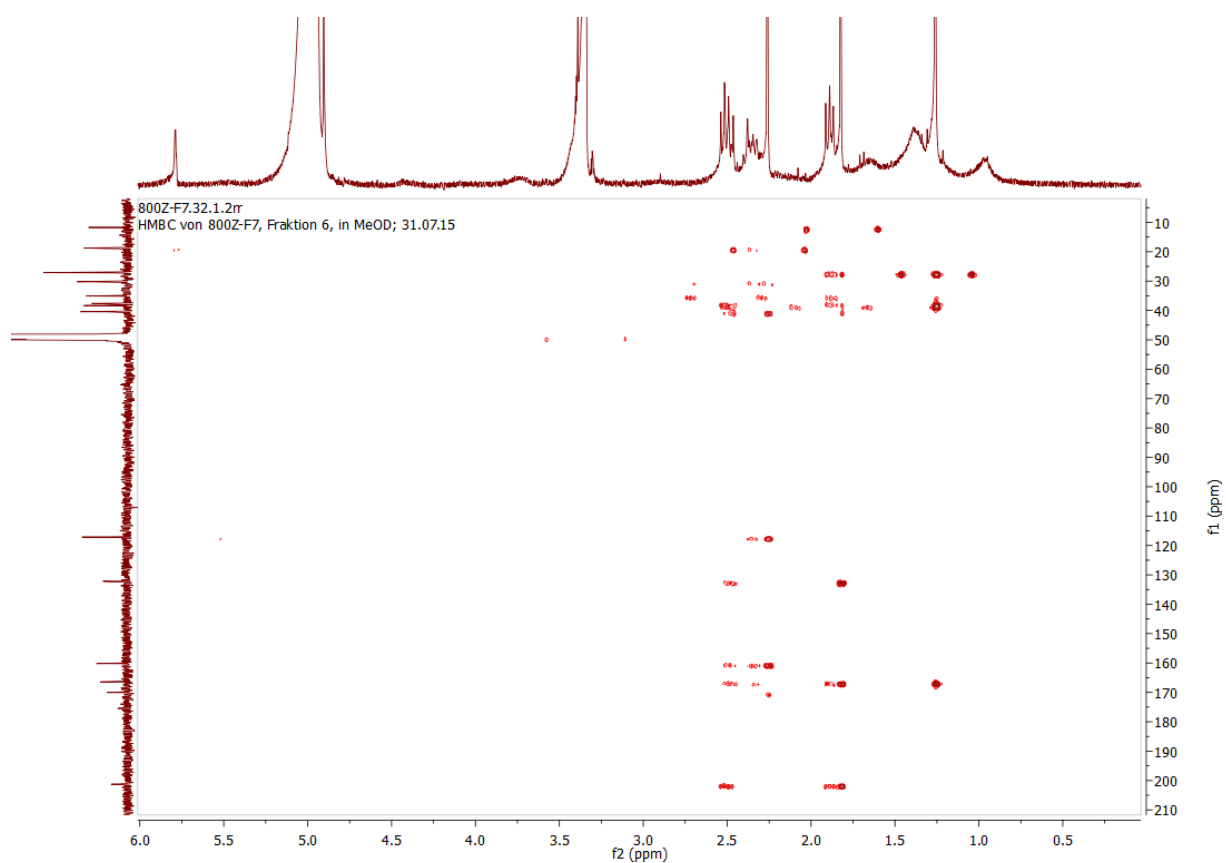
Fig. 8.75: HMBC of epicaronic acid (**13**) in MeOH-d_4.
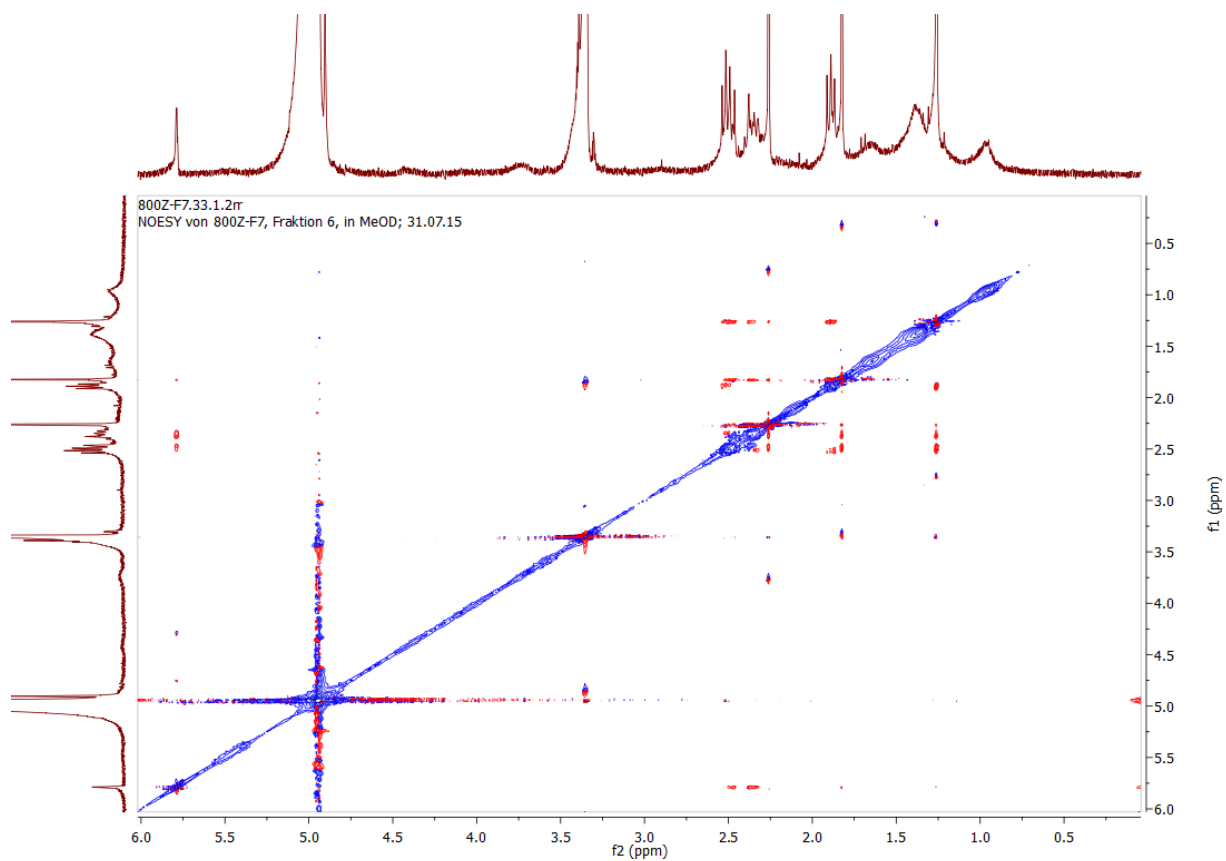
Fig. 8.76: NOESY of epicaronic acid (**13**) in MeOH-d_4.
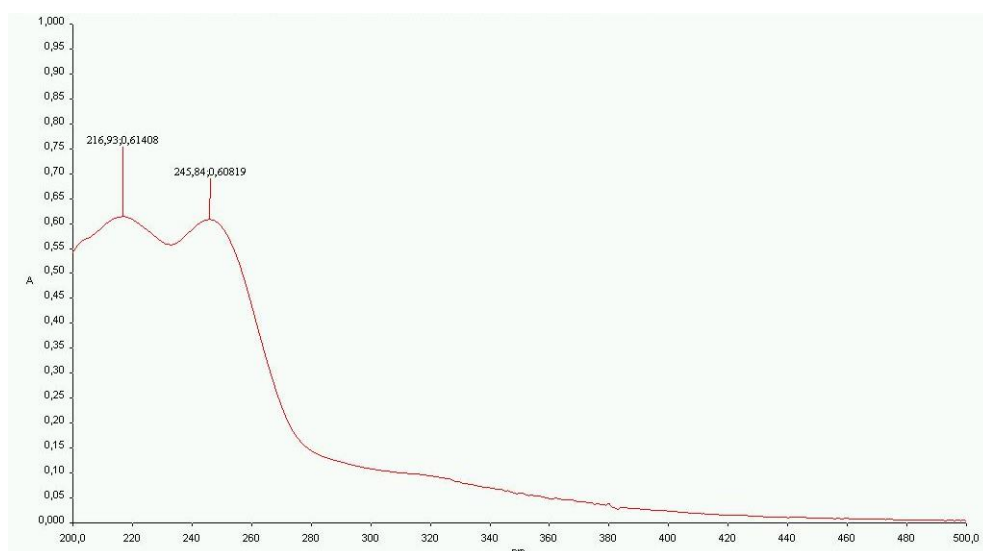
Fig. 8.77: UV-spectrum of epicaronic acid (**13**) in MeOH.
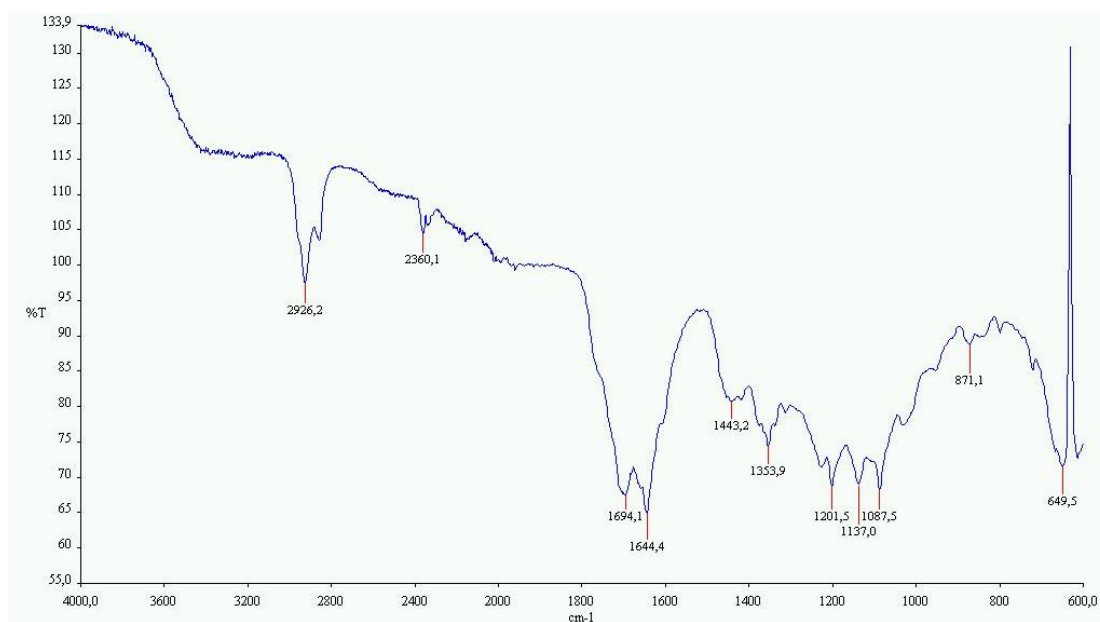
Fig. 8.78: IR-spectrum of epicaronic acid (**13**).
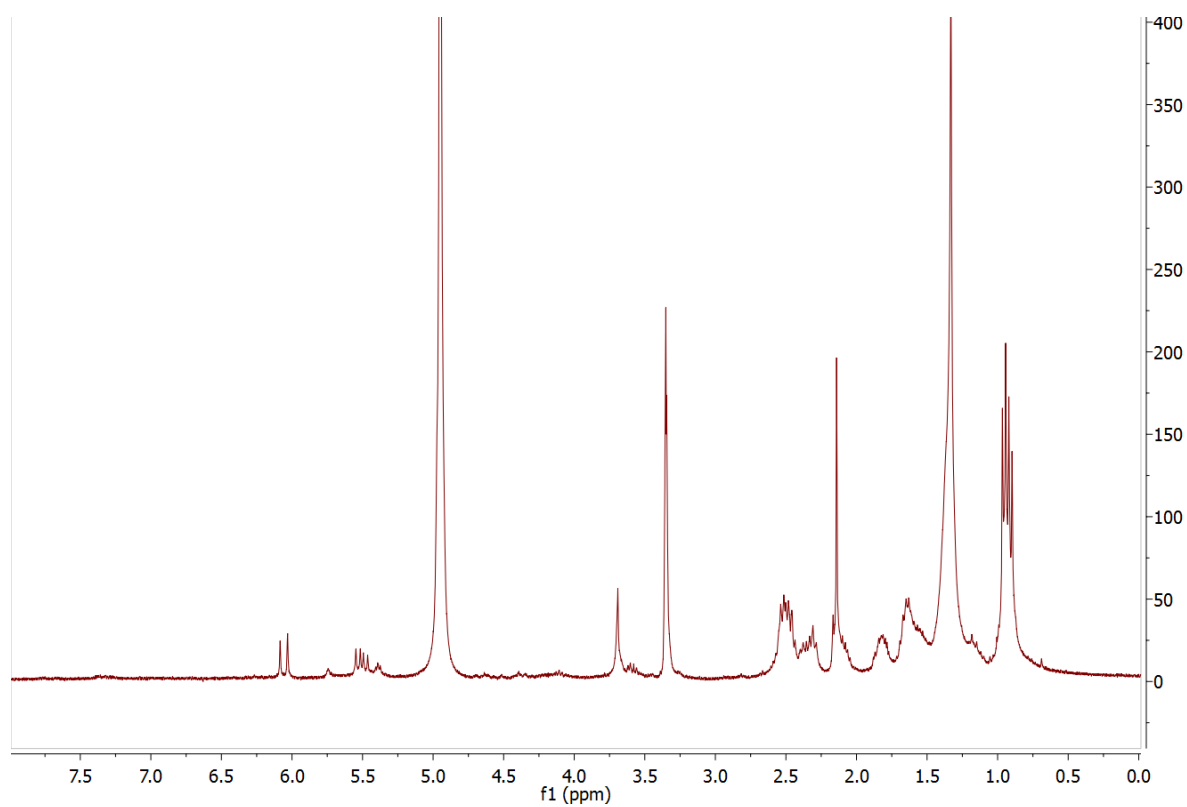
Fig. 8.79: ^{1}H-NMR of tricinonoic acid (**14**) in MeOH-d_4.
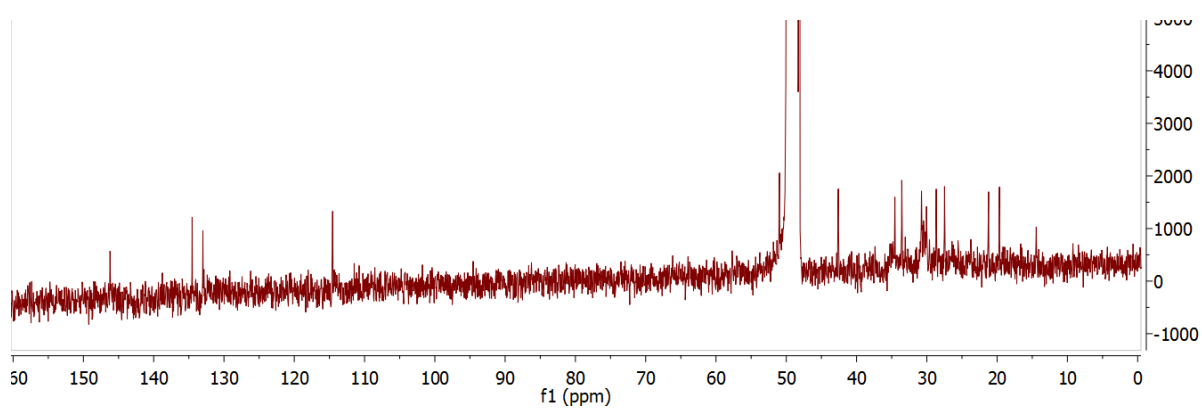
Fig. 8.80: ^{13}C-NMR of tricinonoic acid (**14**) in MeOH-d_4.
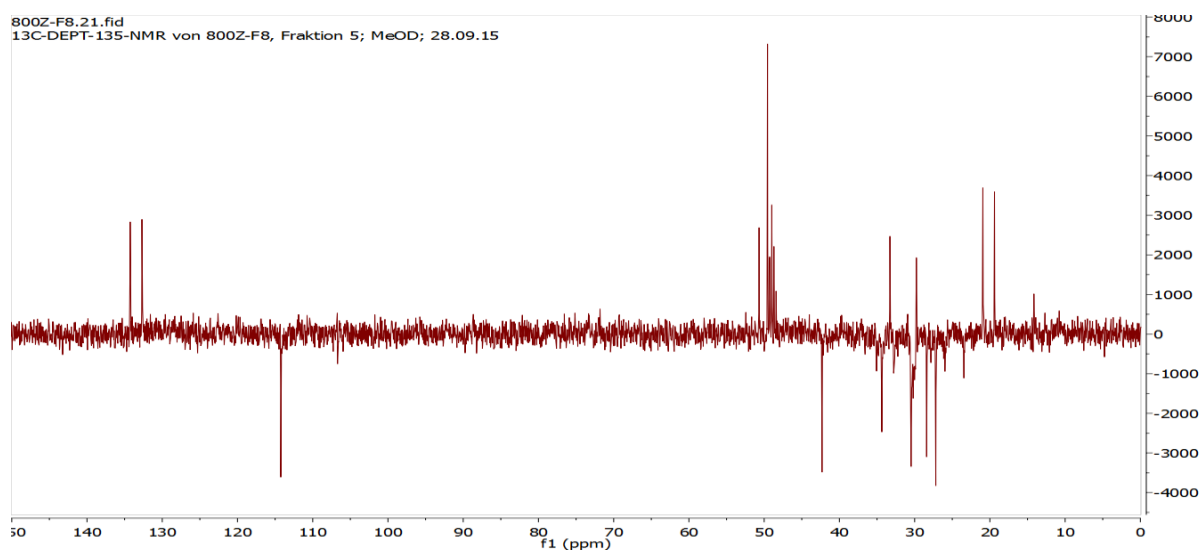
Fig. 8.81: DEPT-135 of tricinonoic acid (**14**) in MeOH-d_4.
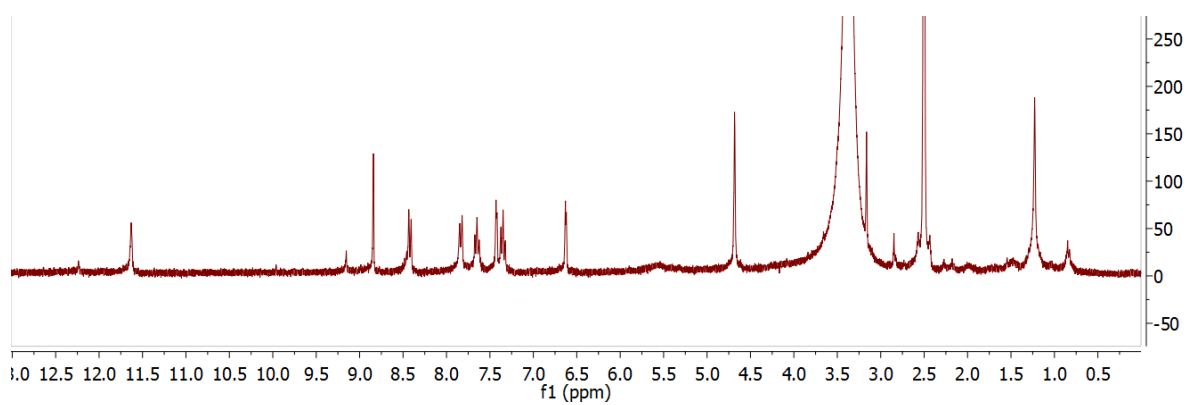
Fig. 8.82: ^{1}H-NMR of flazin (**15**) in DMSO-d_6.
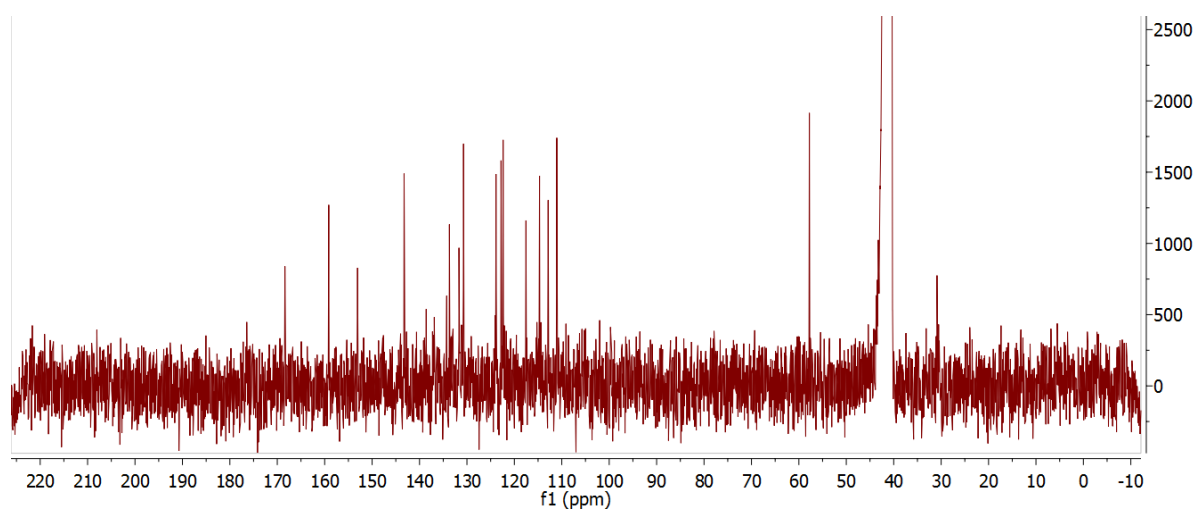
Fig. 8.83: ^{13}C-NMR of flazin (**15**) in DMSO-d_6.
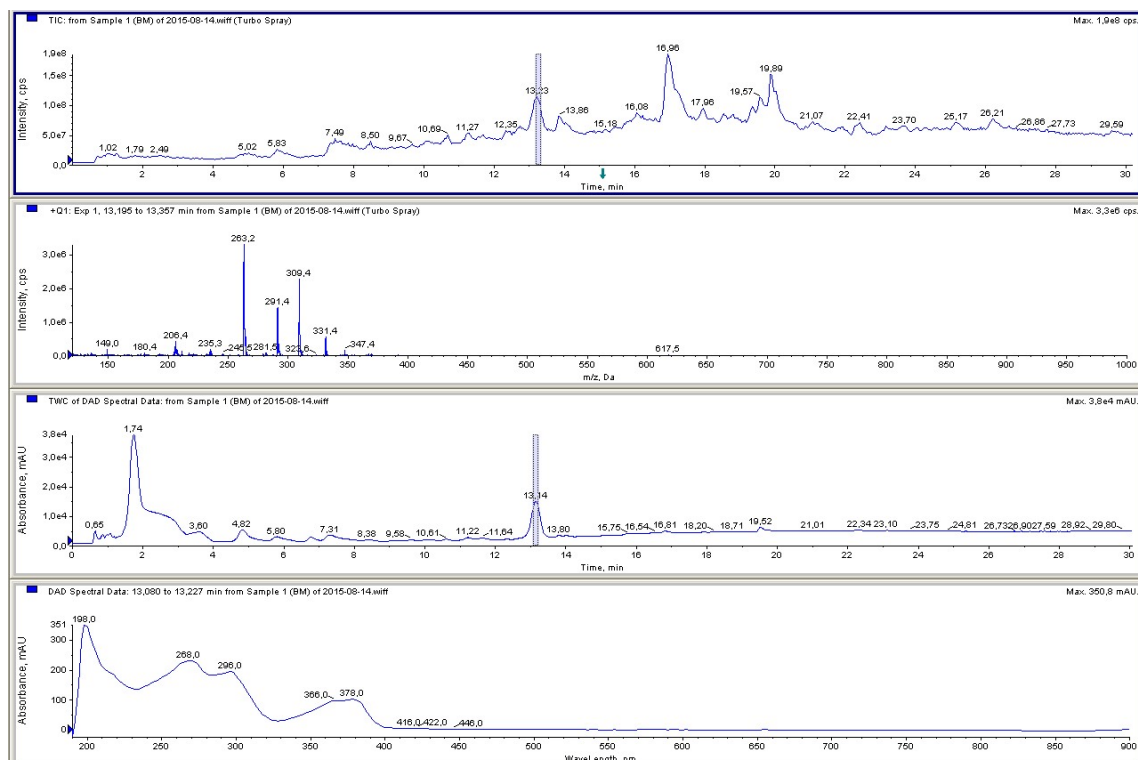
Fig. 8.84: LC-ESI-MS data sheet for the crude extract of pure malt extract showing the total ion chromatogram (TIC), the mass signal for flazin (*m/z* 309 [M+H]$^+$), the total wavelength chromatogram (TWC) and the DAD spectral data for flazin (from top to bottom).

normalized data
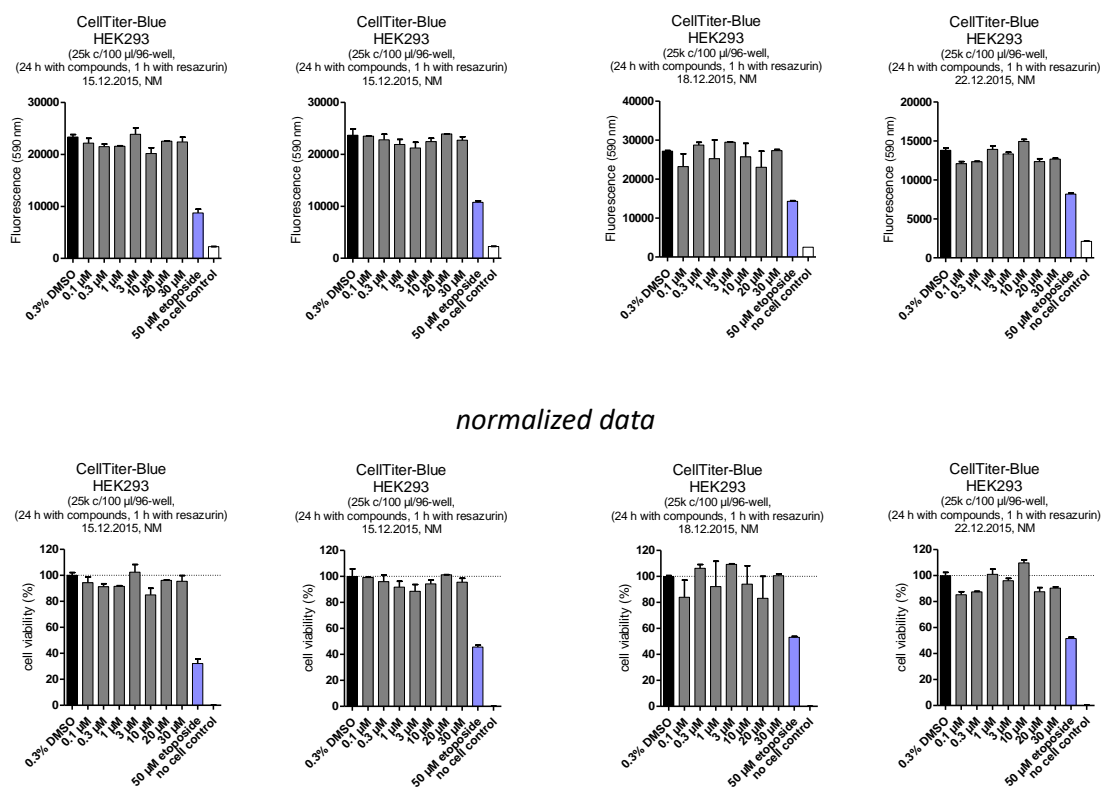
Fig. 8.85: Raw data of the resazurin-based cell viability assay, performed with acetosellin (**4**) in a concentration range of 0.1 µM – 30 µM. 0.3% DMSO was used as control.
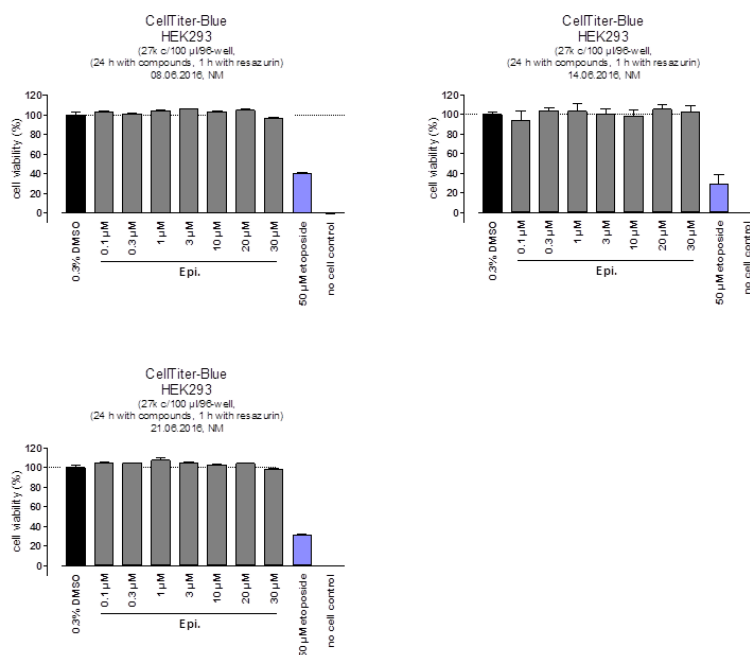
Fig. 8.86: Raw data of the resazurin-based cell viability assay, performed with epicoccolide B (**9**) in a concentration range of 0.1 µM – 30 µM. 0.3% DMSO was used as control.

Tab. 8.2: Effect of compounds **1**-**3**, **4**, **6**, **10**, **13**, **14**, **15** on human cerebroside sulfotransferase (hCST). Inhibitory activity is given as residual activity of the tested enzyme in %. Assay was performed in duplicates on two days, respectively.

Tested compound	Residual activity [%]
Epipyrone triacetate (**6**)	88.43 ± 5.9
Flazin (**15**)	46.36 ± 7.1
Acetosellin (**4**)*	11.86 ± 5.7
Epicaronic acid (**13**)	53.44 ± 3.4
Tricinonoic acid (**14**)	57.08 ± 2.3
(3R,4S)-4-Hydroxymellein (**10**)	88.72 ± 3.4
Epipyrones (**1**-**3**)	18.21 ± 6.8

* Activity on first testing. Acetosellin did not show inhibitory activity after repeated testing on hCST.
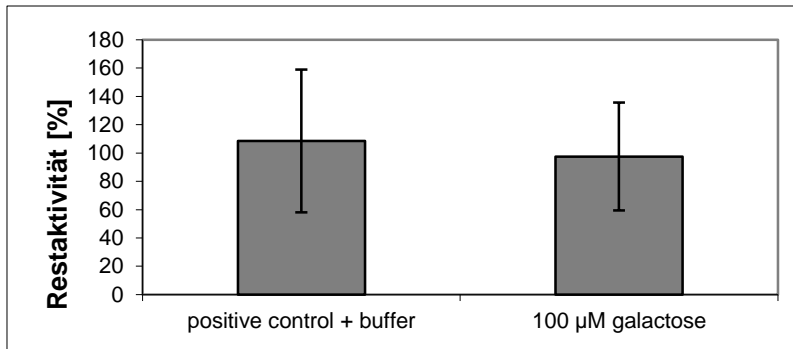
Fig. 8.87: Assay for inhibitory activity of pure β-D-galactose on human cerebroside transferase. The assay was repeated four times. Error bars indicate standard deviation. No significant inhibition could be observed. The positive control was carried out without inhibitor.
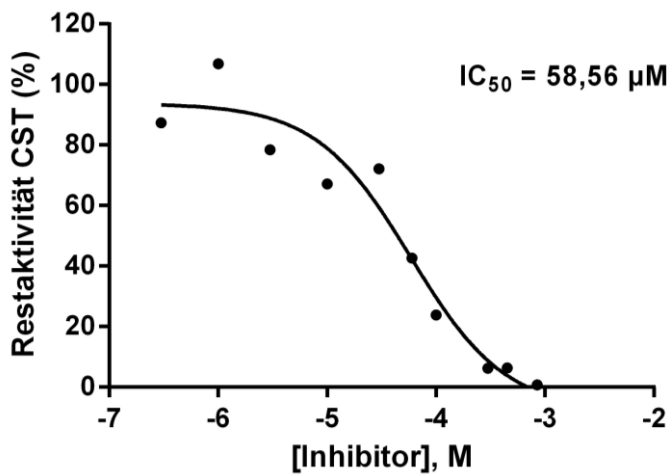

Fig. 8.88: Inhibitory activity of citreoviridin C on human cerebroside sulfotransferase (hCST). The assay was performed in duplicates, of which the mean values of are given.
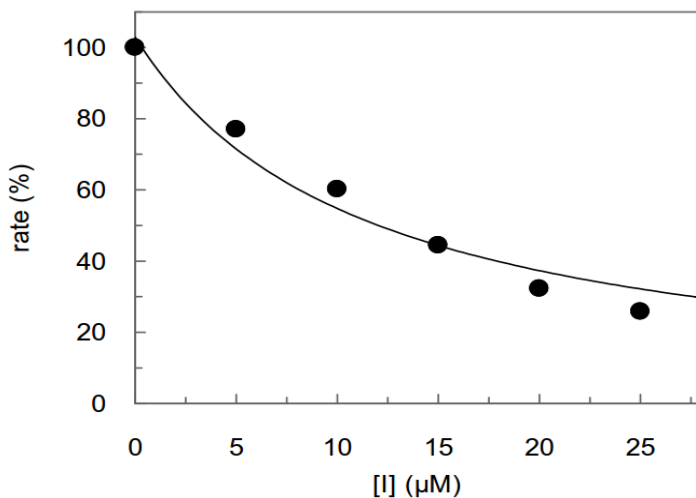

Fig. 8.89: Inhibitory activity of epipyrones (**1-3**) on cathepsin K. The assay was performed in duplicates for each concentration.
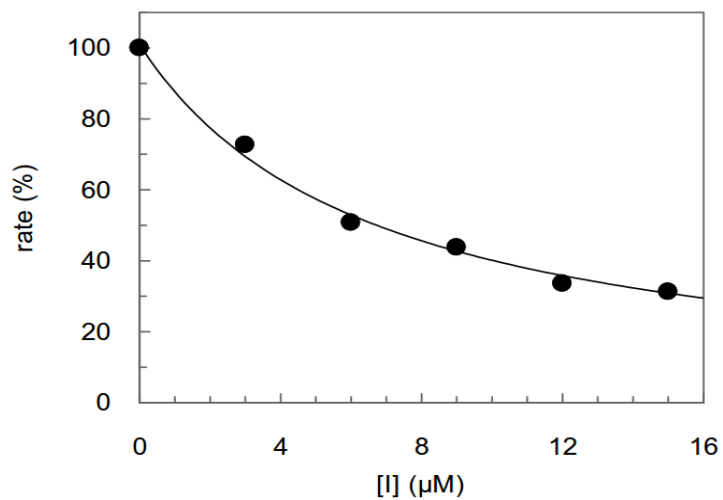
Fig. 8.90: Inhibitory activity of epipyrones (**1**-**3**) on cathepsin S. The assay was performed in duplicates for each concentration.
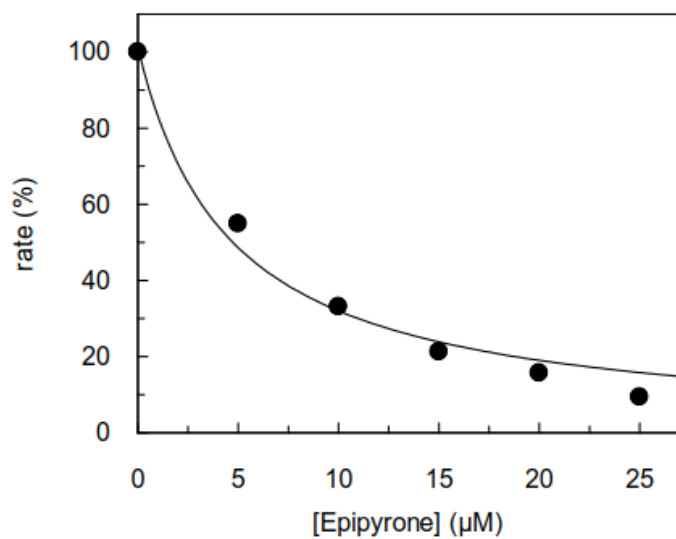

Fig. 8.91: Inhibitory activity of epipyrones (**1**-**3**) on human leukocyte elastase (HLE). The assay was performed in duplicates for each concentration.
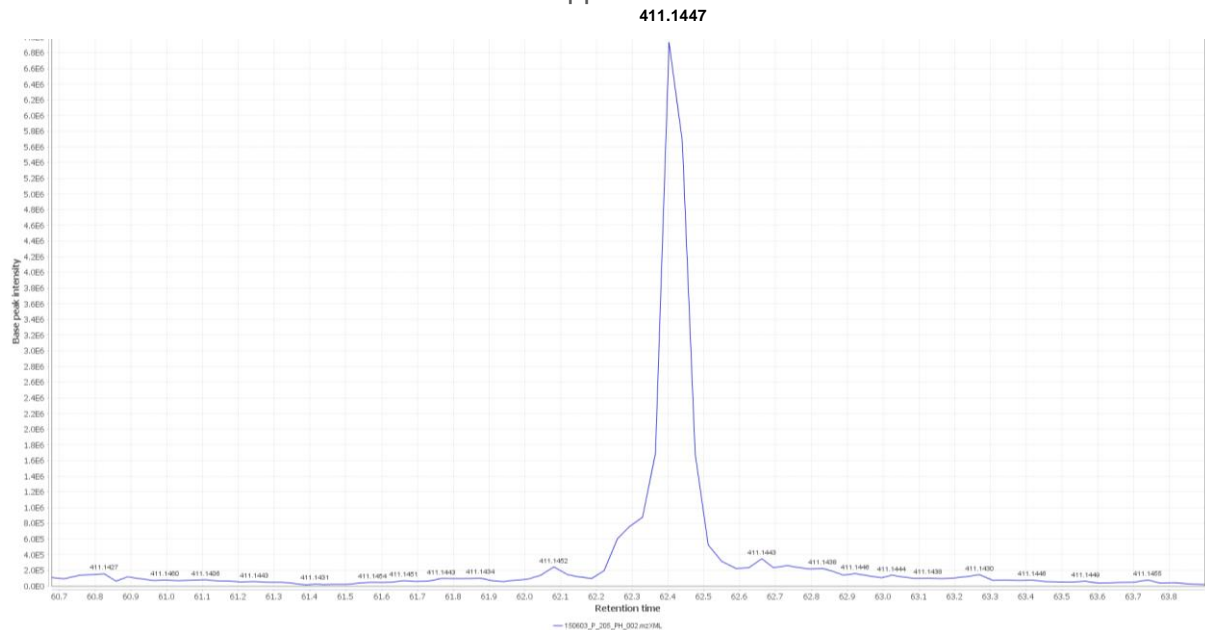
Fig. 8.92: Part of chromatogram showing the presence of epicocconone (**8**) in guttation droplets on mycelium of *E. nigrum* strain 749, grown on Czapek-Dox agar under continuous illumination with white light. Analysis was performed by LC-HR-ESI-MS in positive mode. Data were viewed with MZmine 2.21.

Fig. 8.93: Mass spectrum and fragmentation of epicocconone (**8**), analyzed in the extract of *E. nigrum* strain 749, grown on Czapek-Dox agar under continuous illumination with white light, by LC-HR-ESI-MS in positive mode. Data were viewed with MZmine 2.21.

Fig. 8.94: Part of chromatogram showing the presence of epipyrones (**1-3**), acetosellin (**4**), 5´6´-dihydroxyacetosellin (**7**), epicocconone (**8**) and epicoccolide B (**9**) in guttation droplets on mycelium of *E. nigrum* strain 749, grown on Czapek-Dox agar under continuous illumination with white light. Analysis was performed by LC-HR-ESI-MS in positive mode. Data were viewed with MZmine 2.21.
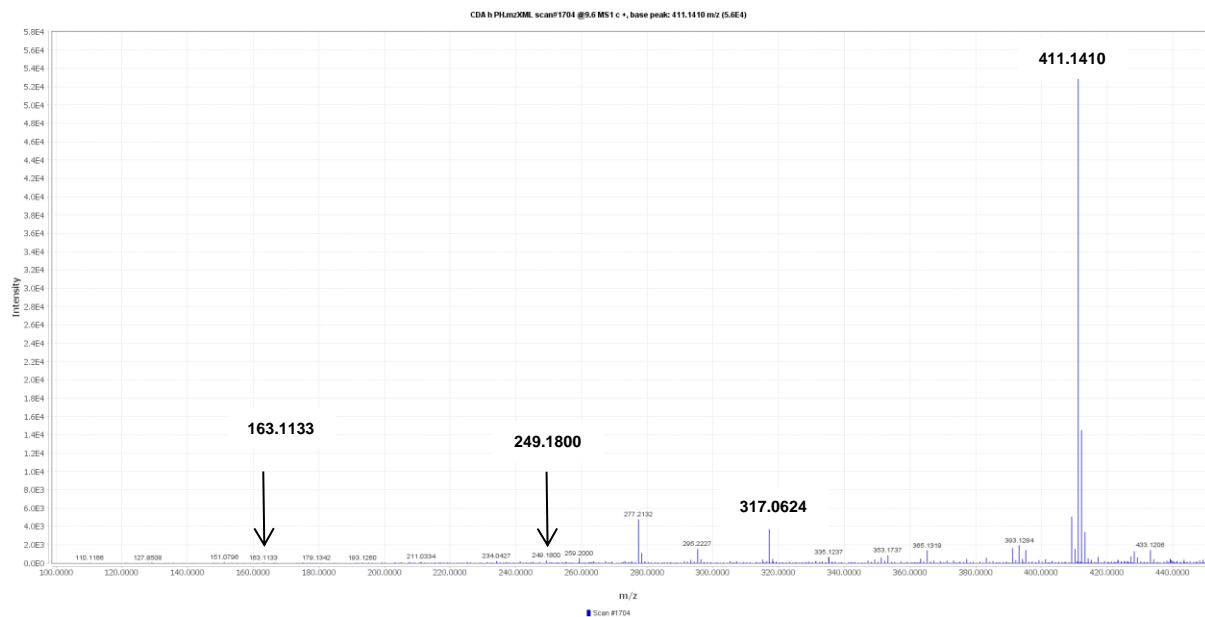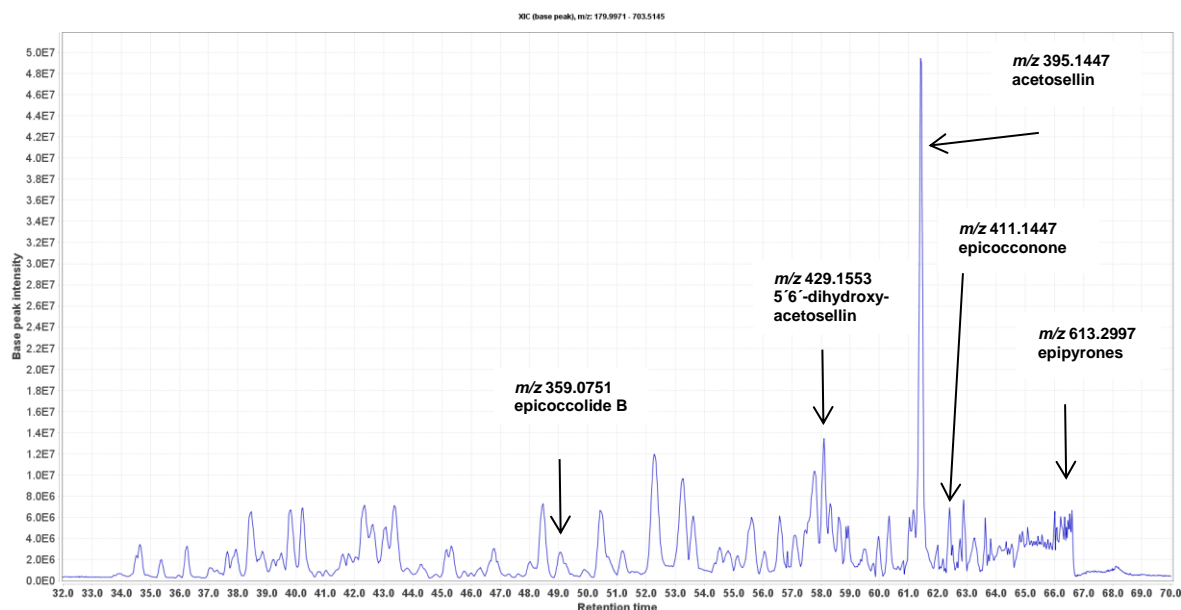

Fig. 8.95: Selected ion chromatogram showing the relative abundance of epipyrones (**1-3**) and acetosellin (**4**) in guttation droplets on mycelium of *E. nigrum* strain 749, grown on CDT (CDA with trace metal solution, upper chromatogram) in darkness and CDA (Czapek-Dox agar, lower chromatogram) under continuous illumination with white light. Analysis was performed by LC-HR-ESI-MS in positive mode. Data were viewed with MZmine 2.21.
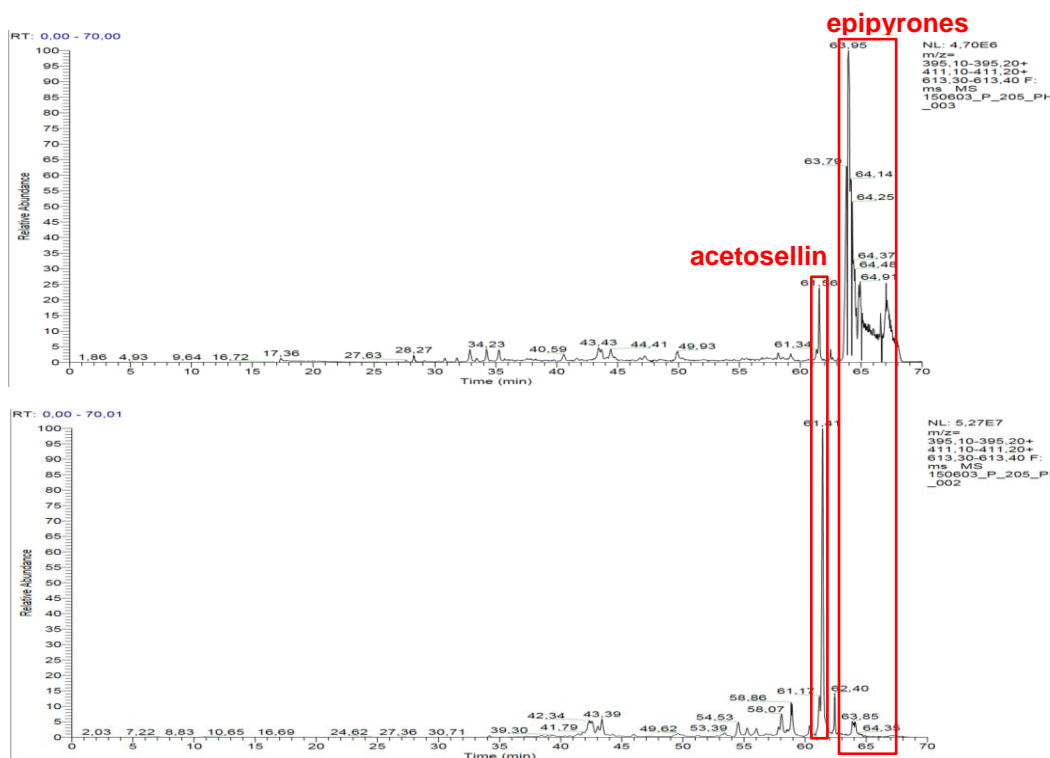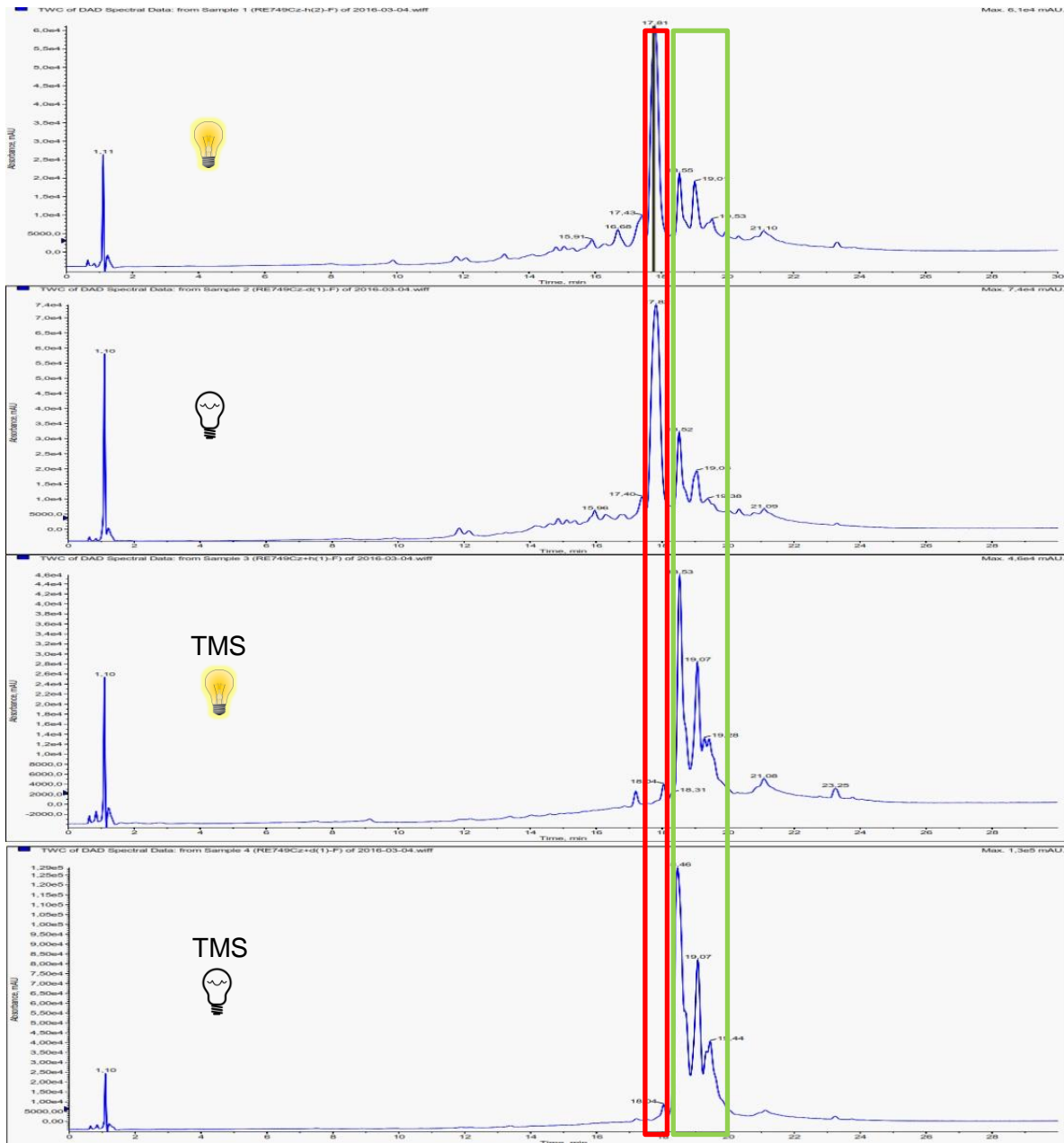
Fig. 8.96: Total wavelength chromatograms showing the relative abundance of epipyrones (**1**-**3**, green box) and acetosellin (**4**, red box) in extracts from *E. nigrum* strain 749, grown on Czapek-Dox agar with or without trace metal solution (first replicate cultivation). Analysis was performed by LC -ESI-MS in positive mode. **TMS** = supplementation with trace metal solution. **Yellow light bulbs** indicate fermentation under continuous illumination with white light, while **colorless light bulbs** indicate fermentation in darkness.

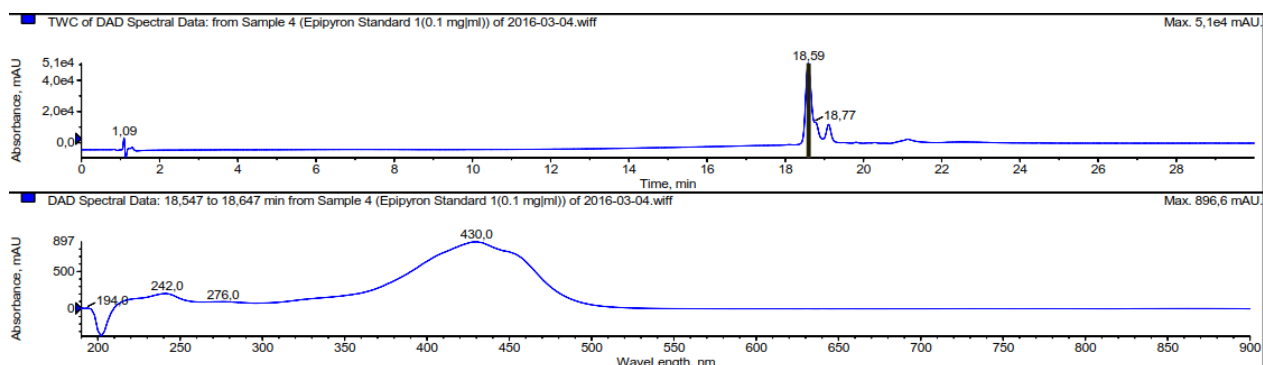**Fig. 8.97a:** Example for DAD data for standard solution of epipyrones (**1**-**3**) with a concentration of 0.1 mg/mL, used for the quantification of extract and guttation droplets.
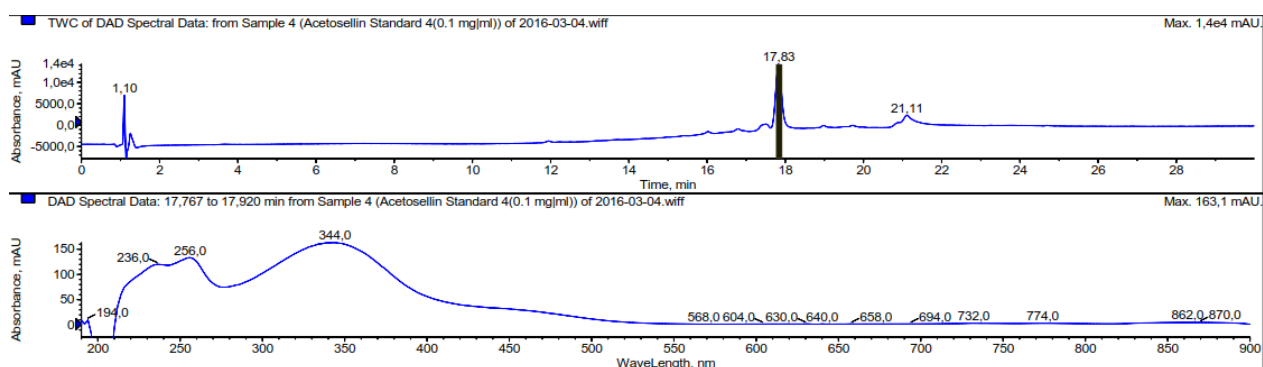
Fig. 8.97b: Example for DAD data for standard solution of acetosellin (**4**) with a concentration of 0.1 mg/mL, used for the quantification of extract and guttation droplets.
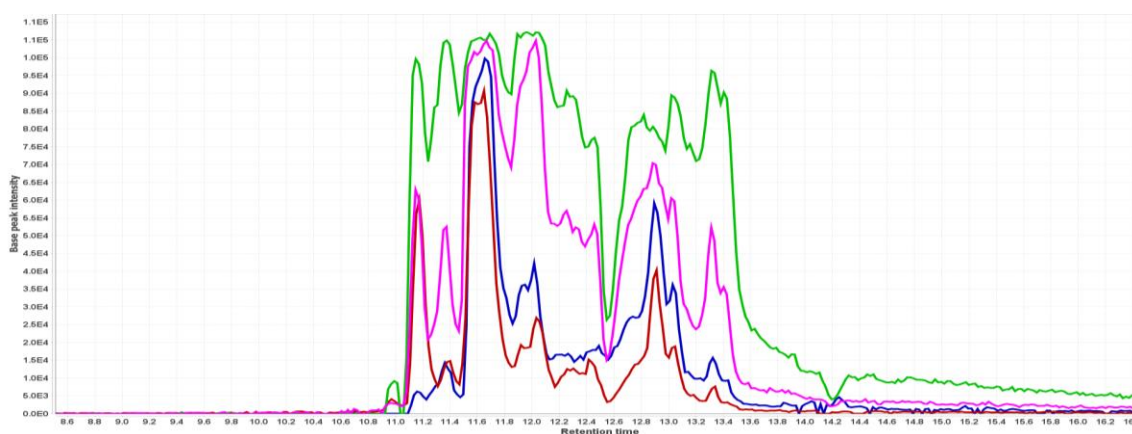
Fig. 8.98: Selected ion chromatogram of different culture extracts from strain 749, showing the mass of epipyrones (**1**-**3**) (m/z 613.3007 $[M+H]^+$, selected range 613.290 - 613.350). Analysis was performed using LC-HR-ESI-MS system C (see **section 3.3.2**). Colored lines represent following extracts (CDA = Czapek-Dox agar, CDT = Czapek-Dox agar with trace metal solution, all cultivations carried out under darkness under the same conditions):): **pink:** CDA**; red:** CDA+Zn^{2+}; **blue:** CDA+Cu^{2+}; **green:** CDT

Tab. 8.3a: Raw data for the quantification of epipyrones (**1**-**3**) and acetosellin (**4**) in the extracts of *E. nigrum* strain 749 on Czapek-Dox agar (see **section 4.7**).

Experiment/ replicate No.	Trace metals/ illumination	Volume of agar	Total mass of epipyrones [mg]	Concentration of epipyrones per L agar [mM]	Total mass of acetosellin [mg]	Concentration of acetosellin per L agar [mM]
1	No/Yes	2.5	8.12	0.005	129.89	0.132
	No/No	1.1	24.95	0.037	338.20	0.780
	Yes/Yes	0.7	11.62	0.027	21.36	0.077
	Yes/No	2.5	207.42	0.135	0.00	0.000
2	No/Yes	1.9	32.50	0.028	217.35	0.290
	No/No	1.8	40.46	0.037	1.79	0.003
	Yes/Yes	1.9	381.57	0.328	0.00	0.000
	Yes/No	1.7	571.21	0.548	0.00	0.000
3	No/Yes	1.7	13.09	0.013	49.02	0.073
	No/No	1.5	16.65	0.018	6.54	0.011
	Yes/Yes	2.1	264.31	0.205	1.98	0.002
	Yes/No	2	293.47	0.239	0.00	0.000

Tab. 8.3b: Mean values of the concentration of epipyrones (**1**-**3**) and acetosellin (**4**) in the extracts of *E. nigrum* strain 749 on Czapek-Dox agar with standard error of the mean (SEM) (see **section 4.7**).

Trace metals/illumination	Mean epipyrones [mM] ± SEM	Mean acetosellin [mM] ± SEM
No/Yes	0,015 ± 0.007	0,165 ± 0.065
No/No	0,031 ± 0.006	0,264 ± 0.258
Yes/Yes	0,187 ± 0.087	0,027 ± 0.025
Yes/No	0,308 ± 0.124	0,000 ± 0.000

Tab. 8.3c: Volumes of collected guttation droplets of *E. nigrum* strain 749 on Czapek-Dox agar (see **section 4.7**). Guttation droplets from all cultures of a specific fermentation condition. The mean values with standard error of the mean (SEM) are given from three replicate experiments.

Collection date[†]	Trace metals/ Illumination	Total volume [µL]			Volume per petri dish [µL]			Mean volume per petri dish [µL]
		n = 1	n = 2	n = 3	n = 1	n = 2	n = 3	
14	No/Yes	166	646	234	6.6	34.0	13.8	18.1
14	No/No	168	420	177	15.3	23.3	11.8	16.8
14	Yes/Yes	0	26	254	0.0	1.4	12.1	4.5
14	Yes/No	12	6	115	0.5	0.4	5.8	2.2
28	No/Yes	36	494	234	1.4	26.0	13.8	13.7
28	No/No	260	178	49	23.6	9.9	3.3	12.3
28	Yes/Yes	0	8	365	0.0	0.4	17.4	5.9
28	Yes/No	227	125	80	9.1	7.4	4.0	6.8

[†]Date of cultivation. n = experiment/replicate number (see **tab. 8.3a**).

Tab. 8.3d: Raw data for the quantification of epipyrones (**1**-**3**) in the guttation droplets of *E. nigrum* strain 749 on Czapek-Dox agar (see **section 4.7**). The mean values with standard error of the mean (SEM) are given from three replicate experiments.

Collection date[†]	Trace metals/illumination	c(epipyrone) [mmol/l]			Mean value ± SEM
		n = 1	n = 2	n = 3	
14	No/Yes	0.16	0.69	1.23	0.69 ± 0.31
14	No/No	0.73	0.76	0.66	0.72 ± 0.03
14	Yes/Yes	*	0.2	0.57	0.39 ± 0.19
14	Yes/No	0.24	4.43	1.32	2.00 ± 1.26
28	No/Yes	0.14	0.51	0.92	0.52 ± 0.23
28	No/No	0.27	0.29	0.12	0.23 ± 0.05
28	Yes/Yes	*	0.92	1.54	1.23 ± 0.31
28	Yes/No	0.81	1.29	1.12	1.07 ± 0.14

*No data recorded, since guttate production was too low for collection of droplets. [†]Date of cultivation. n = experiment/replicate number (see **tab. 8.3a**).

Tab. 8.3e: Raw data for the quantification of acetosellin (**4**) in the guttation droplets of *E. nigrum* strain 749 on Czapek-Dox agar (see **section 4.7**). The mean values with standard error of the mean are given from three replicate experiments.

Collection date[†]	Trace metals/illumination	c(acetosellin) [mmol/l]			Mean value ± SEM
		n = 1	n = 2	n = 3	
14	No/Yes	0.11	0.09	0	0.07 ± 0.03
14	No/No	0.25	0.01	0	0.09 ± 0.08
14	Yes/Yes	*	0.01	0	0.01 ± 0.01
14	Yes/No	0	0.01	0	0.00 ± 0.00
28	No/Yes	0.11	0.15	0	0.09 ± 0.04
28	No/No	0.22	0	0	0.07 ± 0.07
28	Yes/Yes	*	0	0	0.00 ± 0.00
28	Yes/No	0	0	0	0.00 ± 0.00

*No data recorded, since guttate production was too low for collection of droplets. [†]Date of cultivation. n = experiment/replicate number (see **tab. 8.3a**).